HUMBOLDT-UNIVERSITÄT ZU BERLIN

Interactome of TNRC6 W-motifs and their conserved Role in miRNA-mediated silencing

DISSERTATION

zur Erlangung des akademischen Grades

Doctor of Philosophy (Ph.D.)

eingereicht an der
Lebenswissenschaftlichen Fakultät der Humboldt-Universität zu Berlin

von
MSc Marta Mauri

Präsidentin der Humboldt-Universität zu Berlin

Prof. Dr.-Ing. Dr. Sabine Kunst

Dekan der Lebenswissenschaftlichen Fakultät
der Humboldt-Universität zu Berlin

Prof. Dr. Bernhard Grimm

Gutachter/innen

1. Prof. Dr. Ana Pombo
2. Prof. Dr. Matthias Selbach
3. Dr. Benedikt Beckmann

Tag der mündlichen Prüfung: July 12th 2017

Erklärung

Hiermit erkläre ich, die Dissertation selbstständig und nur unter Verwendung der angegebenen Hilfen und Hilfsmittel angefertigt zu haben. Ich habe mich anderwärts nicht um einen Doktorgrad beworben und besitze keinen entsprechenden Dok-torgrad. Ich erkläre, dass ich die Dissertation oder Teile davon nicht bereits bei einer anderen wissenschaftlichen Einrichtung eingereicht habe und dass sie dort weder angenommen noch abgelehnt wurde. Ich erkläre die Kenntnisnahme der dem Verfahren zugrunde liegenden Promotionsordnung der Lebenswis-senschaftlichen Fakultät der Humboldt-Universität zu Berlin vom 5. März 2015. Weiterhin erkläre ich, dass keine Zusammenarbeit mit gewerblichen Promotionsberaterinnen/Promotions-beratern stattgefunden hat und dass die Grundsätze der Humboldt-Universität zu Berlin zur Sicherung guter wissenschaftlicher Praxis eingehalten wurden.

Declaration

I hereby declare that I completed the doctoral thesis independently based on the stated resources and aids. I have not applied for a doctoral degree elsewhere and do not have a corresponding doctoral degree. I have not submitted the doctoral thesis, or parts of it, to another academic institution and the thesis has not been accepted or rejected. I declare that I have acknowledged the Doctoral Degree Regulations, which underlie the procedure of the Faculty of Life Sciences of Humboldt-Universität zu Berlin, as amended on 5th March 2015. Furthermore, I declare that no collaboration with commercial doctoral degree supervisors took place, and that the principles of Humboldt-Universität zu Berlin for ensuring good academic practice were abided by.

Berlin,

…….

Marta Mauri

The work presented in this thesis was performed between the years 2013-2017 in the laboratory of Dr. Marina Chekulaeva at the Berlin Institute for Medical Systems Biology, part of the Max Delbrück Center for Molecular Medicine in the Helmholtz Association in Berlin, Germany.

To my Family,

Abstract

MicroRNAs (miRNAs) guide Argonaute (AGO) proteins to silence complementary mRNA targets. In bilaterians, AGO interact with GW182/TNRC6 proteins, which recruit CCR4-NOT deadenylases via short tryptophan-containing motifs (W-motifs), thereby promoting the translational repression and decay of target mRNAs. To gain deeper insights into miRNA silencing mechanisms, I determined the W-motif-specific interactome of human TNRC6C proteins using quantitative proteomics. I identified 23 proteins that were at least two-fold enriched with wild type TNRC6C as compared to mutants where W-motifs were disrupted. Besides known functional interactors, such as subunits of the CCR4-NOT complex, I identified components of clathrin-coated vesicles (CCVs), metabolic enzymes, mitochondrial proteins, RNA helicases, kinases, and phosphatases with potential roles in miRNA-mediated repression. I showed that AGO and TNRC6 localize on CCVs via interactions between W-motifs and CCV adaptor protein 2A (AP2A). Depletion of AP2A intensified miRNA-mediated repression of RLuc-hmga2 reporters, but it did not increase CCR4-NOT binding to W-motifs. Conversely, knockdown of CCR4-NOT increased W-motif-mediated interactions between TNRC6C and AP2A. Hence, binding to either CCR4-NOT or AP2A may be governed by specific modifications of TNRC6 proteins, and CCVs may mediate the storage or recycling of TNRC6 and AGO proteins.

The second part of this study addresses the conservation of the mechanisms of miRNA silencing in the cnidarian *Nematostella vectensis*, separated by 600 million years from other Metazoa. Using cultured human cells, I showed that *Nematostella* GW182 (nvGW182) recruits the CCR4-NOT deadenylation complex via its W-motifs, thereby inhibiting translation and promoting mRNA decay. As in bilaterians, nvGW182 is recruited to the miRNA repression complex by AGO proteins, indicating this mechanism of miRNA-mediated silencing was already active in the last common ancestor of Cnidaria and Bilateria.

Keywords: miRNA silencing, Argonaute proteins, TNRC6/GW182 proteins, W-motifs, clathrin-coated vesicles (CCVs), evolution, Cnidaria, Nematostella GW182

Zusammenfassung

MicroRNAs (miRNAs) regulieren die Genexpression, indem sie Proteine der Argonaute Familie (AGO) zu komplementären Sequenzen in mRNAs rekrutieren. In Bilateria interagiert AGO mit GW182/TNRC6 Proteinen, die wiederum CCR4-NOT Deadenylasen rekrutieren und so die Inhibition der Translation und den mRNA-Abbau fördern. Die Interaktion zwischen TNRC6 und CCR4-NOT ist abhängig von kurzen, Tryptophan-reichen Motiven (W-Motiven). Um mehr über die Mechanismen der miRNA-abhängigen Genrepression zu erfahren, habe ich W-Motiv-abhängige Interaktionspartner humaner TNRC6C Proteine identifiziert. Hierzu habe ich, mithilfe von quantitativer Massenspektrometrie, das Interaktom von wildtyp TNRC6C Proteinen mit dem von TNRC6C Proteinen, deren W-Motive mutiert wurden, verglichen. Neben bekannten Interaktionspartnern wie Untereinheiten des CCR4-NOT Komplexes, habe ich Komponenten von Clathrin-Vesikeln (CCVs), Stoffwechsel assoziierte Enzyme, mitochondriale Proteine, RNA Helikasen, Kinasen und Phosphatasen mit potentiellen Funktionen in miRNA-assoziierter Repression identifiziert. Darüber hinaus konnte ich zeigen, dass AGO und TNRC6C sich auf CCV befinden und dass die W-Motiv-abhängige Interaktion mit dem CCV-Adapter-Protein 2a (AP2A) hierfür verantwortlich ist. Eine Depletion von AP2A/ Die Reduzierung der zellulären AP2A Menge verstärkt die miRNA-abhängige Repression eines untersuchten Reportergens, hat aber keinen Einfluss auf die Bindung von CCR4-NOT an W-Motiven. Die Reduzierung von CCR4-NOT dagegen verstärkt die Bindung zwischen TNRC6 und AP2A. Es ist vorstellbar, dass post-translationale Modifikationen die Bindung von TNRC6 an CCR4-NOT oder AP2A beeinflussen und möglicherweise spielen CCVs eine Rolle beim recyceln von TNRC6 und AGO Proteinen oder fungieren als Reservoir/ Speicher.

Der zweite Teil dieser Studie befasst sich mit der Konservierung von miRNA vermitteltem Gen-Silencing in Cnidaria (*Nematostella vectensis*), welche sich vor 600 Millionen Jahren von der Ahnenreihe der Metazoa abspalteten. Hier zeige ich in humanan Zellen, dass *Nematostella* GW182 (nvGW182) Teile des CCR4-NOT Komplexes über W-Motive rekrutiert und dadurch die Translation inhibiert und den mRNA Abbau fördert. Wie auch in Bilateria wird nvGW182 durch AGO rekrutiert, was darauf schließen lässt, dass der miRNA Inhibitionsmechanismus bereits in den letzten gemainsamen Vorfahren von Cnidaria und Bilateria aktiv war.

Schlüsselwörter: miRNA Inhibitionsmechanismus, Argonaute Proteine, TNRC6/GW182 Proteine, W-motiven, Clathrin-Vesikeln (CCVs), Evolution, Cnidaria, Nematostella GW182

Publication and Presentations

Parts of this thesis have been published in a peer revewed scientific journal:

Marta Mauri, Marieluise Kirchner, Reuven Aharoni, Camilla Ciolli Mattioli, David van den Bruck, Nadya Gutkovitch, Vengamanaidu Modepalli, Matthias Selbach, Yehu Moran and Marina Chekulaeva (2016) *Conservation of miRNA-mediated silencing mechanisms across 600 million years of animal evolution*. Nucleic Acids Research. doi:10.1093/nar/gkw792

Figures and quotations extracted from the manuscript are explicitely indicated.

Parts of this thesis have been presented at international conferences and workshops:

Marta Mauri, Marieluise Kirchner, Camilla Ciolli Mattioli, Matthias Selbach and Marina Chekulaeva (2016) Conservation of miRNA silencing mechanisms across 600 million years of animal evolution. Poster. Functional RNAs Cell Symposia, Guangzhou, China.

Marta Mauri, Marieluise Kirchner, Matthias Selbach, Marina Chekulaeva (2014) Towards a functional interactome of TNRC6C protein. Poster. The complex Life of mRNA, EMBL, Heidelberg, Germany.

Marta Mauri, Marieluise Kirchner, Cinthia Claudia Amaya Ramirez, Matthias Selbach and Marina Chekulaeva (2014) Role of W-motifs in miRNA Silencing and Other Cellular Pathways. Poster. Non-coding Genome workshop, Institut Curie, Paris, France.

Table of Contents

ERKLÄRUNG ..... **II**

DECLARATION ..... **II**

ABSTRACT ..... **V**

ZUSAMMENFASSUNG ..... **VI**

PUBLICATION AND PRESENTATIONS ..... **VII**

LIST OF FIGURES ..... **XII**

LIST OF SUPPLEMENTARY FIGURES ..... **XIV**

SUPPLEMENTARY TABLES ..... **XV**

1. INTRODUCTION **1**

1.1 CLASSES OF SMALL RNAS 2

1.1.1 siRNAs *3*

1.1.2 piRNAs *4*

1.1.3 miRNAs *4*

1.2 MIRNA BIOGENESIS AND MODES OF ACTION 5

1.3 BIOLOGICAL FUNCTIONS OF MIRNAS 10

1.3.1 miRNA functions in development *11*

1.3.2 Misregulated functions in disease *12*

1.4 MECHANISMS OF MIRNA-MEDIATED REPRESSION 14

1.4.1 Components of the RNA Induced Silencing Complex (RISC) *16*

1.4.1.1 AGO Protein Family 17

1.4.1.2 GW182 Protein Family 20

1.4.1.3 PAN2-PAN3 & CCR4-NOT deadenylase complexes 25

1.4.2 Subcellular localization of miRISC *28*

1.4.3 miRNA-mediated translational repression *30*

1.4.3.1 Basics of eukaryotic translation 30

1.4.3.2 Translational repression by miRNAs: initiation vs. post-initiation mechanisms 34

1.4.4 miRNA-mediated deadenylation and decay *38*

1.4.5 Kinetics of miRNA silencing *39*

1.4.6 Modulation of miRNA silencing *42*

1.4.6.1 Modulation by post translational modifications of miRISC 42

1.4.6.2 Modulation of miRNA processing 43
1.4.6.3 Modulation of miRNA stability 45
1.4.6.4 Modulation by accessory proteins 46
1.5 RNAi ACROSS SPECIES 48
1.6 AIM OF THE STUDY 52
2. RESULTS 53
2.1 IDENTIFICATION OF THE W-MOTIF-DEPENDENT INTERACTOME OF HUMAN TNRC6C PROTEIN 53
2.1.1 Importance of W-motifs for mRNA repression 53
2.1.2 Classes of W-motif-specific Interactors identified by quantitative Mass Spectrometry analysis of TNRC6C and its mutants 55
2.2 ADDRESSING THE ROLE OF CLATHRIN-COATED VESICLES IN REGULATION OF miRNA SILENCING 61
2.2.1 Clathrin-coated vesicles as novel interactors of TNRC6 and AGO2 proteins 61
2.2.2 Knockdown of components of the clathrin-coated vesicles enhances miRNA-mediated repression 66
2.3 CONSERVATION OF THE PLAYERS AND MECHANISM OF miRNA-MEDIATED REPRESSION 72
2.3.1 Nematostella GW182 represses mRNAs via W-motifs within its C-terminal domain 73
2.3.2 W-motifs of Nematostella GW182 recruit the CCR4-NOT complex . 77
2.3.3 Nematostella GW182 represses translation and mediates mRNA degradation via the CCR4-NOT deadenylase complex 81
2.3.4 Nematostella GW182 interacts with Nematostella AGOs, but fails to bind human AGOs 83
2.3.5 W-motifs of Nematostella GW182 contribute to bona fide miRNA silencing 87
3. DISCUSSION 91
3.1 MODULATION OF miRNA SILENCING VIA W-MOTIF SPECIFIC INTERACTOME OF TNRC6 PROTEINS 91
3.1.1 Speculative model for regulation of miRNA silencing by components of clathrin-coated vesicles 91
3.1.2 Potential roles for other classes of identified W-motif interactors in miRNA silencing 96

3.2 Evolutionary Aspects of miRNA-mediated Repression 99
3.2.1 Evolution of the modes of miRNA silencing 99
3.2.2 Conservation of miRISC components 101
4. MATERIALS 104
4.1 Equipment and Consumables 104
4.2 Chemicals and Enzymes 105
4.3 Kits 108
4.4 Buffers, solutions and Media 108
4.4.1 Buffers and solutions 108
4.4.2 Media 109
4.5 Bacterial strains and Cell lines 110
4.5.1 Bacterial strains 110
4.5.2 Cell Lines 110
4.6 Oligos 111
4.6.1 Oligos for sequencing 111
4.6.2 Oligos for cloning 111
4.6.3 Oligos for site directed mutagenesis 114
4.6.4 Oligos for qRT-PCR 116
4.7 siRNAs 116
4.8 Plasmids 117
4.8.1 Backbones 117
4.8.2 List of plasmids 117
4.9 Antibodies 133
4.10 Polyacrylamide gel compositions 134
4.11 Softwares 135
5. METHODS 136
5.1 Cell Culture 136
5.2 DNA work 137
5.2.1 DNA Extraction with Phenol-Chloroform 137
5.2.2 Agarose gel electrophoresis 137
5.2.3 Cloning 138
5.2.4 Mutagenesis 142
5.3 RNA work 143
5.3.1 RNA isolation 143

5.3.2 cDNA synthesis *144*
5.3.3 qRT-PCR *145*
5.4 PROTEIN WORK 147
5.4.1 Protein Extraction *147*
5.4.2 Determination of protein concentration *147*
5.4.3 GST pull-down *148*
5.4.4 TNRC6A IP *150*
5.4.5 Nematostella AGO1 and CNOT9 IP *150*
5.4.6 SILAC and Mass Spectrometry *151*
5.4.7 Western blotting *153*
5.5 CCVS ISOLATION FROM HELA CELLS 155
5.6 TETHERING ASSAYS 155
5.7 MIRNA REPORTER ASSAYS 156
5.8 TNRC6 RESCUE ASSAYS 157
5.9 LUCIFERASE ASSAYS 157
5.10 TRANSFERRIN UPTAKE ASSAYS 158
5.11 GO AND KEGG PATHWAYS ENRICHMENT ANALYSIS 159
5.12 MOTIF ANALYSIS 159
6. APPENDIX 160
6.1 SUPPLEMENTARY FIGURES 160
6.2 SUPPLEMENTARY TABLES 173
7. ABBREVIATIONS 207
8. SYMBOLS AND UNITS 209
9. BIBLIOGRAPHY 210
ACKNOWLEDGEMENTS 247

List of Figures

Figure 1. Canonical and non-canonical pathways of miRNA biogenesis 8

Figure 2. Modes of miRNA silencing in bilaterian animals 15

Figure 3. Argonaute (AGO) protein domains and structure 19

Figure 4. GW182 protein domains and RRM structure 24

Figure 5. The CCR4-NOT deadenylase complex 27

Figure 6. Eukaryotic translation 33

Figure 7. Disruption of W-motifs by Tyr or Ala point mutations progressively alleviates mRNA repression by TNRC6C CED 54

Figure 8. Identification of a TNRC6C W-motif specific interactome 56

Figure 9. TNRC6C CED interacts with vesicular trafficking proteins via its W-motifs 58

Figure 10. Additional classes of W-motif-specific interactors identified by quantitative Mass Spectrometry 60

Figure 11. TNRC6A and AGO2 proteins associate with Clathrin-coated vesicles (CCVs) 63

Figure 12. AP2A appendage interacts with TNRC6C CED via W-motifs 65

Figure 13. No enrichment of wt miRNA reporter mRNA is detected on the isolated CCVs 66

Figure 14. Knockdown of AP2A proteins enhances miRNA-mediated repression 68

Figure 15. Knockdown of CCR4-NOT allows increased AP2A binding to TNRC6C CED 70

Figure 16. Phylogenetic distribution of GW182 proteins 72

Figure 17. nvGW182 represses tethered mRNA via its C-terminal effector domain (CED) 74

Figure 18. nvGW182 represses tethered mRNA via W-motifs 76

Figure 19. Quantitative Mass Spectrometric analysis of proteins associated with nvGW182 and its deletion mutants nv∆CED, nvDNAJ and nvCED 78

Figure 20. nvGW182 recruits subunits of the CCR4-NOT complex via its W-motifs 80

Figure 21. nvGW182 represses translation and mediates mRNA degradation via CNOT6/CNOT7 deadenylases 82

Figure 22. GW182-AGO interaction regions are not conserved between human and Nematostella 84

Figure 23. Multiple tryptophan-containing regions of nvΔCED contribute to nvAGO binding 85

Figure 24. W-binding pockets of human AGOs are conserved in nvAGOs 86

Figure 25. AGO, GW182 and CCR4-NOT natively interact in Nematostella 87

Figure 26. Human/Nematostella GW182 chimera partially rescues miRNA silencing in human HeLa cells 89

Figure 27. Speculative model illustrating CCVs modulation of miRNA silencing .. 95

Figure 28. Modes of miRNA silencing across species 99

List of Supplementary Figures

Figure S 1. Human TNRC6C amino acid sequence 160

Figure S 2. Consensus human W-motif and the corresponding count matrix 161

Figure S 3. TNRC6C CED interacts with AP1 proteins via W-motifs 162

Figure S 4. Ratio of wt to mut RLuc-hmga2 reporter does not vary between input-isolated and CCV-isolated RNA 163

Figure S 5. Knockdown of AP2A proteins does not enhance miRNA repression when using RLuc-3xb artificial miRNA reporters 164

Figure S 6. Knockdown of TNRC6 proteins does not significantly affect CCV-mediated endocytosis 165

Figure S 7. Nematostella GW182 (nvGW182) amino acid sequence 166

Figure S 8. Tethering of nvΔCED does not affect mRNA repression 167

Figure S 9. Consensus W-motif and the corresponding count matrix 168

Figure S 10. Sequence alignment of human and Nematostella DDX6 169

Figure S 11. Proteins other than TNRC6 containing W-motifs 170

Figure S 12. Coexpression of nvGW182 and nvAGOs cannot rescue TNRC6 depletion in mammalian cells 171

Figure S 13. Affinity purification of endogenous TNRC6A shows abundant interactions with CCR4-NOT and less abundant interactions with CLTC 172

Supplementary Tables

Table S1. W-motif enriched interactors identified by SILAC followed by AP-MS/MS 173

Table S2. nvGW182 MS results 176

Table S3. nvΔCED MS results 178

Table S4. nvDNAJ MS results 185

Table S5. nvCED MS results 198

Table S6. W-motif enriched interactors detected in b-isoxazol precipitates 206

1. Introduction

The goal of biology is to understand how life works. Back in 1869 Friedrich Miescher isolated DNA[1]. Years later, in 1944 Avery, MacLeod and McCarty demonstrated that DNA is the molecule that carries the genetic information[2], pointing to DNA as the molecule of life. Within 20 years Watson, Crick and Rosalind Franklin solved the DNA structure[3] and the genetic code was deciphered[4,5]. To then dissect how cells with the same DNA content can differentiate and develop into complex organisms, mechanisms of gene expression regulation had to be studied. To explain that, "the central dogma of biology" was proposed, stating that DNA passes its information onto RNA that acts as a temporary messenger carrying the information to synthesize proteins[6]. In this view, DNA is the crucial storage of information and proteins are the functional protagonists acting as gene regulators, while RNA is an overlooked intermediary. However, in 1982 one exception was identified: rybozymes, RNA molecules that act as catalysts[7,8]. This discovery contributed in refreshing the 'RNA World Hypothesis' stating that earlier forms of life might have been mediated by self-replicating RNA molecules later replaced by more stable DNA molecules[9]. Later on, once the human genome was sequenced and assembled it was observed that nearly 99% of the genome is non-protein-coding and about 90% of it is transcribed into non-coding RNAs[10-12]. The news generated a debate on how functionally relevant the non-coding genome is, with opposing views regarding it as a byproduct of small population size or as an important trait of organisms complexity[13-16]. It is still unclear what percentage of the non-coding genome is actually functional. Current estimates suggest ~8%[17-20], however additional experimental evidence is needed to answer this question. Nevertheless, the past two-three decades have signed an 'RNA revolution' with multiple novel classes of non-coding RNAs and their roles as gene expression regulators being identified[12,21-23]. It became evident that epigenetic regulation is not only mediated by histone modifier and DNA methylases, but also by a subset of RNA molecules[13,16,24] and RNA modifiers (reviewed in[25]). Classes of non-coding RNAs include small RNAs (sRNAs), long non-coding RNAs (lncRNAs) and circular RNAs (circRNAs) amongst others (reviewed in[17,18,20]). Interestingly, some non-coding

RNAs harbor small ORFs (sORFs), potentially encoding peptides[21-23,26-30]. Although a few sORF-encoded peptides have been assigned a function[31-35], the generality of their roles is still to be investigated.

Small RNAs are the most extensively studied group of non-coding RNAs, comprising three classes: siRNAs, miRNAs, and piRNAs.

1.1 Classes of small RNAs

In the past twenty-three years novel classes of short non-coding RNAs, generally called small RNAs (sRNAs) have been described[36-39]. As the name suggests, they are all characterized by a small size, ranging between 20-30 nucleotides and are not translated into proteins[36-39]. sRNAs are derived from longer RNA precursors; which are then processed to mature sRNAs that associate with a member of the Argonaute (AGO) protein family. sRNAs guide AGO proteins to their RNA targets via Watson-Crick base pairing where they then exert their regulatory functions[36,39]. The striking common feature of all classes of sRNAs is that nucleotide base-pairing is used as a strategy for highly specific target recognition[36,39]. They differ in respect to their biogenesis and in some aspects of their modes of action, despite all being governed by similar principles. RNA interference (RNAi)[24,40,41], which refers to the regulatory processes mediated by small RNAs, was a breakthrough discovery and its main contributors, Fire and Mello[24], were awarded with the 2006 Nobel Prize. Generally, all classes of small RNAs function in repressing transcripts and/or potentially harmful genetic elements[18,42,43]. Lastly, it is important to mention that except for the budding yeast, *Saccharomyces cerevisiae*, and a few other species, all eukaryotic organisms analyzed so far express sRNAs and the RNAi machinery[44]. In prokaryotes (bacteria and archaea) sRNAs are on average longer than their eukaryotic counterparts (~50-500 nucleotides)[45]. Yet, they also act via base-pairing to regulate the expression of their targets[45]. Additionally, prokaryotes express an RNAi-like machinery, which is functionally similar to the eukaryotic one despite its components are not homologous to their eukaryotic counterparts[44]. Notably, also the genomes of certain viral families encode for small RNAs (miRNAs)[46].

To date, the best-characterized classes of eukaryotic small RNAs are small interfering RNAs (siRNAs), microRNAs (miRNAs) and Piwi-associated RNAs (piRNAs). As for any human-built classification it is important to bear in mind that

the borders between the different classes are not clearly defined and several exceptions to the rules have been discovered.

1.1.1 siRNAs

Small interfering RNAs are 20–25 nucleotides long RNA molecules. They are usually processed from long double-stranded RNAs (dsRNA) formed by two complementary RNAs. The origin of these longer precursors can be endogenous (endo siRNAs), forming when two complementary DNA strands are transcribed. This can occur for instance in case of antisense transcription, transcription of transposable elements or from hairpin RNAs[26-30,47-51]. Alternatively, the source of dsRNA can be exogenous (exo siRNAs), such as from a viral infection, since many viruses, while replicating their genomes, produce both sense and antisense transcripts[40,41,52]. The longer precursors are then cleaved by a ribonuclease III enzyme (RNase III) known as Dicer into shorter dsRNA fragments (~20-25 base pairs). These shorter dsRNA products have a two nucleotides overhang on 3' ends and phosphate groups on 5' ends[42,43,53]. The duplex is then loaded into a member of the AGO protein family where the siRNA strand with the least thermodynamically stable 5'-end is retained, while the other strand is released[18,47-51,54-56]. The loaded strand is commonly referred to as the guide strand, while the strand that is not loaded is called passenger strand. Once the guide strand is loaded, it forms an effector complex known as RNA induced silencing complex (RISC)[52,57]. The siRNA guide then acts to recruit RISC to perfectly complementary stretches of mRNA sequences, where it then induces gene silencing. Silencing is achieved through mRNA cleavage catalyzed by the endonucleolytic activity of AGOs. AGOs cleave in the middle of the siRNA-mRNA duplex, between the 10th and 11th residues. The two halves of the mRNA are subsequently degraded via 3'→5' and 5'→3' decay pathways (reviewed in[58]). siRNAs do not only function as post-transcriptional gene regulators in the cytoplasm, but can also serve as transcriptional regulators or genome structure modulators in the nucleus (reviewed in[53,59-63]). Additional details about siRNA biogenesis and functions can be found in these reviews[18,54-56].

siRNAs are mostly important to keep the activity of transposons under control and to face viral infections. Nevertheless siRNAs can also regulate protein-coding genes and have therefore been exploited as powerful tools to control gene

expressions not only for research purposes, but also for applications in the clinic and biotechnology industry.

1.1.2 piRNAs

P-element-induced wimpy testis (PIWI)-interacting RNAs (piRNAs) are 25-30 nucleotides long RNA molecules expressed across the animal kingdom, from sponges to humans, but depleted from plants and fungi[57,64]. All piRNAs have a modified 2'-O-methyl 3'-end suggested to increase their stability[59-63]. They were first discovered in *D. melanogaster* as short sequences complementary to intergenic repetitive elements, such as retrotransposons, specifically expressed in animal germ cells[59,64-69]. Most of the repetitive regions complementary to piRNAs were found in discrete genomic regions, later defined as piRNA clusters[64,70-74]. In contrast to siRNAs, piRNAs are generated from long single stranded precursors arising from the transcription of these repetitive regions in a Dicer-independent manner[59,75,76]. To exert their function, piRNAs associate with a member of the Piwi subclade of Argonaute proteins, which is mainly germline-specific[59,64,67-69,77]. The effector complex, piRISC, is then guided by piRNAs to silence the expression and transposition of mobile genetic elements both in the cytoplasm and in the nucleus. Indeed, piRNAs and Piwi proteins are essential for functional gametogenesis and reproduction[57,70-74,78,79]. To date, they are the largest class of small non-coding RNAs[75,76,80]. Importantly, piRNAs can mediate trans-generational silencing thereby protecting newly synthesized genomes from mobile elements[77,81]. More recent analysis extended the presence of Piwi-piRNAs to somatic cells[82-84] and pointed at a novel role of piRNAs in repression of partially complementary mRNA targets, similarly to miRNAs[85,86].

1.1.3 miRNAs

MicroRNAs are 21-23 nucleotide long single-stranded RNAs expressed in animals, plants, unicellular algae and by some viral genomes[80,87]. Current release of miRBase (miRBase v21)[88] annotates 1881 human miRNA precursors and 2588 human mature miRNAs. Their number varies across species, for instance for *D. melanogaster* 256 precursors and 466 mature miRNAs are currently annotated, for *C. elegans* 250 and 434 and for a non-bilaterian animal, such as *N. vectensis*, 141 and 142. Transcription of miRNA-encoding genes produces long single-stranded RNAs that fold back into hairpins and are then processed by two RNAse III

enzymes, Drosha and Dicer, to form mature miRNAs (reviewed in[89]). Mature miRNAs are loaded into AGO proteins and guide them to partially complementary mRNA targets, which are then silenced by the miRISC via translational repression and mRNA degradation (reviewed in[90,91]).

miRNAs were first discovered in 1993 in *Caenorhabditis elegans* in the laboratories of Ruvkun and Ambros[92,93]. A few years later another *C. elegans* miRNA, named let-7, was characterized[87]. Interestingly its sequence and function was conserved from flies to human[94,95]. Since then thousands of miRNAs have been discovered across species[80,96-102] as a class of small RNAs ubiquitously expressed in somatic tissues[103,104]. Most miRNA binding sites are located in the 3'-UTR of protein-coding transcripts[95,105]. Animal miRNAs are only partially complementary to their targets. Typically, they have a uracil (U) at their 5'-end[99,106], a region between nucleotides 2-7, called 'seed', that has perfect complementarity to mRNA targets, and the most 3'-region that has only partial complementarity to targets[103,107,108]. This feature allows single miRNAs to target multiple genes. Considering that more than 60% of human genes contain miRNA binding sites[105,109-111], miRNAs have the ability to regulate nearly every biological process. Therefore, miRNAs are often deregulated in pathologies. As a matter of fact, molecules targeting miRNAs (anti-miRs) or synthetic miRNAs (miR mimics) are being developed for therapeutics (reviewed in[106,112,113]). Functionally important molecules are usually conserved across evolution. However, miRNA sequences as a whole show poor conservation across species. For a few conserved miRNAs, their target sequences complementary to seed regions are also significantly conserved across species, underlying the importance of miRNA-mediated gene regulation[107,108,114].

1.2 miRNA biogenesis and modes of action

miRNA genes are mostly transcribed by RNA polymerase II into hundreds to thousands nucleotide long primary transcripts (pri-miRNAs) that fold into hairpin-containing structure where the miRNA sequences reside[109-111,115]. Processing into mature miRNAs differs in animals and plants. This chapter will focus on animal miRNA biogenesis (**Figure 1**).

In mammals miRNA-encoding genes are mainly located within intergenic regions and introns of protein-coding genes, although some can also be found

within exons. miRNA loci are organized in individual transcription units or, as often is the case, they are clustered together and transcribed as single polycistronic transcripts[112,113,116]. Although some reside within protein-coding genes, their promoters can differ[114,117-120] and miRNA genes can have several transcription start sites (TSS)[115,121-123]. Once RNA polymerase II has transcribed them, pri-miRNAs are capped at their 5'-end and polyadenylated at their 3'-end. They are usually kilobases long and fold in an imperfectly matched stem-loop structure with free ends. In the canonical pathway a nuclear complex called microprocessor digests the free ends of the pri-miRNA to form a ~65 nucleotides long hairpin named pre-miRNA with a typical 2 nucleotides overhang at the 3'-end and a phosphate group at the 5'-end[116,124-128]. The microprocessor is composed of an RNase III enzyme called Drosha and its cofactor DGCR8 (Pasha in *D. melanogaster* and *C. elegans*) that bind dsRNAs. The importance of the microprocessor complex is emphasized by the fact that Drosha depletion is embryonic lethal and lack of DGCR8 leads to DiGeorge syndrome[117-120,129-131]. Pre-miRNAs are exported to the cytoplasm by Exportin 5 with the help of RanGTP[121-123,132,133]. In the cytoplasm, the RNase III enzyme Dicer further processes the pre-miRNA near the terminal loop to form a ~22bp long dsRNA[124-128,134-137]. Similarly to Drosha, depletion of Dicer in mouse is embryonic lethal and causes proliferation and differentiation defects in mouse embryonic stem cells[49-51,129-131]. The RNA duplex is then loaded into Argonaute family protein, forming a premature effector complex called pre-miRNA-induced silencing complex (pre-miRISC). Two heat-shock proteins, HSC70 and HSP90, use ATP to induce a conformational change in AGOs that allows loading of the duplex[132,133,138-142]. Sorting of RNA duplexes in specific AGO proteins is a consequence of (I) which Dicer processes the precursor, (II) the structure of the RNA duplex, (III) the terminal nucleotide, and (IV) its thermodynamic properties (reviewed in[143]). In *D. melanogaster* and *C. elegans* RNA duplexes with central mismatches, as most miRNAs have, are preferentially loaded into AGO1[140-142] and ALG-1 or ALG-2[144,145], respectively. Conversely, perfectly matched duplexes are generally sorted to AGO2[140-142] in flies and RDE-1 in worms[144,145]. By contrast in mammals perfectly and imperfectly matched duplexes are similarly sorted between AGO1-4[135,146,147]. Once the duplex is loaded, one of the two strands, named passenger strand, is then rapidly degraded. Usually the strand that is retained, guide strand,

is the one with the least thermodynamically stable 5'-end and with a uracil as first nucleotide[138-142,148].

A minority of miRNAs can also be generated via non-canonical biogenesis pathways that are either microprocessor independent or Dicer independent. In the so-called mirtron pathway, pre-miRNAs are generated by splicing and de-branching or trimming of a lariat, bypassing the requirement for Drosha-DGCR8[149-153]. Further processing is similar to the canonical pathway. The microprocessor can be bypassed also in the case of short hairpins RNAs generated directly by transcription[120,154] or by tRNAs[148,155-157], snoRNAs[152,158] and small nuclear viral RNAs[95,154,159,160]. For example, miR-451, a conserved miRNA in vertebrates, is processed in a very short hairpin by the microprocessor (~18bp), exported and directly loaded onto AGO2, which cleaves it into a 30 nt RNA, that is then trimmed to produce a mature miRNA[95,99,155-157,161,162]. Lastly, pre-miRNA with only 1 nt 3'-overhang have to be elongated by an additional nt through monourydilation to be efficiently processed by Dicer[158,163-166].

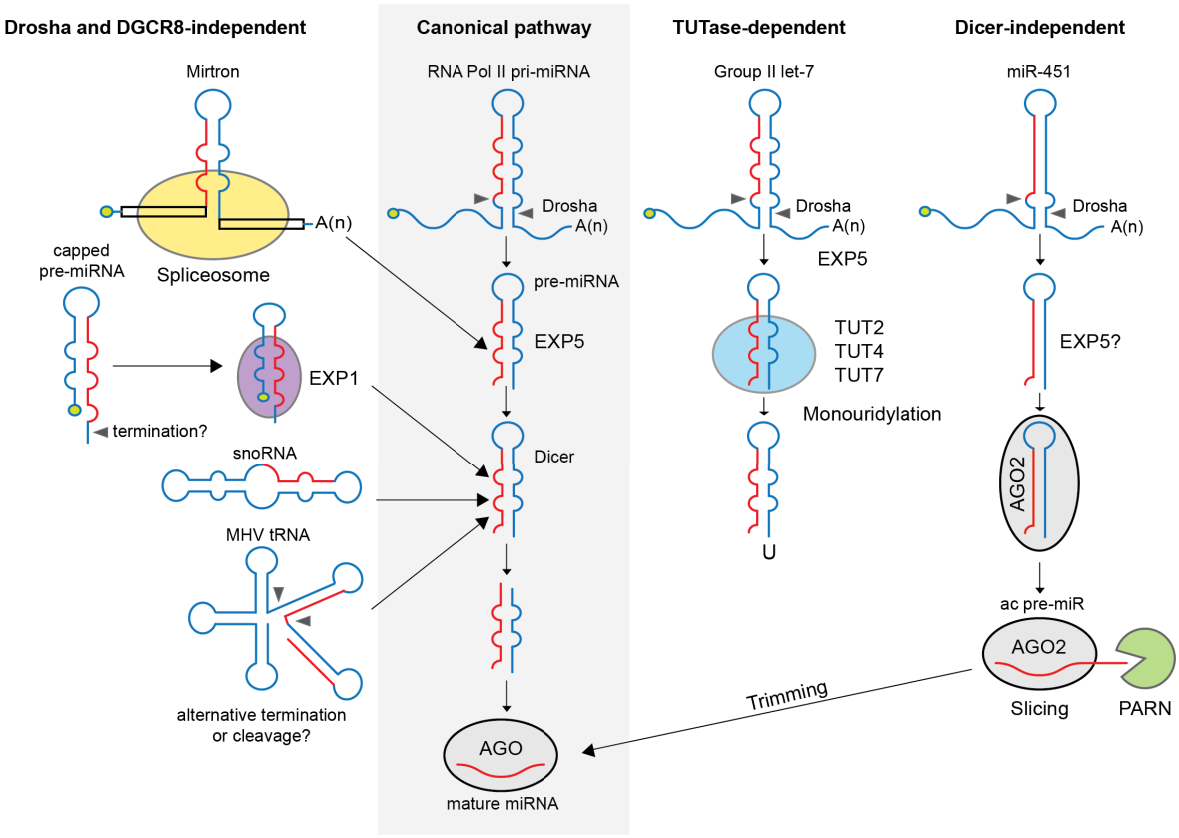

Figure 1. Canonical and non-canonical pathways of miRNA biogenesis In the canonical miRNA biogenesis pathway miRNA genes are mainly transcribed by RNA-Pol II into primary RNA transcripts (pri-miRNAs), nuclear processing of the pri-miRNA is performed by the microprocessor Drosha-DGCR8, and results in a ~65 nt pre-miRNA exported to the cytoplasm by exportin 5 (EXP5). In the cytoplasm the RNaseIII Dicer further processes the pre-miRNA producing double stranded short RNAs that can be loaded onto AGO proteins. In Drosha and DGCR8-independent pathways, transcription generates directly pre-miRNAs, which will be then exported to the cytoplasm by EXP1. Alternatively, mirtron loci produce pre-miRNAs through splicing and debranching. Some mirtrons require additional trimming of the RNA tails before Dicer processing. Cleavage of snoRNAs and tRNAs (or tRNA-like RNAs) can also directly originate pre-miRNAs. In the TUTase-dependent biogenesis pathway, the microprocessor produces pre-miRNAs with shorter 3'-overhang that require monouridylation for efficient Dicer processing. In a Dicer-independent pathway, short pre-miRNAs are produced by Drosha, exported and directly loaded on AGO2, which cleaves the stem of the pre-miRNA that is further trimmed by the 3'-5' exonuclease PARN. Question marks indicate experimental evidence supporting that step is missing. MHV, murine γ-herpesvirus; mmu, *Mus musculus*; Pol II, RNA polymerase II. Figure from Nature review; Minju Ha and V. Narry Kim, 2014[89].

When the mature miRNA is loaded into AGO, it will from a mature miRISC complex and it will guide it to mRNA targets via complementary base pairing. In most cases, miRNA share only partial complementarity with their mRNA targets leading to translational repression and target degradation. Typically, the seed region, nucleotides 2-7 of the miRNA, perfectly matches to its targets, while the 3'-end of the miRNA is imperfectly matched[95,147,159,160,167,168]. Having a uracile as first nucleotide and perfect match also at position 8 increases the activity of the miRNA[95,99,161,162,169-173]. Though, there are reported cases of functional miRNAs with imperfect seed matching to targets[95,163-166,174]. In some instances, miRNAs have extensive perfect complementarity with their targets. If this is the case they lead to silencing via AGO2-mediated cleavage of target mRNAs, similarly to siRNAs[105,147,162,167,168,175,176].

miRNAs mainly target the 3'-UTR of protein-coding genes, but they can also bind the 5'-UTR and the coding region[162,169-173,177-179]. Certain features of the 3'-UTR influence the overall effect exerted by miRNAs. For instance, target sites positioned at least 15 nt away from the stop codon, AU-rich sequences near target sites, targets far from the center of long 3'-UTR and multiple miRNA binding sites across the 3'-UTR increase the effect of miRNA-binding[95,174]. Functionality of 5'-UTR and CDS miRNA sites is not entirely clear. Sites in coding regions were reported to be functional only in case of ribosome stalling, for example, due to a stretch of rare codons[180]. More recently, they have been proposed to function in translation inhibition and to augment the repression effect of sites in the 3'-UTR[181]. miRNA sites within the 5'-UTR are more criptic, they are suggested to repress mRNA targets by preventing ribosomal association due to occupancy of miRISC[182].

Overall, miRNAs affect expression levels of hundreds of genes[105,162,175,176] mostly by moderately (average ~ 30%) downregulating target expression, thereby fine-tuning tissue specific gene expression of nearly all cell types[162,177-179,183,184].

1.3 Biological functions of miRNAs

miRNAs are a wide class of gene regulators. In fact 1-2% of genes in worms, flies and mammals encode for miRNAs[95,185-190]. Their mechanism of targeting by complementary base pairing represents an exquisite strategy to selectively regulate the majority of genes and therefore potentially all biological processes[105,191,192]. Most metazoan miRNAs recruit the RISC to target RNAs via imperfect base-pairing with sites typically within the 3'-UTR of their targets, thereby inducing translational repression and RNA destabilization, with the latter mechanism contributing the most to miRNA silencing[162,176,183,184]. Regardless of their established function as gene expression regulators, increasing evidence suggests that most miRNAs are not master regulators (few examples of those are described in the next chapter), but rather act as a buffering system for stochastic cell to cell variability ensuring robustness against environmental and genetic variations. In spite of numerous overexpression and deletion studies performed in cell culture[185-190,193,194], which indicated crucial roles for miRNAs, *in vivo* knockouts of several specific miRNAs showed mild or no apparent phenotypes[95,105,191,192] supporting their role as buffering agents. It is important to note that although miRNAs lead to mild changes in gene expression (max ~2-fold)[119,129,162,176,195-197], miRNA genes often arise from gene duplication events producing homologous miRNAs that share the same seed sequence[193,194,198-200]. When co-expressed these miRNA families can co-regulate targets enhancing their silencing effects. In addition, combinatorial regulation by multiple miRNAs can occur since most 3'-UTRs have on average four miRNA binding sites[92,93,95,105,201]. Overall, miRNA silencing as a general mechanism of gene expression regulation is of importance to cells. In fact, individual mice knockouts of the enzymes involved in miRNA processing: Drosha[196], Dgcr8[119] and Dicer[129]; of AGO2[202]; and mutant mice of GW182/TNRC6 proteins[203], the downstreat effectors of AGOs are embryonic lethal. Conditional knockouts of Dicer in cell culture lines exhibit an expected reduction in mature sRNAs and severe developmental defects, such us defective differentiation and centromers silencing[130,204]. Drosha depletion in cell culture systems abolishes production of canonical miRNAs[205] and conditional depletion in mice leads to defective spermatogenesis and male infertility[206]. AGO1-AGO4 depletion in mouse embryonic stem cells (mESC) abrogates miRNA silencing and leads to apoptosis[207]. Another line of evidence for the importance of miRNA is the

evolutionary conservation of seed-target base pairing across species[93,198-201] that supports a selective advantage conferred by miRNAs.

1.3.1 miRNA functions in development

Most miRNAs function as fine-tuners of gene expression, however some miRNAs have more prominent physiological roles. A few well-characterized examples are outlined in the following paragraphs.

Lin-4, the first miRNA discovered, regulates developmental timing in *C. elegans* by targeting lin-14 mRNAs[92,93,201,208]. Lin-14 encodes a transcription factor that is necessary to complete the first larval stage[209-212]. Both lin-4 loss of function mutants and lin-14 gain of function mutants lose the ability to differentiate and keep going through early stage fates[93,201,213-216]. To ensure proper development fluctuations lin-14-mRNA levels are promptly regulated by oscillations in lin-4 in a feed-forward loop[208,217].

Similarly, let-7, the second miRNA discovered, contributes to stem cells differentiation by inhibiting cell cycle progression and self-renewal[209,211,212,218]. miRNAs belonging to the let-7 family target c-Myc, ras, high mobility group A (HMGA) , Janus protein tyrosine kinase (JAK), signal transducer and activator of transcription 3 (STAT3) and Np95/ICBP90-like RING finger protein (NIRF), oncogenes involved directly or indirectly in promoting cell proliferation[219]. By targeting these genes let-7 halts cell proliferation and acts as a tumor suppressor[219].

Depletion of the miR-143/145 cluster under normal conditions causes no apparent phenotype. However, depletion upon injury impairs the ability of the intestinal epithelium and of blood vessels to regenerate due to altered insulin-like growth factor signaling[213-216,220]. Additional examples of miRNA knockouts, which manifest phenotypes only under stress conditions, are reviewed by Vidigal and Ventura (2015)[217].

In *Zebrafish*, the miR-430 family controls fluctuations in chemokine receptor signaling, ensuring fidelity in germ cells migration[218,221]. The same family also takes part in maternal mRNA clearance during the maternal to zygotic transition[220,222]. Clearance of maternal mRNAs is as well mediated by miRNAs in other species, such as *X. laevis*, *C. elegans* and *D. melanogaster*[223-225].

miR-128 is a good example of additive effects of miRNAs due to targeting of multiple functionally related mRNAs. In fact, depletion of miR-182 in mice induces de-repression of several members of the mitogen-activated protein kinase pathway (MAPK) leading to fatal epilepsy[221]. An analogous example is miR-205, whose depletion in mice causes neonatal death and results in compromised epidermal and hair follicle growth, due to targeting of several modulators of the phosphoinositide 3 kinase (PI3K) signaling pathway[222].

1.3.2 Misregulated functions in disease

As miRNAs modulate virtually all biological processes, including cell growth, proliferation and differentiation, organismal metabolism and development, they are deregulated in a variety of diseases[226-233]. A large and growing body of literature has investigated the roles of miRNAs in cancer, neurodegenerative, viral, immune and cardiac diseases (reviewed in[231,233-236]). In the majority of cases, aberrant miRNA expression associates with the disease[229,237-239]. In short, the function of miRNAs is conserved in disease, but their expression patterns are altered as a cause or consequence of the pathology. This observation raised hope for using miRNAs as prognostic and diagnostic biomarkers of specific diseases[240]. Additionally, the discovery that nucleotides mimicking or inhibiting the activity of miRNAs could be delivered *in vivo*, promoted the development of therapeutic strategies based on miRNAs[241].

To note, the first genetic disorder to be linked to miRNAs was Fragile X Syndrome (FXS)[226-228,232]. This pathology manifests with severe cognitive and intellectual disabilities and is associated with a CGG trinucleotide repeat expansion within the 5'-UTR of the fragile X mental retardation 1 (FMR1) gene encoding for the FMR1 RNA binding protein[232,234-236,242]. In wild type conditions the *Drosophila* homolog of FMR1, dFXR, associates with components of active miRISC as was shown by cofractionation and affinity purification experiments [226,227] and contributes to sRNA-mediated repression[226]. Contrariwise, the disease mutant loses the ability to associate with RISC as was shown by a shift of the mutant in the cytosolic soluble fraction of a Superose gradient[226]. In the following paragraphs I will outline a few examples of human disease-associated miRNAs.

The first link between cancer and miRNA deregulation came from the observation that 65% of B-cell chronic lymphocytic leukemia (B-CLL) patients had

deletion of genes encoding miR-15 and miR-16[243]. Moreover the expression levels of miR-15 and miR-16 were downregulated in patients without the genetic deletion[243]. In fact miR-15 and miR-16 repress the anti-apoptotic gene *bcl-2*, thus promoting tumor cell death[244]. Expression profiles of several types of cancer showed a correlation between aberrant miRNAs expression and the occurrence or stage of cancer[245,246]. Cancer-related miRNAs are classified as tumor suppressor, such as miR-15, miR-16 and let-7, or oncogenes, such as miR-21 and miR-155[243,244,247].

Viruses often encode their own miRNAs or modulate and take advantage of host miRNAs. For example, miR-122 has been found to be necessary for hepatitis C virus (HCV) replication *in vitro* and *in vivo*, although its levels are not affected by the viral infection[248,249]. On the other hand the Epstein-Barr virus (EBV) upregulates the expression of the host miR-155[250], which spares the infected cells from apoptosis[251]. Similarly the Kaposi's sarcoma associated herpes virus (KHSV) encodes for miR-K12-11 that targets the same set of genes as miR-155[252].

In the autoimmune disease multiple sclerosis (MS) the expression of miR-145 is a hallmark of the disease, which allows to discriminate between patients and healthy controls[253].

Aging-related neurological diseases such as Parkinson (PD) and Alzheimer's (AD) also showed distinct profiles of miRNA expression. In PD patients, the expression of miR-30b, miR-30c and miR-26a correlates with the susceptibility of the disease[254]. Additionally, miR-133b might contribute to the onset of PD since it is involved in a feedback loop essential for maintenance of dopaminergic neurons[255]. In AD patients the expression of miR-29a, miR29-b-1 and miR-9 is downregulated[256], thereby the expression levels of their target BACE1, a protein involved in AD pathogenesis[257], is upregulated.

miR-208 is a cardiac-specific miRNA. Upon cardiac stress miR-208 expression, together with other stress-induced stimuli, leads to upregulation of β-myosin heavy chain (β-MHC) that promotes cardiac remodeling and hypertrophy[258]. Delivery of anti-miR-208 molecules prevented pathological cardiac remodeling[259].

1.4 Mechanisms of miRNA-mediated repression

miRNA-mediated repression is achieved via two mechanisms: translational repression and mRNA degradation, involving mRNA deadenylation, decapping and 5'-3' decay[81,242,260,261]. Genome-wide analysis of the effects of miRNAs on mRNA and protein expression levels indicated that at steady state miRNA-mediated degradation accounts for 66-90% of overall miRNA silencing in several mammalian cultured cells[162,176,183,184,262,263]. In addition, structural and biochemical studies have elucidated many molecular details of miRNA-silencing. The structures of some of its key players: human AGO2 in complex with miRNA mimics[264-266]; subunits of the deadenylase complexes CCR4-NOT and PAN2-PAN3, such as CNOT9[267,268], CNOT1 in complex with the RNA helicase DDX6[267,268] and PAN3[269]; and lastly DDX6 in complex with the enhancer of mRNA decapping EDC3[270] clarified the mode and sequence of events leading to miRNA-mediated repression.

In bilaterian animals miRNA silencing acts via the recruitment of the miRNA induced silencing complex (miRISC) to target mRNAs[232] (**Figure 2**). The core components of miRISC are Argonaute proteins (AGO1-AGO4 in mammals) and GW182/TNRC6 protein (TNRC6A-C in mammals). miRNAs guide miRISC to partially or fully complementary mRNA targets[232]. Fully complementary targets are silenced by cleavage via catalytically active AGOs (only AGO2 in mammals)[232,242]. However, in bilaterian animals the majority of miRNAs are only partially complementary to mRNA targets, thereby impeding cleavage by AGO[242]. Under these circumstances, AGO proteins recruit a member of the GW182 protein family[271-274], which acts as a platform for the recruitment of downstream effector complexes, such as the CCR4-NOT and PAN2-PAN3 deadenylase complexes[275-277]. One of the major advances in the field was the discovery that the CCR4-NOT complex is directly recruited to miRISC by the C-terminal domain of GW182 proteins and mediates both translational repression and mRNA decay[275-277]. Chekulaeva and colleagues demonstrated that the direct recruitment of CCR4-NOT to GW182 proteins is mediated by a series of short linear motifs containing an invariant tryptophan residue (Trp, W), and thus named W-motifs, dispersed throughout the C-terminal domain of GW182 proteins[275]. Point mutations of seven tryptophan residues within W-motifs to alanine abrogated both translational repression and mRNA decay[275]. This discovery revealed that the same set of

proteins mediates both miRNA silencing mechanisms, explaining why the two mechanisms of miRNA-mediated silencing - translational repression and mRNA deadenylation – are coupled.

Interestingly miRNA-mediated translational repression and deadenylation, decapping and decay can be uncoupled in some cellular contexts, such as oocytes, early embryos, cell-free extracts and neuronal cells[225,263,278-285]. Under these circumstances, translationally repressed and possibly deadenylated miRNA targets can escape decay and eventually reinitiate translation[263,281,283].

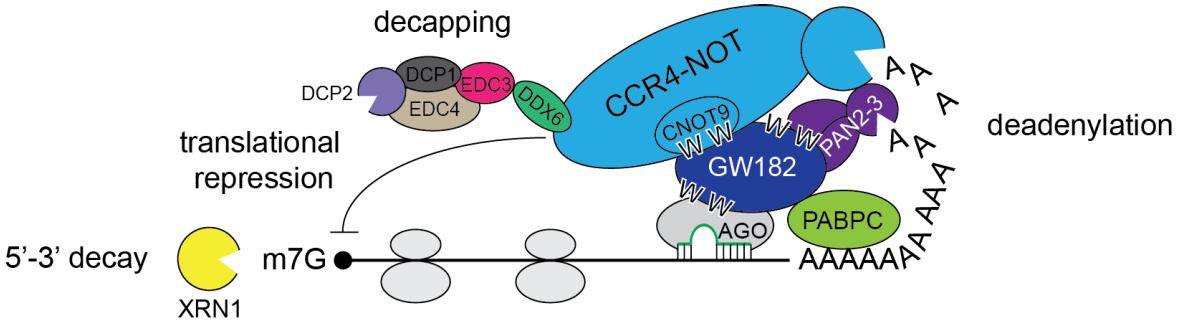

Figure 2. Modes of miRNA silencing in bilaterian animals Sequence of molecular events leading to miRNA-mediated translational repression and deadenylation, decapping and decay supported by structural and biochemical studies. First, miRNAs lead AGO proteins to target mRNAs as pinpointed by structures of human AGO2 bound to miRNA mimics[264-266]. AGO recruit GW182 proteins via two W-binding pockets[264]. GW182 proteins interact with PABPC proteins via a PAM2 motif[286,287] and with the PAN2-PAN3[269,288-290] and CCR4-NOT deadenylation complex via W-motifs present in their C-terminal unstructured domain[267,268]. CNOT1 via its MIF4G domain interacts with both the catalytic module CNOT6-CNOT7[291,292], which can promote shortening of poly(A) tails, and with the RNA helicase DDX6[267,268,293], which can promote translational repression. DDX6 additionally interact with the decapping factor EDC3[270] that in turns bind to the DCP1-DCP2[294,295] complex thereby leading to decapping (it is not yet known whether DDX6 can interact simultaneously with CNOT1 and EDC3). Finally, decapping factors recruit the 5'-3' exonuclease XRN1[296,297]. Cap removal promotes access of XRN1 to target mRNAs, thereby inducing mRNA decay.

The following chapters will further describe the most important players of miRNA silencing and the current knowledge on the mechanisms of miRNA-mediated translational repression and degradation.

1.4.1 Components of the RNA Induced Silencing Complex (RISC)

The term RNA induced silencing complex (RISC) was first used by the Hannon lab in the year 2000 to describe a ribonucleoprotein complex involved in RNAi[298,299]. By purifying mRNA cleavage products from dsRNA-treated *Drosophila* S2 cells, Hammond and colleagues identified RISC, a sequence specific nuclease that co-fractionates with a ~25 nucleotide long RNA, which confers specificity to the enzyme[298,299]. Their observation came right after Tuschl and Zamore recapitulated RNAi *in vitro* using Drosophila melanogaster embryo lysates[300,301]. Their findings indicated that target mRNAs are at least partially degraded by a nuclease[300,301]. Genetic screens performed in *C. elegans* identified Argonaute (AGO) proteins as components of RNAi and possibly of RISC[302-304]. The first biochemical evidence identifying AGO as a central component of RISC came from the Hannon lab[147,299]. Purification of RISC from *Drosophila* extracts and mass spectrometry analysis revealed a yet unknown protein, CG7439, later named AGO2, whose activity matched perfectly the one of RISC[299]. Similarly, the Wang lab and soon after the Siomi lab, revealed that *Drosophila* AGO2 and siRNAs were core components of RISC[301,305]. Affinity purification of the human homologue of AGO2 allowed the detection of the slicing activity of AGO2 proteins[304]. Purification of additional members of the AGO family demonstrated that in humans only AGO2 is catalytically active, while the paralogues AGO1, AGO3 and AGO4 are not[146,147,271,273,274,306,307]. Conversely, a similar study performed in *Drosophila* showed that both dmAGO1 and dmAGO2 are catalytically active, although dmAGO1 has lower slicer activity[305]. *In vitro* reconstitution of a minimal RISC composed of recombinant human AGO2 and a single stranded siRNA was sufficient to catalyze specific cleavage of a target RNA. Importantly, AGO2 with three mutated amino acids (Asp, Asp, His; DDH triad) as well as a form of AGO2 supplemented with duplex, instead of single stranded, siRNAs could not direct target cleavage, pinpointing the region involved in cleavage and the requirement for single stranded RNAs[304].

When miRNAs associate with AGO, the complex is referred to as miRISC. Core components of miRISC in metazoans are not only AGO proteins, either catalytically active or inactive, but also members of the GW182/TNRC6 protein family. GW182 proteins are required for miRNA silencing and were described as direct interactors of AGO proteins[146,271,273,274,307,308]. In fact, artificial tethering of

either AGO or GW182 proteins to a reporter mRNA 3'-UTR repressed protein synthesis[309-311]. It was later discovered that the ability of GW182 proteins to silence is due to the recruitment of downstream effectors of silencing such as the CCR4-NOT deadenylase complex (reviewed in[90,261]). In the following subchapters I will describe in more details the components of animal miRISC.

1.4.1.1 AGO Protein Family

Argonaute (AGO) proteins were first discovered in the plant *Arabidopsis thaliana* and are given their name after the shape of the leaves of the mutant that allowed their discovery, which indeed resembled an argonaute octopus[308]. AGO proteins play a well-established role in RNAi by directly binding sRNAs, thus recruiting effector complexes to target RNAs and mediating their regulation[147,207,271,309,312,313]. However, they have also been implicated in processes such as transcriptional regulation and splicing (reviewed in[314]). They are conserved across species and kingdoms, from archaea to bacteria to higher eukaryotes. The AGO protein family is divided in three subfamilies or clades: PIWI proteins, which are germline-specific and associate with piRNAs; AGO proteins, which are ubiquitously expressed and associate with siRNA or miRNAs and the nematode-specific WAGO subfamily[146,147,315]. Multiple copies of genes encoding for AGOs exist across species. Humans, for instance, express eight AGO paralogs; *D. melanogaster* five and *C. elegans* twenty-six. Four human AGOs belong to the PIWI subfamily (HIWI1-3 and HILI) and four to the AGO subfamily, named respectively AGO1-4[147,316,317]. Mammalian AGO1-4 play partially redundant roles in siRNA and miRNA-mediated silencing; they all can silence when tethered to a reporter mRNA, they all can rescue an AGO knockout mouse embryonic stem cell line and they interact with similar subsets of proteins, small RNAs and mRNA targets[147,207,271,309,312,313,317]. Among the mammalian four AGOs, only AGO2 has cleavage activity[146,147,264,318-323]. Despite their functional redundancies pinpointed in cell culture systems, AGO2 mice knockout are embryonic lethal, and heterozigotes for AGO2 depletion exhibit severe defects in embryonic development possibly due to the peculiar slicing activity of this AGO member[147].

AGO proteins have a molecular mass of about 100 kDa. They are organized in four globular domains: an N-terminal domain, a Piwi-Argonaute-Zwille (PAZ) domain, a MID domain and a PIWI domain (**Figure 3**). PAZ, MID and PIWI are evolutionary conserved, while the N-terminal diverged the most. The crystal

structures of archaeal, eubacterial and eukaryotic AGO proteins revealed a bilobal architecture, with each lobe bearing two globular domains: N-terminal and PAZ, MID and PIWI. Although the relative position of the lobes differs between prokaryotes and eukaryotes, the architecture and domain organization is conserved[265,317,323,324]. The PAZ domain hosts a conserved hydrophobic pocket that binds the 3'-end of small RNAs, while a pocket at the interface between the MID and PIWI domains hosts the small RNA 5'-end[264,318-323,325,326]. MID domains of different species show different preferences for nucleotide binding, thereby determining the specificity for the 5'-nucleotide[327,328]. Human AGO2 has a preference for guide RNAs starting with U or A nucleotide[327]. In addition, the phosphate-ribose backbone of positions 2-8 of the small RNA are in contact with AGO, while the bases are oriented and available for target binding via hydrogen bonds[265,323,324,329]. This finding provided evidence for why perfect complementarity of the seed region is crucial in target recognition. The PIWI domain has an RNase H-like fold and hosts the catalytically active site coordinated by divalent cations[264,325,326]. RNase H recognizes and cleaves DNA-RNA duplexes[325]. This feature is retained in prokaryotic AGOs, which were found to be DNA-guided RNases[321,326]. However, eukaryotic AGOs evolved the ability to bind to, and in case of catalytically active AGOs cleave, RNA-RNA duplexes. The catalytic site is composed by a DDH triad (Asp-Asp-His) that was reported to be necessary, but not sufficient, for target cleavage[146,147,304]. In mammals, both AGO2 and AGO3 have the catalytic motif, but only AGO2 can slice perfectly matched targets between nucleotides 10 and 11 relative to the 5'-end of the guide RNA[147,322,325]. Later studies showed that two additional residues, E and F (Glu and Phe) [328,330] and an unstructured loop in the N-terminal domain[329] are important for slicing. Moreover the PIWI domain hosts two tryptophan (W)-binding pockets that mediate direct binding of AGOs to GW182 proteins[264,331], allowing further downstream processing. The residues forming W-binding pockets are conserved across AGO proteins participating in miRNA silencing, such as human AGO1-AGO4 and *Drosophila* Ago1[264]. Contrariwise, these residues are less conserved in *Drosophila* Ago2, which in fact does not interact with GW182 proteins, and in the PIWI clade of AGO proteins[311,332]. The structural study of human AGO2 revealed that the two W-binding pockets host tryptophan residues that are at least 8-10 amino acids apart (20-25 Å)[264]. Interestingly, multiple W-containing motifs present in GW182

proteins follow this spacing requirement, suggesting several tryptophans mediate high affinity binding with AGO via consecutive or cooperative binding[264]. In agreement with this observation, a peptide array of TNRC6B peptides showed that human AGO2 binds with high affinity peptides containing two W residues spaced by 10 amino acids[331]. Residues flanking W tend to have small side chains and contribute weakly to interactions with AGO. Intriguingly, only a subset of W residues, usually located in the N-terminal unstructured regions of TNRC6/GW182 proteins mediate interactions with AGO, while others located mainly in the unstructured C-terminus lack AGO-binding properties[331,333-340]. Generally, tryptophan-containing motifs are a conserved strategy used by AGO-interacting proteins to bind to the PIWI domain. Till and colleagues named protein regions containing such AGO-binding motifs "AGO-hooks"[333].

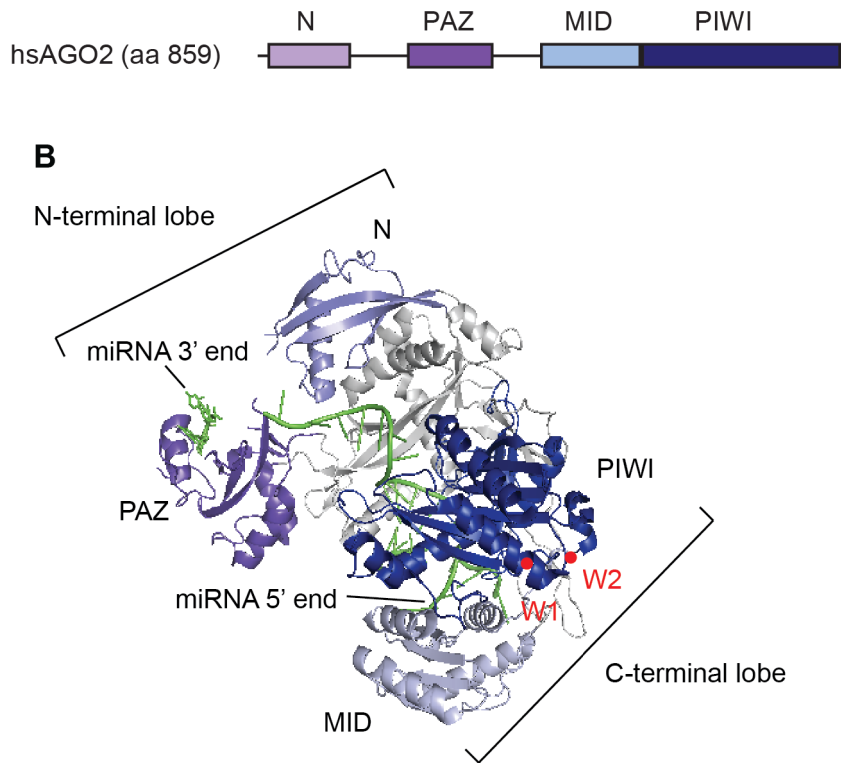

Figure 3. Argonaute (AGO) protein domains and structure (A) *Homo sapiens* AGO2 domain organization: N, N-terminal domain; PAZ, Piwi-Argonaute-Zwille; MID and PIWI domain. HsAGO2 is chosen as a representative example of the AGO family. **(B)** Structure of *Homo sapiens* AGO2 (blue and gray) in complex with a miRNA (green); PDB code: 4W5O[266]. Each domain is color-coded according to (A). Red dots indicate the position of the two W-binding pockets on the surface of the PIWI domain.

1.4.1.2 GW182 Protein Family

GW182 proteins were first described as a 182 kDa autoantigen found in the serum of patients suffering from an autoimmune motor and sensory neuropathy[341]. The protein was named GW because of the multiple Gly-Trp repeats within its amino acidic sequence[271-274,307,310,341,342]. Researchers found GW182 to be enriched in cytoplasmic speckles that they called GW-bodies (also known as processing bodies, P-bodies)[341,343]; sites enriched in proteins involved in mRNA degradation[344,345]. Shortly after, several studies from independent groups demonstrated that GW182 proteins are functional interactors of AGO proteins required for miRNA silencing[271-274,307,310,342]. GW182, AGO and miRNAs were shown to coimmunoprecipitate and colocalize in both mammalian cells[273,307] and *C. elegans*[274]. Moreover *in vitro* binding assays between the *C. elegans* homologs of AGO1 (ALG-1) and GW182 (AIN-1) suggested a direct interaction between these two proteins[274]. Multiple experiments indicated a key function of GW182 proteins in miRNA-mediated repression. In fact, disrupting GW182-AGO interactions or depleting GW182 proteins in mammalian and *D. melanogaster* S2 cells and in *C. elegans* severely impaired miRNA silencing[272-274,310] and lead to a decrease in the number of P-bodies[272,273]. Similarly, transfection of a dominant negative AGO or AGO mutants lacking the ability to load miRNAs also inhibited miRNA silencing and P-bodies formation indicating that AGO and GW182 act in the same pathways and that miRNA-mediated repression and P-body formation are linked[272,273,307]. Experiments in which GW182 proteins were tethered to an mRNA reporter lead to its repression also in absence of AGO proteins, providing evidence that GW182 are the effector proteins acting downstream of AGO[335-338].

The GW182 protein family is present in metazoans. To date, no orthologues have been found in plants or fungi[311,346]. Vertebrates express three paralogues named trinucleotide repeat-containing 6 proteins (TNRC6): TNRC6A, TNRC6B and TNRC6C. *D. melanogaster* encodes for only one member known as Gawky (GW182), and *C. elegans* and most of other nematodes express two divergent members named AIN-1 and AIN-2[346-348]. Except for AIN-1 and AIN-2, orthologues of GW182 share a similar domain organization. They feature an N-GW (N-terminal GW-rich AGO-binding domain), a UBA (ubiquitin-associated)-like domain, a Q (glutamine)-rich region, a PAM2 motif (poly(A)-binding protein interacting motif 2) and an RRM (RNA recognition motif)[349,350] (**Figure 4**). The N-GW domain is

responsible for AGO binding, while PAM2, RRM and the flanking disordered regions constitute the C-terminal effector domain, which is responsible for silencing of mRNA targets via CCR4-NOT binding[275-277,335-338,351]. Aside from recruiting the CCR4-NOT deadenylase complex, a study reported that GW182 proteins function as coactivators of the enzymatic activity of CNOT *in vitro*[277]. GW182 proteins are mainly disordered except for two globular domains: UBA and RRM. The UBA domain is formed by three α helices involved in binding ubiquitinated substrates[311,337,348]. The RRM domain folds into four antiparallel β-sheets and two α-helices and is usually involved in RNA binding[331,340,346,349]. However, the structure of *Drosophila* RRM revealed an additional helix that prevents RNA binding[351], hence GW182 proteins require interactions with AGO (or other RBPs) to be recruited to mRNA targets. The RRM domain is dispensable for localization to P-bodies and for interactions with AGOs[351]. Nevertheless, GW182 RRM partially contributes to miRNA-mediated repression probably by mediating protein-protein interactions[331,351]. The Q-rich region mediates P-bodies localization, but is dispensable for silencing and PAM2 mediates the interactions with PABP proteins, which bind to the mRNA poly(A) tail[311,333,334,337]. An additional study identified a type of proline-rich motif located in the C-terminal region of GW182 proteins and named it P-GL motif[352]. Though, P-GL motifs and UBA and RRM domains are highly conserved across GW182 orthologues, none of these regions is crucial for silencing. In fact mutations or depletion of these regions did not severely affect GW182-mediated repression in reporter assays[335-338,346,351,353,354]. The following paragraph will further describe the two functional N-terminal and C-terminal regions involved in AGO-binding and CNOT-binding, respectively.

As mentioned in the previous subchapter, AGO-GW182 interactions are mediated by short linear motifs containing GW (Gly-Trp) repeats located in the unstructured N-terminal region of GW182 proteins[276,277,331,333,340,346,355]. Pfaff et al.[331] identified the minimal requirements for AGO-binding. The authors of the study showed that a subset of W flanked by amino acids with small side chains engage in interactions with AGO. In the context of a peptide array, one W (W 623 of TNRC6B) is sufficient for AGO binding, however two W residues spaced by ten amino acids have higher affinity, suggesting they might bind sequentially to the two hydrophobic pockets within the PIWI domain of AGO proteins[331]. Additionally,

proteins other than GW182 use the same type of motifs to mediate AGO binding[290,333,334].

Intriguingly, W-motifs, short tryptophan-containing motifs found mostly within TNRC6 CED recruit the PAN2-PAN3 and CCR4-NOT deadenylase complexes, which then mediate translational repression and/or mRNA decay[275,277,290]. W-motifs act in an additive manner to silence mRNA targets[275]. Resolution of the structure of CNOT9 identified two Trp-binding pockets responsible for direct CNOT-GW182 binding[267,356]. However, additional W-motif binding pockets are thought to be present on other CNOT subunits although they have not been identified yet[267,268]. Interaction with PAN2-PAN3 is mediated by a single Trp, which fits into a hydrophobic pocket formed by a PAN3 dimer[290]. The identification of W-motifs clarified what is the mode of action of nematodes GW182 orthologs, AIN-1 and AIN-2, which lack the typical GW182 domain organization, but possess multiple W-motifs[357]. It also provided an explanation for why multiple Trp-containing N-terminal and C-terminal fragments of Gawky could silence when tethered to an RNA[336,355]. Similarly to AGO-interacting proteins, also other CCR4-NOT-interacting proteins evolved short linear motifs (SLIMs) containing aromatic residues that fit into CNOT hydrophobic pockets underlining the importance of SLIMs in mediating protein-protein interactions[358,359]. Despite the similarities between AGO-binding and CNOT-binding Trp-containing motifs they exhibit exquisite specificity for their binding partners. Which features allow the discrimination between binding partners is still unclear.

In addition, GW182 proteins interact with PABPC proteins via the PAM2 motif and partially via the disordered regions downstream of PAM2[286,360]. Both binding sites are required for binding in *Drosphila* GW182, while PAM2 alone is sufficient in mammalian TNRC6 proteins[286,287,360-362]. PABPC are highly conserved eukaryotic proteins known to stabilize mRNA and enhance translation by interacting with eIF4G at mRNA 5'-end and thereby forming so-called mRNA closed-loop structure[363-366]. Additionally GW182-PABPC interactions are conserved across species suggesting they are functionally important[357]. However, the role of GW182-PABPC interactions in miRNA silencing is not entirely clear. Some evidence showed that AGO binds more efficiently to polyadenylated mRNAs *in vitro*[367] and repression of polyadenylated mRNAs is stronger in human and *Drosophila* cells[368-370], suggesting PABPC promotes recruitment of RISC to

targets. Another possibility is that GW182 prevents PABPC from stimulating translation. In fact, it has been reported that once PABPC binds to GW182 it can no longer bind to EIF4G, a cap-binding protein; potentially disrupting a “closed-loop” structure that facilitates translation[361,362]. PABPC was shown to be required for miRNA-mediated repression in rabbit reticulocytes[371] and its depletion from mammalian cell free extracts[361] abolished miRNA-mediated deadenylation. In addition, mutations of PABPC binding regions in GW182 proteins partially impair repression in human cells and aggravate the inability of W-motifs mutants to rescue GW182-depleted cells[275,353,370]. However, these effects are mild and by contrast, tethering of PAM2 mutants efficiently silence target mRNAs suggesting PABPC may indeed facilitate miRISC recruitment to mRNA targets[275,352,353,360,370]. Moreover depletion of PABPC from *Drosophila* cell-free extracts[372] and in zebrafish embryos[352] does not abolish silencing, indicating PABPC role in silencing is not essential. Accordingly, miRNAs can silence mRNA reporters lacking poly(A) tails, hence PABPC, in human and *Drosphila* cells[275-277,352,368,370,372-374]. Thus, the emerging picture is that GW182-PABPC interactions may enhance miRNA-silencing, at least in some cellular contexts where poly(A) tail length is coupled with translational efficiency.

A

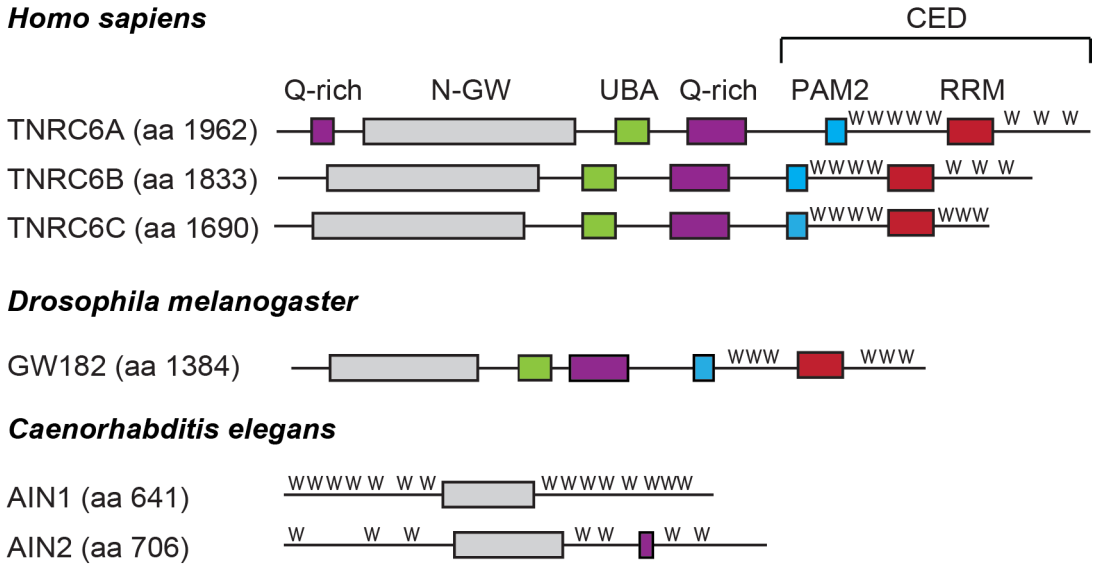

B

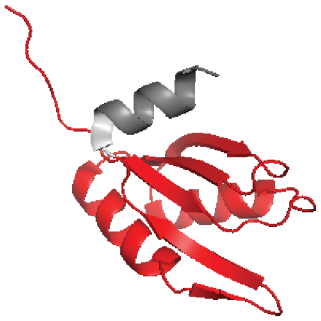

Figure 4. GW182 protein domains and RRM structure (A) Domain organization of GW182 protein family. N-GW: GW-repeat–rich region (grey); UBA: ubiquitin associated domain (green); PAM2: PABP associated motif 2 (light blue); RRM: RNA-recognition motif (red); W stands for W-motifs. The C-terminal effector domain (CED) is composed of RRM, PAM2 and the unstructured flanking regions with W-motifs. Human paralogues TNRC6A-C are shown together with the *D. melanogaster* homologue GW182 and the *C. elegans* functional analogues AIN1 and AIN2 **(B)** Structure of *D. melanogaster* GW182 RRM domain (red and grey); PDB code: 2WBR[351]. The C-terminal alpha helix shown in gray, and the absence of aromatic residues crucial for RNA binding, prevent binding of the RRM to RNA and is conserved throughout GW182 homologues[351].

1.4.1.3 PAN2-PAN3 & CCR4-NOT deadenylase complexes

Two deadenylase complexes, PAN2-PAN3 and CCR4-NOT, account for most of general and miRNA-mediated mRNA deadenylation (reviewed in[375]). The contribution of PAN2-PAN3 to overall deadenylation is unclear, but a bulk of evidence suggests it is minor compared to CCR4-NOT-induced deadenylation, which is indeed sufficient for mRNA deadenylation[267,268,275-277,311,353,370,375-378]. The current models of mRNA deadenylation and decay suggests that PAN2-PAN3 initiates shortening of poly(A) tails[377,379]. Once shortening has reached a certain threshold CCR4-NOT takes over and catalyzes the removal of poly(A) tails in a processive manner[376,380,381]. Deadenylated mRNAs can then be decapped and degraded by the 5'-3' exonuclease activity of XRN1[375,376,382,383].

The PAN2-PAN3 complex is formed by three subunits: the catalytic subunit PAN2 and a homodimer of PAN3 subunits[269,290]. PAN3 subunits homodimerize via a coiled-coil region connecting an N-terminal pseudo-kinase domain with a C-terminal globular domain[269]. The N-terminus of the dimer forms a W-binding pocket, which mediates binding to GW182 proteins[269]. Instead the C-terminal domain of the dimer binds to the catalytic PAN2 subunit[269,288,290]. The PAN2-PAN3 complex is recruited to mRNA targets via interactions with the PAN3 adaptor dimer. PAN3 interacts directly with PABPC proteins, via a PAM2 motif, and with RNA, via a zinc-finger domain[289,375,384]Additionally, interactions between PAN2-PAN3 and GW182 contribute to the recruitment of the deadenylase complex to miRNA targets. Depletion of PAN2-PAN3 or overexpression of a catalytically inactive form of PAN2 only partially alleviate silencing in human and *Drosophila* cells[276,377]. Yet, depletion of PAN2-PAN3 aggravates the alleviation of silencing observed upon CNOT1 depletion, supporting a role for PAN2-PAN3 in the degradation of miRNA reporters[276].

The CCR4-NOT deadenylase complex (mammalian carbon catabolite repression 4-negative on TATA-less) is a multi-subunits complex that weighs approximately 1 MDa (**Figure 5**). It is highly conserved in eukaryotes and regulates all layers of gene expression ranging from transcription to mRNA export, to mRNA deadenylation, translational repression and decay, to protein ubiquitination and degradation by the proteasome (reviewed in[382]). In mammals the complex has seven core subunits: CNOT1, which is the biggest subunit that acts as a central scaffold, CNOT2, CNOT3, CNOT6 or CNOT6L, CNOT7 or

CNOT8, CNOT9 and CNOT10 (reviewed in[382]). CNOT1 consists of a series of α-helixes related to HEAT repeat domain, two domains homologous to the middle domain of the eukaryotic initiation translation factor eIF4G, MIF4G-like (MIF4G-L) and MIF4G, a CNOT9/CAF40 binding domain (CN9BD) and a C-terminal NOT1 superfamily homology domain (reviewed in[90]). The HEAT domains interact with the CNOT10-CNOT11 module, while the MIF4G domain docks the formation of the catalytic module composed by the two catalytically active deadeanylases: CNOT7, or its paralogue CNOT8, (also known as CAF1 and POP2, respectively) and CNOT6, or its paralogue CNOT6L, (also known as CCR4a and CCR4b)[291,292,375]. Via a different surface of its MIF4G domain CNOT1 also recruits the RNA helicase DDX6, which functions in translational repression[267,268]. Thus, interactions with the catalytic module do not exclude interactions with DDX6[267,291]. DDX6 additionally interacts with decapping factors, such as EDC3 and EDC4[267,268,297,385]. The decapping proteins EDC4 in vertebrates and Dcp1 in *Drosophila* recruit the exonuclease XRN1 promoting further decay of mRNA targets[296,297]. Hence, the MIF4G domain allows coupling of deadenylation with decapping and 5'-3' decay and provides insights into how CCR4-NOT can mediate translational repression in absence of deadenylation. Next to the MIF4G domain, the CN9BD binds CNOT9 in a 1:1 stoichiometry[267,268]. Via CNOT1-CNOT9 the CCR4-NOT complex is recruited to GW182 proteins. Two W-motifs present in the C-terminus of GW182 proteins bind to two hydrophobic pockets on the CNOT9 subunit[267,268]. Similarly to the two W-binding pockets of AGO proteins[264], CNOT9 pockets can host two W spaced by 8-10 amino acids (20-25 Å apart)[267,268]. It is likely that CCR4-NOT bears additional W-binding pockets for GW182 proteins, although they have not been identified yet. This hypothesis is supported by the finding that a CNOT1 mutant unable to bind to CNOT9 still retains the ability to bind to GW182 proteins[267,268] and by the observation that sequential mutations of up to seven W-motifs within GW182 proteins cause a progressive alleviation of repression[275]. Lastly, the SHD domain located in the C-terminal region of CNOT1 binds the CNOT2-CNOT3 module[386,387], which provides an additional binding surface for RNA binding proteins, such as Nanos and *Drosophila* Bicaudal-C[358,388,389]. The central role of CCR4-NOT in mRNA deadenylation and decay is supported by the fact that upon depletion of CNOT subunits, deadenylation and decay of mRNA and miRNA targets is abrogated[311,375,376,390]. Accordingly,

overexpression of CNOT6 and CNOT7 catalytic mutants prevents miRNA-induced deadenylation and results in stabilization of miRNA targets[267,275,370,377,390-393]. Additionally, CCR4-NOT can repress translation independently of deadenylation and decay[267,275,370,391,393,394]. The same holds true also in the context of the miRNA pathway[275-277,353,370,378,395].

A

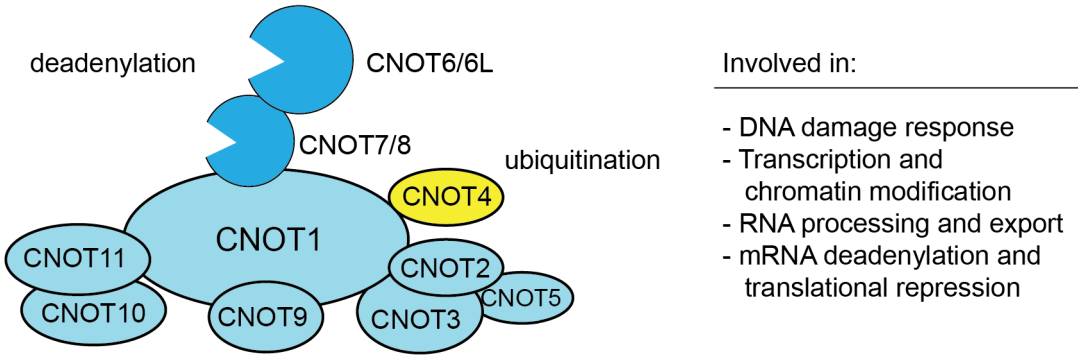

B

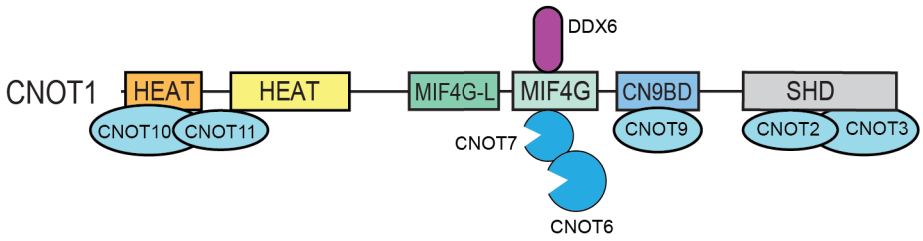

Figure 5. The CCR4-NOT deadenylase complex (A) Schematic representation of the mammalian CCR4-NOT complex and its main functions. The catalytic module comprehend CNOT6/CNOT6L and CNOT7/CNOT8 deadenylase subunits; CNOT4 is shown in yellow since it does not stably associate with CCR4-NOT in human and flies[396,397]. Scheme based on[382,398]. **(B)** Schematic illustration of CNOT1 domain organization including the binding sites for other CNOT modules and for the RNA helicase DDX6. HEAT, folded α-helical repeat domain; MIFG-L (MIF4G-like) and MIF4G, domains structurally related to the middle eIF4G domain; CN9BD, CNOT9/CAF40 binding domain; SHD, superfamily homology domain. Illustration based on[90].

1.4.2 Subcellular localization of miRISC

miRISC components play primarily cytoplasmic functions[399]. However, a growing body of evidence identified miRISC components also in the nucleus, suggesting possible uncharacterized nuclear roles[400-404]. In the next paragraphs I will describe the evidence supporting localization of miRISC to distinct cell compartments.

P/GW-bodies are dynamic cytoplasmic foci composed of aggregates of proteins and translationally repressed mRNAs[344]. They contain the key components of mRNA degradation, miRNA silencing, non-sense mediated decay (NMD) and translational repression[280,405-407]. As the name suggests, GW182 proteins are found in P/GW-bodies in addition to the CCR4-NOT complex, AGO proteins, miRNAs and their targets, decapping enzymes and the 5' to 3' exonuclease XRN1[339,406,408]. P/GW bodies are depleted from ribosomes and initiation factors except for the cap-binding protein eIF4E and its inhibitor eIF4ET[409,410]. A necessary requirement in P/GW-body assembly is the presence of a pool of repressed mRNAs[272,411,412] that can later be reactivated for translation[278-280]. Characterization of these mRNP granules raised the question on whether they are sites required for mRNA catabolism. Upon depletion of P/GW bodies *Drosophila* S2 cells still exhibit functional miRNA silencing, mRNA decay and NMD pathways[413]. On the other hand microscopically visible P/GW bodies are disrupted by the inhibition of siRNA or miRNA-mediated repression[307,413,414], suggesting P/G bodies are rather a consequence than a cause of small RNA silencing[413]. miRNA-loaded AGO proteins are also localized to another type of cytoplasmic mRNP granules named stress granules[342,415-417]. Stress granules are aggregates of stalled translation initiation complexes forming upon stress[418-420]. They are enriched in components of the translational machinery and can be clearly distinguished from GW/P-bodies[406,413]. Nevertheless, upon certain stresses they can dock or overlap with P/GW granules and share their components[421-423].

Membrane fractionation analysis identified active miRISC as an enriched component of endosomes and multi vesicular bodies (MVBs), late endosomes that can fuse with lysosomes or with the plasma membrane, thus connecting miRNA silencing and endosomal trafficking[424,425]. It has been proposed that MVBs promote GW182 turnover, and therefore modulate miRNA silencing[424,425]. These observations were in agreement with the initial identification of AGO2 as a membrane-bound protein[426].

In 2013 three studies reported that specific forms of active RISC localize to the rough endoplasmic reticulum (ER)[427-429]. In *Drosophila* S2 cells a form of miRISC lacking GW182 proteins, named polysomal miRISC (P-miRISC), co-sediments with the ER[427]. P-miRISC is composed of AGO1, miRNAs and Loqs-PB and is induced upon serum starvation. The authors of the study found that miRNA silencing under starvation increased 5- 10-fold compared to non-stress conditions and was independent of GW182 proteins[427]. In *Arabidopsis thaliana*, AMP1, an integral membrane protein of the rough ER, recruits miRNA loaded AGO1 and promotes translational repression of miRNA targets[428]. In humans, the homologue of Loqs-PB, TRBP, associates with the ER and recruits AGO in complex with sRNAs via protein-protein interactions[429]. Recently, a study performed in *Drosophila* cells reported that active miRISC containing GW182 copurifies with ribosome complexes in an RNA-dependent manner[430].

Additionally, AGO and TNRC6 proteins can shuttle between the cytoplasm and the nucleus. Increasing evidence points at a role for AGO proteins in nuclear RNAi[400,402,431,432], while the nuclear role of TNRC6 proteins is mostly unknown. The nuclear import of AGO proteins has been suggested to involve Importin 8[433]. Instead, nuclear import of TNRC6 proteins is mediated by the Importin β pathway[404]. The first line of evidence supporting the presence of TNRC6 proteins in the nucleus showed that TNRC6B actively shuttles to the nucleus[333]. Later studies showed that also TNRC6A is imported into the nucleus[403,404]. Nuclear levels of AGO and TNRC6 proteins have been suggested to be mutually dependent, indicating the existence of a mechanism that fine tunes the cytoplasmic and nuclear levels of both protein families[404].

1.4.3 miRNA-mediated translational repression

miRNA-mediated translational repression is one of the two modes of miRNA silencing. In the following chapters I will first give a brief overview of eukaryotic translation and then a summary of the current knowledge of the mechanism of miRNA-induced translational repression.

1.4.3.1 Basics of eukaryotic translation

Translation is a multi-steps process consisting of initiation, which is the rate limiting step, elongation, termination and ribosomes recycling[434] (**Figure 6**). In the initiation step the small ribosomal subunit 40S associates with a set of eukaryotic initiation factors, eIF1, eIF1A and eIF2-GTP-Met initiator tRNA ($tRNA_i$), eIF3 and eIF5 to form a 43S pre-initiation complex (PIC). The 43S PIC binds to the m^7G cap-structure at the 5'-end of mRNAs. This crucial interaction is mediated by eIF3, within the 43S PIC, and the cap-binding complex eIF4F. eIF4F is composed by three subunits: eIF4E, which is the protein directly binding to the mRNA 5'-cap; the DEAD box RNA helicase eIF4A; and eIF4G, a scaffold that binds to eIF4E, eIF4A and helps recruiting the 43S PIC[435]. Once the cap is recognized, 43S PIC scans the mRNA in a 5' to 3' direction until it finds a start codon. Both 43S recruitment and scanning are helped by the unwinding activity of the eIF4A helicase, which is essential to unfold secondary RNA structures[435]. Recognition of the start codon by the $tRNA_i$ anticodon arrests ribosomal scanning and induces a conformational change of 43S. This rearrangement leads to the release of eIF1, which consequently allows the irreversible hydrolysis of GTP from eIF2-GTP-Met-$tRNA_i$ stimulating the formation of the 48S initiation complex. 48S can then associate with the 60S ribosomal subunit forming an elongation competent 80S ribosome[436,437]. During elongation the ribosome moves towards the 3'-end of the bound mRNA helped by several eukaryotic elongation factors (eEF) while catalyzing the formation of a polypeptide chain[438]. The 80S ribosome hosts three pockets for tRNA-binding named exit site (E), peptidyl site (P) and aminoacyl site (A) oriented in a 5'-E-P-A-3' direction in respect to the mRNA[439]. The incoming aminoacyl-tRNA binds to the complementary mRNA codon in the A site. The P-site hosts the tRNA bound to the growing polypeptide chain and the E-site hosts a deacetylated tRNA. Once a peptide bond is formed between the amino acid carried by the tRNA in the A site and the polypeptide chain in the P-site, the

growing peptide is transferred to the A-site. Upon ribosome translocation the peptidyl tRNA is transferred to the P-site. The now unloaded tRNA that was in the P-site is relocated to the E-site, from which the previous deacetylated tRNA has been released. Lastly, a new amynoacil tRNA enters the A-site and the process is repeated until the ribosome encounters a stop codon. When a stop codon (UAA, UGA, or UAG) enters the A site termination occurs[439-441]. The proteins eRF1 and eRF3 ensure the fidelity of termination and the release of the polypeptide chain[442,443]. The deacetylated tRNA is then released; the ribosome dissociates in its 40S and 60S subunits and is recycled for another round of translation. In some cases the 40S subunits stays bound to the mRNA where it can resume scanning and reinitiate translation[444].

The 5'-m^{7}G cap and 3'-poly(A) are two mRNA features that enhance translation initiation efficiency[434]. This is explained by the fact that components of the eIF4F cap-binding complex help the recruitment of the ribosomal 40S subunits and that poly(A) tails are bound by PABP proteins, which directly interact with the cap binding complex eIF4F via eIF4G[363,365,445]. The interactions between a 3'-end binding protein and a 5'-end binding protein potentially result in the circularization of an mRNA, which is suggested to help translation by facilitating ribosome recycling[436]. Another explanation is that PABP tethers eIF4F to the mRNA bypassing the need for *de novo* recruitment of cap-binding proteins[436,446]. Irrespective of the mechanism, the interactions between 5'-end and 3'-end binding proteins are crucial for efficient translation. In fact histones mRNAs, which lack poly(A) tails, are efficiently translated thank to interactions between the protein module SLBP-SLIP1 (stem loop binding protein-SLBP interacting protein 1), which recognizes stem-loop structures near the 3'-end and the cap-binding complex eIF4F[447].

Translation initiation can also be cap-independent. A subset of mRNAs, especially viral mRNAs, uses internal ribosome entry sites (IRES) to directly recruit the ribosomes. Structurally related types of viral IRESs have different requirements for translation initiation. Picornaviruses IRES, such as poliovirus and encephalomyocarditis virus (PV, EMCV) do not require eIF4E binding, but need all the other canonical initiation factors[448-450]. HCV-like IRESs as hepatitis C virus (HCV) function independently of eIF1, eIF1A, eIF4A, eIF4B, eIF4F, but require eIF3[451,452]. Dicistrovirus intergenic regions IRESs, such as cricket paralysis virus

(CrPV), directly recruit the 40S subunit without the need of any canonical initiation factors and the initiator tRNA. The P site of the 40S subunit is instead occupied by an IRES domain mimicking codon-anticodon base pairing[453,454]. Cellular IRESs do not exhibit structural similarity and their mechanism of action is mostly unknown. However, they are thought to require all canonical factors except for eIF4E, similarly to picornaviruses IRESs[455,456]. In some cases, IRES-mediated initiation also requires IRES *trans*-activating factors (ITAFs); RNA binding proteins (RBPs) that might stabilize the optimal IRES 3D structure[456].

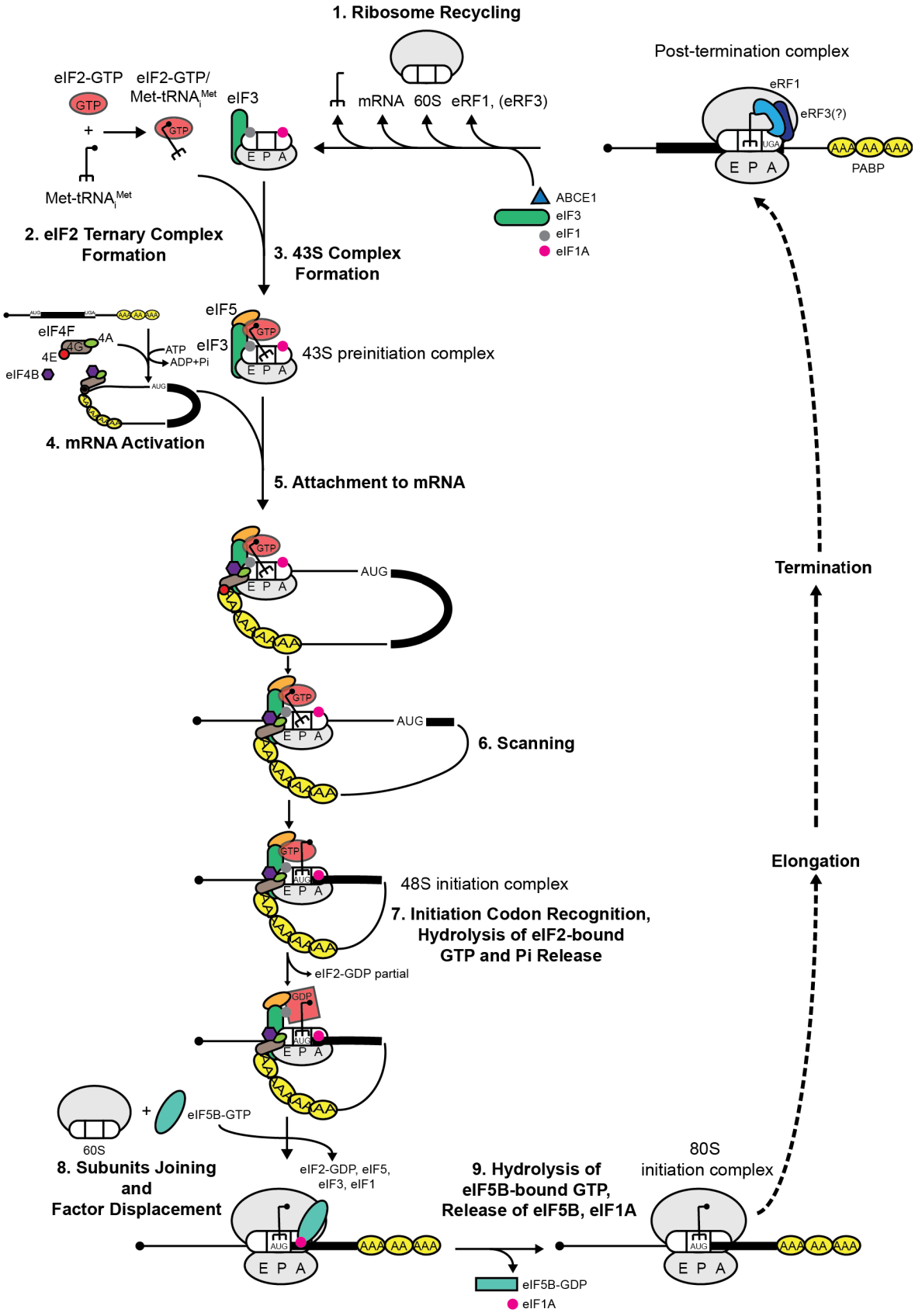

Figure 6. Eukaryotic translation Schematic illustration of the steps occurring during eukaryotic translation. Figure from Nature review by Jackson et al., 2010[436].

1.4.3.2 Translational repression by miRNAs: initiation vs. post-initiation mechanisms

The past years have seen contradictory observations supporting models postulating miRNA-mediated translational repression occurrence at the translation initiation step or at the post-initiation steps. In the following paragraph I will briefly summarize the historical controversy and the emerging consensus on the mechanism of miRNA-mediated translational repression.

Six-eight years after the first miRNA was described in *C. elegans*, two groups reported a model of miRNA-mediated translational repression by studying the miRNA lin-4 in *C. elegans*. Both groups observed that lin-4 inhibited proteins synthesis from its mRNA targets *lin-14* and *lin-28*, despite target mRNA levels did not vary considerably[457,458]. Since lin-4 targets were detected in a polysome-associated fraction, the authors suggested that inhibition of translation occurs post-initiation[457,458]. Accordingly, later studies performed in mammalian cell culture observed that miRNAs repress protein synthesis without affecting target mRNA expression levels nor their co-sedimentation with a translationally active polysomal fraction[180,459-461]. In addition, miRISC and miRNA targets were both found to be associated with polysomal fractions[459,460,462,463]. The authors interpreted this piece of evidence as an additional argument in support of inhibition at post-initiation steps[459]. A third line of evidence in support of this model comes from the study on the expression of internal ribosome entry site (IRES)-driven mRNAs. Two reports showed that miRNAs repress HCV and CrPV IRES-driven translation of mRNAs[171,461]. Given that HCV IRES function independently of several translation initiation factor (eIF) factors, but eIF3, and CrPV IRES do not require any conventional eIFs, Petersen and colleagues[461] concluded that miRNA repress translation of these targets independently of the cap structure, thus at post-initiation steps. One issue of the study by Petersen and colleagues was that the authors did not test repression of the IRES-driven mRNAs at the mRNA level. Hence, they could not exclude whether miRNAs induced degradation of their targets. The authors proposed that miRNAs cause ribosome drop off, as miRNA targets dissociated from polysomes more rapidly than a control insensitive to miRNAs when translation was inhibited using the eIF4A inhibitor hippuristanol[461]. Alternatively, Nottrott et al. (2006)[460] proposed a model in which miRNAs induce co-translational protein degradation. Yet, an independent study by Pillai and

colleagues[412] showed that targeting of nascent polypetides to the ER, as a strategy to protect them from proteolysis, does not prevent miRNA-mediating repression arguing against the model proposed by Nottrot et al. (2006).

In parallel, several other studies provided contrasting evidence. Two groups reported [412,464] that endogenous let-7 miRNA as well as synthetic miRNAs cause their targets to shift to lighter polysome fractions in HeLa cells[412,464]. Subsequent studies showed that miR-122 causes its endogenous CAT-1 mRNA target to associate with lighter polysomal fraction in Huh7 cells[279]. Similar shifts were observed for miR-16 reporters in HEK 293T cells and for endogenous targets of let-7 in HeLa cells[465,466]. Another study performed in *C. elegans* also demonstrated that miRNAs cause a decrease in the number of ribosomes associated with their targets[467]. Genome-wide studies looking at transcriptome and translatome changes upon miRNAs induction noticed that miRNA targets associate with fewer ribosomes[183,184,262,284]. Additionally, the distribution of ribosomes along the length of translationally repressed miRNA targets remained uniform; arguing against ribosome drop-off or inhibition at elongation step, which would imply higher ribosomal density at the 5'-end of the transcript compared to the 3'-end[183,284]. A second line of conflicting evidence came from experiments on cap-independent reporters. Translation of miRNA reporters driven by EMCV[412,468], HCV[412], CrPV IRESs[464] or by an ApppG-cap structure[464] was refractory to miRNA-mediated repression in cell cultures. Similarly tethering of translation initiation factors, such as eIF4E or eIF4G, upstream of miRNA reporters coding sequence would prevent miRNA silencing[412]. This bulk of evidence suggested that miRNA-mediated repression targets translation initiation. Accordingly, *in vitro* studies supported a model of miRNA-mediated inhibition of translation initiation. miRNAs were shown to interfere with the formation of the 48S and 80S ribosomal complexes in embryonic *D. melanogaster* extracts[469] and in mouse Krebs-2 ascites lysate[470]. Additionally, several studies demonstrated that miRNAs cannot silence IRES-driven mRNAs as well as mRNAs with artificial Appp-cap structures in cell-free extracts, suggesting a critical role of the m^7G cap in miRNA silencing[371,469-473]. miRNA-mediated translational repression of miRNA reporters in ascites extracts was gradually released in presence of increasing amounts of eIF4F, pointing at displacement of cap binding proteins as a potential repressive mechanism[470]. Furthermore, use of specific cap analogues was shown to augment miRNA-

mediated repression of target mRNAs without affecting the expression of non-targets[474].

The emerging consensus in the miRNA field is that miRNAs can inhibit translation initiation by targeting the cap binding complex eIF4F[90]. To date, the best-characterized model of miRNA-mediated translational repression involves the recruitment of AGO and GW182 proteins, the CCR4-NOT deadenylase complex and RNA helicases, such as the decapping activator DDX6 and the initiation factor paralogues eIF4A1 and eIF4A2[90]. Several groups have shown that the CCR4-NOT complex can silence independently of its deadenylase activity and of mRNA poly(A) tails, indicating that it mediates translational repression[267,268,275,276,353,370,391,393]. Consistently, tethering of CNOT subunits induces translational repression of poly(A)- minus reporters without causing their decay[275,276,391,393]. CNOT1, the scaffold subunit of the CCR4-NOT complex, recruits the DEAD-box RNA helicase DDX6 via its MIF4G domain, which has been shown to contribute to translational repression[267,268,293]. The binding CNOT1-DDX6 induces a conformational change of DDX6 that promotes its ATPase activity, which is required for miRNA-mediated translational repression[267]. DDX6 also binds to decapping factors, such as EDC3, EDC4, LSm14, PatL1, and to eIF4E transporter (4E-T), an eIF4E binding protein that represses translation by targeting the cap-binding protein complex eIF4F via a yet unclear mechanism[475-477]. Although it is by now clear that human DDX6 and its *D. melanogaster* ortholog Me31B repress translation, activate decapping, and play a role in miRNA silencing; a detailed mechanism of repression is still not defined[267,268,293,478-480]. Another documented strategy to induce miRNA-mediated translational repression involves the RNA helicase eIF4A, which is crucial in unwinding highly structured 5'-UTR, thus promoting scanning of the 43S complex. However, conflicting evidence prevented a clear understanding of how eIF4A contributes to this process. One group reported that miRNAs repress translation initiation by preventing ribosomal scanning and that miRNA reporters with unstructured 5'-UTR are refractory to miRNA inhibition[371]. Another study by Meijer and colleagues[481] reported that eIF4A2, but not eIF4A1, is recruited to miRISC by interactions with the MIF4G domain of CCR4-NOT and blocks scanning of the 43S complex. Questions have been raised about these findings when structural studies demonstrated that CNOT1 MIFG domain binds DDX6, but not eIF4A2[267,268,293].

Secondly, eIF4A2 knock out in human cells revealed that eIF4A2 is not required for miRNA-mediated repression[482]. Moreover, studies performed in human and *Drosophila* cell-free extracts showed that eIF4A1 and eIF4A2 are both released from miRNA targets, instead of being recruited, thereby repressing translation[483,484]. Consistently, tethering of GW182 in *Drosophila* lead to displacement of eIF4A and depletion of eIF4A from S2 cells impaired miRNA-mediated translational repression[483]. The role of CCR4-NOT in this process is still unclear[483,484]. Interestingly, at least in *Drosophila*, dissociation of eIF4A can also occur independently of GW182, supporting the existence of a GW182-independent mechanism of miRNA silencing in insect cells[372,427,483,485]. Arguing against inhibition of scanning as a mode of miRNA-mediated translational repression is a recent study by the Izaurralde group[486]. Using luciferase reporters with short 5'-UTRs (<10 nt) and the TISU 5'-UTR (translation initiator of short 5'-UTRs), whose translation is cap-dependent but scanning-independent[487], the authors could show that miRNAs repress these targets independently of scanning in human and *Drosophila* cells[486]. In addition, modifying the 5'-UTR secondary structure did not affect the degree of translational repression indicating eIF4A helicase activity is not required for miRNA-mediated translational repression[486]. As a strategy to uncouple miRNA-mediated translational repression from deadenylatyon and decay researchers have long taken advantage of miRNA reporters without poly(A) tails[275,276,352,370-374,412,464,470,473,485]. Using poly(A)- miRNA reporters Kuzuoğlu-Öztürk and colleagues confirmed that interactions between AGO(dmAGO1)/GW182/CCR4-NOT/DDX6 are necessary for miRNA-mediated translational repression in both human and *Drosophila* cells[486]. Despite dmAGO1 was reported to also induce miRNA-mediated translational repression independently of GW182[485], disrupting W-binding pockets responsible for GW182 binding abolished repression[486]. The authors suggested that another AGO-binding proteins might be recruited via the same pockets and mediate repression in flies[486]. Lastly, miRNA-mediated translational repression via DDX6 was also reported to occur independently of CCR4-NOT in mouse embryonic stem cells[488]. In this case DDX6 recruitment depends on the module GW182-EED (mammalian hyperplastic disc EED protein)[488].

Irrespective of the inconsistencies, multiple studies support a role for miRNAs in inhibiting translational repression at the initiation step by modulating

directly or indirectly one of the three components of the eIF4F cap-binding complex: eIF4E, eIF4G or eIF4A. Nevertheless, the detailed dynamics of this process and whether one or more mechanisms are at play in a context or species-specific manner remains to be established.

1.4.4 miRNA-mediated deadenylation and decay

miRNAs accelerate mRNA degradation[90]. The first biochemical studies reporting this finding in animals observed a negative correlation between miRNA expression levels and the mRNA levels of specific miRNA targets[489-492]. Genome-wide studies could provide evidence for miRNA-induced mRNA decay as a widespread mechanism of miRNA-mediated repression. In fact, expression of definite miRNAs in multiple cell lines and primary cells was shown to cause downregulation of hundreds of target transcripts[162,176,183,184,262,489]. Accordingly, depletion of specific miRNAs caused an opposite effects: upregulation of hundreds of miRNA targets[162,176,490]. This mode of miRNA silencing was also supported by the observation that miRNA target expression levels increase upon depletion of essential components of the miRNA pathway, such as AGO, GW182 and Dicer[220,310,311,378,479,493,494].

miRNAs promote degradation of their targets via the canonical mRNA decay pathway[220,310,311,373,378,390,479]. The canonical mechanism of mRNA degradation involves mRNA deadenylation followed by decapping and 5' to 3' degradation by the exonuclease XRN1 or 3' to 5' degradation by the exosome and subsequent removal of the cap by the scavenger enzyme DcpS[495,496].

In the context of the miRNA pathway, GW182 proteins have been shown to directly recruit the deadenylase complexes PAN2-PAN3 and CCR4-NOT to miRNA targets, allowing their priming for degradation[275-277,310,311,377,390]. The two deadenylase complexes, PAN2-PAN3 and CCR4-NOT, act consecutively to deadenylate target mRNAs[298,375]. Depletion of PAN2-PAN3 or overexpression of a catalytic mutant of PAN2 had mild effects on miRNA-mediated deadenylation[276,377,390]. Conversely, depletion of CCR4-NOT as well as overexpression of dominant negative forms of its catalytic subunits (CNOT6 and CNOT7) severely impaired miRNA-mediated deadenylation and decay, indicating CCR4-NOT is the major deadenylase of miRNA silencing[311,336,377,378,390,392,485]. Similarly, point mutations of W-motifs within GW182 proteins prevented CCR4-

NOT binding, causing abrogation of mRNA repression in tethering assay and rescue assays[275]. Interestingly, GW182 was shown to not only recruit CCR4-NOT to miRNA targets, but also to act as a co-activator of its deadenylase activity in Krebs extracts[277]. Aside from the catalytic CNOT module, the main subunit CNOT1 can directly recruit the RNA helicase DDX6 via its MIF4G domain[267,356]. A structural study solved the details of the interactions between the RecA-like domain of DDX6 and an FDF-motif in the enhancer of decapping EDC3[270]. EDC3 is one of the several cofactors of the decapping enzyme DCP2 and the decapping activator DCP1[270,310,311,476,479]. DDX6 also binds additional decapping and decay factors containing and FDF-motif, such as PatL1, LSm14, and 4E-T. Thus, sequential interactions between CCR4-NOT/DDX6/EDC3 link the deadenylation step to decapping. After cap removal the major cytoplasmatic 5' to 3' exoribonuclease XRN1 is free to access the 5' monophosphate end of mRNA targets and degrade them[310,311,378,479,491,497]. The decapping cofactors EDC4 in human cells and Dcp1 in *Drosophila* cells recruit XRN1, connecting decapping to 5' to 3' mRNA decay[296]. Depletion of cofactors involved in cap removal was shown to cause an increase in the abundance of miRNA targets, accumulating in their deadenylated forms[479].

Hence, the CCR4-NOT complex can couple deadenylation to decapping to 5'-3' exonuclelytic degradation by XRN1, leading to mRNA degradation (reviewed in[383]). Apart from members of the GW182 family several additional proteins, such as Nanos, *Drosohila* CUP, Bicaudal, Smaug, PUM and vertebrates Roquin and TTP proteins, can recruit the CCR4-NOT complex to target RNAs, thereby enhancing deadenylation and decay of their bound mRNAs[358,359,388,498-503].

1.4.5 Kinetics of miRNA silencing

In 2012 three individual studies sought out to investigate the order of events leading to the establishment of miRNA-mediated repression[284,392,504]. Two studies addressed the dynamics of miRNA silencing using inducible miRNA reporters in human[392] and *Drosophila* S2 cell lines[504]. A third study looked at the expression of the endogenous targets of miR-430 in zebrafish embryos, taking advantage of the known expression pattern of miR-430, which is induced ~2.5 hours post fertilization (hpf)[284]. Controlling the timing of miRNA reporters/miR-430 expression enabled the authors to follow the effects of miRNAs on the expression of their

targets at specific time points. Béthune et al.[392] generated HeLa cell lines expressing inducible luciferase reporters either sensitive to the endogenous miRNA let-7 (wt) or insensitive (mutated let-7 binding sites) as a negative control. By comparing the expression of the wt and mut reporters upon induction, the authors observed that up to 2 h post-induction wt reporter mRNA levels were unaltered, but protein synthesis was already repressed. Between 3 and 48 h protein inhibition was accompanied by a decrease in target mRNA levels, demonstrating that miRNA-mediated translational repression precedes mRNA decay and mRNA decay is the predominant mechanism of miRNA silencing at steady state. Similar results were obtained with reporters sensitive to miR-21 bearing fewer miRNA binding sites. Overall, the results indicated that translational repression prevails on newly synthesized miRNA targets, irrespective of the miRNA and of the number of miRNA binding sites; while mRNA decay dominates at steady state. By measuring poly(A)-tail length of wt and mut reporters at different time points post-induction the authors observed that miRNA-dependent deadenylation can be observed after translational repression and before mRNA decay. Moreover upon knockdown of the CCR4-NOT deadenylase complex or overexpression of dominant negative mutants of its catalytic subunits, miRNA targets would undergo translational repression, but not deadenylation or decay. This study provided evidence that miRNA silencing is a three steps process. First, miRNAs inhibit translation in absence of mRNA decay and independently of deadenylation. Translational repression is then followed by mRNA deadenylation either as a consequence of translation inhibition or because it occurs at a slower rate. Third, deadenylation leads to mRNA decay. Analogously, Djuranovic et al.[504] demonstrated a similar mechanism of miRNA silencing in *Drosophila* S2 cells. Using natural and artificial inducible miRNA reporter, sensitive to either endogenous or ectopically expressed miRNAs, they could demonstrate the same sequence of events. miRNA-mediated translational repression occurs at early stages (first 6 h after induction) independently of deadenylation, mRNA deadenylation follows (10 h) and later on (24 h) mRNA is degraded.

Using mRNA-Seq and ribosome profiling in wt and in Dicer knock out (thus, with impaired small RNAs processing) zebrafish embryos, Bazzini and colleagues[284] showed that the protein outcome of miR-430 targets decreased at 4 hours post fertilization (hpf), while their mRNA levels were stable. At 6 hpf both

mRNA and protein levels decreased. Comparably to Bethune and Djuranovic studies, the authors could demonstrate that (I) translational repression precedes decay; (II) for a specific target of miR-430 deadenylation could be detected only after translational repression; and (III) a miR-430 reporter with an internal poly(A) tail could be repressed, irrespective of deadenylation. A later report by Subtelny et al.[263] confirmed that miRNAs, other than miR-430, first induce translational repression and then degradation in zebrafish embryos. However, using poly(A)-tail length profiling in combination with RNA-Seq and ribosome profiling the authors showed that several miRNA targets were both translationally repressed and deadenylated, providing an *in vivo* example where deadenylation is uncoupled from degradation.

In 2014 a study tested if the dynamics of miRNA silencing observed using miRNA reporter genes could be recapitulated by endogenous miRNA targets in several mammalian cell types[184]. Using inducible miRNA systems, the authors concluded that (I) the time lag between translational repression and mRNA decay is shorter than the one observed for reporter genes; (II) translational repression of endogenous miRNA targets is weaker than the one of reporters and hardly detectable for lowly expressed miRNAs.

Collectively these data provide evidence that miRNA silencing involves translational repression, deadenylation and decay. Undoubtedly, miRNA-mediated translational repression precedes miRNA-mediated decay and is independent of deadenylation. Interestingly, translational repression, deadenylation and decay can be uncoupled artificially using reporters lacking poly(A) tails or catalytically inactive CCR4-NOT subunits; or *in vivo* as it seems to occur in zebrafish embryos at pre-gastrulation stages. It is well established that mRNA deadenylation is a prerequisite for miRNA-mediated mRNA decay[311,377,392], yet it is still unclear whether translational repression is required for degradation to occur[90].

1.4.6 Modulation of miRNA silencing

To ensure proper regulation of gene expression in response to different cellular stimuli, miRNA silencing is regulated at multiple levels: miRNA transcription, nuclear export, miRNA processing and turnover, subcellular localization, post-translational modifications (PTMs) of miRISC components and by accessory proteins[91,505].

1.4.6.1 Modulation by post translational modifications of miRISC

Several PTMs have been reported for AGO proteins. The first AGO2 modification to be described was phosphorylation of the S387 residues, reported to facilitate AGO2 localization to P-bodies[506] and to enhance miRNA-mediated repression[507]. Mass spectrometry analysis identified several phosphorylation sites in AGO2[508]. Among them, phosphorylation of the conserved residue Y529, positioned in the 5' sRNA-binding pocket of AGO2, has been shown to decrease the efficiency of sRNA loading[508]. Under hypoxic conditions, EGFR signaling induces elevated phosphorylation of AGO2 Y393, which inhibits miRNA maturation from pre-miRNAs by altering interactions with Dicer[509]. As hypoxia characterizes the environment of several solid tumors, this modification was shown to correlate with poor survival of breast cancer patients[509]. AGO2 hydroxylation at P700 under hypoxic conditions was reported to enhance AGO2 stability or localization to P-bodies and miRNA silencing[510,511]. In contrast, AGO2 sumoylation at K402 was related to a decrease in AGO2 stability[512] and ADP-ribosylation of AGO2 has been shown to alleviate miRNA-mediated repression[513]. Additionally, it was reported that upon T-cell activation AGO proteins are ubiquitinated and marked for proteasomal degradation and that miRNA levels decrease[514]. Notably, unloaded AGO proteins are less stable than their corresponding guide RNA-loaded form[515,516].

Despite GW182/TNRC6 proteins were first identified as phosphoantigens localizing to cytoplasmic foci[341], little is known about the function of such PTMs. The intrinsically disordered regions of GW182/TNRC6 proteins containing W-motifs are enriched in serine and threonine residues, which are the main targets of phosphorylation[517]. Huang et al.[518] reported that upon phosphatase treatment interactions between TNRC6C and PABPC were reduced, suggesting a potential mechanism for PABP displacement.

Little is known about how PTMs in the CCR4-NOT complex and PABPC proteins modulate miRNA silencing. The yeast homologue of CCR4-NOT can be phosphorylated in the CNOT1, CNOT4 and CNOT7 subunits[519]. CNOT4 phosphorylation is required for the yeast stress response, however the functions of the other phosphorylations are not clear[519]. PABPC proteins are target of extensive PTMs, such as acetylation and di-methylation of lysine residues, mono-methylation and phosphorylation[520]. The phosphorylation state of PABPC has been reported to modulate interactions with poly(A) tails and translation initiation factors[521].

1.4.6.2 Modulation of miRNA processing

As explained previously miRNA processing is a two steps process that leads to the production of mature miRNAs. The first step of miRNA maturation involves the microprocessor, whose minimal components are the RNA helicase III Drosha and the dsRNA binding protein DGCR8[116,522-525]. The second step involves the RNase III enzyme Dicer[124-128]. Modulations of the levels and activity of these proteins affects miRNA processing. Drosha and DGCR8 can regulate each other with a mode that is conserved across the animal kingdom[526]. DGCR8 stabilizes Drosha by binding to it[526,527], while Drosha cleaves a hairpin-containing exon in *DGCR8* mRNA, thereby destabilizing it[120,526,528]. PTMs modulate the activity of Drosha and DGCR8. For instance phosphorylation of Drosha by glycogen synthase kinase 3β (GSK3β) is necessary for its nuclear localization[529,530]. Acetylation of Drosha was shown to prevent its degradation by the proteasome[531]. Deacetylation of DGCR8 by histone deacetylase 1 (HDAC1) was reported to increase the affinity for pri-miRNAs binding[532]. Phosphorylation of DGCR8 by the kinase ERK increased its stability[533]. Additionally, DGCR8 can be sequestered from the microprocessor by a phosphorylated form of methyl-CpG-binding protein 2 (MeCp2)[534]. DGCR8 is released upon dephosphorylation of MeCp2 induced by neuronal activation[534]. Among the accessory proteins that work together with the microprocessor, p68 (DDX5) and p72 (DDX17) are two RNA helicases that have been shown to be necessary for the maturation of a subset of pri-miRNAs[196]. TGF-β and BMP signaling pathway were reported to promote the maturation of pri-miR21 and pri-miR199a[535]. Upon TGF-β and BMP signaling, SMAD proteins translocate in the nucleus where they can directly interact with p68[536], which promotes the activity of the microprocessor and increase levels of pre-miRNAs, while leaving unchanged

the corresponding pri-miRNA levels[535]. The tumor suppressor p53 is another cofactor shown to promote maturation of pri-miRNAs via interactions with the helicase p68[537,538]. Conversely the estrogen pathway leads to inhibition of the microprocessor[539,540]. Binding of estradiol (E2) to the estrogen receptor α (ERα) leads to displacement of Drosha-p68/p72 from the ERα targeted pri-miRNAs[539].

Another way of regulating miRNA biogenesis is mediated by RBPs, which recognize and bind to specific sequences of the pri-, pre-miRNAs and sequester them from the processing pathway or promote their maturation. For example the RBPs LIN-28 and the KH-type splicing regulatory factor (KSRP) bind in a mutually exclusive way to two sequences of the let-7 precursor loop to either prevent or promote[541] its maturation, respectively[542]. LIN-28 can block maturation via the microprocessor and via Dicer thank to the recruitment of the terminal poly(U) polymerases TUT4 and TUT7, which urydilate pre-let-7 and trigger its degradation[543-545]. Similarly to KSRP, the heterogeneous nuclear ribonucleoprotein 1A (hnRNP1A) enhances processing via the microprocessor by binding to the loop of pri-mir-18a and relaxing the stem region[546,547]. The RBP TDP43 was also reported to bind to Drosha and increase microprocessor activity[548,549].

Dicer activity is regulated by accessory proteins. In *Drosophila melanogaster* Loquacious proteins (Loqs-PA and Loqs-PB) were shown to be necessary for the maturation of most miRNAs by binding to Dcr-1, whereas Loqs-PB is specifically required for a subset of miRNA isoforms[550-552]. The mammalian Loqs homologue, TRBP, and the cofactor PACT, also associate with Dicer and were reported to increase the efficiency of Dicer processing of certain pre-miRNAs[550,553-557]. However, none of the two proteins seem to be necessary for Dicer function, which can in fact work alone[555]. Moreover phosphorylation of TRBP was reported to increase processing of miRNAs promoting growth and to downregulate processing of the let-7 family[558].

Additionally, miRNA sequence and structure can modulate processing. A C to T single nucleotide polymorphism (SNP) in *pri-miR-15a~16-1* decreases processing by Drosha and consequently reduces the levels of mature miR-16[559]. Target specificity can also be affected by SNPs in miRNA genes and some SNP variants are associated with different types of cancer[560-564]. RNA editing, such as conversion of adenosine to inosine catalyzed by adenosine deaminases (ADARs) was shown to diminish the efficiency of Drosha and Dicer processing of pri-

miR142[565] and pri- and pre-miR-151[566]. O-methylation of the 5'-phosphate of pre-miR-145 and pre-miR-23b by the RNA methyltransferase BCDIN3D was shown to alter Dicer binding, thereby decreasing pre-miRNA processing and consequently mature miR levels[567].

1.4.6.3 Modulation of miRNA stability

The abundance of miRNAs, thus their effect on gene expression, is also regulated by miRNA turnover[568]. In certain cellular contexts miRNAs have long half-lives up to several days[258,569-571], by contrast miRNA half-lives are considerably shortened in neuronal cells[572-574]. One strategy to destabilize miRNAs in mammalian cells is their degradation by highly complementary mRNA targets, named target RNA-directed miRNA degradation (TDMD)[571,575-579]. TDMD induces miRNA tailing, which is the template-independent addition of nucleotides at the 3'-end of miRNAs, and their 3'-5' trimming and decay[571,578,580]. Although association of miRNAs and AGO proteins stabilizes miRNAs by protecting their 5' and 3' termini[264,265], miRNA tailing occurs when miRNA are still associated with AGOs[578]. AGOs additionally interact with the exonuclease DIS3L2 responsible for miRNA decay[579]. This mechanism competes with miRNA-mediated decay of miRNA targets and is particularly prominent in neurons[578]. It was initially reported as a strategy employed by a number of viruses to downregulate host miRNAs disadvantageous to viral replication[154,580-582].

Notably, RNA tailing can trigger either stabilization or destabilization of pre- and mature miRNAs[232]. For instance, polyurydilation of pre-let-7 by the terminal urydil transferases TUT4 and TUT7 prevents processing by Dicer and enhances decay[583] via the 3'-5' exonuclease DIS3L2[584,585]. Conversely, monourydilation of group II pre-let7 by TUT7, TUT4 and TUT2 promotes let-7 maturation[158]. Adenylation of miRNAs induced by the pox viral protein VP55 causes degradation of tailed miRNAs[586]. By contrast adenylation of the hepatic miRNA-122 has been reported to stabilize this miRNA[587].

Members of the miR-16 family, which target genes involved in the cell cycle G1-S transition, have been reported to rapidly increase during G0 arrest and to rapidly decrease upon cell cycle re-entry with a yet unknown mechanism[588].

Several nucleases have been associated with miRNA degradation. The endoribonuclease MCP-induced protein 1 (MCPIP1/ZC3H12A) has been reported to cleave pre-miR146a and 135b[589]. Endoplasmic reticulum stress induces

cleavage of a subset of pre-miRNAs (pre-miR17, 34a, 96 and 125b) by the kinase/endoribonuclease IRE1α leading to derepression of pro-apoptotic caspase 2[590]. Similarly an interferon-mediated response induces the polynucleotide phosphorylase PNPase old-35 (PNPT1) 3'-5' exonuclease to degrade a subset of miRNAs in melanoma cells[591]. Loss of 3'-5' exonuclease ERI1 was shown to correlate with increased expression of certain miRNAs[592]. miR-382 was shown to be degraded by the 3'-5' exonucleolytic activity of the exosome with the minor help of XRN1[593]. Other nucleases have been implicated in miRNA decay in other species. In *C. elegans*, the 5'-3' exonuclease XRN1 and XRN2 have been reported to degrade mature miRNAs when miRISC is not associated with its targets[594,595]. In *A. thaliana*, small degrading nucleases (SDNs) have been implicated for the first time in active miRNA degradation[596].

Lastly, miRNAs can be sequestered from their targets by competing endogenous RNA molecules (ceRNAs) that have complementary binding sites. For example, long non-coding RNAs (lncRNAs), such as HULC lncRNA upregulated in liver cancer cells can titrate miR-372 away from its targets[597]. Similarly, lncRNA MD1 competes for binding of miR-133 and contributes to muscle differentiation[598]. Likewise, a brain specific circular RNA (circRNA) has been reported to act as a sponge for miR-7[599,600]. However, the idea of ceRNAs has been recently challenged by a study showing that the physiological concentration of a ceRNA required to sequester miRNAs in wild type conditions is unrealistic[601].

1.4.6.4 Modulation by accessory proteins

miRNA silencing is also modulated by accessory proteins, which either antagonize or promote miRNA-mediated repression.

The RNA binding protein (RBP) HuR, a member of the embryonic lethal abnormal vision (ELAV) protein family, was reported to alleviate miR-122 mediated repression of *CAT-1* mRNA in the Huh7 hepatoma cell line[279]. Upon stress, HuR translocates from the nucleus to the cytoplasm where it is free to bind AU-rich sequences in the 3'-UTR of *CAT-1* mRNA. The binding induces miRISC dissociation[285], release of the *CAT-1* mRNA from P-bodies and association of *CAT-1* mRNA with polysomes[279]. Similarly, the germline specific RBP Dead end 1 (DND1) was reported to alleviate miR-430 mediated repression of *NANOS1* and *TDRD7* mRNAs in primordial zebrafish germ cells by binding to sequences overlapping with miR-430 binding sites[602,603]. Overexpression of DND1 in human

HEK293 cells also antagonizes *p27* and *LATS2* mRNA repression by miR-221 and miR-327, respectively[603]. The apolipoprotein B mRNA-editing enzyme polypeptide-like 3G (APOBEC3G) alleviates miRNA-mediated repression independently of its deaminase activity in human cells[465]. Expression of APOBEC3G was shown to correlate with the release of miRNA reporters from P-bodies and their active translation[465].

In contrast, *C. elegans* Pumilio family (PUF) homolog PUF-9 promotes let-7 mediated silencing of *hbl-1* mRNA[604]. Likewise, in flies and humans Pumilio enhances miRNA silencing of the oncogene *E2F3*[605]. Moreover in humans, several PUF-binding motives are found in proximity of miRNA-binding sites suggesting extensive interaction between PUF proteins and miRISC[606].

The TRIM–NHL family of E3 ubiquitin ligase proteins was shown to interact with miRISC[607]. Mammalian TRIM32 and *C. elegans* NHL-2 were reported to enhance the activity of a subset of miRNAs, including let-7, without altering their levels[608,609]. Both proteins promote neuronal differentiation[608,609]; interestingly TRIM32 is asymmetrically distributed in neuronal progenitors[608]. Conversely, *D. melanogaster* Mei-P26 leads to a reduction in mature miRNA levels[610]. TRIM71 was attributed a role in degradation of AGO2 via ubiquitination[611]. However, these findings were later challenged by the observation that TRIM71 enhances miRNA repression of the *Cdkn1* gene thereby promoting embryonic stem cells proliferation[612].

HuR also has a dual role in modulating miRNA silencing. In fact it can enhance let-7 mediated repression of *MYC* mRNA[613].

The RBP polypyrimidine tract binding protein (PTB) competes with miRISC binding of a subset of mRNAs involved in neuronal differentiation and enhances miRISC binding of a different subset of mRNAs by modifying their 3'-UTR structure[614]. PTB depletion caused alleviation of miRNA-mediated repression of neuronal genes and resulted in the transdifferentiation of fibroblasts into neurons[614].

In neuronal cells reversible modulation of miRNA silencing is an important mechanism to maintain synaptic plasticity and long-term memory[281,615]. The neurotrophic factor BDNF has been reported to partially alleviate *Limk1* mRNA repression by miR-134 in rat hippocampal neurons[281]. The RNA helicase MOV10, involved in miRNA silencing, or its *Drosophila* homolog Armitage have been

shown to be degraded at synapses upon neuronal stimulation, thereby promoting the expression of dendritically localized mRNAs[282,616,617].

Generally, RBPs are likely candidates for regulating miRNA silencing since their binding sites are mainly localized in 3'-UTRs, similarly to miRNAs, and hundreds of different RBPs are encoded by the genome (reviewed in[618]).

1.5 RNAi across species

Silencing of RNA molecules via small complementary RNAs is a widespread process, known as RNA interference (RNAi), present across most forms of life[44]. Small RNAs act as guides for the recruitment of a set of protein to target nucleic acids[619,620]. RNAi was first described in eukaryotes[24] where it consists of three major pathways: siRNA-mediated, piRNA-mediated and miRNA-mediated pathways[621]. Despite differences in the biogenesis of these sRNAs, degree of complementarity to targets and modes of action, they all share some components of the RNAi molecular machinery, suggesting gene regulation via RNAi appeared in a common ancestor of Eukarya[44,619]. Also prokaryotes possess an ancestral form of RNAi, however prokaryotes and eukaryotes RNAi seem to have evolved independently since the respective RNAi machineries are not homologous[44]. Nevertheless, the mechanistic principles and its function as a defense mechanism are shared features between prokaryotic and eukaryotic RNAi[622].

RNAi-like mechanisms in prokaryotes are functional analogues of eukaryotic miRNA, siRNA and piRNA pathways. Similarly to miRNAs, a subset of small RNAs (on average longer than eukaryotic sRNAs) identified in archaea and bacteria exhibit partial complementarity to mRNA targets and leads to translation inhibition or degradation of targets via the RNA chaperone Hfq[623,624]. In addition, most bacteria and archaea evolved an sRNA-based adaptive immunity that protects cells from foreign and mobile genetic elements, such as bacteriophages and plasmids, resembling the function of siRNAs and piRNAs[625]. This interference pathway involves clustered, regularly interspaced short palindromic repeats (CRISPRs) interspaced by stretches of DNA derived from the genomes of past invaders, which encode sRNAs that guide CRISPR associated (Cas) nucleases to target invasive nucleic acids[622,626-629].

Amongst eukaryotes, the core conserved components of RNAi are Argonaute proteins, including both AGO and PIWI subclades, and Dicer-like

proteins generally having an RNase III domain and a helicase domain[44]. Many species also express RNA-dependent RNA polymerases[44]. Interestingly, the RNAi machinery seem to originate from the assembly of simpler prokaryotic and viral proteins with roles in processes other than prokaryotic RNAi: the helicase domain of Dicer and AGO from archaea[630,631], the RNaseIII domain from bacteria[632] and RdRP from viruses[633,634]. Multiple paralogues of these proteins emerged in eukaryotes via duplication events and, together with accessory proteins, contributed to the evolution of different RNAi pathways[44,619]. Given a non-homogenous distribution of these proteins across species, multiple losses might have occurred throughout evolution[619,635]. Several unicellular eukaryotes including *Trypanosoma cruzi, Leishmania major, Cyanidioschyzon merolae, Plasmodium falciparum* and the budding yeast *Saccharomyces cerevisiae* do not express the RNAi machinery[619]. It is hypothesized that these organisms lost, independently from each other, the RNAi components suggesting that RNAi is dispensable in unicellular eukaryotes[619]. Conversely, RNAi in multicellular eukaryotes seem essential as suggested by the embryonic lethality of Dicer mutants[129,636]. Yet, siRNAs, and Dicer and AGO homologues were found in other unicellular eukaryotes as the fission yeast *S. pombe*[637] and in the budding yeasts *S. castelli* and *K. polysporus*[638,639]. Additionally, siRNAs were reported to be produced by several fungi, plants, protozoans and metazoans species[637,640-643] leading researchers to hypothesize that siRNA-mediate pathways against viruses and transposons were the most ancestral modes of RNAi. By contrast, regulation of endogenous gene expression by miRNAs was only reported in multicellular species[644]. Thereby, miRNAs were thought to have appeared together with multicellularity. Interestingly, the discovery that the unicellular alga *Chlamydomonas reinhardtii* expresses plant-like miRNAs argued against this hypothesis and suggested that at least a common eukaryotic ancestor between plants and unicellular algae already developed siRNA and miRNA-mediated RNA silencing[101,102]. Despite many eukaryotic organisms express miRNAs, the number of miRNA-encoding genes differ largely amongst genomes and seem to rise with increasing organismal complexity, ranging from dozens of genes in sponges to nearly 1500 genes in humans[232].

Given substantial differences between plants/algal and animals miRNA genes, miRNA biogenesis and miRNA targeting[101,102,645], miRNA pathways have

been thought to have evolved separately in the two lineages[645]. miRNA sequences and their respective targets diverged across the animal and plant kingdoms[108]. Despite some miRNA families being conserved within animals (thirty miRNA gene families including the oldest conserved let-7 family)[194,646] and within plants (miR-165 and miR-166 families)[647], no overlap is present between the two kingdoms, exception made for the miR-884 family and their *UBP1*-like mRNA targets[648]. In addition, most of plant miRNAs are encoded from single transcription units located in intergenic regions[96]. Plants lack a Drosha homolog and are processed in two nuclear steps by the Dicer homologue Dicer-like 1 (Dcl-1) helped by the dsRNA binding protein hyponastic leaves 1 (HYL1) and Serrate[649]. Although homologs of Serrate are present in animals (named ARS2)[650,651], HYL1 homologues have only been found in plants. Most mature plant miRNAs have high complementarity to their targets, thus mostly act via AGO-mediated target slicing[199,649,652]. Additionally, plants lack the key miRISC component GW182. Contrariwise, animal miRNA genes are mostly found within introns and often form clusters, transcribed as a single primary transcript[653]. They are processed in two steps; firstly in the nucleus by the microprocessor Drosha-Pasha/DGCR8 and secondly in the cytosol by Dicer and its partners Loquacious/TRBP and PACT[55]. The majority of animal miRNAs have only partial complementarity to targets and mostly mediates translational repression and mRNA deadenylation and decay via the AGO-GW182 miRISC complex[81,652]. Yet, most studies performed in animals looked at a subgroup of metazoan called bilaterians (animals with bilateral symmetry such as humans, flies and worms), which does not include the older phyla of Porifera (sponges), Ctenophora (comb jellies), Placozoa (Trichoplax) and Cnidaria (corals, sea anemons, hydroids and jellyfish), which diverged more than 600 million years ago (Mya) from the rest of metazoa[654]. Thus, the term “animal” has been used improperly in this context and to gain evolutionary insights into miRNA-mediated regulation is important to also look at more ancient animal species. sRNAs and most of the components of the RNAi machinery have not been found in Placozoa and Ctenophora[655-657]. However, studies performed in cnidarians and sponges identified piRNAs, miRNAs and siRNAs (with piRNAs being the most abundant sRNAs)[655,658,659] and homologues of the RNAi machinery[654]. Two cnidarian species, namely *Hydra* and the sea anemone *Nematostella vectensis* were shown to express about 100 miRNAs without sequence similarities to any of the most

conserved bilaterian or plant miRNA families, exception made for *Nematostella* miR-100, which is conserved among bilaterians[655,658,659]. Unlike bilaterians and similar to plants, *Nematostella* miRNAs tend to have high complementarity to their targets and mediate target slicing[659]. Both *Nematostella* AGO1 and AGO2 in fact possess the five residues previously found to be important for AGO slicing activity in bilaterians[304,330,654]. Analogously to plants, most cnidarian sRNAs are methylated, possibly by the ubiquitously expressed protein HEN1; whose expression is instead restricted to the germline in bilaterians[655,658,659]. Furthermore, cnidarians, sponges and ctenophores express a homologue of plant Dicer partner HYL1, but no homologues of Loquacious/TRBP and PACT[654]. However, unlike plants *Nematostella* also possesses a GW182 homolog[654], a protein required for miRNA-mediated deadenylation and translational repression in Bilateria. Of note, plant miRNAs are also able to mediate both slicing and translational repression[649], although via the non-GW182 SUO protein family[414]. Together these findings argued against the independent evolution of miRNA pathways in animals and plants. They instead suggested that animals and plants miRNA pathways might have had a common ancestor and that slicing might have been the predominant ancestral mode of action of miRNAs, leaving open the question as to what role GW182 plays in cnidarians.

1.6 Aim of the Study

The aim of this study was to gain further mechanistic and evolutionary insights on miRNA-mediated regulation of gene expression. The miRNA field has been extremely prolific and extensive research efforts have brought a clearer understanding of the detailed modes of miRNA silencing. Despite these efforts, multiple layers of modulation of miRNA silencing keep emerging and it is not yet clear whether miRNA-mediated repression might function differently in different contexts and species. Given that members of the GW182 protein family are crucial components of miRISC in animals, research presented in this thesis focuses on these proteins. Specifically, W-motifs dispersed throughout GW182 proteins mediate miRNA-silencing by recruiting the CCR4-NOT deadenylase complex. With this in mind, I sought out to identify the W-motif-specific interactome of one of the three mammalian paralogues of GW182 proteins, TNRC6C. The aim was to identify novel factors interacting with W-motifs that could function as competitors of the CCR4-NOT complex and thereby modulate miRNA silencing. Further, I aimed to investigate the evolution and conservation of the mechanisms of miRNA-mediated silencing between bilaterians and cnidarians, focusing on the role of GW182 orthologue in the cnidarian *Nematostella vectensis.* Because the modes of miRNA silencing differ substantially in plants and bilaterian animals, it was important to explore the mechanism of miRNA-mediated repression in non-bilaterian animal species, which separated more than 600 million years ago from the rest of the metazoan lineages.

2. Results

2.1 Identification of the W-motif-dependent interactome of human TNRC6C protein

2.1.1 Importance of W-motifs for mRNA repression

miRNA silencing is mediated by short tryptophan-containing T/LWG/S repeats, named W-motifs because of their invariant tryptophan residue, dispersed throughout disordered regions of TNRC6/GW182 proteins[275] (**Figure 7A** and **7B**). These motifs act in an additive manner to recruit the CCR4-NOT and PAN2/PAN3 deadenylation complexes and are necessary and sufficient to mediate translational repression and deadenylation of target mRNAs. In case of human TNRC6 homologs, TNRC6A, TNRC6B and TNRC6C, most of the silencing W-motifs are located in the C-terminal effector domain (CED) as shown in **Figure 7A** and in **Figure S1** for TNRC6C[275-277]. Indeed, disruption of W-motifs by point mutations of tryptophan to alanine (W→A) in TNRC6A CED, TNRC6C CED and in the *Drosophila* homologue dmGW182 abrogates mRNA repression[275,355]. To test whether mimicking the aromaticity of the tryptophan residues is sufficient to restore repression, a tryptophan to tyrosine (W→Y) mutant of TNRC6C CED was tested in tethering assays. HEK293 cells were co-transfected with plasmids encoding a *Renilla* luciferase (RLuc) mRNA containing five boxB hairpins in its 3'-UTR, and TNRC6C CED or its W-motifs mutants (7W7Y and 7W7A) fused with HA-tag and lambda (λ) phage N peptide, which binds the boxB sites[309,660]. *Firefly* luciferase (FLuc) without boxB serves as transfection control (**Figure 7C**). An untethered TNRC6 CED, lacking the N peptide, was used as a negative control for RLuc-5boxB repression. As expected, TNRC6C CED represses the tethered mRNA more than 5 fold, while the 7W7A mutant led to a pronounced alleviation of repression. Interestingly, the 7W7Y mutant shows an intermediate phenotype, leading to a partial alleviation of repression (~2.5 fold). This result further supports the key role of W-motifs in mRNA repression and indicates that aromaticity of the central residue of W-motifs is an important feature of repression (**Figure 7D**).

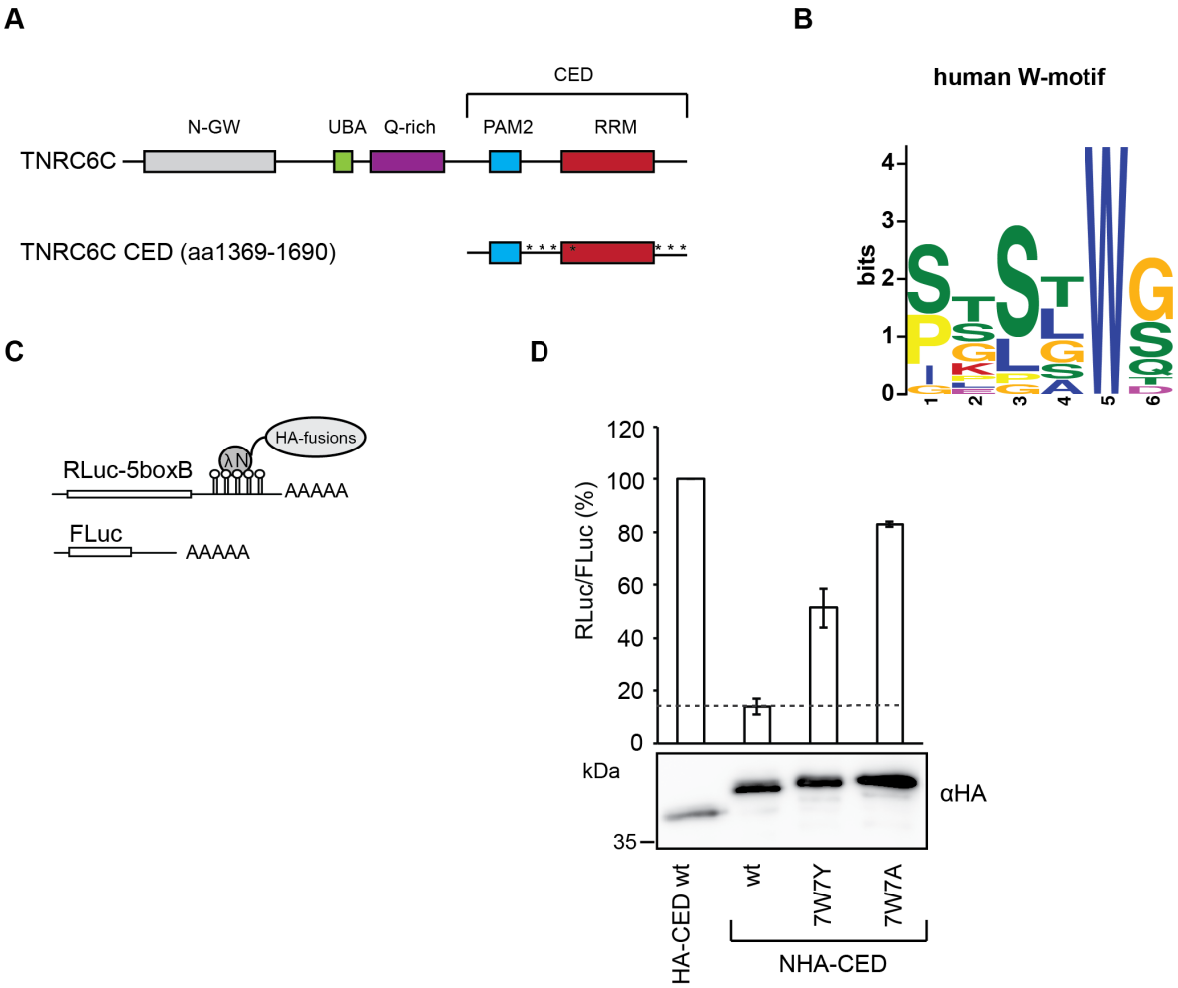

Figure 7. Disruption of W-motifs by Tyr or Ala point mutations progressively alleviates mRNA repression by TNRC6C CED (A) Schematic representation of human TNRC6C and its C-terminal Effector Domain (CED) used in this study. Individual domains and regions of TNRC6C: N-GW, GW-repeat–rich region; UBA, ubiquitin associated-like domain; RRM, RNA-recognition motif; PAM2, PABP associated motif. The CED includes PAM2, RRM domain and the unstructured regions flanking the RRM, which contain several W-motifs. The positions of seven Trp residues within W-motifs are depicted with asterisks. Those residues were either mutated into Ala or Tyr in the 7W7A and 7W7Y mutants, respectively. Numbers correspond to the amino acid position. **(B)** Graphic representation of a human W-motif obtained by aligning experimentally validated W-motifs of TNRC6A and TNRC6C [275]. The sequence was derived with MEME suite[661], see also **Figure S2**. **(C)** Schematic representation of reporter constructs used in tethering experiments: RLuc-boxB encodes for *Renilla* luciferase (RLuc) coding sequence fused to a 3'UTR with five boxB sites that specifically bind to λN peptide; FLuc encodes for Firefly luciferase (FLuc) coding sequence without boxB sites and serves as a control[309]. **(D)** 7W7Y and 7W7A CED mutants progressively alleviate repression of tethered mRNA. Human HEK293 cells were co-transfected with plasmids encoding RLuc-boxB, FLuc, and

NHA-CED or its indicated 7W7Y, 7W7A mutants. As negative control, a plasmid encoding untethered HA-CED was used. RLuc activity was normalized to that of FLuc and presented as a percentage of RLuc produced in the presence of the untethered HA-fusion. Values represent means ± SD from 3 individual experiments (n=3). Expression levels of HA-fusion proteins were estimated by western blotting with antibodies directed against HA-peptide.

2.1.2 Classes of W-motif-specific Interactors identified by quantitative Mass Spectrometry analysis of TNRC6C and its mutants

To identify novel interactors of TNRC6C proteins recruited via W-motifs, HEK293 cells were transfected with plasmids expressing GST-fusions of either wild-type (wt) CED, CED with mutated W-motifs (7W7A and 7W7Y) or GST alone as a control on background binders. The content of GST pull-downs was analyzed by quantitative proteomics using stable isotope labeling of amino acid in cell culture (SILAC) coupled to liquid chromatography-tandem mass spectrometry (LC-MS/MS) in collaboration with Dr. Marieluise Kirchner (**Figure 8A**). By comparing the interactome of TNRC6C CED wt and the two mutants, we were able to identify proteins that are pulled by TNRC6C CED via its W-motifs. 80 proteins were identified as at least 1.3 fold enriched with TNRC6C CED wt as compared to both mutants and to the GST control, indicating they are W-motif-specific (**Figure 8B** and **Table S1**). As expected, subunits of the CCR4-NOT complex were found enriched with the wt CED. Gene ontology (GO) and Kyoto Encyclopedia of Genes and Genomes (KEGG) pathways enrichment analysis performed with DAVID[662,663] identified RNA degradation as the most enriched pathway, which is consistent with the main function played by TNRC6 proteins in miRNA-mediated repression. Interestingly, endocytosis resulted as another enriched pathway among W-motif specific interactors. In agreement with this, the most enriched GO cellular components terms (GO CC) were cytosol, coated pit and plasma membrane (**Figure 8C**). Quantitative proteomic experiments illustrated in figure 8 were done in collaboration with Dr. Marieluise Kirchner, who ran the samples on the Mass Spectrometer, processed the raw data with MaxQuant, and supervised the data analysis I performed.

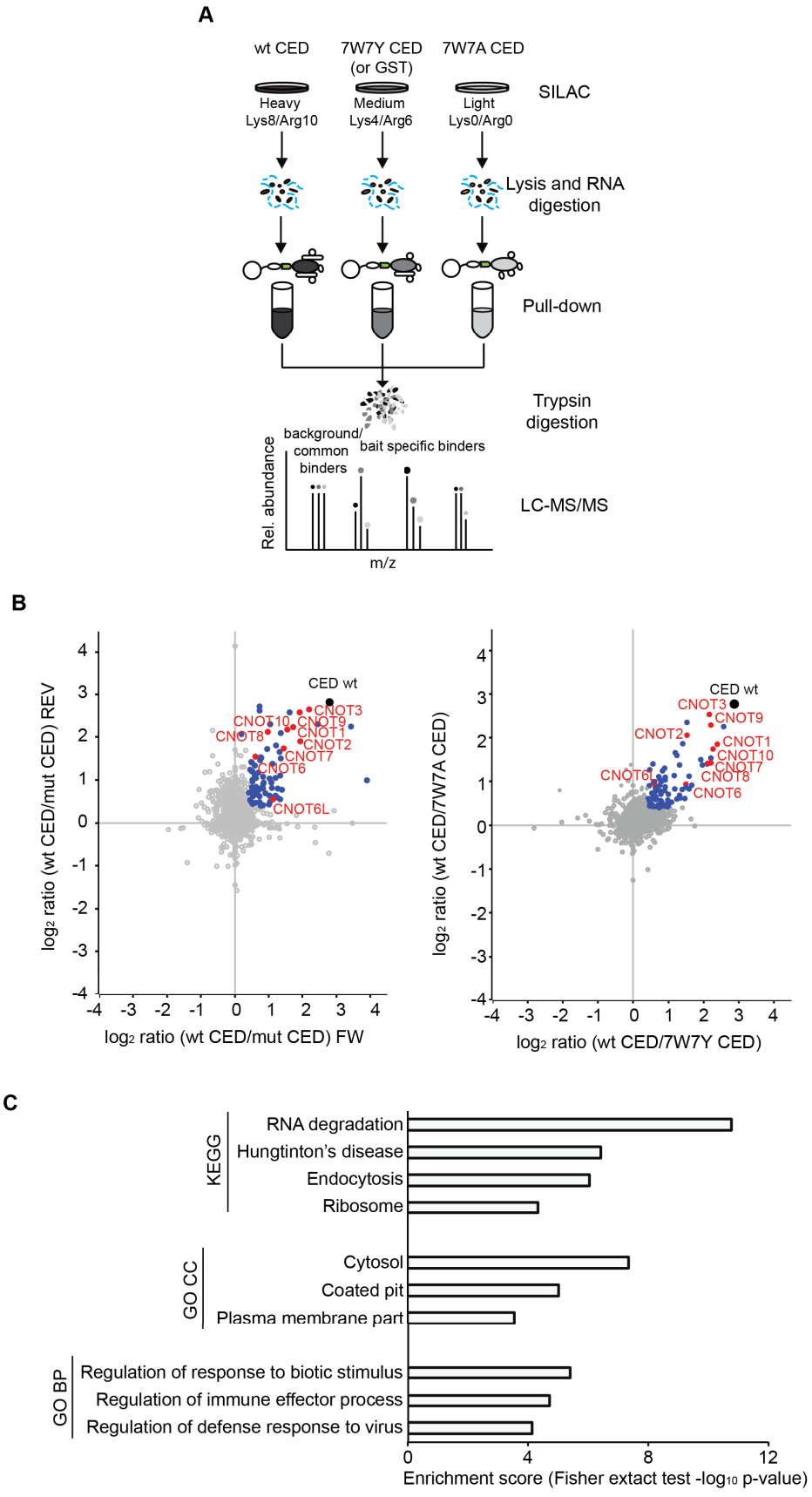

Figure 8. Identification of a TNRC6C W-motif specific interactome (A) Experimental strategy: GST-TNRC6C CED wt, 7W7A and 7W7Y mutants (or GST tag alone) were

transiently transfected in differentially SILAC labeled HEK293 cells (heavy, medium and light). Nuclease-treated HEK293 lysates were used in GST pull-down followed by Mass Spectrometry. For the forward experiment CED wt was labeled with heavy amino acids (dark grey) and the 7W7A mutant was labeled with light amino acids (light grey). For the reverse experiment the SILAC labels were swapped. **(B)** SILAC-MS results. The data are presented as a $\log_2$ enrichment of a given interactor with wt TNRC6C CED relative to mutants. On the left, forward experiment (*x*) is plotted against reverse (*y*). On the right, the same data are presented as enrichments relative to the two different mutants: wt/7W7Y enriched interactors (*x*) are plotted against wt/7W7A enriched interactors (*y*). Values represent means from 4 to 9 individual experiments. The cutoff to define the enrichment was set at $\log_2$=0.4 (~1.3-fold change). All the interactors that passed the cutoff are displayed in blue. The bait, CED wt, is represented in black. Subunits of the CCR4-NOT complex (positive control) are shown in red. **(C)** Gene ontology analysis on W-motif-specific CED interactors. wt CED-enriched interactors (mean $\log_2$FC≥ 0.4; one sample t-test p-value< 0.05) were subjected to GO and KEGG Pathways enrichment analysis using DAVID[662,663]. The enrichment was calculated over the total proteins identified by Mass Spectrometry. The bar graph shows the most enriched enriched GO terms (cellular component, CC: and Biological Process, BP) and KEGG pathways, and their respective enrichment scores (-$\log_{10}$ p-value).

Amongst the 80 enriched W-motif-specific interactors of TNRC6C CED, MS identified proteins involved in vesicular trafficking (**Figure 9A**). In particular, components of the clathrin-coated vesicles (CCVs), such as clathrin (CLTC, CLTA) and subunits of the adaptor protein of class 2 complex (AP2), were significantly enriched with TNRC6C CED, but not with its mutants (**Figure 9B**). Clathrin heavy chain (CLTC) is also one of the most abundant interactors of wt CED (**Figure 9C**). Importantly, interactions between wt TNRC6C CED and CCV components could be validated using GST pull-down of TNRC6C CED and its mutants followed by western blotting (**Figure 9D**). Consistently, previous proteomic analysis on CCVs isolated from HeLa cells identified TNRC6A, TNRC6B and Argonaute 2 (AGO2) proteins as components of clathrin-coated vesicles[664]. In addition, affinity purification of AGO2 from mouse embryonic fibroblasts (MEF) followed by Mass Spectrometry[665] identified clathrin as an AGO2 interactor. Our data suggest that recruitment of the AGO-TNRC6 complex to CCVs is mediated by W-motifs of TNRC6 proteins, as interaction with CCV components was lost upon mutation of W-motifs.

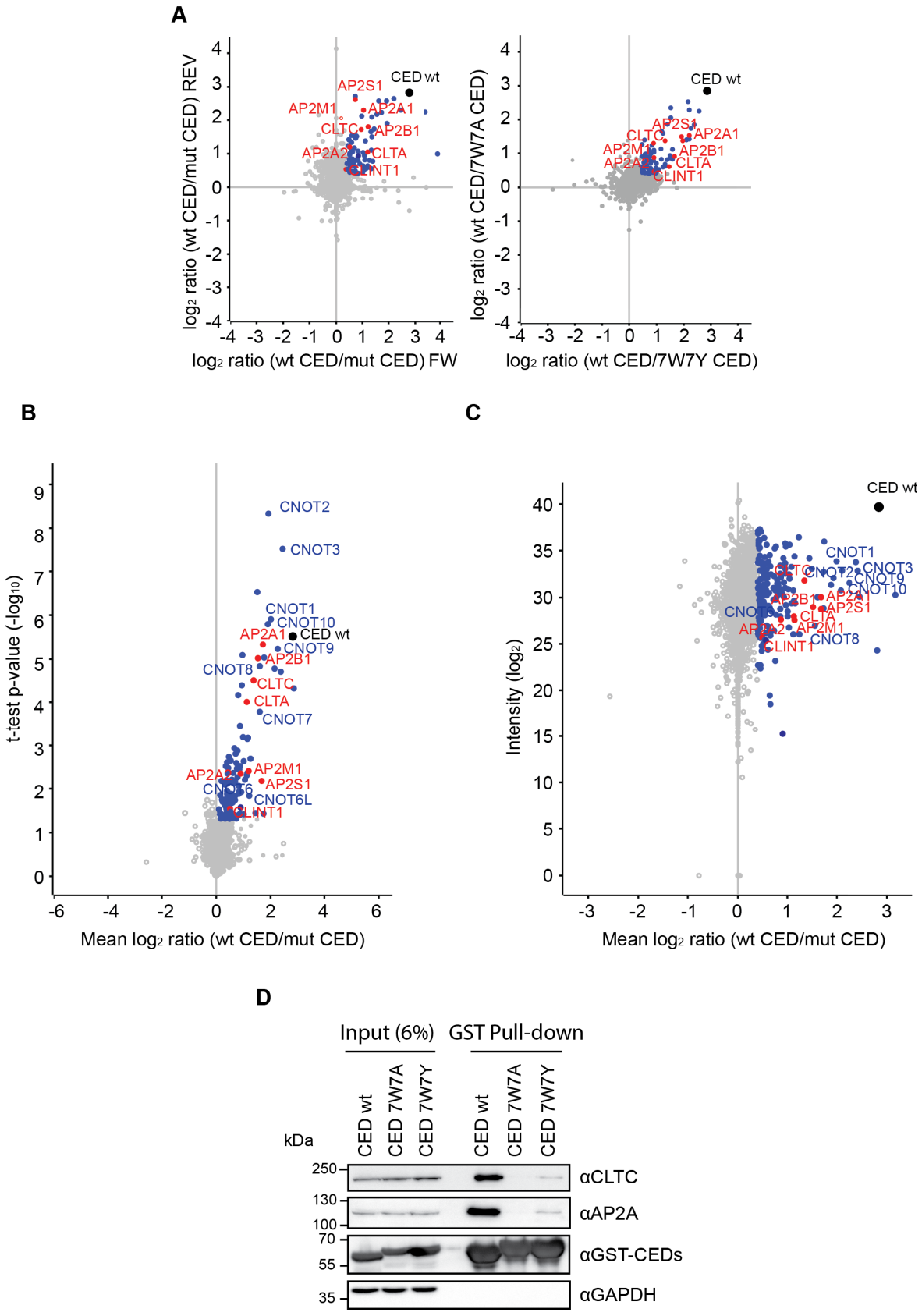

Figure 9. TNRC6C CED interacts with vesicular trafficking proteins via its W-motifs

(A) SILAC-MS results. Scatter plots identifying proteins involved in vesicular trafficking (shown in red) as enriched interactors of wt TNRC6C CED over its mutants. Data were

analyzed and presented as in Figure 8B. **(B)** SILAC-MS results. Scatter plot showing wt CED W-motif-specific interactors (*x*; mean $\log_2$ enrichment wt CED/mut CED) and their significance (*y*; -$\log_{10}$ p-value) (one sample t-test; p-value < 0.05). Significant interactors are shown in blue. Vesicular trafficking proteins are highlighted in red. **(C)** Estimate of W-motif-specific interactors abundance. The mean $\log_2$ enrichment wt CED/mut CED (*x*) is plotted against the intensity (*y*). Enriched interactors are shown in blue and vesicular trafficking proteins are shown in red. **(D)** Validation of interactions between wt TNRC6C CED and vesicular trafficking proteins identified in (A). Nuclease-treated cell lysates from HEK293 expressing GST-fusions of TNRC6C CED were used in GST pull-downs, and inputs (6%) and GST pull-downs were analyzed by western blotting using the indicated antibodies.

Additional classes of TNRC6C W-motifs specific interactors could be identified with this approach (**Figure 10**). For instance two DEAD-box RNA helicases, DDX20 and DDX46, were able to interact with TNRC6 CED, but not with its mutants. Despite two recent studies identifying DDX6 as a direct interactor of CNOT1 that promotes translational repression[267,268], we could not identify this protein as enriched in our dataset. Similarly, three metabolic enzymes involved in nucleotides metabolism and amino acid biosynthesis (CAD, PHGDH and PYCRL) interact with TNRC6C via its W-motifs. Moreover mitochondrial proteins such as intermembrane chaperones (TIMM proteins) and ADP/ATP translocases or metabolite carriers (SLC25A proteins), and kinases and phosphatases were among wt CED interactors. Interestingly, by comparing the wt CED-enriched interactors with 7W7A and 7W7Y interactors we were able to observe that the 7W7Y mutant preserves the interactions with PABP1 and PABP4, and PCBP1 proteins (**Figure 10**, right). PABP proteins bind poly(A) RNA stretches and PCBP proteins bind poly(C) RNA stretches, and are both involved in RNA stabilization. This observation may indicate that these protein families could be responsible for the residual repressive activity of 7W7Y CED. Despite all CED domains, wt, 7W7Y and 7W7A mutants, have an intact PAM2 motif (**Figure 7A** and **Figure S1**), which is responsible for direct interaction with PABPs[286,360], our SILAC-MS data shows that PABP binding to 7W7A CED is significantly impaired. Secondary regions in TNRC6 CED have already been attributed PABP binding abilities [275,286,360,362]. Thus, our data suggest W-motifs constitute these secondary regions that reinforce

interactions with PABPs and that Y-motifs can also suffice in mediating PABPs binding.

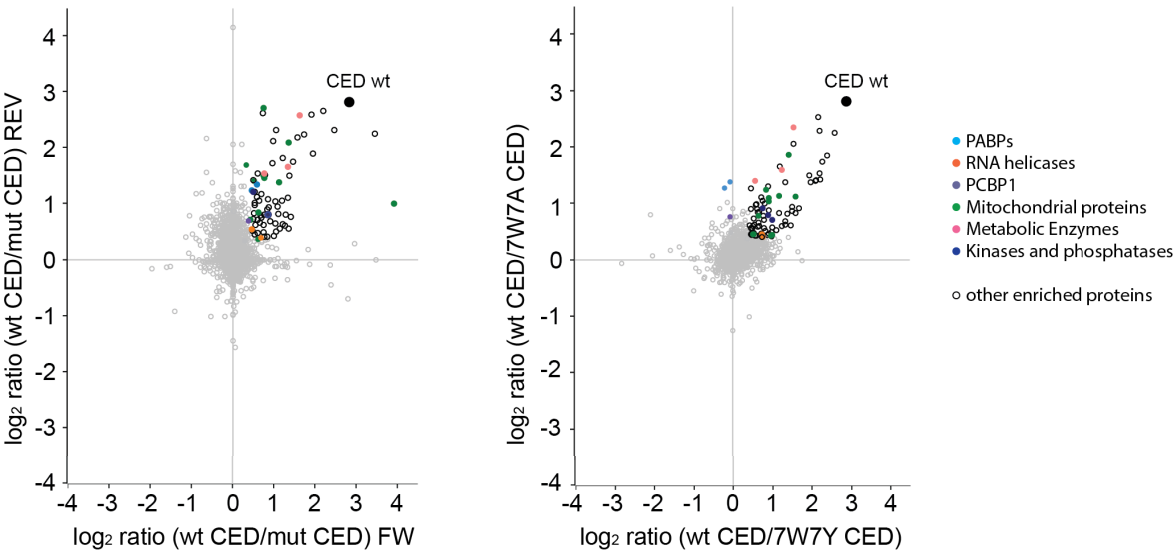

Figure 10. Additional classes of W-motif-specific interactors identified by quantitative Mass Spectrometry Different classes of W-motif-specific interactors identified by quantitative Mass Spectrometry are shown with different colors. Metabolic enzymes (CAD, PHGDH, PYCRL) in light red; mitochondrial proteins (TIMM and SLC25A proteins) in green; kinases and phosphatases in blue; poly(A) binding proteins (PABPC1 and PABPC4) in light blue; poly(C) binding proteins (PCBP1) in purple and DEAD-box RNA helicases (DDX20, DDX46) in orange. The data are presented as described in Figure 8B. All enriched proteins are shown in black.

Overall this analysis identified previously unstudied interactors of TNRC6C proteins. Given that W-motifs are indispensable for miRNA silencing, these novel interactors are likely to play a role in the regulation of miRNA-mediated repression.

2.2 Addressing the role of clathrin-coated vesicles in regulation of miRNA silencing

In light of the finding that several proteins involved in vesicular trafficking are W-motif-specific binders of TNRC6C, the next questions to ask were where these interactions are taking place within a cell, and what their functional meaning is. More specifically, if and how they modulate miRNA-mediated repression.

2.2.1 Clathrin-coated vesicles as novel interactors of TNRC6 and AGO2 proteins

Clathrin-coated vesicles (CCVs) are a type of vesicles in charge of sorting cargos between the plasma membrane, trans-Golgi network, and endosomal compartments (reviewed in[666]). Clathrin forms a spherical scaffold that coats the vesicles, while a heterotetrameric complex of proteins, called adaptor proteins (AP proteins), crosses the clathrin scaffold and is capable of binding clathrin, membranes lipids and proteins, and accessory proteins on the external side the vesicles. Depending on which class of AP proteins binds to clathrin, CCVs mediate different membrane trafficking pathways. Clathrin, together with AP2, mediate specifically the formation of endocytic vesicles from the plasma membrane (**Figure 11A**), while AP1 and AP3 CCVs mediate trans-Golgi trafficking (**Figure S3A**) (reviewed in[666]). The SILAC-MS/MS data indicated that clathrin and AP2 are W-motif-specific interactors of TNRC6C, while AP1 and AP3 subunits did not pass the established cutoffs; suggesting these interactions might be occurring selectively on endocytic CCVs. However coexpression of AP1 subunits and GST-fusions of TNRC6C CED wt and 7W7A mutant, followed by GST pull-down and western blotting also showed W-motif dependent interactions with AP1 subunits (**Figure S3 B**), indicating TNRC6 might weakly interact also with AP1-CCVs.

Given that all four subunits of AP2: AP2A, AP2B, AP2M and AP2S, are interacting with wt CED, clearly supporting the idea that endocytic CCVs interact with TNRC6C, the focus was placed on AP2-CCVs. AP2A and AP2B are the biggest subunits of AP2 and share the same domain organization. They have a trunk domain, which binds to the plasma membrane with the help of AP2M, and to the receptors to be internalized; a hinge unstructured region that connects the trunk to the appendages, and in case of AP2B contributes to the interaction with the

clathrin triskelion; and appendage domains that protrude from the clathrin coat and are free to bind accessory proteins (**Figure 11A**; reviewed in[667]).

To investigate whether TNRC6 interactions with CCV proteins are occurring on the vesicles, CCV-enriched fractions were isolated from HeLa cells as illustrated in **Figure 11B**. The presence of TNRC6 proteins was tested via western blot. In agreement with a previous proteomic study[664], CCVs were found to interact with endogenous TNRC6A and AGO2 proteins (**Figure 11C**). Due to unavailability of specific antibodies against TNRC6B and TNRC6C their presence could not be tested.

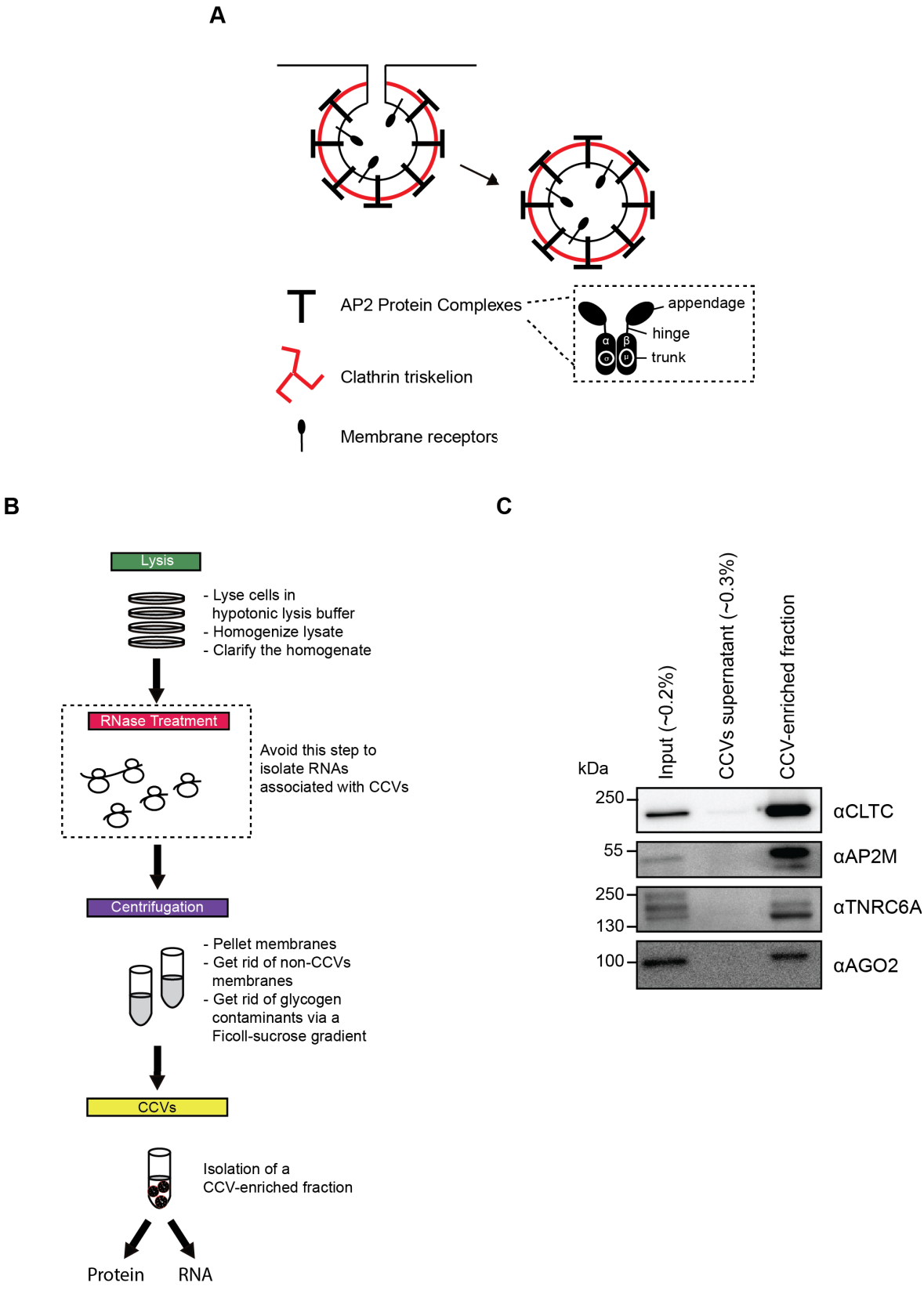

Figure 11. TNRC6A and AGO2 proteins associate with Clathrin-coated vesicles (CCVs) (A) Schematic drawing representing the formation and structure of CCVs. The clathrin coat and its triskelion shape are shown in red, and adaptor proteins (AP) are represented by a black T-shape protruding from the clathrin-coat. The four subunits

forming AP complexes, AP2A (α), AP2B (β), AP2M (μ) and AP2S (σ) and their domains (trunk, hinge and appendages) are illustrated. **(B)** Scheme summarizing the procedure adopted to isolate CCVs and the modification introduced; adapted from Borner et al., (2012)[664]. **(C)** CCVs were isolated from HeLa cells as illustrated in (B). Input (~0.2%), CCVs supernatant (~0.3%) and the CCV-enriched fraction were analyzed by western blotting using the indicated antibodies. For proper comparison the same protein content was loaded in input and CCV-enriched lanes.

TNRC6-CCVs interactions were detected by either pulling down TNRC6C CED and probing for components of CCVs or by isolating CCVs and probing for TNRC6 proteins. However, it was still not clear whether these interactions occur on the outer surface of CCVs or within the vesicles. To discriminate between these possibilities flag-tagged AP2A appendage and AP2B appendage-hinge domains, which protrude from the clathrin-coat, were overexpressed in HEK293 cells, together with GST-fusions of TNRC6 CED wt or 7W7A. The presence of AP2 appendages was then tested in GST pull-down by western blotting with αflag antibody (**Figure 12**). AP2A appendages interacted with wt TNRC6 CED, but not with the 7W7A mutant where W-motifs are disrupted; suggesting CCV-TNRC6 interactions are located on the outer vesicles coat and are mediated by contacts between TNRC6C W-motifs and the appendage regions of AP2A proteins.

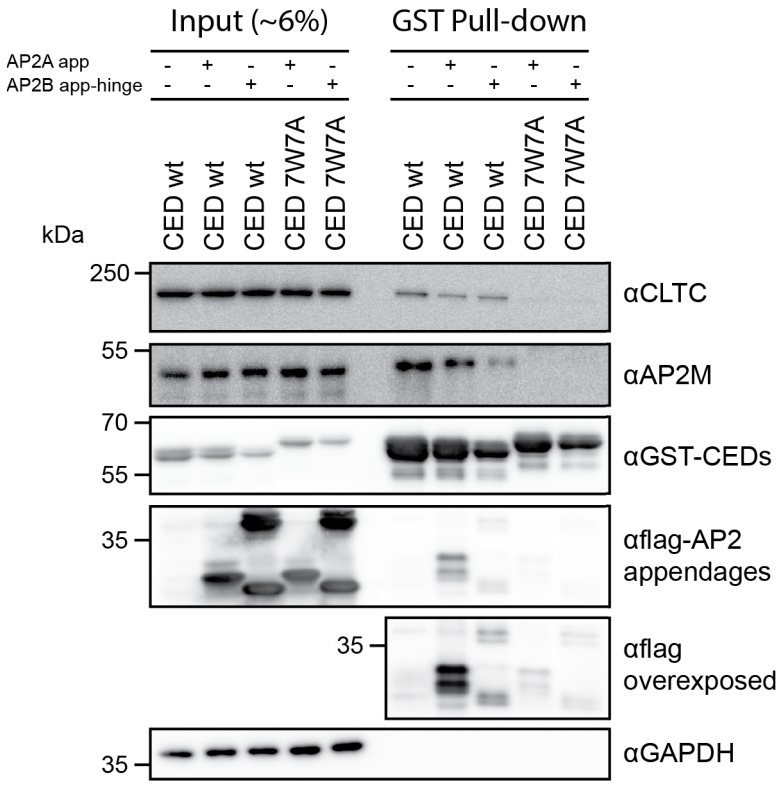

Figure 12. AP2A appendage interacts with TNRC6C CED via W-motifs HEK293 cells were co-transfected with plasmids encoding GST-fusions of TNRC6C CED and plasmids encoding flag-tagged AP2A appendage or AP2B appendage-hinge regions. Nuclease-treated cell lysates were used in GST pull-down, and inputs (~6%) and GST pull-downs were analyzed by western blotting with the indicated antibodies. TNRC6C 7W7A was used as negative control.

Next, to test whether TNRC6 and AGO, two core components of the miRISC complex, on CCVs are also associated with miRNA targets, CCV-enriched fractions were isolated from HeLa cell lines expressing doxycycline inducible miRNA reporters, and their RNA content was analysed (**Figure 13A**). One of the HeLa line carries a stably integrated inducible FLuc/RLuc-hmga2 reporter where RLuc is fused to the 3'-UTR of the hmga2 gene targeted by let-7 miRNA, which is endogenously expressed in HeLa cells (for simplicity called RLuc-hmga2 wt)[392]. A second HeLa line carries a FLuc/RLuc-hmga2 construct fused to a mutated hmga2 3'-UTR with disrupted let-7 sites that serves as a negative control (RLuc-hmga2 mut) [392]. In both cell lines FLuc is used as a normalization control. Thus, if TNR6C proteins associated with CCVs are bound to a let-7 loaded form of AGO2 and to the corresponding target mRNA, one would expect an enrichment of wt RLuc-

hmga2 mRNA on CCVs when compared to mut RLuc-hmga2 mRNA. However, no significant difference could be observed between normalized wt and mut RLuc mRNAs on CCVs relative to their corresponding inputs (**Figure 13B** and **Figure S4**). These results may suggest that TNRC6-AGO complexes interacting with CCVs are not associated with miRNA targets, and are consequently inactive in miRNA silencing.

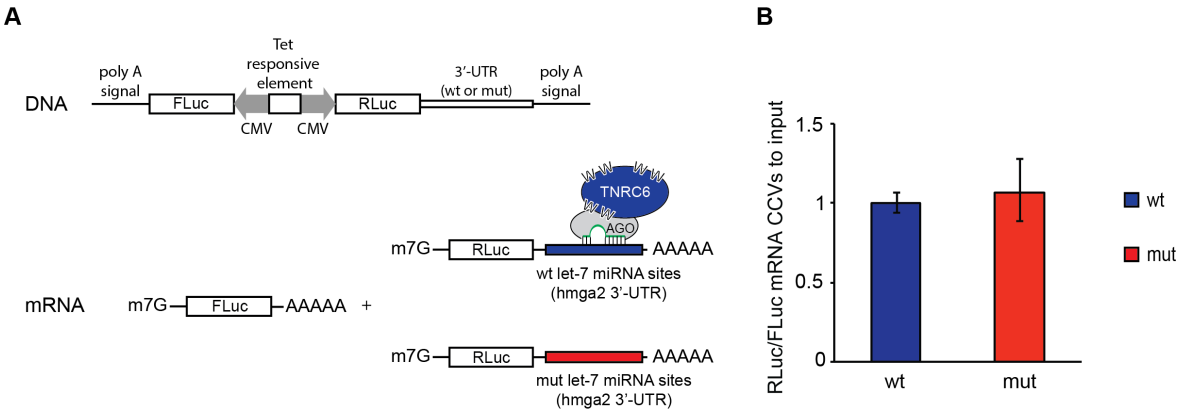

Figure 13. No enrichment of wt miRNA reporter mRNA is detected on the isolated CCVs (A) Schematic representation of FLuc/RLuc-hmga2 dox-inducible reporters expressing FLuc insensitive to miRNAs and RLuc fused to the wt 3'UTR of hmga2, thus sensitive to let-7 miRNA (wt, blue) or its mutant version with disrupted let-7 sites (mut, red). Reporters were previously described in[275,392] **(B)** CCV-enriched fractions were isolated from HeLa cell lines carrying stably integrated inducible FLuc/RLuc-hmga2 wt or mut miRNA reporters illustrated in (A). Expression of miRNA reporters was induced for 1 day prior to CCVs isolation. RNA was isolated from inputs and CCV-enriched fractions and reporter RNA expression levels were analyzed by qRT-PCR. RLuc mRNA levels were normalized to that of FLuc and presented as ratios of RLuc isolated from CCVs over RLuc isolated from inputs (wt ratio, shown in blue, was set to 1; mut ratio is shown in red). Values represent means ± SD from 3 technical replicates.

2.2.2 Knockdown of components of the clathrin-coated vesicles enhances miRNA-mediated repression

To understand whether the interactions between TNRC6 proteins and CCVs affect miRNA-silencing, components of CCVs were knocked down in HeLa cells transiently or stably expressing the previously described FLuc/RLuc-hmga2 inducible reporters sensitive to let-7 miRNA (chapter 2.2.1). Their effects on miRNA-mediated repression were tested 4 h after inducing the expression of miRNA reporters using luciferase reporter assay (**Figure 14A**). In the initial setup,

HeLa cells were co-transfected with either wt RLuc-hmga2 or mutant RLuc-hmga2 reporter and siRNAs against TNRC6A/B/C, CLTC and AP2A1/2 gene transcripts or a scramble siRNA (**Figure 14A**, left). In a second setup, HeLa cells stably integrating the same set of inducible hmga2 reporters were transfected with siRNAs against the same genes (**Figure 14A**, right). In both cases, in the control samples let-7 efficiently repressed wt RLuc-hmga2 mRNA, when compared with the mutant reporter (compare the blue bar with the red bar in the scramble sample in **Figure 14A**). As expected, upon depletion of endogenous TNRC6 proteins, repression of the wt RLuc-hmga2 reporter was alleviated. Intriguingly, depletion of AP2A1/A2 proteins caused a decrease of nearly twofold in the expression of the let-7 regulated reporter. Instead, depletion of CLTC did not significantly affect miRNA silencing. To ensure that tested proteins were indeed efficiently depleted, their expression levels were assessed by qRT-PCR and by western blotting (**Figure 14B** and **14C**).

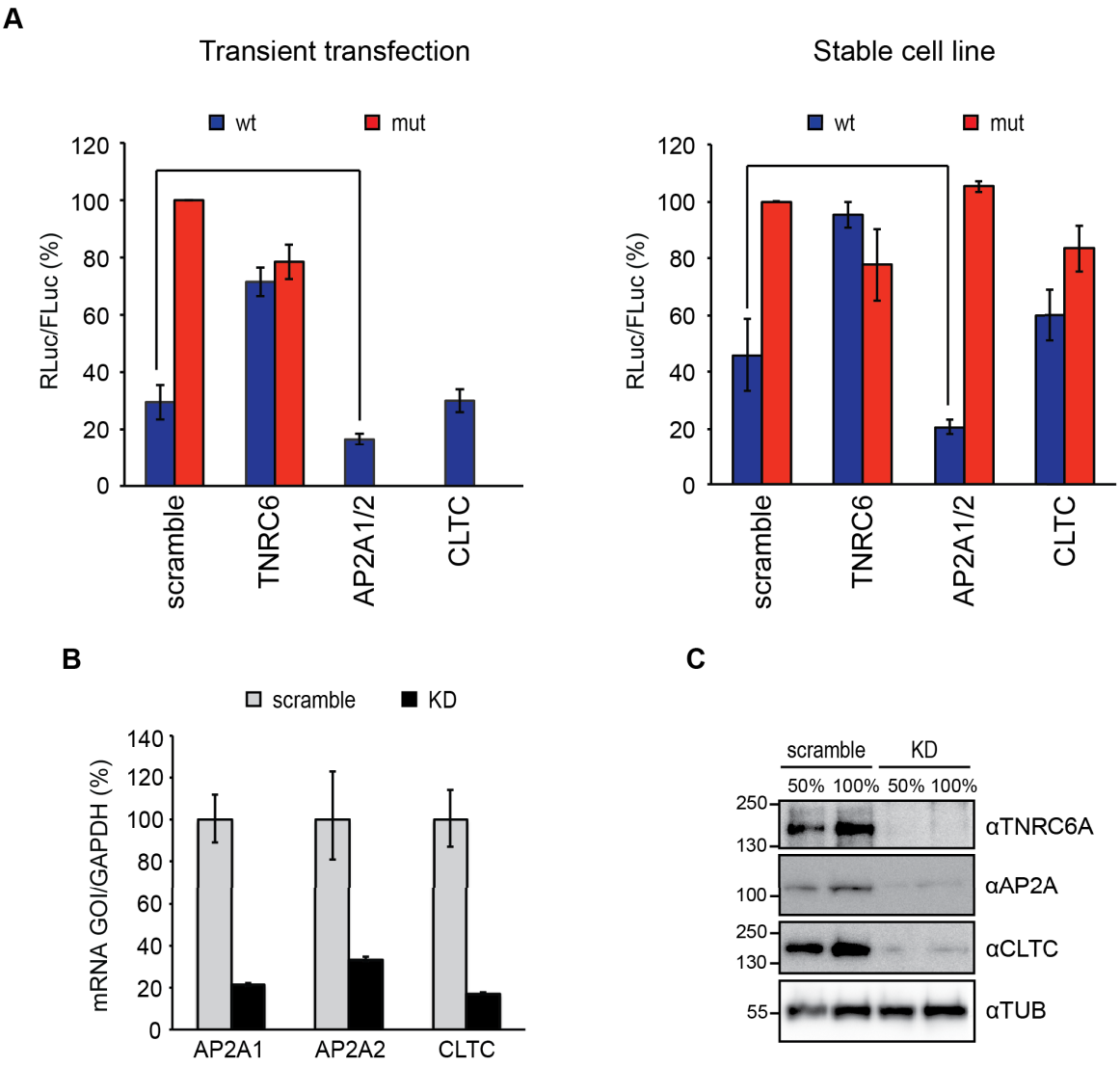

Figure 14. Knockdown of AP2A proteins enhances miRNA-mediated repression (A) siRNAs against the indicated genes were either co-transfected with plasmids encoding the dox-inducible let-7 miRNA reporters (hmga2-wt and hmga2-mut) illustrated in Figure 13A (left plot; means ± SEM, n=6) or transfected in HeLa cells stably carrying the same inducible miRNA reporters (right plot; means ± SEM, n=3). In both cases expression of the reporters was induced for 4 h with doxycycline. RLuc activity was normalized to FLuc and expressed as a percentage of RLuc activity produced by hmga2-mut reporter in samples transfected with scramble siRNA (set to 100%). Knockdown of TNRC6 proteins was used as a positive control on alleviation of miRNA-mediated repression. **(B)** Knockdown efficiency was estimated by qRT-PCR. Total RNA was reverse transcribed and cDNA was amplified using primers specific for AP2A1, AP2A2 and CLTC. mRNA levels of the indicated genes were normalized to GAPDH levels and expressed as a percentage of the corresponding mRNAs in the scramble control (set to 100%). Values represent means ± SD of 2 individual experiments. **(C)** Knockdown efficiency was estimated by western blotting using the indicated antibodies.

Given that W-motifs are necessary for miRNA silencing, proteins recruited via these motifs may promote or alleviate repression. As knockdown of AP2 proteins enhanced silencing, I reasoned AP2 could compete with the well-known repressor complex CCR4-NOT for W-motifs binding. To test this possibility, HEK293 cells depleted of either the CCR4-NOT complex (CNOT1-CNOT9 KD) or CCV components (AP2A-CLTC KD), and control cells treated with a scramble siRNA were transfected with plasmids encoding GST-TNRC6C CED wt and GST-7W7A mutant as a negative control. Nuclease-treated cell lysates were used in GST pull-downs, and analyzed by western blotting (**Figure 15A**). In the control samples, wt TNRC6C CED interacts with subunits of CCR4-NOT (CNOT9 and CNOT1) and components of CCVs (AP2A and CLTC), while 7W7A CED loses the ability to interact with both CCR4-NOT and CCV components, as expected. Depletion of CCR4-NOT increases AP2A binding to wt CED (~3- to 4-fold, **Figure 15B** and **15C**), supporting competitive or alternative interactions. Nonetheless, upon depletion of AP2A-CLTC no significant difference in CCR4-NOT binding could be detected between the knockdown sample and the scramble control. These results suggest CCR4-NOT is a stronger W-motifs interactor than AP2A, and competition occurs only in one direction.

It is indeed important to mention that depletion of AP2A proteins did not affect miRNA-mediated repression of bulged RLuc-3xb luciferase reporters bearing an artificial 3'-UTR sensitive to let-7^{412} (**Figure S5**). I will further comment possible reasons for the discrepant results observed when using RLuc-hmga2 reporters and RLuc-3xb reporters in the discussion session.

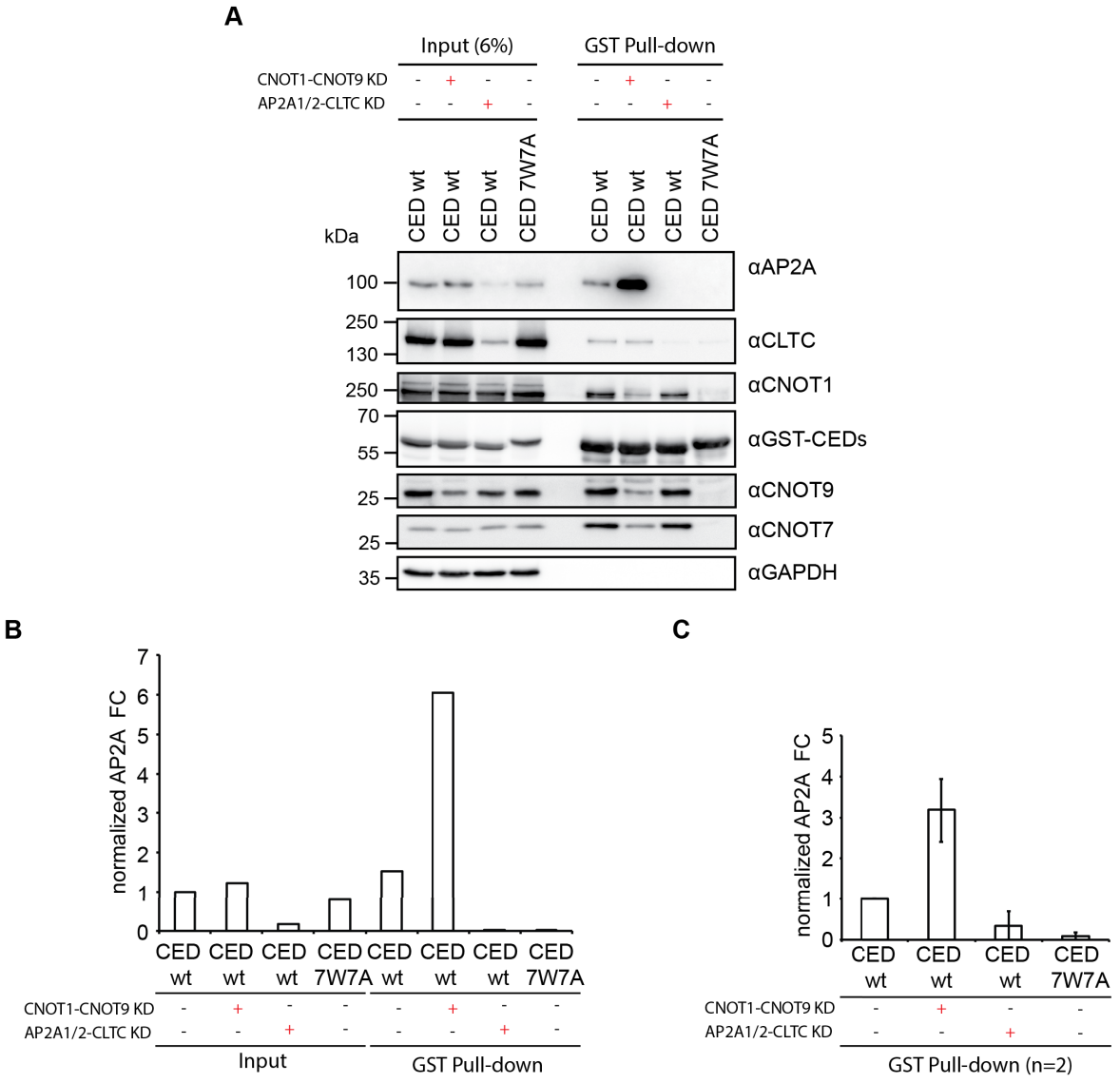

Figure 15. Knockdown of CCR4-NOT allows increased AP2A binding to TNRC6C CED (A) HEK293 cells were co-transfected with plasmids encoding GST-fusions of TNRC6C CED and siRNAs against CNOT1-CNOT9, AP2A-CLTC or a scramble siRNA as control. Nuclease-treated cell lysates were used in GST pull-down, and inputs (6%) and GST pull-downs were analyzed by western blotting using the indicated antibodies. TNRC6C 7W7A was used as negative control on CCR4-NOT, and AP2A and CLTC binding **(B)** AP2A levels shown in (A) were quantified with ImageJ software. Quantification of AP2A band intensities normalized to GST band intensities is shown for inputs and GST pull-downs. Normalized intensity ratios are relative to input control (CED wt co-transfected with scramble siRNA; set to 1). **(C)** AP2A binding to TNRC6C CED increases 3- 4-fold upon CCR4-NOT KD. Normalized fold change of AP2A binding in pull-down samples expressed relatively to the wt pull-down control are shown (pull-down of CED wt co-transfected with scramble siRNA was set to 1; means ± SEM; n= 2, individual experiments).

As interactions between TNRC6C and CCVs could also indicate potential function for TNRC6 proteins in the CCV pathway, I collaborated with Dr. Caroline Bruns (Hauchke lab, FMP, Berlin) to test this hypothesis. To evaluate whether TNRC6 proteins modulate clathrin-mediated endocytosis, Dr. Caroline Bruns tested the effect of depleting TNRC6 proteins on the uptake of transferrin (Tfn) receptor, which is a well-accepted proxy of clathrin-mediated endocytosis. The evidence indicates no significant difference between the control samples and samples depleted from TNRC6A proteins. Thus, these data did not support the hypothesis of TNRC6 involvement in regulation of endocytosis (**Figure S6**).

2.3 Conservation of the players and mechanism of miRNA-mediated repression

miRNA silencing is a layer of post-transcriptional gene regulation active in diverse eukaryotic lineages. Given that miRNA pathways differ substantially between plants and bilaterian animals, their study in more ancient clades is important to infer the evolution of this regulatory mechanism. The starlet sea anemone *Nematostella vectensis*, a representative of Cnidaria that diverged ~600 Mya from bilaterians, was shown to frequently cleave its miRNA targets via nearly perfect matches[659]. While this mechanism exhibits unexpected resemblance to the mode of action of plant and algae miRNAs, *Nematostella* and other cnidarians possess genes encoding for GW182 homologs as bilaterians do (**Figure 16**;[654]). Here, I sought out to investigate what is the function of *Nematostella* GW182. The following chapters (2.3.1—2.3.5) were adapted from my first-author manuscript (Mauri et al., 2016)[668]. Direct quotes are delimited by inverted commas: “ “.

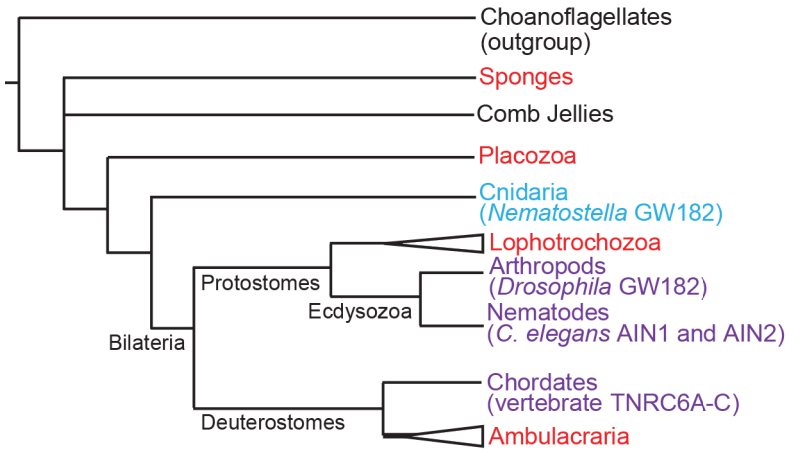

Figure 16. Phylogenetic distribution of GW182 proteins Schematic phylogenetic tree of Metazoa at the phylum level (based on[669,670]). Phyla where GW182 proteins were functionally and biochemically studied appear in purple and the studied protein appear within brackets. Phyla where GW182 homologs are found in the genome, but have not been functionally studied yet appear in red. Cnidaria appear in blue. Phylogenetic groups of multiple phyla are indicated by a triangle. The illustrated polytomy of sponges and comb jellies is due to the current uncertainty regarding their relative phylogenetic positions. This figure and figure legend was a panel of Figure 1 in Mauri et al., 2016.

2.3.1 *Nematostella* GW182 represses mRNAs via W-motifs within its C-terminal domain

"Proteins of the GW182 family show relatively low global sequence conservation, but are characterized by a conserved domain organization that includes an N-terminal GW-rich region, an ubiquitin-associated (UBA) domain, a glutamine-rich (Q-rich) region, PABP-associated motif 2 (PAM2) and a C-terminal RNA recognition motif, flanked by tryptophan-motifs-containing regions (reviewed in[90]). *Nematostella* GW182 (nvGW182), in addition, contains an N-terminal DNAJ domain that has been proposed to assist loading of small RNA duplexes into AGO proteins together with HSP70[654] (**Figure 17A** and **Figure S7**). The N-terminal GW repeats bind AGOs[311,331,333,335,355], and the C-terminal part of the protein (CED) recruits the CCR4-NOT and PAN2/PAN3 deadenylation complexes to repress mRNA[275-277]. Chekulaeva et al.[275], previously identified tryptophan-containing WG/S/T and G/S/TW repeats (W-motifs) as the key silencing elements, both necessary and sufficient for the direct recruitment of deadenylases and for mRNA silencing. The structural aspects of this recruitment were dissected in further studies by Filipowicz, Conti, Weichenrieder, and Izaurralde groups[267,268]. Importantly, the function of these motifs was shown to be conserved between human and *Drosophila*[275]. As nvGW182 contains similar motifs in its C-terminal region (W; **Figure 17A** and **Figure S7**), the working hypothesis is that it may function via a similar mechanism.

To test if the function of nvGW182 in mRNA repression is conserved, RNA-protein tethering assay were performed in human HEK293 cells and the effect on mRNA expression was analyzed. Tethering was achieved by co-expressing *Renilla* luciferase mRNA containing five boxB hairpins in its 3´-UTR (RLuc-5boxB; shown previously in **Figure 7C**), and nvGW182 protein or its deletion mutants fused with HA-tag and lambda phage N peptide, recognizing the boxB sites[309,660]. As untethered controls that were not expected to repress RLuc-5boxB, analogous HA-fusions lacking N peptide were used. As expected, human homologs TNRC6A, B and C, used as positive controls, led to efficient repression of tethered mRNA (**Figure 17B**; ~10- to 5-fold). Importantly, tethering of nvGW182 leads to ~3.5-fold repression. To identify the domains of nvGW182 that function in repression, C- and N-terminal deletions (nvΔCED and nvCED, respectively) were generated and their ability to repress tethered mRNA was tested. Consistently with the prior

mapping studies in human and Drosophila[335-338], nvCED effectively represses mRNA (~5-fold), while nvΔCED has practically no effect (**Figure 17B** and **Figure S8**)."

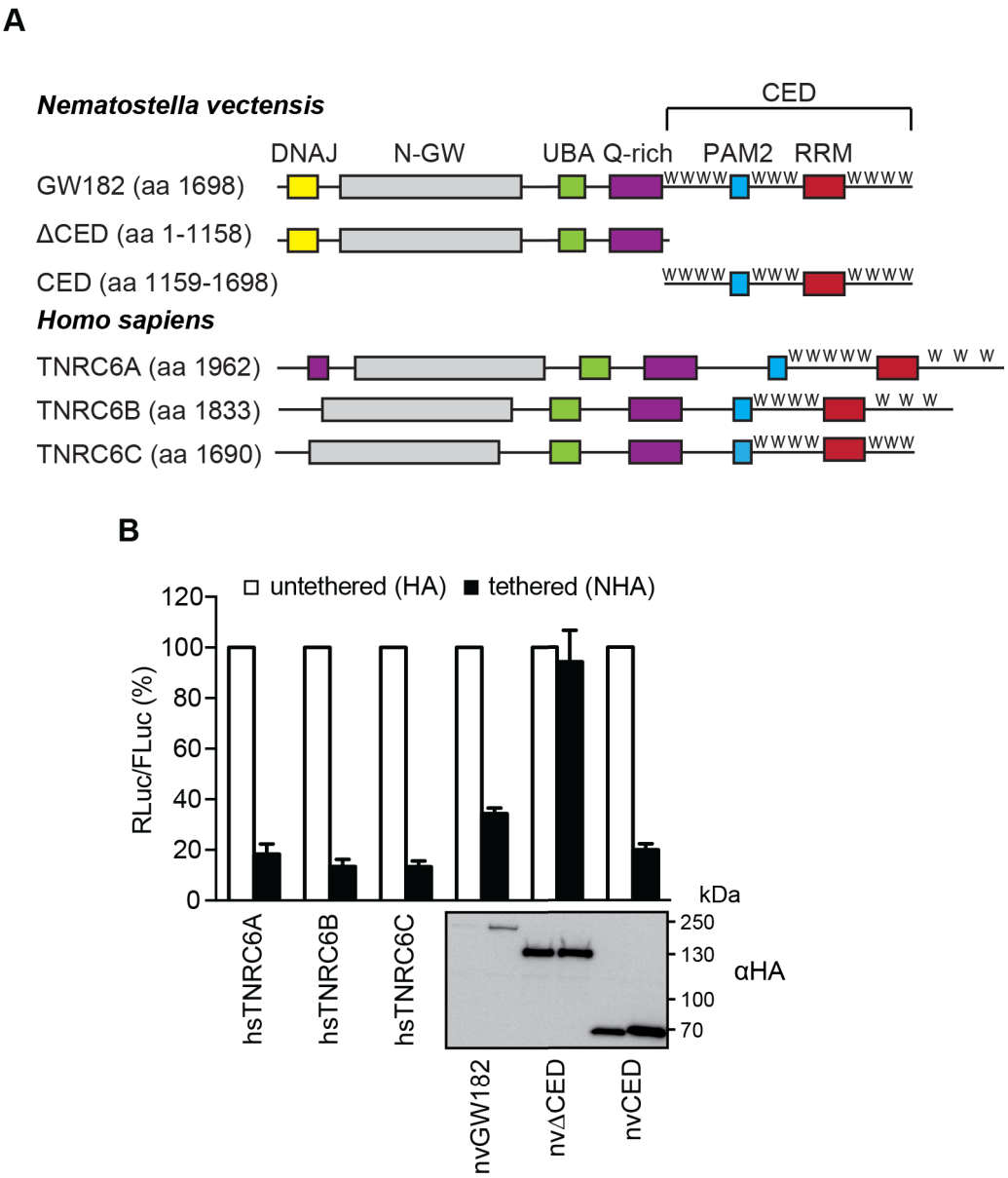

Figure 17. nvGW182 represses tethered mRNA via its C-terminal effector domain (CED) (A) Schematic representation of *Nematostella vectensis* GW182 (nvGW182), its human homologs TNRC6A, B and C, and their deletion mutants. DNAJ domain (yellow); N-GW: GW-repeat–rich region (grey); UBA: ubiquitin associated domain (green); PAM2: PABP associated motif 2 (light blue); RRM: RNA-recognition motif (red). The C-terminal effector domain (CED) is formed by RRM, PAM2 and the unstructured flanking regions with tryptophan-containing motifs, or W-motifs (W). The numbers correspond to the amino acid positions. **(B)** Repression of RLuc-boxB mRNA by NHA-nvGW182 and its deletion

mutants. Human HEK293 cells were co-transfected with plasmids encoding RLuc-boxB, FLuc, and full-length NHA-nvGW182 or indicated NHA-nvGW182 deletion mutants. As positive controls, plasmids encoding human NHA-TNRC6A, NHA-TNRC6B and NHA-TNRC6C were co-transfected. As negative controls, plasmids encoding untethered HA-fusions were used. RLuc activity was normalized to that of FLuc and presented as a percentage of RLuc produced in the presence of the corresponding untethered HA-fusions (open bars). Values represent means ± SD from 5 to 6 individual experiments (n=5-6). Expression levels of HA-fusion proteins were estimated by western blotting with antibodies directed against HA-peptide. This figure and figure legend was a panel of Figure 1 in Mauri et al., 2016.

Next, I tested if nvCED mediates repression via presumptive W-motifs (**Figure 18A**; W-motifs are shown in bold). For that, W residues in W-motifs were mutated (W → A) starting from the C-terminus and the effect of these mutations on expression of the tethered mRNA was analyzed (**Figure 18B**). Mutations of W-motifs indeed led to alleviation of repression by nvCED. As most alleviation was achieved when mutating the four N-terminal W-motifs, I decided to test if these motifs are the most critical for repression. For that, nvCED with sequential mutations of the four N-terminal W-motifs were generated (**Figure 18C**). These mutations lead to partial alleviation of repression (~2.5-fold), and repression was completely abrogated only when all eleven motifs were mutated (11W11A). These results suggest that W-motifs act in an additive manner to mediate silencing. Importantly, W-motifs were also required for mRNA silencing in the context of the full-length nvGW182 (**Figure 18D**). Western blot analysis of the NHA-nvCED and NHA-nvGW182 confirmed that the differences in their repressive potential cannot be attributed to differences in expression levels (**Figure 18B-D**).

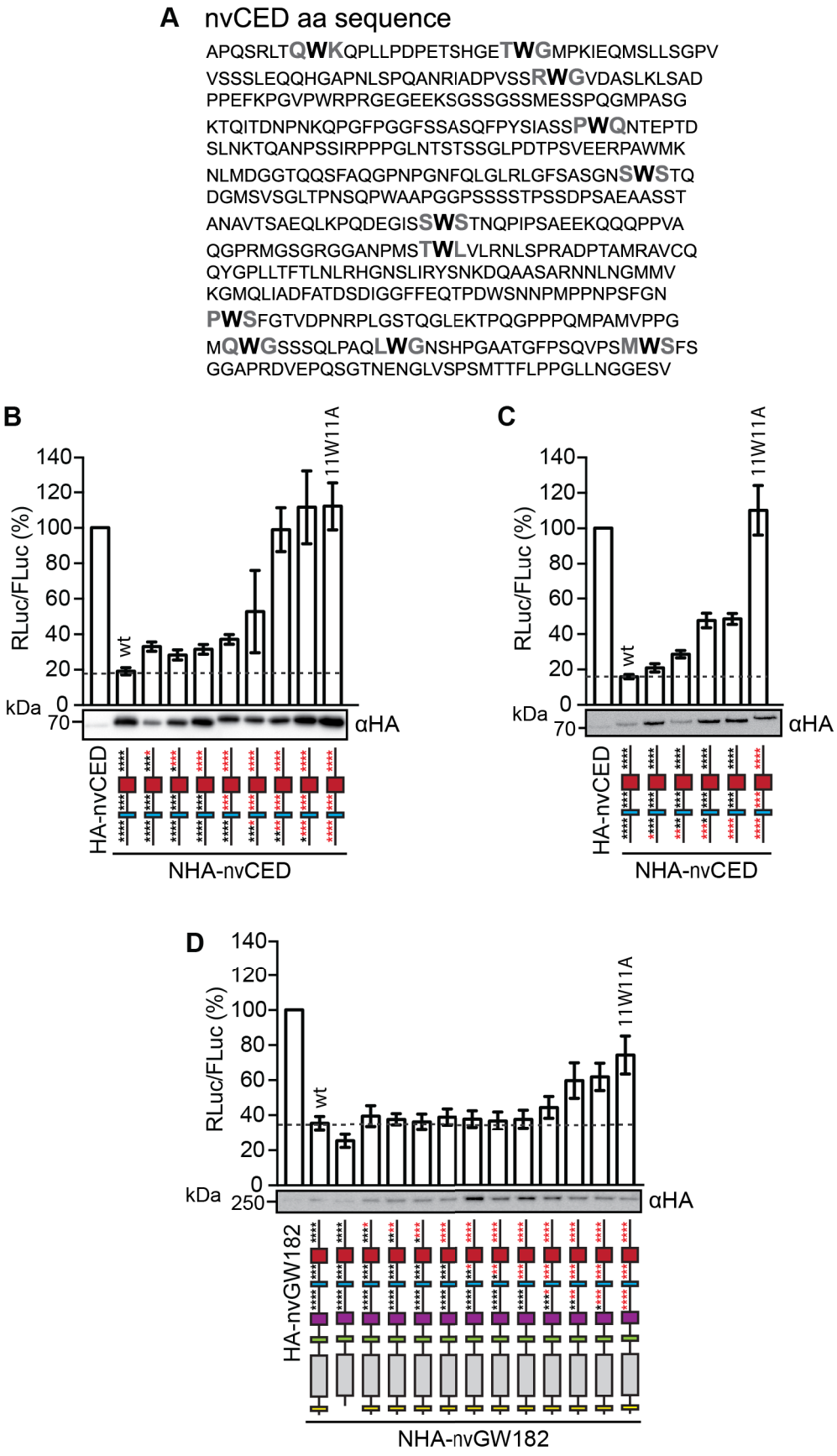

Figure 18. nvGW182 represses tethered mRNA via W-motifs (A) Sequence of the nvGW182 CED (nvCED) with tryptophans in presumptive W-motifs shown in bold. **(B)**

Mutations of W residues (W→A) in W-motifs alleviate repression by the nvCED. Plasmids encoding either wt NHA-nvCED or its indicated mutants were co-transfected into HEK293 cells, together with RLuc-5BoxB and FLuc. As negative control, untethered HA-nvCED was used. Mutants 1W1A through 11W11A contain up to eleven mutated W residues (for details, see Materials and Methods). Schematic representations of nvCED constructs are drawn below the corresponding bars. Asterisks indicate presumptive W-motifs; W residues are shown in black and W→A mutations in red. Data were analyzed and presented as in Figure 17B (means ± SD; n=4-10). Expression of NHA-fusion proteins was estimated by western blotting. **(C)** W-motifs additively contribute to repression by tethered nvCED. Experiment was performed as in (B), except that nvCED with four N-terminal W-motifs mutated were used (means ± SD; n=4). (D) W-motifs contribute to repression by the full-length nvGW182. Experiment was performed as in (B), except that full-length nvGW182 was used instead of nvCED domain (means ± SD; n=4-12). This figure and figure legend corresponds to Figure 2 in Mauri et al., 2016.

2.3.2 W-motifs of *Nematostella* GW182 recruit the CCR4-NOT complex

To understand how nvGW182 mediates repression, proteins interacting with nvGW182 and its repressive domain nvCED were identified. Either full-length GST-nvGW182 or its deletion mutants (GST-nvΔCED, GST-nvDNAJ, GST-nvCED) were expressed in HEK293 cells; pulled down with a GST tag and analyzed by mass spectrometry (**Figure 19A-D**; **Tables S2-S5**). Similarly to their mammalian counterparts[275-277,286,361,362], the full-length nvGW182 and wt CED associated with components of the human CCR4-NOT complex, CNOT1, CNOT2, CNOT3, CNOT9 and PABP proteins.

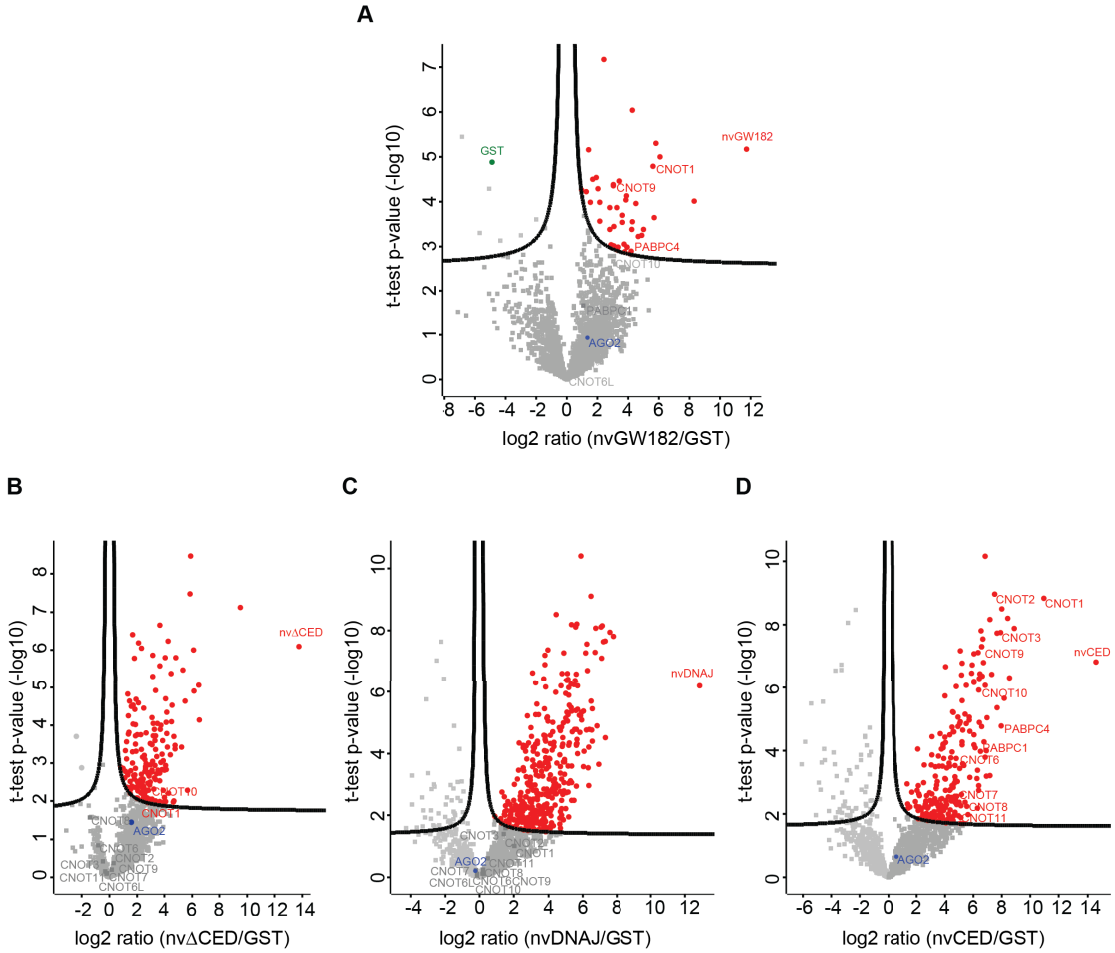

Figure 19. Quantitative Mass Spectrometric analysis of proteins associated with nvGW182 and its deletion mutants nvΔCED, nvDNAJ and nvCED Subunits of the CCR4-NOT complex and PABP proteins interact with nvGW182 via its CED. Human AGO2 (labeled in blue) is not capable of interacting with nvGW182 or with its domains. **(A)** Volcano plot showing nvGW182-enriched interactors over GST control. The logarithmic ratios of protein intensities were plotted against negative logarithmic p-values of a two sample t-test (two sided). A hyperbolic curve separates significantly enriched proteins (shown in red) from common binders (FDR≤ 0.05; S0=0.1; n=2, biological replicates). CCR4-NOT subunits and PABP proteins are labeled in red if enriched or in grey if not enriched, AGO2 is labeled in blue and the baits are shown in red. **(B-D)** Volcano plots showing, from left to right, nvΔCED, nvDNAJ and nvCED-enriched interactors (shown in red) over GST control. Only proteins identified in (A) as nvGW182 binders (log_2 ratio nvGW182/GST> 0; 1337 proteins total) were considered for the analysis. Analysis was done as described in (A). CCR4-NOT subunits and PABP proteins are labeled in red if enriched or in grey if not enriched, AGO2 is labeled in blue and the baits are shown in red.

As silencing was mediated by W-motifs present in nvCED, the 11W11A nvCED mutant was included as a negative control. Importantly, interactions with the CCR4-NOT subunits were lost in nvCED 11W11A mutant, demonstrating that nvGW182 recruits deadenylases via W-motifs (**Figure 20A**). As both wt and 11W11A mutant nvCED proteins contain the PAM2, they both interacted with PABP. The PAN2/PAN3 deadenylation complex was not detected among the interactors of nvGW182, although it was previously found to bind human and Drosophila GW182 via W-motifs[275,276]. Thus, interaction with PAN2/PAN3 might not be conserved in *Nematostella*. Alternatively, it is possible that PAN2/PAN3 was not detected in the nvCED pull-downs because it is a weaker interactor than CCR4-NOT. To validate the results of the mass spectrometry, the content of GST pull-downs was analyzed by western blotting. Indeed, both CNOT7/CAF1 and CNOT9 interacted with the wt nvCED, but not with the 11W11A mutant variant (**Figure 20B**). When only four N- or C-terminal W-motifs were mutated (N-4W4A and C-4W4A), nvCED retained most of its affinity to the CNOT7 subunit (**Figure 20C**), suggesting an additive role of W-motifs in the CCR4-NOT recruitment.

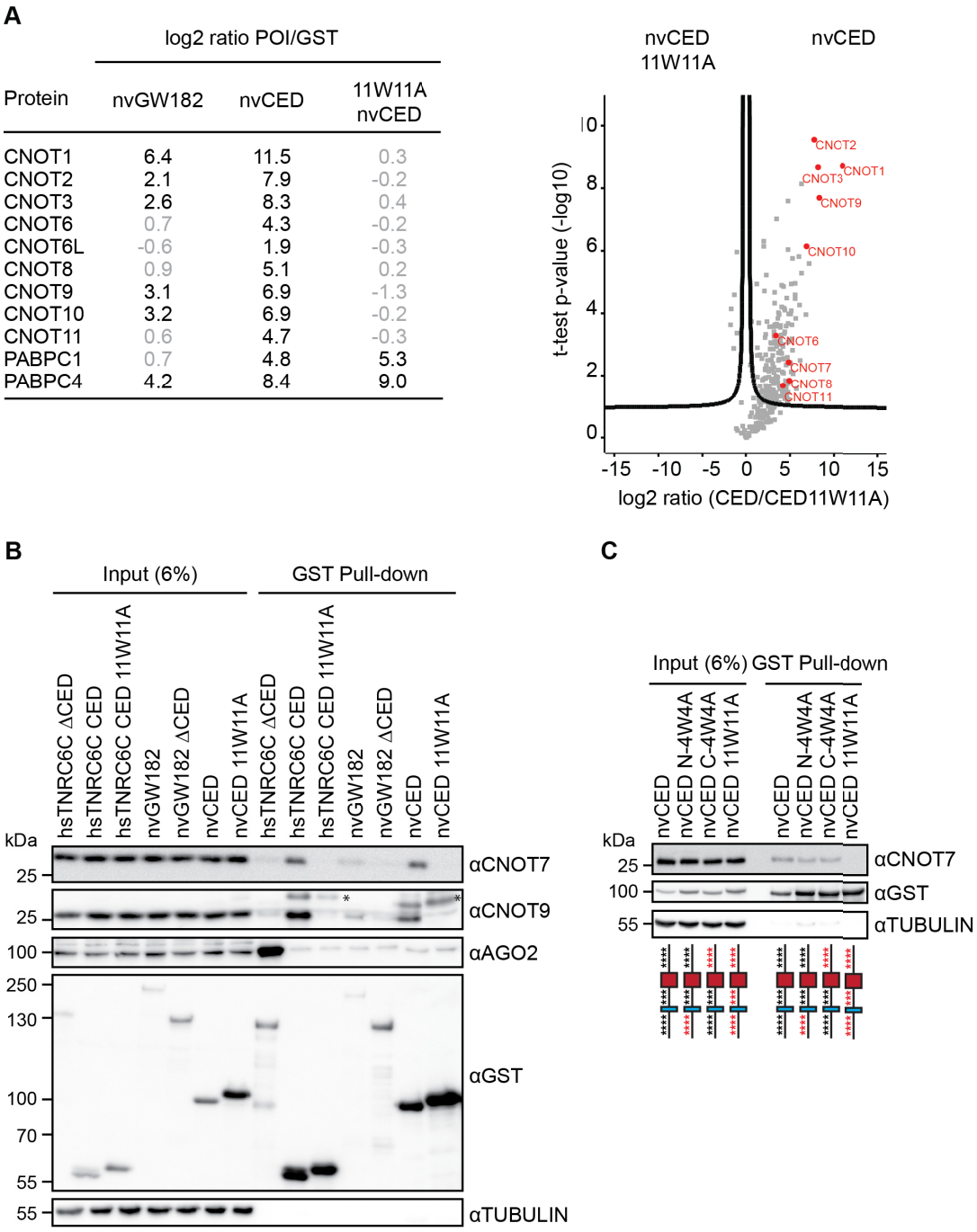

Figure 20. nvGW182 recruits subunits of the CCR4-NOT complex via its W-motifs

(A) Quantitative mass spectrometric analysis of proteins associated with nvGW182. The GST-nvGW182 full-length constructs, the nvCED domain only, as wild type and 11W11A mutant variant, were expressed in HEK293 cells and affinity purified using GST. GST alone was used as a negative control. On the left, relevant interactors for each variant are listed along with their corresponding enrichment factor (the $\log_2$ ratios of label-free quantification values (LFQ intensity) over corresponding LFQs detected in pull-down of GST tag alone). On the right, volcano plot showing proteins with differential binding to

nvCED and nvCED11W11A variant. The logarithmic ratios of protein intensities were plotted against negative logarithmic p-values of a two sample t-test (two sided). A hyperbolic curve separates significantly enriched proteins from common binders. Selected interactors recruited via W-motifs of nvCED are labeled in red (FDR≤ 0.05; S0=0.1; n=2, individual experiments). **(B)** Validation of CCR4-NOT-nvCED interactions identified in (A). Nuclease-treated cell lysates from HEK293 expressing GST-fusions of the indicated proteins were used in GST pull-downs, and inputs (6%) and GST pull-downs were analyzed by western blotting using the indicated antibodies. Human TNRC6CΔCED was used as positive control for AGO2 binding. TNRC6C CED and TNRC6C 7W7A CED were used as positive and negative controls for CNOT7 and CNOT9 binding. Asterisks (*) indicate unspecific bands. **(C)** W-motifs function additively to recruit the CCR4-NOT complex. The experiment was performed as in (B), except that nvCED with four N-terminal (N-4W4A) or C-terminal (C-4W4A) W-motifs mutated were used for pull-downs. nvCED and nvCED 11W11A were used as positive and negative controls for CNOT7 binding, respectively. Schematic representations of nvCED domains are shown below the corresponding lanes. Asterisks indicate W-motifs; W residues are shown in black and W→A mutations in red. This figure and figure legend corresponds to Figure 3 in Mauri et al., 2016.

2.3.3 *Nematostella* GW182 represses translation and mediates mRNA degradation via the CCR4-NOT deadenylase complex

"The CCR4-NOT complex includes two deadenylation enzymes, CNOT6/CNOT6L and CNOT7. To test if the deadenylation activity of the recruited CCR4-NOT complex contributes to nvGW182-mediated repression, catalytically inactive mutants of CNOT6 ($CNOT6_{cat}$) and CNOT7 ($CNOT7_{cat}$) subunits were used[377]. These mutants function as dominant negative and their overexpression leads to mRNA stabilization because of decrease in deadenylation rates. Therefore, if function of nvGW182 involves CCR4-NOT-mediated deadenylation, I expect that interfering with CNOT6 and CNOT7 deadenylation activity would affect repression by nvGW182. Indeed, when co-expressing increasing amounts of $CNOT6_{cat}$ and $CNOT7_{cat}$, partial alleviation of repression by nvGW182 and nvCED is observed (**Figure 21A**) accompanied by stabilization of tethered mRNA (**Figure 21B**). In bilaterians GW182 mediates not only mRNA deadenylation via CCR4-NOT, but also translational repression[267,275]. To test if *Nematostella* protein functions similarly, I tested the silencing effects of nvGW182 and of nvCED on the tethered RLuc-boxB reporter mRNA and on its protein product by qRT-PCR and luciferase

assay, respectively, and compared their expression levels (**Figure 21C**). This analysis confirmed that inhibition of protein production (filled bars) couldn't be fully explained by changes in mRNA levels (open bars), suggesting that nvGW182 affects both mRNA stability and translation. Importantly, no silencing was observed with the 11W11A nvCED mutant, defective in CCR4-NOT recruitment, indicating a role for W-motifs in both mRNA decay and translational repression. Altogether, these results suggest that the mechanism by which GW182 protein represses mRNA may be conserved between *Nematostella*, flies and mammals."

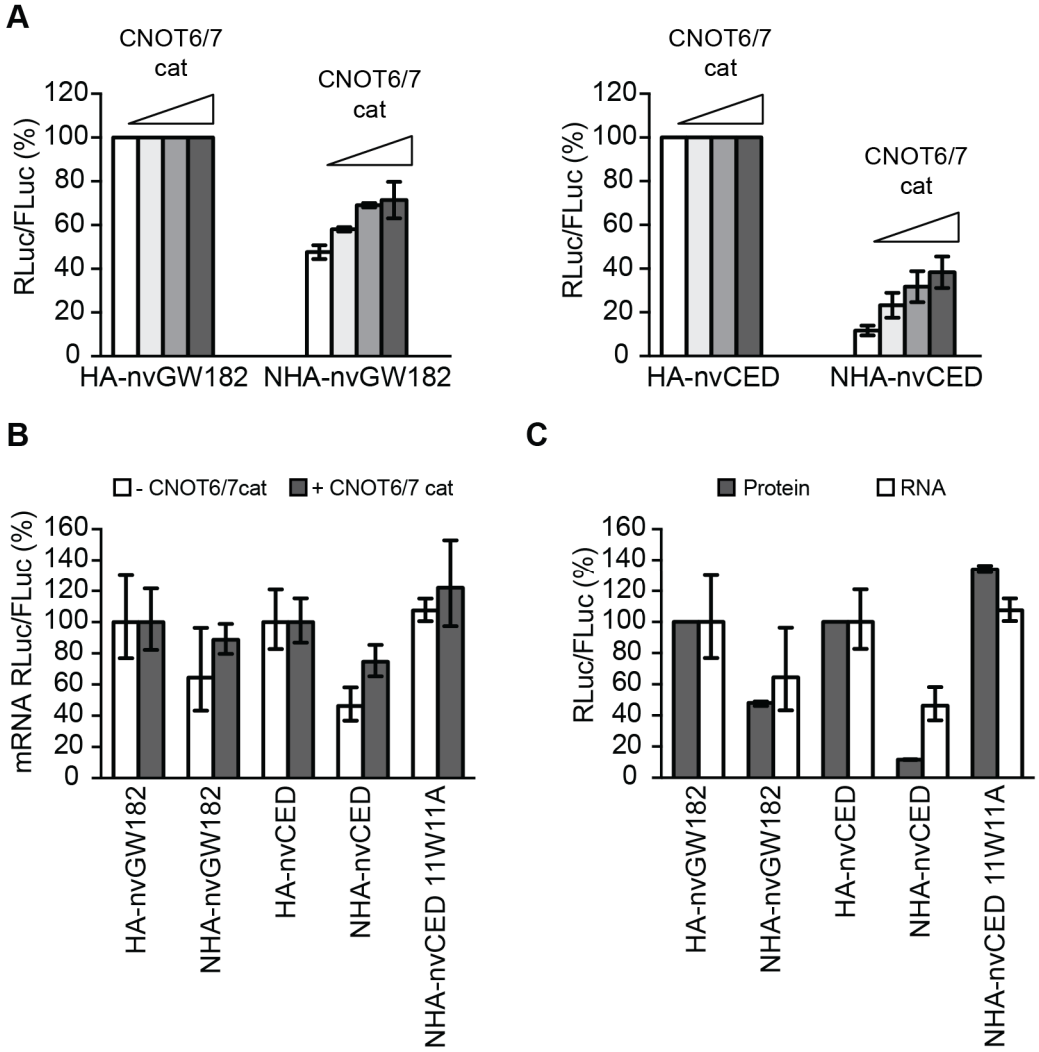

Figure 21. nvGW182 represses translation and mediates mRNA degradation via CNOT6/CNOT7 deadenylases (A) The deadenylation catalytic activity of the CCR4-NOT complex contributes to nvGW182-mediated silencing. HEK293 cells were co-transfected with RLuc-boxB, FLuc, tethered NHA-nvGW182 or NHA-nvCED, and increasing amounts of CNOT6 and CNOT7 catalytic mutants ($CNOT_{cat}$). Untethered HA-fusions were used as negative controls (means ± SD; n=3-6). **(B)** Interfering with the CCR4-NOT deadenylation

activity leads to stabilization of nvGW182-bound mRNAs. RLuc and FLuc mRNA from nvGW182-tethering experiments shown in (A) were estimated by qRT-PCR. Filled bars: +$CNOT_{cat}$; open bars: -$CNOT_{cat}$. RLuc values were normalized to FLuc mRNA. Untethered HA-fusions were used as negative controls (means ± SD; n=2). **(C)** nvGW182 silences tethered mRNA via translational repression and stimulation of mRNA decay. RLuc and FLuc mRNA and protein levels from nvGW182-tethering experiments were estimated by qRT-PCR (RNA, open bars) and luciferase assays (protein, filled bars). Data were normalized and presented as in (A and B). This figure and figure legend corresponds to Figure 4 in Mauri et al., 2016.

2.3.4 *Nematostella* GW182 interacts with Nematostella AGOs, but fails to bind human AGOs

In order to function in the miRNA silencing pathway, GW182 proteins need to be recruited to an mRNA via direct interaction with AGO:miRNA complex, which is happening via the N-terminal GW repeats[311,331,333,335,355]. Intriguingly, mass spectrometry performed on the GST pull-downs of nvGW182 or its N-terminal regions (nvΔCED, nvDNAJ) did not detect any significant interaction with human AGO proteins (shown previously in **Figure 19**). This result was validated by western blotting on the GST pull-downs with αAGO2 antibody; the N-terminal domain of human TNRC6C (TNRC6C ΔCED) was used as a positive control for AGO2 binding (**Figure 22A** and previously **in 20B**). Indeed, a strong interaction between AGO2 and human TNRC6C ΔCED was detected, but not with nvGW182 domains overexpressed in HEK293 cells. The possible explanations of this result are that (I) nvGW182 binds only *Nematostella*, but not human AGOs, because of low conservation of binding sites or (II) nvGW182 is recruited to mRNA via a different RNA-binding protein. To discriminate between these possibilities, HA-tagged *Nematostella* AGOs, nvAGO1 and nvAGO2, were overexpressed in human HEK293 cells, together with GST-nvGW182 domains. Binding of nvAGO1 and nvAGO2 to nvGW182 was then tested in GST pull-downs (**Figure 22A**). Western blotting with αHA antibody showed that nvAGOs interact with the N-terminal domain of nvGW182 protein (nvGW182 ΔCED), but not with its human homolog (TNRC6C ΔCED). These results suggest that GW182-AGO interaction regions are not conserved between human and *Nematostella*. Consistently with this result, *Nematostella* AGOs were not able to repress tethered mRNA, unlike human AGO2 (hsAGO2) used as a positive control (**Figure 22B**).

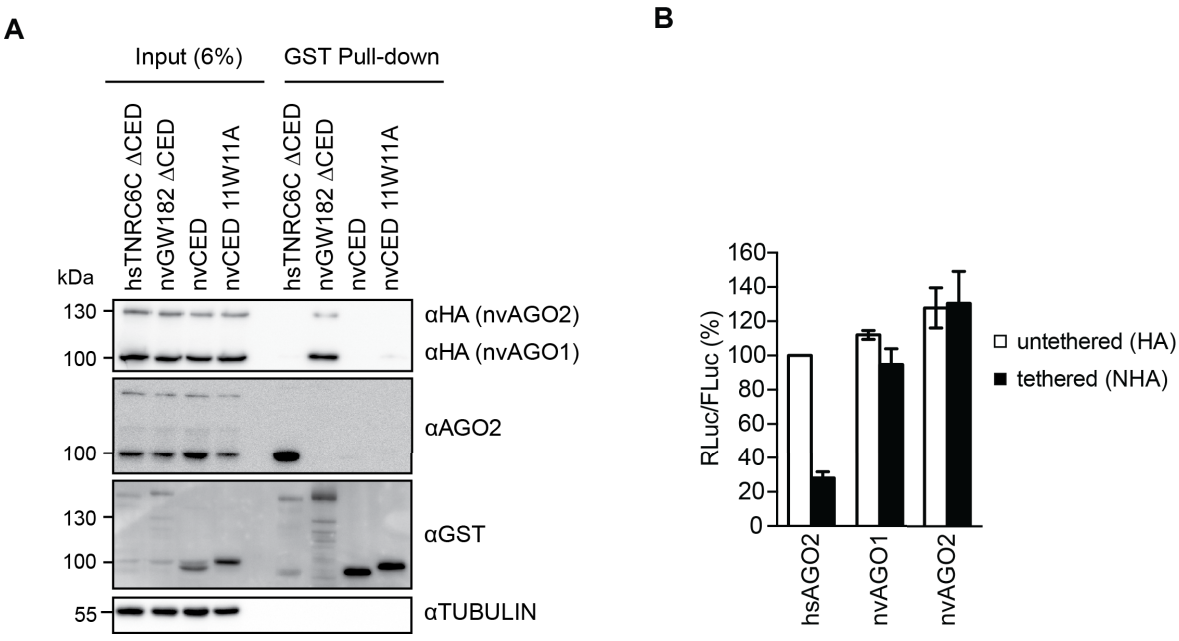

Figure 22. GW182-AGO interaction regions are not conserved between human and Nematostella (A) nvGW182 binds nvAGOs, but not human AGO2. GST-fusions of nvGW182 or its domains were co-expressed with HA-tagged nvAGO1 and nvAGO2 in HEK293 cells, pulled down with GST tag, and inputs (6%) and GST-pulldowns were analyzed by western blotting using the indicated antibodies. Human TNRC6CΔCED was used as positive control for human AGO2 binding. **(B)** *Nematostella* AGOs are not able to repress tethered mRNA in human cells. Human HEK293 cells were co-transfected with RLuc-boxB, FLuc, and NHA-nvAGO1 or NHA-nvAGO2. Human AGO2 (NHA-hsAGO2) was used as a positive control. As negative controls, plasmids encoding untethered HA-fusions were used (means ± SD; n=3). This figure and figure legend correspond to panel A and B of Figure 5 in Mauri et al., 2016.

Previous works[331,339] have shown that human GW182 proteins have multiple regions capable of AGO binding. Interaction with AGO is mediated by tryptophan residues, but these AGO-binding motifs are functionally distinct from the CCR4-NOT-binding W-motifs[275,355]. Analogously to human TNRC6 proteins, nvGW182 has several tryptophan residues within its disordered N-terminal domain (**Figure S7**) suggesting interaction with AGO proteins may also occur via multiple tryptophan-containing motifs. To test this possibility, a set of N-terminal deletion mutants containing different amount of potential AGO-binding tryptophans was generated (asterisks; **Figure 23A**). In order to assess the ability of the generated nvGW182 deletions to recruit nvAGOs, GST pull-down assays were performed (**Figure 23B**). Deletion of N-terminal portions lead to gradual reduction of nvAGOs

signal, suggesting that nvGW182 recruits nvAGOs via multiple regions, similarly to human orthologs.

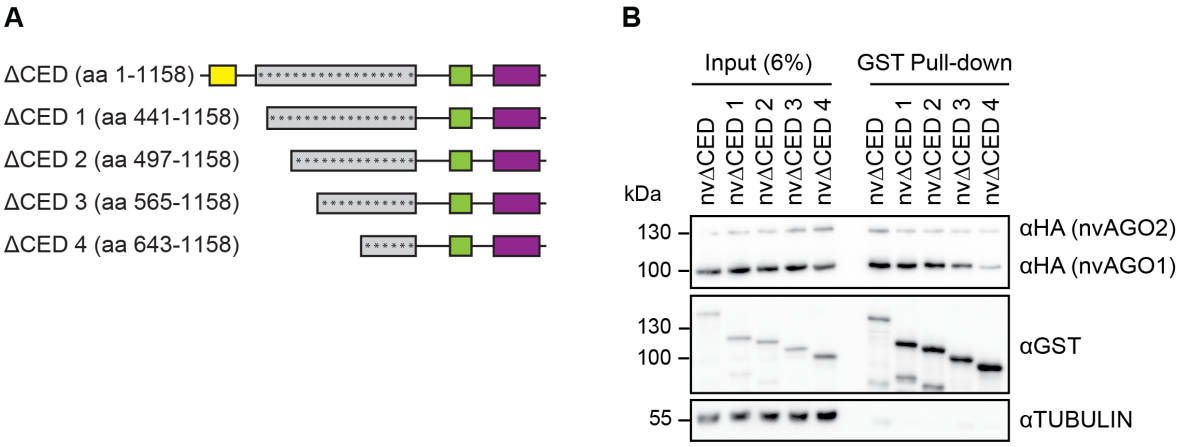

Figure 23. Multiple tryptophan-containing regions of nvΔCED contribute to nvAGO binding (A) Schematic representation of nvΔCED deletion mutants used in (B). The numbers correspond to the amino acid positions. Asterisks represent putative AGO-binding motifs. **(B)** Multiple regions of nvΔCED contribute to nvAGOs binding. GST-fusions of nvΔCED deletion mutants were co-expressed with HA-nvAGOs in HEK293 cells, nuclease-treated lysates were used in GST pull-downs and inputs (6%) and GST pull-downs were analyzed by western blotting using the indicated antibodies. This figure and figure legend corresponds to panel C and D of Figure 5 in Mauri et al., 2016.

To understand whether the lack of inter-species interactions between AGO and GW182 proteins could be explained by a divergence in AGO sequences, human, *Drosophila* and *Nematostella* AGO proteins were aligned (**Figure 24**). The alignment shows how the residues forming the tryptophan binding pockets responsible for direct interactions with TNRC6 proteins in humans are mostly identical (pocket 1, orange and red residues; pocket 2 green residues). This observation, together with the results obtained from deletion mutants shown in **Figure 23B** suggests that the mode of interaction between AGO-GW182 proteins may be conserved. Probably, the structures of nvΔCED and/or nvAGOs are sufficiently different from their human counterparts, thus preventing inter-species interactions.

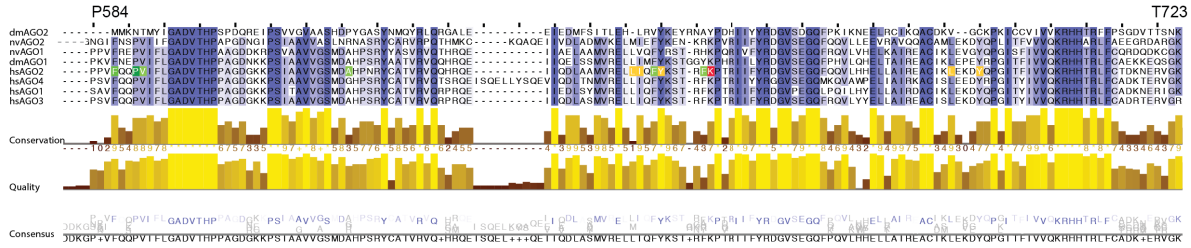

Figure 24. W-binding pockets of human AGOs are conserved in nvAGOs Amino acid sequence alignment of *Nematostella* AGOs (nvAGO1, nvAGO2), *Drosophila* AGOs (dmAGO1, dmAGO2) and human AGOs (hsAGO1, hsAGO2, hsAGO3, hsAGO4). The region aligning to aa 584-723 of hsAGO2 is displayed. Blue indicates amino acid conservation, the darker the blue the more conserved residues are. The residues forming two tryptophan-binding pockets hosting two W residues of TNRC6 proteins identified by Schirle et al., 2012[264] are highlighted in yellow (pocket 1; central residue is shown in red) and in green (pocket 2; central residue is shown in dark green). Histograms indicative of sequence conservation and quality of the alignment, and a consensus AGO sequence are displayed below the alignment. Sequence alignment of AGO proteins was performed with Clustal Omega (EBI) and visualized with Jalview.

Together, these results provide strong evidence that *Nematostella* GW182 can interact with human CCR4-NOT and *Nematostella* AGOs. Yet, they were obtained under overexpression conditions and in human cell cultures. To test whether those interactions also occur naturally in the sea anemone itself, Reuven Ahroni, in the laboratory of our collaborator Yehu Moran, performed immunoprecipitation (IP) from *Nematostella* embryonic lysates, using a custom antibody raised against nvAGO1 and a commercially available antibody against a region of human CNOT9 that is 94% identical to its *Nematostella* homolog. Both IPs were then tested by western blot, and showed the presence of nvGW182 in nvAGO1 and CNOT9 IP, but not in control mock IP performed with unspecific rabbit IgGs (**Figure 25**). These results indicate that AGO, GW182 and CNOT9 interact with one another in *Nematostella* like in mammals[267,268,275-277,361].

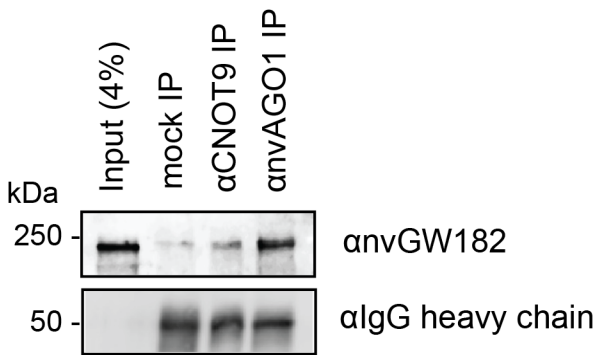

Figure 25. AGO, GW182 and CCR4-NOT natively interact in Nematostella *Nematostella* embryonic lysates were used in IP with α nvAGO1 and α CNOT9 antibody, and the co-immunoprecipitated proteins were analyzed by western blotting with α nvGW182 antibody. Unspecific rabbit IgG was used as a negative control. This figure and figure legend corresponds to panel E of Figure 5 in Mauri et al., 2016.

2.3.5 W-motifs of *Nematostella* GW182 contribute to bona fide miRNA silencing

"As nvGW182 does not interact with human AGOs, it cannot be used to rescue the depletion of TNRC6 proteins in mammalian cells. To overcome this issue and test whether nvGW182 can function in miRNA silencing, I generated a chimeric construct containing the N-terminal AGO-binding domain of human TNRC6A protein and C-terminal CCR4-NOT-binding domain of nvGW182 (**Figure 26A**). This chimeric construct was generated in two versions: wt and 11W11A mutant that does not interact with CCR4-NOT. The constructs were used in GST pull-downs to make sure that both wt and 11W11A chimeras are able to bind human AGO2 with the same efficiency (**Figure 26B**).

Next, chimeric human*/Nematostella* GW182 were tested in a *bona fide* miRNA repression assay. For that, HeLa cells were depleted of the endogenous TNRC6A and B using stably integrated inducible shRNA constructs, and chimeric GW182 proteins were tested for their ability to rescue miRNA repression. To assess miRNA-mediated silencing, cells were co-transfected with the Fluc/RLuc-hmga2 reporter, targeted by let-7 miRNA, which is endogenously expressed in HeLa cells (**Figure 26C**). In control cells let-7 efficiently repressed wt Rluc-hmga2 mRNA, when compared with the mutant reporter from which let-7-binding sites were disrupted (compare Rluc-hmga2 wt with RLuc-hmga2 mut, filled bars). Upon depletion of endogenous TNRC6 proteins (open bars), repression of the hmga2

reporter was alleviated. As shown previously, transfection of a plasmid encoding wt TNRC6A resistant to shRNA rescued the repression, and its unfuctional mutant TNRC6A 8W8A could not rescue[275]. Intriguingly, the chimeric protein carrying nvCED was also able to partially rescue miRNA-mediated silencing (wt chimera). Importantly, its function in miRNA silencing was dependent on the CCR4-NOT-recruiting W-motifs, as 11W11A mutant was not able to complement the knockdown of TNRC6 proteins." To summarize, these data suggest that W-motifs of nvGW182 mediate miRNA silencing in a genetic rescue experiment. In order to determine the consensus sequence of the CCR4-NOT-recruiting W-motif, shared between bilaterians and cnidarians, experimentally validated W-motifs in human, *Drosophila*[275] and *Nematostella* GW182 proteins (**Figure 18B-D**) were used as inputs for the MEME motif-searching algorithm[661]. The resulting consensus sequence of W-motif (**Figure 26D** and **Figure S9**) is rich in S, T and G residues, surrounding the invariant W suggesting W-motifs could be modulated by post-translational modifications (PTMs) such as S/T phosphorylation.

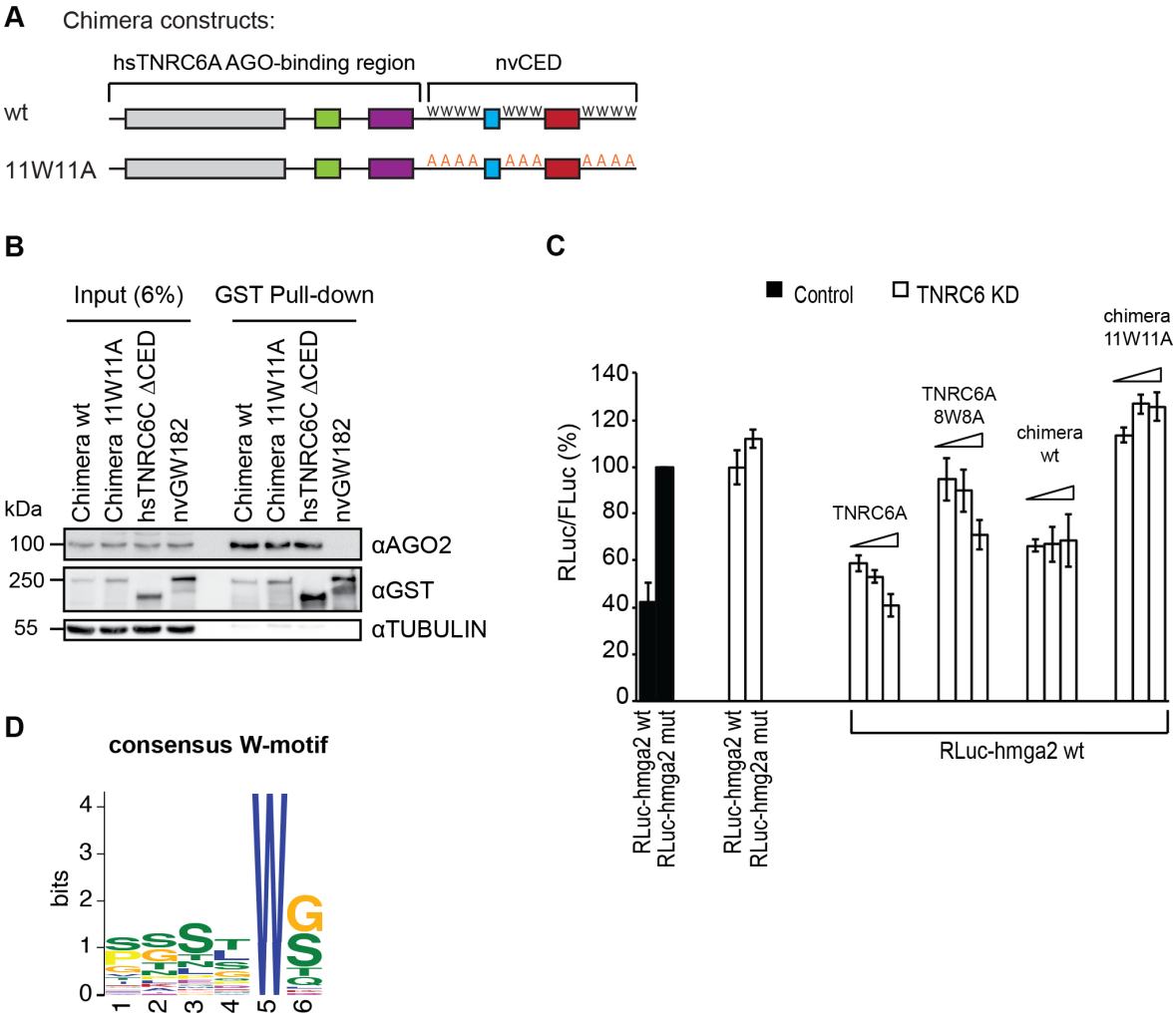

Figure 26. Human/Nematostella GW182 chimera partially rescues miRNA silencing in human HeLa cells (A) Schematic representation of human/*Nematostella* GW182 protein chimeras (h/nvGW182) used in (B) and (C). AGO-binding N-terminal region of human TNRC6A was fused to nvCED, either wt or 11W11A mutant. **(B)** h/nvGW182 chimera binds endogenous human AGO2. Nuclease-treated lysates from HEK293 cells expressing GST-fusions of the indicated proteins and their domains were used in GST pull-downs, and inputs (6%) and GST pull-downs were analyzed by western blotting using the indicated antibodies. **(C)** W-motifs of h/nvGW182 chimera are required to rescue depletion of endogenous TNRC6 proteins. HeLa cell line carrying stably integrated inducible shRNAs construct against endogenous TNRC6A and B was used for TNRC6 knockdown experiments (open bars); HeLa cells not expressing TNRC6-directed shRNAs was used as a control (filled bars). Expression of shRNAs was induced for 2 days prior to transfection of miRNA reporters and rescue constructs. Cells were transfected with RLuc-hmga2 reporter containing let-7 sites or its mutant version (RLuc-hmga2 mut), and increasing amounts of plasmids expressing h/nvGW182 chimera or its 11W11A mutant. TNRC6A was used as a positive control. Values represent percentages of RLuc activity

produced by hmga2-mut reporter without TNRC6 depletion (means ± SD; n=3). **(D)** Graphic representation of the W-motif that recruits the deadenylation complexes and is conserved in human, *Drosophila* and *Nematostella,* The consensus was derived with the MEME suite[661], see also **Figure S9**. This figure and figure legend was adapted from Figure 6 in Mauri et al., 2016.

3. Discussion

3.1 Modulation of miRNA silencing via W-motif specific Interactome of TNRC6 proteins

W-motifs are the effectors of miRNA-mediated silencing in animals. In fact proteins of the GW182 family recruit the downstream effectors of miRNA silencing specifically via these short type of linear tryptophan-containing motifs present throughout unstructured regions of the GW182/TNRC6 protein family[275]. The functional relevance and mode of interactions between GW182 W-motifs and the CCR4-NOT deadenylase complex have been well established[267,268,275,277]. Hence, previously unstudied interactors recruited via W-motifs are likely candidates to modulate or mediate miRNA-mediated repression. In this study, the W-motif-specific interactome of human TNRC6C was identified and a potential role of clathrin-coated vesicles (CCVs) as modulator of miRNA-silencing has emerged.

3.1.1 Speculative model for regulation of miRNA silencing by components of clathrin-coated vesicles

GW182/TNRC6 proteins are crucial components of metazoans miRISC that direct miRNA silencing by binding to AGO and CCR4-NOT proteins[81]. Previous reports identified the C-terminal domain of GW182 proteins as their silencing domain (CED)[335,337,338,340]. Through the action of multiple W-motifs, GW182 CED recruits the CCR4-NOT deadenylase complex, thereby leading to repression of mRNA targets[267,268,275-277]. Using TNRC6C CED wt and mutants where W-motifs were disrupted, a TNRC6C W-motif-specific interactome was identified (**Figure 8**). Since W-motifs are indispensable for miRNA-silencing, these novel protein-protein interactions are likely to modulate miRNA-mediated repression. Several components of the coat of clathrin-coated vesicles (CCVs) resulted enriched with wt CED as compared to 7W7A and 7W7Y CED mutants (**Figure 9**). For instance, binding of clathrin heavy and light chains (CLTC and CLTA) and of various subunits of adaptor proteins of class 2 (AP2 complex including AP2A, AP2B, AP2M, and AP2S) was lost when mutating the central tryptophan residue of W-motifs to either alanine or tyrosine. Having identified not only one, but several

components of CCVs, further supported the idea that these interactors could be functionally relevant candidates. Consistently, previous studies identified CLTC as an interactor of TNRC6B in HeLa cells [331], and CLTC and AP2A proteins as RNA-independent interactors of AGO in mouse embryonic fibroblasts (MEFs)[665]. Given that AGO and TNRC6 interact in the miRISC complex, and that the C-terminal domain of TNRC6C used in this study is incapable of binding AGO, our data suggests that interactions with CLTC and AP2A proteins are mediated by W-motifs of TNRC6 proteins. Thus, AGO proteins are indirectly recruited to AP2A-CLTC via TNRC6 proteins. Additionally, AGO and TNRC6A/B were identified by MS as novel components of CCV coats[664]. By isolating CCVs from human HeLa cells, I could show that TNRC6 and AGO proteins co-sediment with these vesicles (**Figure 11**). Moreover, AP2A appendage regions protruding from the clathrin coat mediated interactions with TNRC6C CED via W-motifs (**Figure 12**), indicating TNRC6-CCV interactions are localized on the outer surface of the vesicles. Interestingly, the RNA isolated from CCV preparations obtained from HeLa cells expressing RLuc-hmga2 wt or mut let-7 reporters was not enriched in wt reporter mRNA (**Figure 13**). This result possibly suggests that the CCV-associated TNRC6-AGO module is not engaging in miRNA-mediated silencing. Accordingly, Frohn et al.[665] observed that interactions between CLTC, AP2A and AGO2 are 2- to 4-fold stronger in a Dicer knock out MEF cell line as compared to wt MEF. Since Dicer knock out prevents the maturation of small RNAs, including miRNAs, this piece of evidence suggests that clathrin and AP2A interact better with a miRNA-unloaded form of AGO2.

Upon depletion of AP2A1/2 proteins, let-7-mediated silencing of RLuc-hmga2 reporters became approximately twofold stronger (**Figure 14**), pointing to a potential role of AP2A proteins in opposing miRNA-mediated repression. An implication of these results is the possibility that CCVs sequester TNRC6-AGO2 from the repression machinery (the CCR4-NOT deadenylation complex), thereby modulating the degree of miRNA-mediated silencing. Consistently, knockdown of two subunits of the CCR4-NOT complex, namely CNOT1 and CNOT9, promoted binding of TNRC6C CED to AP2A proteins by ~3- 4-fold (**Figure 15**). However, knockdown of AP2A/CLTC did not increase interactions with CCR4-NOT, arguing against the sequestration model. One possibility is that, since CCR4-NOT is abundant in cells (**Figure 9D** and **Figure S13**), TNRC6C CED could already be

saturated by CNOT interactions. As clathrin forms CCVs in association with different classes of adaptor proteins (AP1, AP2, AP3 and AP4), another possibility is that the knockdown of multiple AP families is required to observe increased CNOT binding. Alternatively, this observation could mean that the increase in miRNA silencing upon AP2A knockdown is mediated by a W-motif-binding factor other than CCR4-NOT. Hence, this evidence may suggest CCVs are sites of storage or recycle of TNRC6 and AGO proteins. It is also possible that the pool of CCV-interacting TNRC6-AGO complex has posttranslational modifications that prevent it from binding to the CCR4-NOT complex.

It is worth noting that, in contrast to the results obtained using RLuc-hmga2 reporters (**Figure 14**), AP2A depletion did not enhance let-7-mediated repression of RLuc-3xb reporters (**Figure S5**). One possible explanation for this discrepancy is that AP2A affects silencing of only a specific subset of miRNA targets, as was previously shown to be the case for enhancers of decapping[479]. Additionally, the endogenous hmga2 3'-UTR (with six endogenous let-7 binding sites) may recapitulate miRNA repression *in vivo* better than the artificial 3'-UTR of Rluc-3xb reporters (with three artificial let-7 binding sites). To test this hypothesis, one would need to perform additional assays using more reporters bearing endogenous 3'-UTRs. Another possibility is that the effect of AP2A knockdown on miRNA silencing can only be observed on newly synthesized targets. In fact RLuc hmga2 reporters were inducible and luciferase assays were performed 4 h post induction, when miRNAs silence via a combination of translational repression and mRNA decay[392]. RLuc-3xb reporters were instead analyzed at steady state, when mRNA decay is the prevalent mode of miRNA silencing. To investigate this possibility one would need to deplete AP2A proteins and perform kinetic analysis using inducible miRNA reporters in order to monitor reporters mRNA and protein expression levels at different time points.

Taken together, these results have shown that CCVs recruit TNRC6-AGO2 complexes via interactions between AP2A appendages and TNRC6 W-motifs. Despite AP2A depletion enhanced silencing of RLuc-hmga2 reporters, it did not increase interactions with the CCR4-NOT complex. However, depletion of CCR4-NOT promoted interactions between AP2A and TNRC6C proteins. Possibly, different modifications of TNRC6 proteins control the switch between CCVs and CCR4-NOT interactions. Earlier studies already suggested a link between

vesicular trafficking and miRNA-mediated repression by identifying miRISC as a component of endosomes and multi vesicular bodies (MVBs)[424,425]. The authors of these two studies proposed that MVBs modulate miRNA silencing by promoting GW182 turnover[424,425]. Similarly, interactions between TNRC6-AGO and CCVs could represent a cellular strategy to store and recycle core components of miRISC. Indeed CCV-bound TNRC6-AGO complex seems to be freed from its miRNA targets (**Figure 13**). A speculative model illustrating the possible functions of CCV-TNRC6 interactions is shown in **Figure 27**. Moreover, clathrin-mediated vesicular trafficking is more prominent in neuronal cells and brain tissues, specifically AP2-CCVs mediate recycling at synaptosomes[671]; and AP1 and CLTC have been shown to contribute to the establishment of cell polarity in mice and worms[666]. These observations leave open the intriguing possibility that this mechanism could primarily regulate the neuronal concentrations of TNRC6-AGO proteins available to engage in interactions with miRISC, thereby controlling neuronal miRNA-mediated regulation of gene expression.

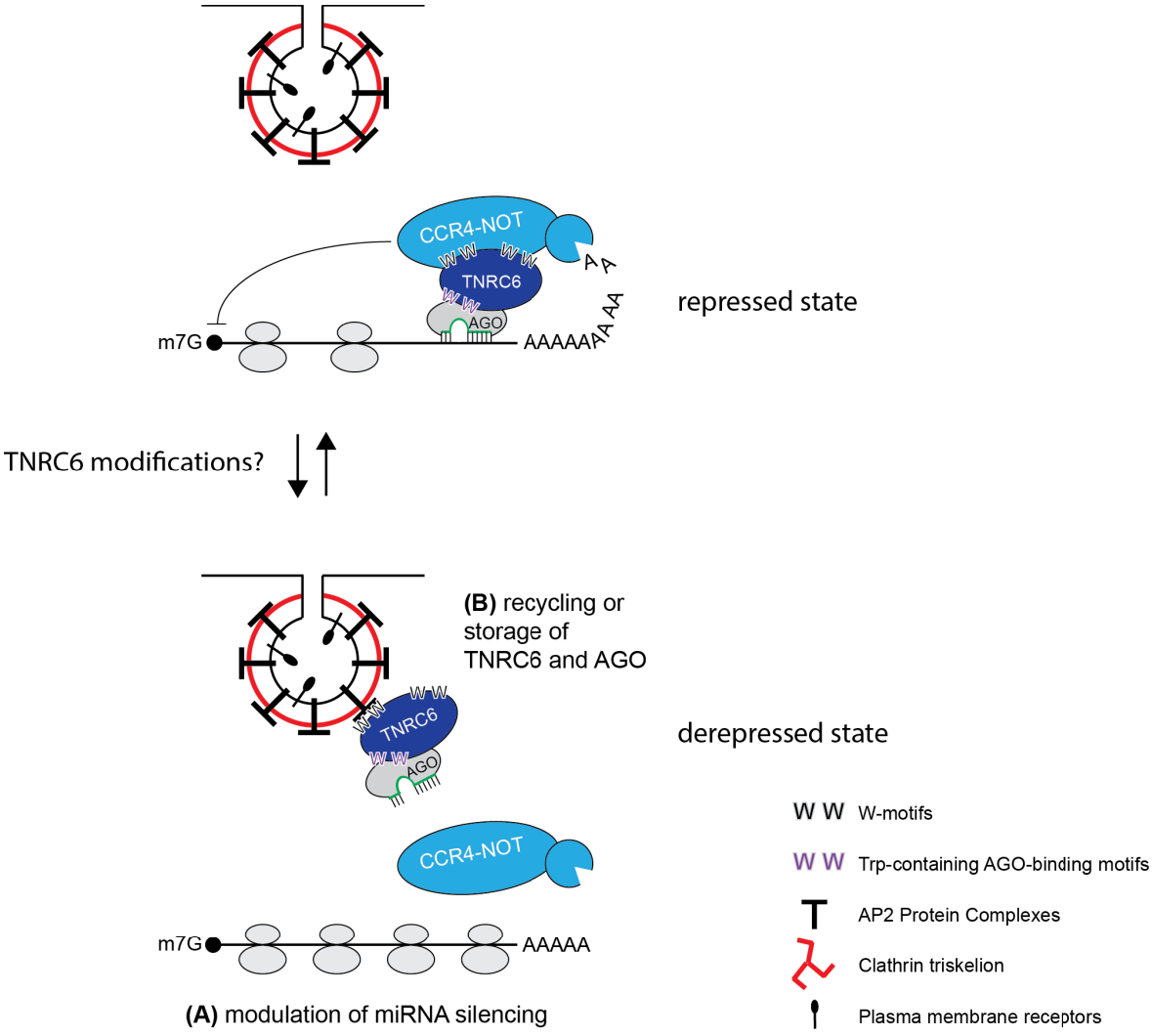

Figure 27. Speculative model illustrating CCVs modulation of miRNA silencing miRNA-loaded AGOs directly recruit TNRC6 proteins to target mRNAs. TNRC6 recruit the CCR4-NOT deadenylase complex to promote translational repression and the decay of target mRNAs through direct interactions with W-motifs. Alternatively, TNRC6 W-motifs direct the TNRC6-AGO complex to CCVs via interactions with AP2A proteins. **(A)** CCVs may free miRNA targets from the repressor complex TNRC6-AGO, thus alleviating miRNA silencing. **(B)** Another option is that CCVs are storage or recycling sites for TNRC6 and AGO proteins that are not actively participating in miRNA silencing. Possibly, modifications of TNRC6 proteins determine which pool of TNRC6 proteins interacts with CCVs and which pool interacts with the CCR4-NOT complex.

3.1.2 Potential roles for other classes of identified W-motif interactors in miRNA silencing

Using a quantitative SILAC-based proteomic approach and loss of functions mutants of TNRC6C CED, multiple sets of proteins that bind TNRC6C via W-motifs were identified in this study. Only components of CCVs were characterized in more detail, but additional groups of interactors such as RNA helicases, translational regulators, metabolic enzymes, mitochondrial proteins, phosphatases and kinases, ribosomal proteins and RNA binding proteins (RBPs) were discovered (**Figure 10** and **Table S1**). Thus, this study provides a repository of additional modulators of miRNA silencing for future research. I will now speculate on the possible functional roles of these interactions.

Two DEAD-box RNA helicases, DDX20 and DDX46, bind TNRC6C CED in a W-motif specific manner (**Figure 10**, in orange). Generally RNA helicases function in unwinding RNA secondary structure and therefore are essential player of RNA metabolism. DDX20 has been implicated in transcriptional regulation (reviewed in[672]), while DDX46 was already found to interact with AGO complexes independently of RNA[673]. Despite the fact that two recent studies identified DDX6 as a direct interactor of CNOT1 that promotes translational repression[267,268], this protein was not enriched in our dataset. Exportin 1 (XPO1) was nearly 1.5-fold enriched with wt TNRC6C CED. In light of the recent evidence demonstrating that XPO1 mediates nuclear export of TNRC6 and AGO proteins[404], it is tempting to suggest that W-motifs mediate this shuttling via XPO1. GW182/TNRC6 proteins are also found in P-granules. A *C. elegans* genetic screen revealed that certain nucleoporins (Nup) are required for P granules integrity[674]. Interestingly the human orthologue of one of these proteins, Nup93, was a TNRC6C enriched interactor together with Nup205. Nuclear pore proteins are enriched in FG (phenylalanine-glycine) repeats found within intrinsically disordered regions and contain short stretches of hydrophobic amino acids, spaced by hydrophilic residues[675]. The high local concentration of FG repeats has been shown to form elastic and reversible hydrogel-like structures[675], leading the authors of the study to propose a model of nuclear transport whereby gel-like structures at nuclear pores filter nuclear trafficking to and from the nucleus. Specificity of transport is achieved by the ability of nuclear transporters to transiently break the FG-mediated hydrophobic non-covalent bonds[675]. Similarly, TNRC6 proteins are characterized by stretches of

numerous W-motifs, suggesting they might mediate interactions via a similar mechanism. Along the same line, two innovative studies led by Han, Kato and colleagues demonstrated that disordered regions with aromatic-containing motifs, comparable to W-motifs, drive the formation of granules by self-aggregating and assuming a polymeric amyloid-like structure[676,677]. The authors suggest that such polymerisation could be the mechanism underlying formation of various RNP granules in the cell, such as P-bodies, stress granules, Cajal bodies and others, and therefore mediate compartmentalization of multiple cellular processes[676,677]. Importantly, increasing evidence shows that disordered regions can form pathological aggregates, especially in neurodegenerative diseases[678,679] strengthening their physiological relevance. Han, Kato and colleagues also observed that exposing cell lysates of different species and of different cell types to biotinylated-isoxazol (b-isoxazol) would selectively precipitate RNA granules components enriched in KH (K protein homology) and RRM (RNA recognition motif) domains, and low complexity (LC) sequences (disordered motifs)[676,677]. Intriguingly, among the precipitated proteins they could find TNRC6B and C as well as ~20% of W-motifs enriched interactors identified by our SILAC approach (**Table S6**)[676,677]. Some examples are FMR1 (fragile X mental retardation syndrome), FXR1 (fragile X related 1) and PCBP1 (poly(C) binding protein 1) proteins, which contain KH domains; and poly(A) binding proteins PABPC1 and 4, which have four RRM domains. FMR1 and its autosomal homolog FXR1 are RNA binding proteins involved in RNA transport and translational regulation[680] and are known to interact with components of miRISC[226-228]. C14orf166 has also been proposed as a regulator of RNA transport[681]. PABPCs and PCBPs proteins bind poly(A) or poly(C) RNA stretches, respectively and modulate RNA stability. PABPCs have long been known to bind TNRC6 proteins and PAN2-PAN3 deadaenylase complex via a PAM2 motif (here present in wt and mut CEDs), however their role in general miRNA silencing is dispensable (see chapter 1.4.1.3). Here we show mutations of W-motifs to alanine disturb PABP-TNRC6C interactions. Importantly, PABPs and PCBP1 interactions were preserved by the 7W7Y mutant indicating that an aromatic tyrosine residue within the motifs is sufficient to promote binding; and suggesting PABPs and PCBP1 could be responsible for the residual repressive activity of 7W7Y CED (**Figure 7D**). These findings argue that W-motifs in TNRC6 proteins could function via alternative

mechanisms: by recruiting CCR4-NOT, as it has been established[275] when in soluble state; and by oligomerizing into large RNP granules, possibly P-bodies, with other proteins. One strategy to control the reversible formation of these aggregates is through phosphorylation of serine and threonine residues in LC sequences, which was shown to promote FUS (fused in sarcoma) hydrogels disassembly *in vitro*[677]. Given that W-motifs are S/T-rich and TNRC6 are extensively phosphorylated[341], phosphorylation is likely to regulate TNRC6 interactions, and thus functions. Possibly because of this reason, kinases and phosphatases were another category of W-motif enriched interactors (**Figure 10**, in blue).

Notably, three metabolic enzymes involved in nucleotides metabolism and amino acid biosynthesis, CAD (Glutamine-dependent carbamoyl-phosphate synthase; aspartate carbamoyltransferase; dihydroorotase), PHGDH (D-3-phosphoglycerate dehydrogenase) and PYCRL (pyrroline-5-carboxylate reductase 3) also exhibit preferential binding for W-motifs. A growing body of evidence supports the existence of moonlighting enzymes, i.e. enzymes with a role other than their catalytic metabolic activity, and of a REM (RNA-enzyme-metabolite) network that connects cellular metabolism with gene regulation (reviewed in[682]). Hence, one possibility is that CAD, PHGDH and PYCRL are moonlight enzymes playing an additional role in RNA metabolism by interacting with TNRC6 proteins. A second possibility is that a catabolic process such as miRNA-silencing, which leads to mRNA decay, is coupled to recycle of the mRNA degradation products generated by the miRNA pathway. Lastly, a group of mitochondrial proteins, such as inter-membranes chaperones (TIMM13, 8A and 8B proteins); ADP/ATP translocases (SLC25A5 and A6 proteins); phosphate and 2-oxoglutarate/malate carriers (SLC25A3 and A11 proteins) and a single strand DNA binding protein SSBP1, were identified as W-motif specific TNRC6C binding partners. Since mitochondria are the cells energy providers, and regulate processes as apoptosis, calcium homeostasis and production of ROS (reactive oxygen species), the function of these interactions might have to do with metabolic aspects similarly to metabolic enzymes. Alternatively, miRNA have been reported to modulate mitochondrial gene expression and AGO has been found in mitochondria (reviewed in[683]), suggesting these interactions may mediate miRISC uptake and function within mitochondria.

3.2 Evolutionary Aspects of miRNA-mediated Repression

3.2.1 Evolution of the modes of miRNA silencing

Earlier studies have shown that multiple cnidarian species, including *Nematostella vectensis,* and sponges possess the miRNA pathway[655,658,659]. Unlike mammals and flies and similarly to plants, *Nematostella* miRNAs tend to have high complementarity to their targets and mediate target slicing[659]. This finding suggested that slicing might have been the ancestral mode of action of miRNAs in animals. However, unlike plants *Nematostella* also possesses a GW182 homolog, a protein required for miRNA-mediated deadenylation and translational repression in Bilateria. Using human cultured cells I could show that nvGW182 functions via a similar mechanism as its bilaterian homologs: it recruits the CCR4-NOT deadenylation complex via its W-motifs, to affect both mRNA stability and translation. Interestingly, also the helicase DDX6, which was shown to contribute to miRNA-mediated translational inhibition in mammals[267,268,293] is highly conserved in *Nematostella* (72% identity and 85% similarity between human and *Nematostella,* **Figure S10**). Interactions between AGO, GW182 and CCR4-NOT could also be observed *in vivo* in *Nematostella* (**Figure 25**). Thus, the set of experiments presented in section 2.3 supports a model where the mechanism of miRNA silencing via W-motifs is conserved between cnidarians and bilaterians (**Figure 28**).

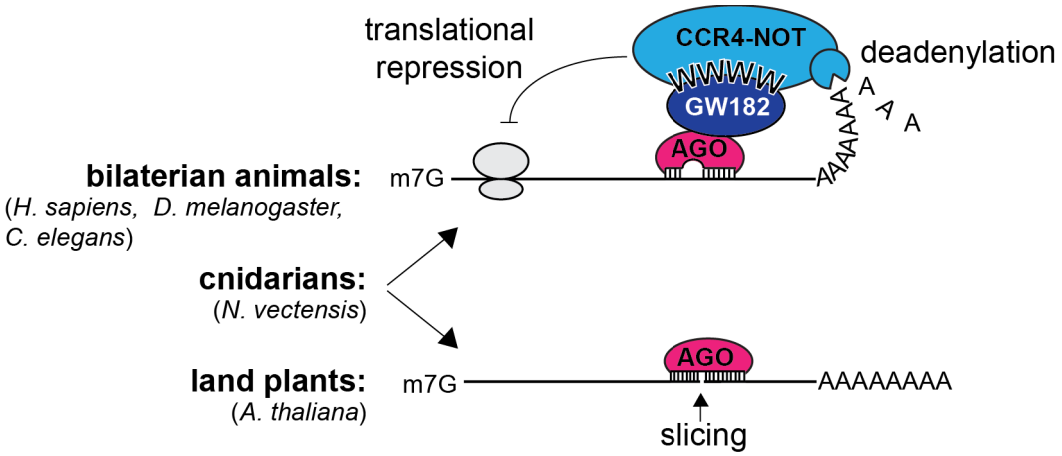

Figure 28. Modes of miRNA silencing across species Speculative model illustrating the mechanisms of miRNA-mediated silencing in bilaterian animals (recruitment of the CCR4-NOT complex via W-motifs of GW182), land plants (slicing by AGO and translational repression via an unknown mechanism that depends on AGO), and

cnidarians (both slicing and GW182-dependent mechanism). This figure and figure legend was adapted from panel D of Figure 6 in Mauri et al., 2016.

It still remains to be elucidated why and how *Nematostella* miRNAs employ two different mechanisms of action: AGO-mediated slicing and AGO/GW182/CCR4-NOT-mediated deadenylation and translational repression. The most likely possibility is that the latter mechanism is employed by a subset of *Nematostella* miRNAs that are only partially complementary to their targets and therefore cannot mediate slicing. It is unlikely that only one of two *Nematostella* AGOs possesses slicing activity, and the second relies on nvGW182-dependent mechanism, because both nvAGO1 and nvAGO2 possess the five residues previously found to be important for AGO slicing activity in bilaterians[304,330,654]. Alternative explanations are that the *Nematostella* miRNA-mediated repression system employs each of the two modes of action under different conditions or for different targets. A possible way of switching the mode of action would be modification of AGO catalytic site; as such modification can interfere with the slicing activity. Another possibility could be via conformational changes of AGOs upon binding of GW182 or other proteins, which would prevent target slicing.

Being able to silence miRNA targets via AGO-mediated cleavage or via translational repression and degradation allows *Nematostella* to either quickly degrade miRNA targets or to reversibly silence them. These results suggest that a less stringent and reversible mechanism of function – mRNA deadenylation and translational repression – was already active in non-bilaterian animals. Since this mechanism became the predominant mode of silencing in bilaterians it might have been advantageous and therefore preserved by evolution.

Previously, Chekulaeva and colleagues have demonstrated that W-motifs are both necessary and sufficient to recruit the deadenylation complexes and repress tethered mRNA, thereby playing a key role in miRNA silencing in human and *Drosophila*[275]. The results of section 2.3 indicate that the function of these potent elements is conserved in over 600 million years of evolution. The consensus sequence of the W-motif, shared between bilaterians and cnidarians (**Figure 26D**) shows that these motifs are rich in serine and threonine residues, which makes them hotspots for phosphorylation[341,518]. Such reversible phosphorylation of W-motifs in TNRC6/GW182 proteins could interfere with their

ability to recruit the CCR4-NOT complex and, thus, represent an interesting mechanism for regulation of miRNA silencing in response to various stimuli.

Knowingly, W-motifs are not restricted to the GW182 family. They can in fact be found in a number of proteins involved in different aspects of RNA metabolism and in a wide spectrum of species, from yeast to human (**Figure S11**). Such proteins might recruit the CCR4-NOT complex to specific targets, thereby competing with GW182 for CNOT binding and consequently modulating miRNA silencing or regulating gene expression in a miRNA-independent way. Interestingly, Nanos and tristetraprolin (TTP) proteins have been reported to directly recruit CCR4-NOT via multiple short linear motifs (SLIMs) found within regions predicted as disordered[358,359,502]. Such SLIMs contain aromatic and hydrophobic residues, whose side chains are inserted into pockets on CNOT surfaces[358,359,502]. Striking features of W-motifs are also the location within unstructured regions of GW182 proteins, the aromatic and hydrophobic side chain of the invariant W residue and the ability to bind two hydrophobic pockets on CNOT9 and probably additional ones on CNOT1 surfaces[267,268,275]. Moreover, CCR4-NOT is a multifunctional complex broadly involved in RNA metabolism (reviewed in[382]). Thus, W-motifs or alternatively aromatic/hydrophobic SLIMs recruiting CCR4-NOT might represent a conserved protein-protein interaction platform employed by several cellular regulatory pathways.

3.2.2 Conservation of miRISC components

miRNA pathway components are conserved throughout bilaterian animals, which include the most commonly studied species of *H. sapiens, M. musculus, D. melanogaster* and *C. elegans*[44]. More ancient animal species, such as members of cnidarians, have been reported to encode for several bilaterian miRISC homologues, including Argonaute, GW182/TNRC6 and CCR4-NOT proteins, and interestingly for the plant-specific Dicer helper homolog HYL1[654]. These observations raised questions on how these miRISC components evolved and which functions they were playing in cnidarians.

The results of cross-species experiments presented in this thesis showed that nvGW182 can interact with the human CCR4-NOT complex through multiple W-motifs embedded in the CED, but fails to recognize human AGOs (**Figure 19, 20B, 22A**), pointing to a scenario where two domains of GW182 experienced

different evolutionary trajectories. The relative conservation of W-motifs in the CED (**Figure 18**) might be the result of the very high conservation of the CCR4-NOT complex that is connected to numerous cellular pathways and hence has very low sequence flexibility (reviewed in[382]). In support of this view, tryptophan-containing motifs are the only conserved feature of AIN1 and AIN2, the two *C. elegans* functional analogues of GW182 proteins, which lack the typical domain organization of GW182 homologues[357] (**Figure 4**). In contrast, the N-terminal part of GW182 protein, which was shown to be crucial for AGO recognition[311,331,333,335,355]), seems to have evolved more rapidly. Although the presence of several GW AGO-binding motifs is conserved between human TNRC6 proteins and nvGW182 and AGO residues forming W-pockets are also conserved (**Figure 24**), human GW-motifs can only bind human AGOs and nvGW-motifs can only bind nvAGOs (**Figure 22A**). The inability of nvAGOs to repress when tethered to mRNAs in human cells (**Figure 22B**) confirmed that they are unable to recruit TNRC6 proteins and consequently the downstream effectors of silencing. Additionally, co-expression of nvGW182 and nvAGOs failed to rescue miRNA silencing in human cells depleted from TNRC6A and B (**Figure S12**), raising the possibility that nvAGOs are not capable of loading human miRNAs.

Nevertheless, the overall ability of nvGW182 to bind nvAGOs and CNOT9 (also verified in *Nematostella*, **Figure 25**), and the well-documented ability of bilaterian GW182/TNRC6 proteins to bind their respective AGOs and the CCR4-NOT complex[267,268,271,275-277,357,361] support a parsimonious view that the last common ancestor of Cnidaria and Bilateria carried at least one GW182 and one AGO and those were forming a miRNA-mediated silencing complex together with units of the CCR4-NOT complex. Further, it is likely that AGOs and the N-terminal domain of GW182 proteins have gone through separate co-evolutionary processes in the cnidarian and bilaterian lineages that are the reason for the observed lack of inter-lineage interaction. This escalating process might have started from a mildly disadvantageous mutation in one of the proteins that reduced the AGO-GW182 affinity and hence made a compensatory mutation in the partner protein advantageous[684].

Overall, the results presented in section 2.3 provide new insights into the evolution of the miRNA-mediated silencing mechanisms using a cnidarian species, Nematostella vectensis, separated by more than half a billion years from the vast

majority of Metazoa. The results show that the core component of the miRNA pathway GW182 is conserved in cnidarians and, analogously to bilaterians, is able to inhibit translation and stimulate mRNA decay by recruiting the CCR4-NOT deadenylation complex via W-motifs. An important task for the future is to test the functionality of nvGW182-mediated silencing in vivo and understand how the two mechanisms – slicing and translational regulation/mRNA deadenylation – interact with each other.

4. Materials

4.1 Equipment and Consumables

Name	Company	Description
C100 Touch Thermal cycler	Biorad	PCR machine
S1000 Thermal cycler	Biorad	PCR machine
CFX96 Real Time System	Biorad	qPCR machine
Trans-Blot Turbo	Biorad	WB semi-dry transfer cassette
ImageQuant LAS 4000	GE Healthcare	Chemiluminescent detector
Alpha Imager HP	Proteinsimple	UV light detector
Berthold Centro XS^3 LB960 DLReady	Berthold Technologies	Microplate reader (luminometer)
5424 centrifuge	Eppendorf	Table top centrifuge
5424 R centrifuge	Eppendorf	Table top centrifuge with cooling system
5804 centrifuge	Eppendorf	Centrifuge
5810 R centrifuge	Eppendorf	Centrifuge with cooling system
Avanti J-26 XP	Beckman Coulter	High performance centrifuge
Sorvall MTX 150 micro-ultracentrifuge	ThermoFisher Scientific	Micro-ultracentrifuge
Binder CB incubator	Binder	CO_2 incubator
Incu-Line VWR	VWR	Incubator
Innova 42 incubator shaker	Eppendorf	Incubator shaker
Thermomixer compact	Eppendorf	Thermomixer
Biospectrometer basic	Eppendorf	Spectrometer
Leica DMIL LED	Leica	Light microscope
Dino-Lite digital microscope	Dino-Lite	Digital microscope
LUNA automated cell counter	Logos biosystems	Cell counter
Qubit fluorometer	Life Technologies	Fluorometer
1.5 and 2.0 ml tubes	Eppendorf	
15 and 50 ml falcon	Lab supplier	
PCR tubes 0.2 ml	LifeScience	
Low binding tubes	Sigma Aldrich	
Amber tubes	Kisker Biotech	
Cryotubes	Simport	
Cuvettes	Carl Roth	
Microseal 96-well skirted qPCR plates	Biorad	
Optical adhesive covers	Biorad	
Microplates	Greiner	
Electronic pipettes	VistaLab Technologies	
Manual pipettes	Eppendorf	
Electronic multichannel pipettes	Eppendorf	
Electronic multistep pipette	Eppendorf	
Pipetboy tips	Eppendorf	
Gel loading tips	Lab supplier	
Combitips	Eppendorf	
Filter tips	Sarstedt	
Pipette buoy tips	Lab supplier	
Glass homogenizer	Wheaton USA	

Name	Company	Description
Magnetic rack	Millipore	
Petri dishes	Sarstedt	
CellStar greiner tissue culture dishes	Lab supplier	
CellStart greiner tissue culture flasks	Lab supplier	
PVDF roll	Millipore	

4.2 Chemicals and Enzymes

Reagent	Catalogue number	Company
Acetic Acid technical grade	A2083, 2500	Applichem
40% Acrylamide/Bisacrylamide Solution 37.5:1	10688,03	Serva
Agarose	2267,1	Carl Roth
Agarose	A8963, 0500	Applichem
Ammonium persulfate	A3678-25G	Sigma-Aldrich
Ampicillin Sodium Salt	K029.2	Carl-Roth
ATP	R0441	Thermo Scientific
Attractene Transfection Reagent	301005	Qiagen
Biorad Protein Assay	500-00006	Biorad
Biotin	29129	Thermo Fisher
BLasticidin	Ant-bl-1	Invitrogen
Boric acid	B7901-500G	Sigma-Aldrich
Boric acid	15166,02	Serva
Bromphenol blue	2830	OmniPur/Calbiochem
Bovine Serum Albumin	A9418-5g	Sigma-Aldrich
Albumin Fraction V	A9418-50g	Carl Roth
Albumin Fraction V	8076,4	Carl Roth
Calcium chloride dihydrate	208291	Calbiochem
Chloramphenicol	3886,2	Carl Roth
Chloroform	C2432-500ml	Sigma-Aldrich
Coelenterazine	102171	PJK
Coenzyme A	102211	PJK
Complete Mini EDTA-free Protease Inhibitor tablets	4693159001	Roche
Complete Mini Protease Inhibitor tablets	4693124001	Roche
Copper (II) sulphate pentahydrate	C8027-500G	Sigma-Aldrich
Coomassie Blue G250 (Serva Blue G)	35050-02	Serva
p-Coumaric acid	C9008-5G	Sigma-Aldrich
Deoxycholic Acid salt	6613-SOG	Amrexo
Diamidino-2-Phenylinarte-Dilactate	13130215-093M4106V	Sigma-Aldrich
Diethyl pyrocarbonate	159220-100g	Sigma-Aldrich
Dimethylsufoxid	A994.1	Carl Roth
Dimethylsulfoxid for cell culture	P60-36700100	PAN
Disodium-EDTA	E5134-500G	Sigma-Aldrich
Dithiothreitol	3870	OmniPur
DMEM (1x)-GlutaMAX	61965-026	Life Technologies
DNA (Sodium salt) from salmon testes	D1626-1g	Sigma-Aldrich
DNase I	A3778.0010	Applichem
dNTP Mix 10mM each	R0193	Thermo FIsher
DPBS	P04-36500	PAN
Doxycycline Hyclate	Cay14422-5	Biomol
DreamTaq DNA Polymerase	EP0702	Thermo Scientific

Reagent	Catalogue number	Company
Dynabeads protein G	100040	Life Technologies
EGTA MB grade	324626	VWR
EZ PCR Mycoplasma Test Kit	20-700-20	Biological Industries
Ethanol 99% pure		MDC store
Ethidium bromide		Carl Roth
Ethylenediaminetetra-acetic acid	EDS-500G	Sigma-Aldrich
EZ-Link Plus Activated Peroxidase	31487	Thermo Fisher
Fast AP Thermosensitive Alkaline Phosphatase	EF0651	Thermo Scientific
Fetal Bovine Serum	10270	Life Technologies
FBS heat inactivated	F4135-500ML	Sigma
Ficoll PM 400 MB grade	SA/F2637/000025	Th. Geyer
Fungizione	15290026	Life Technologies
Ganciclovir	SYN-001B	Linaris/Prospec
Gel Code Blue Stain reagent	24592	Thermo Scientific
GeneRuler 1kb ladder	SM0311	Thermo Scientific
Geneticin sulphate solution	M3118.0100	Genaxxon
Gentamicin/Amphotericin	10R01	Life TEchnologies
Gibson Assembly Master Mix	E2611S	NEB
L-Glutathione reduced	G4251-10g	Sigma-Aldrich
Glutathion Sepharose 4B	170756-01	GE Healthcare
Glycerol	G5516-500ml	Sigma-Aldrich
Glycine	23391,03	Serva
GlycoBlue Blue Coprecipitant	AM9516	Life TEchnologies
Guanidine Hydrochloride	G3272-100g	Sigma-Aldrich
Hepes	H3375-500G	Sigma
Hydrochloric acid	A0625.2500	Applichem
Hydrogen Peroxide 30%	216763-500ml	Sigma-Aldrich
4-(2-Hydroxyethyl)piperazine-1-ethanesulfonic acid	H3375-100G	Sigma-Aldrich
Hygromycin B	sc-29067	Santa Cruz
Igepal CA-630	18896-50ML	Sigma-Aldrich
Imidazole	26081,01	Serva
Iso-Propanol (2-Propanol)	1.09634.1011	Merck
jetPrime Transfection Reagent	114-01	Polyplus
Kanamycin sulfate	T832.2	Carl Roth
LB-agar	X969.3	Carl Roth
LB-medium	X968.3	Carl Roth
Lithium acetate dihydrate	62395-250G-F	Sigma-Aldrich
Lithium Chloride	4490410000	Acros Organics
D-luciferin 500mg	102212	PJK
Luminol	A8511-5G	Sigma-Aldrich
Magnesium acetate tetrahydrate	M5661-250G	Sigma-Aldrich
Magnesium chloride hexahydrate	M2670-100G	Sigma-Aldrich
Magnesium sulfate heptahydrate	S3264-500G	Sigma-Aldrich
Manganese (II) cloride tetrahydrate	M3634-500g	Sigma-Aldrich
Maxima First Strand cDNA Synthesis Kit for RT-qPCR	K1642	Thermo Scientific
MEM Non-Essential Amino Acids Solution, 100X	11140035	Life Technologies
MES free acid	M8250	Sigma-Aldrich
2-Mercaptoethanol	M3148-100ml	Sigma
Methanol	4627,6	Carl Roth
Micrococcal Nuclease	EN0181	Thermo Scientific

Reagent	Catalogue number	Company
MOPS, free acid	475922	Calbiochem
Mung Bean Nuclease	M0250S	NEB
Non-fat skimmed milk powder	54650,1	Biomol
PageRuler Plus Prestained Protein Ladder	26620	Fermentas Life Sciences
5x Passive Lysis Buffer	E1941	Promega
Pefabloc	50985,1	Biomol
Polyethylenimine		Polysciences Inc.
Penicillin 10KU/Streptomycin Solution 10 mg	A2213	Biochrom
Pfu DNA Polymerase	EP0571	Thermo Scientific
Phenol/Chloroform 25:24:1	KP31757	Calbiochem
lambda-phosphatase	sc-2003124	Santa Cruz
Phosphatase Inhibitor Mix I	39050,02	Serva Electrophoresis
Phusion DNA Polymerase	F-530L	Thermo Scientific
Polyethylene glycol	33136,01	Serva Electrophoresis
Ponceau S Sodium	P3504-50g	Sigma-Aldrich
Potassium acetate	529543	Calbiochem
Potassium chloride	P9541-500G	Sigma-Aldrich
Potassium hydroxide	1.05012.1000	Merck
Potassium phosphate monobasic	P9791-500G	Sigma-Aldrich
Potassium phosphate tribasic	P5629-25G	Sigma-Aldrich
Precision Plus Protein Standard Dual Color	161-0374	Biorad
PreScission Protease	270843-0.5KU	VWR
propylgallate	P3130-100g	Sigma
Proteinase K	SAFSP4850	Sigma
Puromycin dihydrochloride	P9620-10 ml	Sigma
Restriction Endonucleases	P10-020500	New England Biolabs
RNase A	K0489	Thermo Scientific
RNase A	K0509	Thermo Scientific
RNAseOUT	10000000P40	Invitrogen
RQ1 DNase Kit	M610A	Promega
Rubidium Chloride	83980-50g	Sigma
SensiFast Sybr Green No-Rox Kit	BIO-98002	Bioline
SOB medium	AE27.1	Carl Roth
Sodium acetate trihydrate	71188-250G	Sigma-Aldrich
Sodium azide	K305.1	Carl Roth
Sodium chloride	A2942,1000	Applichem
Sodium dodecyl sulfate	A2263,0100	AppliChem
Sodium deoxycholate	SAFS30970	VWR
Sodium hydroxide	1064621000	Merck
sodium phosphate monobasic	A2901,1000	Applichem
Sodium phosphate dibasic	S3264-500G	Sigma-Aldrich
Sodium phosphate tribasic	342489-25g	Sigma-Aldrich
Spermidine	85558-1G	Sigma-Aldrich
Sucrose	A2211,1000	Applichem
Super Signal West Femto Maximum Sensitivity Substrate	34096	Pierce
T4 DNA Ligase	EL0011	Thermo Scientific
T4 Polynucleotidkinase	EK0031	Thermo Scientific
N,N,N',N'-Tetramethyl-ethylenediamine	T9281-25ML	Sigma-Aldrich
Topo TA cloning Kit	450641	Life Science
TriFast FL PeqGold	30-2110	VWR

Reagent	Catalogue number	Company
Trypsin	P10-020500	PAN
Tris(hydroxymethyl)aminomethane molecular biology grade	37186,03	Serva
Triton X-100	A4975,1000	AppliChem
Trizma base	93362-1KG	Sigma-Aldrich
Trypan Blue	15250-061	Life Technologies
Tryptone/Peptone from Casein	8952,3	Carl Roth
L-Tryptophan	6540-100GM	Calbiochem
Tween 20	P9416-100ML	Sigma-Aldrich
Urea	666122	Calbiochem
Western Blocking Reagent	11921673001	Roche
X-beta-Gal	2315,3	Carl Roth
Xylene yanol FF	X4126-10G	Sigma-Aldrich
YPD agar	X971.1	Carl Roth
YPD medium	X970.1	Carl Roth
Zeocin	ant-zn-1	InvivoGen

4.3 Kits

Kit Name	Company	Catalogue number	Application
Plasmid miniprep DNA kit	Roboklon	E3500-02	Plasmid isolation (mini)
NucleobondXtra	Macherey-Nagel	00740412/000050	Plasmid isolation (midi)
GeneJET gel extraction kit	Thermo Fisher	K0692	DNA purification from gel
GeneJET PCR purification kit	Thermo Fisher	K0702	DNA purification from PCR

4.4 Buffers, solutions and Media

4.4.1 Buffers and solutions

Buffers	Composition	Application
Lysis buffer	50 mM Tris-HCl pH 7.4, 150 mM KCl, 0.5% (v/v) Triton X-100, 0.2 mM Pefabloc (or 1 tablet Roche protease inhibitor cocktail in 10 ml buffer)	Cell lysis and GST pull-down, IP (*)
Washing buffer	50 mM Tris-HCl pH 7.4, 150 mM KCl, 0.1% (v/v) Triton X-100, 0.2 mM Pefabloc (or 1 tablet Roche protease inhibitor cocktail in 10 ml buffer)	GST pull-down, IP
Elution buffer	50 mM GSH in washing buffer; pH ajusted to 7.5 with 1 M Tris	GST pull-down
Hypotonic buffer A	0.1 M MES, pH 6.5 adjusted with NaOH, 0.2 mM EGTA, and 0.5 mM $MgCl_2$	CCVs isolation (*)
5x SDS loading buffer	50% (v/v) glycerol, 300 mM Tris-HCl pH 6.8, 5% (v/v) 14.3 M β2-mercapto-ethanol, 0.1% (w/v) bromophenol blue, 10% (w/v) SDS	SDS-PAGE
Running buffer	25mM Tris-base, 191 mM glycine, 0.1% (w/v) SDS	SDS-PAGE
Transfer buffer	25mM Tris-base, 191 mM glycine, 20% (v/v) MetOH	western blotting (transfer)
PBS	0.137 mM NaCl, 2.6 mM KCl, 10 mM Na_2HPO_4, 1.8 mM KH_2PO_4	Cell culture
TBS	50 mM Tris-HCl pH 7.5, 150 mM NaCl	western blotting (washing)

Buffers	Composition	Application
PBS-T	PBS and 0.1-0.2% (v/v) Tween-20	western blotting (washing)
TBS-T	TBS and 0.1% (v/v) Tween-20	western blotting (washing)
Blocking solution	5% (w/v) milk or BSA in TBS-T or PBS-T (depending on antibody requirements)	western blotting (blocking)
ECL	100 mM Tris-HCl pH 8.5, 1.25 mM luminol, 225 µM coumaric acid, 0.01% H_2O_2	western blotting (developing)
Comassie staining solution	50% (v/v) H2O, 50% (v/v) EtOH, 0.1% (w/v) Blue G powder	Comassie staining
Comassie destaining solution	60% (v/v) H2O, 30% (v/v) EtOH, 10% (v/v) acetic acid	Comassie destaining
TBE	89 mM Tris-HCl pH 6.8, 89 mM boric acid, 2.5 mM EDTA	DNA electrophoresis
Fluc reagent	75 mM Hepes pH 8.0, 0.1 mM EDTA, 4 mM $MgSO_4$, 530 µM ATP, 270 µM Coenzyme A, 470 µM DTT and 470 µM luciferin	Luciferase assays
Rluc reagent	2.2 mM Na_2EDTA, 220 mM K_3PO_4 pH 5.1, 0.44 mg/ml BSA, 1.1 M NaCl, 1.3 mM NaN_3 and 0.6 µg/ml colenterazine	Luciferase assays

*Buffers for RNA work were prepared in DEPC-treated water

4.4.2 Media

Medium	Composition	Cell type
DMEM	DMEM-GlutaMAX high glucose (Gibco) with 10% (v/v) FBS (Gibco)	Mammalian cells
SILAC DMEM	DMEM high glucose without L-Arg, L-Lys and L-Gln; with 10% (v/v) dialyzed FBS (Sigma-Aldrich), 100 U-ml penicillin-streptomycin (Invitrogen), 4 mM stable Gln, and 28 mg/L L-Arg and 48 mg/L L-Lys. Light medium (Arg0/Lys0, Sigma-Aldrich); medium heavy (Arg6/Lys4, Sigma-Aldrich); heavy (Arg10/Lys8, Sigma-Aldrich)	Mammalian cells
LB (Lysogeny Broth)	25 g LB powder (Carl Roth) in 1 L Millipore water	*E. coli*

4.5 Bacterial strains and Cell lines

4.5.1 Bacterial strains

Strain	Species	Genotype
XL1-blue	*E. coli*	endA1 gyrA96(nalR) thi-1 recA1 relA1 lac glnV44 F'[::Tn10 proAB+ lacIq Δ(lacZ)M15] hsdR17(rK- mK+)
DH5α	*E. coli*	F– endA1 glnV44 thi-1 recA1 relA1 gyrA96 deoR nupG purB20 φ80dlacZΔM15 Δ(lacZYA-argF)U169, hsdR17(rK–mK+), λ–
Mach1	*E. coli*	ΔrecA1398 endA1 tonA Φ80ΔlacM15 ΔlacX74 hsdR(rK- mK+)
dam-/dcm- (NEB; C2925)	*E. coli*	ara-14 leuB6 fhuA31 lacY1 tsx78 glnV44 galK2 galT22 mcrA dcm-6 hisG4 rfbD1 R(zgb210::Tn10) TetS endA1 rspL136 (StrR) dam13::Tn9 (CamR) xylA-5 mtl-1 thi-1 mcrB1 hsdR2

4.5.2 Cell Lines

Cell Line	Species	Source	Description	Use
HEK 293	*Homo sapiens*	Matthias Selbach Lab	Human embryonic kidney cells with the morphology of epithelial cells	Pull-down experiments and tethering assays
HeLa-EM2-11ht (HeLa rtTA)	*Homo sapiens*	Kai Schoenig (Weidenfeld et al., 2009, NAR)[685]	HeLa line carrying reverse tetracycline transactivator for doxycycline (dox) inducible expression; and hygromycin/ganciclovir cassette flanked by FRT site (F&F3) for generation of arbitrary stable lines with dox-inducible expression via RMCE (ganciclovir to be used for negative selection)	miRNA reporter assays, rescue assays, CCV isolation
HeLa-rtTA-1266 clone 27 (TNRC6A&B-KD)	*Homo sapiens*	Marina Chekulaeva and Camilla Ciolli Mattioli (Mauri et al., 2016, NAR)[668]	HeLa line with dox inducible KD of TNRC6A&B	Rescue assays, CCV isolation
HeLa-rtTA-755 (hmga2 wt)	*Homo sapiens*	Julien Bethune (Bethune et al., 2012, EMBO Rep)[392]	HeLa line with dox inducible expression of FLuc/RLuc-hmga2 wt let-7 miRNA reporter	miRNA reporter assays, CCV isolation
HeLa-rtTA-756 (hmga2 mut)	*Homo sapiens*	Julien Bethune (Bethune et al., 2012, EMBO Rep) [392]	HeLa line with dox inducible expression of FLuc/RLuc-mutated hmga2 let-7 miRNA reporter	miRNA reporter assays, CCV isolation

4.6 Oligos

4.6.1 Oligos for sequencing

MCh	Name	Sequence (5'-3')	Purpose
26	Fluc upstream sequencing	TTCATAGCCTTATGCAGTTGCTC	Sequencing oligo for upstream region of Firefly luciferase
814	pCiNeo-upstream	CACAGGTGTCCACTCCCAGTTC	Sequencing primers for pCiNeo plasmids
815	pCiNeo-downstream	ACTGCATTCTAGTTGTGGTTTGTCC	
816	pEBG-upstream (GST)	ATAGCATGGCCTTTGCAGGG	Sequencing primers for pEBG plasmids.
817	pEBG-downstream	ACAGGGATTTCTTGTCTCCCAC	
1002	Rluc sequencing upstream	TAGTTGATGAAGGAGTCCA	Sequencing upstream of Renilla luciferase
1042	GST upstream	CAAGGCCCTTAATTTTCCAATAACC	Sequencing upstream of GST-Tag
1125	CMV rev sequencing	CACCGTACACGCCTAAAGC	Sequencing primer binding the flanking region between CMV and Tet-O sites
1268	Rluc sequencing, downstream	CTGAGGAGTTCGCTGCCTAC	Sequencing primer binding in the 3' terminal region of Renilla luciferase
2279	pEBH upstream sequencing primer	ATGGCTTACCCATACGATGTTC	Upstream oligo to sequence pEBH

4.6.2 Oligos for cloning

MCh	Name	Sequence (5'-3')	Purpose
658	TNRC6A N-terminus rev	CACACCACCTCCTTTGTTTGTGTTAAC	Use oligos 658&1209 to amplify siRNA resistant N-terminus of TNRC6A isoform 2 (Q8NDV7-2) from p1218
659	TNRC6A-middle-fw	GTTAACACAAACAAAGGAGGTGGTGTG	Use oligos 659&660 to amplify C-terminus of TNRC6A with NotI site at the 3'end. Then mix two PCR products (from 1209&658 and 659&660 PCRs) and amplify the full-length with 1209 and 660. Digest with SbfI-NotI and clone into SbfI-NotI cut pCiNeo-HA and pCiNeo-NHA
660	NotI-Cterm-reverse	AGGGAAGCGGCCGCTTACATGGACTCTCCACCCC	
1183	SbfI-hAP2A2 fw	AACCTGCAGGCATGCCGGCCGTGTCCAAG	Primers to amplify full length AP2A2. Use total human cDNA as template, digest with SbfI-NotI and clone into SbfI-NotI-cut p1238
1184	NotI-hAP2A2 rev	aagcggccgcCTAAAACTGCGCTGAGAGCA	
1185	SbfI-hAP2A2 appendage fw	AACCTGCAGGCGCGCCTCTCGCTCCTGG	Fw primer to be used with MCh 1184 as rev to amplify AP2A2 appendage. Use total human cDNA as template, digest with SbfI-NotI and clone into SbfI-NotI-cut-p1238
1186	SbfI-hAP2B1 hinge_appendage fw	AACCTGCAGGCGAACAGCCTCAGGTTATC	Primers to amplify hinge and appendage region of AP2B1. Use total human cDNA as template, digest with SbfI-NotI and clone into SbfI-NotI-cut p1238
1187	NotI-hAP2B1 hinge_appendage_rev	aagcggccgcTTAGTTTTTCAAAATGCTGTCG	
1188	SbfI-hAP2M fw	AACCTGCAGGCatgattggaggcttattcat	Primers to amplify full length AP2M. Use total

MCh	Name	Sequence (5'-3')	Purpose
1189	NotI-hAP2M rev	aagcggccgcctagcagcgagtttcataa	human cDNA as template, digest with SbfI-NotI and clone into SbfI-NotI-cut p1238
1209	SbfI-TNRC6A-fw (full clone)	tacgctcctgcaggcATGGATGCTGATTC TGCCTCCAG	To be used with mch658 (instead of 657) and p1218 as a template to amplify N-terminus of TNRC6A
1648	CHC miR-1	gcgatgctgttgacagtgagcgaAATCGCCC ATCTGAAGGTCCTctgtgaagcca	Oligos for cloning anti-CHC miR into BsaI-cut p1010 (Tet-inducible expression) based on the siMCh17 sequence deposited into the collection. PNK and anneal mch1648&1651 and mch1649&1650; ligate the two pairs; gel purify the shRNA, clone in dephosphorylated BsaI cut p1010 vector. miR seq: tgctgttgacagtgagcgaGCCTAATCTCCGTGCTCAA ctgtgaagccacagatgggTTGAGCACGGAGATTAGG Cctgcctactgcctcggacttcaaggg, GCGA and GCAG are compatible cohesive ends for BsaI site.
1649	CHC miR-2	cagatgggAGGACCTTCAGATGGGCG ATTctgcctactgcctcggacttcaaggg	
1650	CHC miR-3	gcagcccttgaagtccgaggcagtaggcagAAT CGCCCATCTGAAGGTCCTccca	
1651	CHC miR-4	tctgtggcttcacagAGGACCTTCAGATG GGCGATTtcgctcactgtcaacagca	
1735	SbfI-nvGW182 fw	aaatacctgcaggcATGCCTAAGGATGA CAAGAAGGAATT	Primers for cloning nvGW182 into SbfI-NotI cut pCiNEo-NHA and pCiNeo-HA for tethering and rescue
1736	NotI-nvGW182 rev	AGGGAAGCGGCCGCCTTAGACACT CTCACCACCGTTCAG	
1795	NotI_Nterm-nvGW182 rev	AGGGAAGCGGCCGCtcaAGGGCTC TGCTGAGTTATTCGC	Primer to amplify the N-terminus of nvGW182. To be used with oligo 1735 as forward and p1429 as a template
1796	SbfI_Cterm-nvGW182 fw	aaatacctgcaggcATGGCCCCACAGTC CAGGCTGAC	Primer to amplify the C-terminus of nvGW182. To be used with oligo 1736 as reverse and p1429 as a template
1855	SbfI-nvGW182 NED ΔDnaJ fw	aaatacctgcaggcCACGACGGGATCAA TGACAGCC	Primer to amplify the N-terminus of nvGW182 depleted of the DnaJ domain (aa 11-61). To be used with oligo 1795 as reverse and p1429 as a template
1861	NotI_nvDnaJ rev	AGGGAAGCGGCCGCCTGACGAGG TACTCGAATGCTTTAG	To be used with oligo 1735 as forward and p1429 as template to amplify the DNAJ domain of NvGW182 between SbfI-NotI, to be cloned in pCiNeo and pEBG
1889	SbfI-hAP2B fw	aaatacctgcaggcATGACTGACTCCAA GTATTTC	Primer to amplify full-length hAP2B flanked by SbfI and NotI sites.
1890	NotI-hAP2B rev	AGGGAAGCGGCCGCCTTTAGTTTT TCAAAATGCTGTCG	
1894	SbfI-hAP2Bappendage fw	aaatacctgcaggcGGCATGGCACCTGG TG	To be used with 1187 as reverse to amplify hAP2B appendage w/o hinge
1899	TNRC6A NEDiso2-nvCED rev	CCTGGACTGTGGGGCctgcgctaacaat cgctgtaactg	To be used with oligo 1209 as forward and p1377 as template to amplify TNRC6Aiso2 NED (aa1-1169) with 15 nt overlapping with nvGW182 CED. Final aim is to have a human-Nematostella GW182 chimera to be used in rescue and pull-down assays.
1900	TNRC6A NED iso2-nvCED fw	cgattgttagcgcagGCCCCACAGTCCAG GCTG	To be used with oligo 1736 as reverse and p1468 and p1498 as templates to amplify nvGW182 CED (aa1159-1698) wt or 11W11A mut with 15 nt

MCh	Name	Sequence (5'-3')	Purpose
			overlapping with TNRC6A NED. Final aim is to have a human-Nematostella GW182 chimera to be used in rescue and pull-down assays.
1907	nv4W4A CED rev	GACAGAGGGGGTATCGGGGA	To be used with oligo 1796 as fw and p1498 as template to amplify a first fragment (fragment 1) of nvCED containing the first 4 W-motifs mutated. See below
1908	nv4W4A CED fw	TCCCCGATACCCCCTCTGTC	To be used with oligo 1736 as rev and p1429 as template to amplify a second fragment of wt NvCED. Fragment 1 obtained with 1796&1895 and fragment 2 (57bp overlap) obtained with 1896&1736 will be then used as templates with oligos 1796&1736 to produce an nvCED with only the first 4 W-motifs mutated to test whether it is the position or number of mut W-motifs that affect repression. The final amplicon will be SbfI-NotI dig and cloned into SbfI-NotI digested pCiNeo-NHA and pEBG.
1909	SbfI-nvAGO1 fw	aaatacctgcaggcATGGCTTCTAATAATCCAGTGAAT	Use to amplify nvAGO1, digest with SbfI and NotI and clone into p1238 and p1227 SbfI-NotI digested. Co-transfect with nvGW182 constructs and test it in pull-down
1910	NotI-nvAGO1 rev	AGGGAAGCGGCCGCCTTCAAGCAAAGTACATTCCCTG	
1911	SbfI-nvAGO2 fw	aaatacctgcaggcATGCCGAAGAAATCGAAA	Use to amplify nvAGO2, digest with SbfI and NotI and clone into p1238 and p1227 SbfI-NotI digested. Co-transfect with nvGW182 constructs and test it in pull-down
1912	NotI-nvAGO2 rev	AGGGAAGCGGCCGCCTTTAGGTAAAGTACATGGATGCTTC	
2024	SbfI-CNOT6/CCR4 fw	aaatacctgcaggcatgcccaaagaaaaatacg	Primers to amplify CNOT6 and CNOT7 catalytic mutants and re-clone them into SbfI-NotI digested high copy and high expression vectors: pEBG-flag and pEBG-HA
2026	SbfI-CNOT7/CAF1 fw	aaatacctgcaggcatgccagcggcaactgta	
2027	NotI-CNOT7/CAF1 rev	AGGGAAGCGGCCGCCTtcatgactgcttgttggcttc	
2059	NotI-CNOT6/CCR4 rev	AGGGAAGCGGCCGCCTCTACCTCCTGCCAGGAAG	
2166	SbfI-nvΔCED del mut1 fw	aaatacctgcaggcGAGGATTGGGAGGAGAACATCG	Oligos to amplify deletion mutants of Nematostella ΔCED.To be used with oligo 1795 as reverse.
2167	SbfI-nvΔCED del mut2 fw	aaatacctgcaggcAGTAACAGCAAAAACAGCAGTGAGAC	
2168	SbfI-nvΔCED del mut3 fw	aaatacctgcaggcGGCATGGGTACAGGCGGAT	
2169	SbfI-nvΔCED del mut4 fw	aaatacctgcaggcGAGACTAGCGGGACTGAGACCA	
2237	NotI-NO_nvΔCEDmut1 rev	AGGGAAGCGGCCGCtcaGTTCTCAAGGGAAGAATTGGGCT	Use with oligo 2166 as fw and p1597 as template to amplify a non-overlapping (NO) deletion mutant of nvΔCED
2238	NotI-NO_nvΔCEDmut2 rev	AGGGAAGCGGCCGCtcaAACCCAATTGACTCCCCCA	Use with oligo 2167 as fw and p1597 as template to amplify a non-overlapping (NO) deletion mutant of nvΔCED
2239	NotI-NO_nvΔCEDmut3	AGGGAAGCGGCCGCtcaCACCCAGGCGGAAGAAGAGTC	Use with oligo 2168 as fw and p1597 as template to amplify a non-overlapping (NO) deletion mutant

MCh	Name	Sequence (5'-3')	Purpose
	rev		of nvΔCED
2240	NotI-NO_nvΔCEDmut N-term rev	AGGGAAGCGGCCGCtcaGCTAGTC CCTTCCCATCCAGA	Use with oligo 1735 as fw and p1479 as template to amplify a non-overlapping (NO) deletion mutant of nvΔCED

4.6.3 Oligos for site directed mutagenesis

MCh	Name	Sequence (5'-3')	Purpose
476	W1445A FW	atcaaatcgacggcctcctctggccctacctcc	Primers for site-directed mutagenesis to introduce W→A mutation in human TNRC6C CED domain.
477	W1445A REV	GGCCAGAGGAGGCCGTCGATTTGATGTCTGACAG	
478	W1487A FW	TCCACCGCCGGTGCCAGCCCCCTC	
479	W1487A REV	TGGCACCGGCGGTGGAGGAGGGCTTG	
480	W1494A FW	CTCGGCGCCACCAGCTCCTACTCCTCG	
481	W1494A REV	AGCTGGTGGCGCCGAGGGGGCTG	
482	W1504A FW	GTTCTGCCGCCAGCACCGACACCTCAGG	
483	W1504A REV	TCGGTGCTGGCGGCAGAACCCGAGGAG	
484	W1515A FW	CCAGCAGCGCCCTCGTTCTTCGAAACC	
485	W1515A REV	AGAACGAGGGCGCTGCTGGTTCTTCCTG	
486	W1605A FW	TCCAGCGCCCAGTCCAGCAGCGCG	
487	W1605A REV	TGGACTGGGCGCTGGAAGTGGGTGGC	
488	W1648A FW	CTGCTGGCCGGCGGGGTGCCCC	
489	W1648A REV	CCGCCGGCCAGCAGCTCACTGCTCC	
490	W1659A FW	AGCAGCCTGGCCGGCCCGCCCAGCGC	
491	W1659A REV	CGGGCCGGCCAGGCTGCTGGAGTACTGGG	
884	W1445Y FW	atcaaatcgacgTATtcctctggccctacctcc	Primers for site-directed mutagenesis, to mutate W→Y in W-motifs of TNRC6C CED
885	W1445Y REV	GGCCAGAGGAataCGTCGATTTGATGTCTGACAG	
886	W1487Y FW	TCCACCtacGGTGCCAGCCCCCTC	
887	W1487Y REV	TGGCACCgtaGGTGGAGGAGGGCTTG	
888	W1494Y FW	CTCGGCtatACCAGCTCCTACTCCTCG	
889	W1494Y REV	AGCTGGTataGCCGAGGGGGCTG	
890	W1504Y FW	GTTCTGCCtacAGCACCGACACCTCAGG	
891	W1504Y REV	TCGGTGCTgtaGGCAGAACCCGAGGAG	
896	W1659Y FW	AGCAGCCTGtatGGCCCGCCCAGCGC	
897	W1659Y REV	CGGGCCataCAGGCTGCTGGAGTACTGGG	
908	W1648Y FW	AGCTGCTGtacGGCGGGGTGCCCCAG	
909	W1648Y	CCCCGCCgtaCAGCAGCTCACTGCTCCC	

MCh	Name	Sequence (5'-3')	Purpose
	REV		
911	W1605Y FW	cccacttccagctatcagtccagcagcgcgtccag	
912	W1605Y REV	gctgctggactgatagctggaagtgggtggcagcg	
1196	W1387,1397Y FW	TTCACTCtatGGGACCCCGCATTATTCCACAAGCCTGtacGGTCCCCCAAGCAG	
1197	W1387,1397Y REV	GGGACCgtaCAGGCTTGTGGAATAATGCGGGGTCCCataGAGTGAAGTGCCGTG	
1198	W1340Y FW	TCTCCCGGCtatCAGTCTCTCGGGTCCAGCCAG	
1199	W1340Y REV	ACCCGAGAGACTGataGCCGGGAGAAGGGGTCAG	Primers for site-directed mutagenesis of W-motifs W→Y in TNRC6A CED. Use siRNA-insensitive TNRC6A clone as a template.
1200	W1239Y FW	CAGGTTCCAGCtacGGTGAGAGCAGCTCAGG	
1201	W1239Y REV	GCTCTCACCgtaGCTGGAACCTGGGGTATATCTG	
1202	W1226,1215Y FW	tctacgTATgataattctccccttcgtataggtggaggaTACggaaattctgacgc	
1203	W1226,1215Y REV	atttccGTAtcctccacctatacgaaggggagaattatcATAcgtagaCAAGGGTG	
1204	W1171Y FW	ccaaattgacaTATtctcctggttcagttacaaacacctc	
1205	W1171Y REV	tgtaactgaaccaggagaATAtgtcaatttggAATCACTA	
1206	W1141Y FW	aactagtgccTATtcatccattcgtgcctccaac	
1207	W1141Y REV	cacgaatggatgaATAggcactagttGAAGGCAG	
1813	W1167 FW	GCTGACCCAGgcgAAACAACCACTCCTC	
1814	W1167 REV	GTTGTTTcgcCTGGGTCAGCCTGGACTG	
1815	W1183 FW	CGAAACAgcgGGCATGCCCAAGATTGAG	
1816	W1183 REV	GCATGCCcgcTGTTTCGCCATGAGAGGT	
1817	W1227 FW	CTCACGGgcgGGCGTTGACGCCTCTCTTAAG	
1818	W1227 REV	CAACGCCcgcCCGTGAGCTCACGGGATC	
1819	W1309 FW	GCAGTCCCgcgCAGAACACTGAACCCAC	
1820	W1309 REV	GTGTTCTGcgcGGGACTGCTGGCTATAG	Primers for site directed mutagenesis of W→A in nvGW182 CED. Numbers refer to the W position according to the annotation of full-length nvGW182
1821	W1391 FW	CAATTCCgcgAGTACCCAGGACGGGATG	
1822	W1391 REV	GTACTcgcGGAATTGCCGCTGGCGGAG	
1823	W1453 FW	CTCAAGTgcgTCCACCAACCAGCCAATTC	
1824	W1453 REV	GGTGGAcgcACTTGAGATCCCTTCATCC	
1825	W1574 FW	CCCGACgcgTCCAACAACCCAATGCCAC	
1826	W1574 REV	GTTGGAcgcGTCGGGTGTCTGCTCAAAAAAC	
1827	W1589 FW	GCAACCCTgcgTCCTTCGGAACAGTTGATC	
1828	W1589 REV	CGAAGGAcgcAGGGTTGCCGAAGCTAG	
1829	W1627 FW	GGCATGCAAgcgGGAAGTAGTTCTCAGCTCC	
1830	W1627 REV	TACTTCCcgcTTGCATGCCCGGCGGAAC	
1831	W1638 FW	CTCAACTCgcgGGCAACTCCCATCCTGG	
1832	W1638 REV	GAGTTGCCcgcGAGTTGAGCGGGGAGC	
1833	W1657 FW	ATCCATGgcgTCTTTCAGCGGAGGAGCC	
1834	W1657 REV	CTGAAAGAcgcCATGGATGGCACCTGAGAC	

4.6.4 Oligos for qRT-PCR

MCh	Name	Sequence (5'-3')	Primer Bank ID/ source	Amplicon size
845	GAPDH fw	CTGGGCTACACTGAGCACC	378404907c3	101
846	GAPDH rev	AAGTGGTCGTTGAGGGCAATG		
1001	RLuc fw	ATGGCTTCCAAGGTGTAC	J. Bethune[392]	120
1002	RLuc rev	TAGTTGATGAAGGAGTCCA		
1043	FLuc fw	GAGCACGGAAAGACGATGACGG	J. Bethune[392]	165
1044	FLuc rev	GGCCTTTATGAGGATCTCTCTG		
1238	AP2A1 fw	TGAAGCCGTCAAGACGCAC	19913413c2	109
1239	AP2A1 rev	CCGGTCACACATGGCGTAG		
1240	AP2A2 fw	TCTCTAGGCTAAGCAGAATCGT	338827683c3	77
1241	AP2A2 rev	GGGAGCCGGGACAAAATAGTAA		
1242	AP1B1 fw	GACCTCATCTCCGACTCTAACC	260436859c1	75
1243	AP1B1 rev	GTGAGACTCGGCAATTTCTGA		
1244	AP1G1 fw	TGCAATCCGGTCATCTTTTAGAG	71772941c1	108
1245	AP1G1 rev	AACTGTCCAAAGTGAGCAGGG		
1246	AP2M1 fw	ACGTTAAGCGGTCCAACATTT	68798812c2	109
1247	AP2M1 rev	GCCATCACGTCACACATCTTAT		
1248	CLTC fw	ACGGTTGCTCTTGTTACGGAT	115527063c2	92
1249	CLTC rev	AGGCTAGAATGGCGATCAAAC		
1499	CNOT1 fw	ACCCTGAAAAACGGGACATTC	46275836c3	103
1500	CNOT1 rev	ACTTCTTGCATGAAATCAGCCA		
1501	CNOT7 fw	AGGAACTTCAACTTGGCAGTTT	85067506c2	195
1502	CNOT7 rev	GACAACCATTTGACCCCTTCA		
1529	CNOT9 fw	CACTGGCACAAGTGGATAGAG	4885578c1	99
1530	CNOT9 rev	GCTTCTTACTTAGCTCCAGCAAA		

4.7 siRNAs

All siRNAs listed below are designed against human targets. siMCh7 can also function on mouse targets.

siMCh	Name	Sequence (sense)	Source
1	AllStar	Not provided	Negative control from Qiagen
5	TNRC6C	GCAUUAAGUGCUAAACAAAdTdT	Chekulaeva et al. 2011[275]
6	TNRC6A	GCCUAAUCUCCGUGCUCAAdTdT	Huntzinger et al. 2010[360]
7	TNRC6B	GGCCUUGUAUUGCCAGCAAdTdT	Huntzinger et al. 2010[360]
8	CNOT1	GGAACUUGUUUGAAGAAUAdTdT	
9	AP2A1 and AP2A2	CAACAACGCCATCAAGAATdTdT	
17	CLTC	AAUCGCCCAUCUGAAGGUCCUdTdT	
33	CNOT9	GAUCUAUCAGUGGAUC AAUdTdT	Ajiro et al. 2009[686]

4.8 Plasmids

4.8.1 Backbones

pMCh	Vector	Purpose	Source
805	pEBG	High expression of GST-fusions in mammalian cells	Addgene 22227 (Tanaka et al., 1995)[687] gift from D. Baltimore
1238	pEB-flag	High expression of 3xflag-fusions in mammalian cells	M. Chekulaeva
1239	pEBH	High expression of HA-fusions in mammalian cells	M. Chekulaeva
1124	pCiNeo-NHA	Expression of NHA-fusions for tethering	R. Pillai[309]
1125	pCiNeo-HA	Expression of HA-fusions for tethering (untethered controls)	R. Pillai[309]
1010	pBI-F3	Dox-inducible expression of shRNAs	K. Schoenig[688]

4.8.2 List of plasmids

Plasmids listed in the table below were cloned by the author:

pMCh	Name	Vector	Insert	Insert species	Cloning strategy	Purpose
1299	pEBG-3xflag-mAP1G1	pEBG without GST-tag	3xflag tag-mAP1G1iso2	M. musculus	Plasmid was generated by amplifying AP1G1 ORF with MCh 1068&1066 from p1243, digesting the insert with SbfI-NotI and cloning it into NotI-SbfI digested p1238	
1300	pEBG-3xflag-hAP1B1	pEBG without GST-tag	3xflag tag-hAP1B1iso2	H. sapiens	Plasmid was generated by amplifying AP1B1 ORF with MCh 1071&1069 from p1244, digesting the insert with SbfI-NotI and cloning it into NotI-SbfI digested p1238	Vector for high-level expression (EF1A promotor) of flag-tagged adaptor proteins. Used for pulldown/OE experiments.
1302	pEBG-3xflag-mAP1G1 appendage	pEBG without GST-tag	3xflag tag-mAP1G1iso2-appendage	M. musculus	Plasmid was generated by amplifying AP1G1 appendage region from p1251 with MCh 1066&1067, digesting the insert with SbfI-NotI and cloning it into NotI-SbfI digested p1238	
1303	pEBG-3xflag-hAP1B1 appendage	pEBG without GST-	3xflag tag-hAP1B1iso2-appendage	H. sapiens	Plasmid was generated by amplifying AP1B1 appendage region from	

pMCh	Name	Vector	Insert	Insert species	Cloning strategy	Purpose
		tag			p1252 with MCh 1072&1069, digesting the insert with SbfI-NotI and cloning it into NotI-SbfI digested p1238	
1304	pEBG-3xflag-hAP1B1 N-term+hinge region	pEBG without GST-tag	3xflag tag-hAP1B1iso2-hinge region	H. sapiens	Plasmid was generated by amplifying AP1B1 hinge region from p1244 with MCh 1071&1070, digesting the insert with SbfI-NotI and cloning it into NotI-SbfI digested p1238	
1316	pEBG-3xflag-hAP2A appendage	pEBG without GST-tag	3xflag tag-hAP2A-appendage	H. sapiens	Plasmid was generated by amplifying AP2A appendage region from HEK293 cDNA with 1185&1184, digesting the insert with SbfI-NotI and cloning it into NotI-SbfI digested p1238	
1318	pEBG-3xflag-hAP2B appendage+hinge	pEBG without GST-tag	3xflag tag-hAP2B-appendage+hinge	H. sapiens	Plasmid was generated by amplifying AP2B appendage-hinge region from HEK293 cDNA with 1186&1187, digesting the insert with SbfI-NotI and cloning it into NotI-SbfI digested p1238	
1377	pCiNeo-NHA-TNRC6A	pCiNeo	NHA flTNRC6A siRNA insensitive	H. sapiens	flTNRC6A was amplified from 2 fragments: an N-terminal fragment amplified using primers mch1209&658 and pMCh1218 as a template. The C-terminal fragment was amplified using mch659&660 as primers and pMCh833 as template. A 1:1 mix of the resulting PCR fragments was used as template with primers mch1209&660 to amplify the full length TNRC6A. The resulting fragment was digested with Sbfi-NotI and cloned in SbfI-NotI cut p1124	Expression constructs for NHA flTNRC6A wt, 8W8A mut and 8W8W+PAM2 mut insensitive to siRNA targeting TNRC6A (siMCh6). Used in tethering and rescue experiments.
1378	pCiNeo-NHA-TNRC6A 8W8A	pCiNeo	NHA-fl TNRC6A 8W8A, siRNA insensitive	H. sapiens	fl8W8A TNRC6A was amplified from 2 fragments: an N-terminal fragment amplified using primers	

pMCh	Name	Vector	Insert	Insert species	Cloning strategy	Purpose
					mch1209&658 and pMCh1218 as a template. The C-terminal fragment was amplified using mch659&660 as primers and pMCh860 as template. A 1:1 mix of the resulting PCR fragments was used as template with primers mch1209&660 to amplify the full engths TNRC6A. The resulting fragment was digested with Sbfi-NotI and cloned in SbfI-NotI cut p1124	
1379	pCiNeo-NHA-TNRC6A 8W8A/PAM2	pCiNeo	NHA-fl TNRC6A 8W8A/PAM2MUT, siRNA insensitive	H. sapiens	fl8W8A+PAM2 mut TNRC6A was amplified from 2 fragments: an N-terminal fragment amplified using primers mch1209&658 and pMCh1218 as a template. The C-terminal fragment was amplified using mch659&660 as primers and pMCh863 as template. A 1:1 mix of the resulting PCR fragments was used as template with primers mch1209&660 to amplify the ful length TNRC6A. The resulting fragment was digested with Sbfi-NotI and cloned in SbfI-NotI cut p1124	
1380	pCiNeo-HA-TNRC6A	pCiNeo	HA-flTNRC6A siRNA insensitive	H. sapiens	flTNRC6A was amplified from 2 fragments: an N-terminal fragment amplified using primers mch1209&658 and pMCh1218 as a template. The C-terminal fragment was amplified using mch659&660 as primers and pMCh833 as template. A 1:1 mix of the resulting PCR fragments was used as template with primers mch1209&660 to amplify the full length TNRC6A. The resulting	Expression constructs for HA flTNRC6A wt, 8W8A mut and 8W8W+PAM2 mut insensitive to siRNA targeting TNRC6A (siMCh6). Used in tethering as negative controls and in rescue experiments.

pMCh	Name	Vector	Insert	Insert species	Cloning strategy	Purpose
					fragment was digested with Sbfi-NotI and cloned in SbfI-NotI cut p1125	
1381	pCiNeo-HA-TNRC6A 8W8A	pCiNeo	HA-fl TNRC6A 8W8A, siRNA insensitive	H. sapiens	fl8W8A TNRC6A was amplified from 2 fragments: an N-terminal fragment amplified using primers mch1209&658 and pMCh1218 as a template. The C-terminal fragment was amplified using mch659&660 as primers and pMCh860 as template. A 1:1 mix of the resulting PCR fragments was used as template with primers mch1209&660 to amplify the full engths TNRC6A. The resulting fragment was digested with Sbfi-NotI and cloned in SbfI-NotI cut p1125	
1382	pCiNeo-HA-TNRC6A 8W8A/PAM2	pCiNeo	HA-fl TNRC6A 8W8A/PAM2MUT, siRNA insensitive	H. sapiens	fl8W8A+PAM2 mut TNRC6A was amplified from 2 fragments: an N-terminal fragment amplified using primers mch1209&658 and pMCh1218 as a template. The C-terminal fragment was amplified using mch659&660 as primers and pMCh863 as template. A 1:1 mix of the resulting PCR fragments was used as template with primers mch1209&660 to amplify the ful length TNRC6A. The resulting fragment was digested with Sbfi-NotI and cloned in SbfI-NotI cut p1125	
1383	pCiNeo-NHA-TNRC6A-W1387,1397Y	pCiNeo	NHA-fl TNRC6A-2W2Y, siRNA insensitive	H. sapiens	Plasmid 1377 was used for site-directed mutagenesis with primers 1196&1197 to mutate W1387 and W1397 to Y	Expression constructs for NHA-flTNRC6A bearing W-->Y mutations within W-motifs; the construct is insensitive to siRNA targeting TNRC6A
1384	pCiNeo-NHA-TNRC6A-W1387,1397,13	pCiNeo	NHA-fl TNRC6A-3W3Y, siRNA	H. sapiens	Plasmid 1383 was used for site-directed mutagenesis with primers 1198&1199 to	

pMCh	Name	Vector	Insert	Insert species	Cloning strategy	Purpose
	40Y		insensitive		mutate W1340 to Y	(siMCh6). Used in tethering and rescue experiments.
1385	pCiNeo-NHA-TNRC6A-W1387,1397,1340, 1239Y	pCiNeo	NHA-fl TNRC6A-4W4Y, siRNA insensitive	H. sapiens	Plasmid 1384 was used for site-directed mutagenesis with primers 1200&1201 to mutate W1239 to Y	
1386	pCiNeo-NHA-TNRC6A-W1387,1397,1340, 1239,1226,1215Y	pCiNeo	NHA-fl TNRC6A-6W6Y, siRNA insensitive	H. sapiens	Plasmid 1385 was used for site-directed mutagenesis with primers 1202&1203 to mutate W1226, 1215 to Y	
1387	pCiNeo-NHA-TNRC6A-W1387,1397,1340,1239,1226,1215,1171Y	pCiNeo	NHA-fl TNRC6A-7W7Y, siRNA insensitive	H. sapiens	Plasmid 1386 was used for site-directed mutagenesis with primers 1204&1205 to mutate W1171 to Y	
1388	pCiNeo-NHA-TNRC6A-W1387,1397,1340, 1239,1226,1215,1171,1141Y	pCiNeo	NHA-fl TNRC6A-8W8Y, siRNA insensitive	H. sapiens	Plasmid 1387 was used for site-directed mutagenesis with primers 1206&1273 to mutate W1141 to Y	
1389	pCiNeo-HA-TNRC6A-W1387,1397,1340, 1239,1226,1215,1171,1141Y	pCiNeo	HA-fl TNRC6A-8W8Y, siRNA insensitive	H. sapiens	flTNRC6A-8Y was amplified with oligos 1209&660, digested with SbfI-NotI and inserted into sbfI-notI digested p1125	
1391	pCiNeo-NHA-TNRC6A-W1387,1397,1340, 1239, 1226Y	pCiNeo	NHA-fl TNRC6A-5W5Y, siRNA insensitive	H. sapiens	Plasmid 1385 was used for site-directed mutagenesis with primers 1202&1203 to mutate W1226, 1215Y, but only one mut was effective	
1392	pCiNeo-NHA-TNRC6A-W1387,1397,1340, 1226, 1215Y	pCiNeo	NHA-fl TNRC6A-5W5Y, siRNA insensitive	H. sapiens	Plasmid 1384 was used for site-directed mutagenesis with primers 1202&1203 to mutate W1226, 1215 to Y	
1427	pBIF3-CHC (siMCh17) miRNA-d1GFP	p1010	tgctgttgacagtgagcgaAATCGCCCATCTGAAGGTCCTctgtgaagccacagatgggAGGACCTTCAGATGGGCGATTctgcctactgcctcggacttcaaggg	synthetic	miRNA sequence was generated by oligo anneling/ligation: PNK and anneal oligos mch1648&1651 and mch1649&1650, ligate the two pairs ON at RT, gel-purify the shRNA, clone in dephosphorylated BsaI-cut pMCh1010.	Plasmid expressing CHC-targeting siRNA (corresponds to siRNA from the lab collection siMCh17) under Tet-inducible promoter. Can be used to generate stable cell lines with conditional miRNA-

pMCh	Name	Vector	Insert	Insert species	Cloning strategy	Purpose
						mediated KD of clathrin heavy chain (CHC).
1468	pCiNeo-HA-nvGW182 (Addgene 82418)	pCiNeo	HA-nvGW182	*N. vectensis*	nvGW182 was amplified using primers mch1735&1736 and pMCh1429 as a template. The resulting fragment was digested with SbfI-NotI and cloned in SbfI-NotI cut and dephosphorylated p1125 (pCiNeo-HA) and p1124 (pCiNeo-NHA) vectors.	Expression constructs for HA-nvGW182 and NHA-nvGW182. Used in tethering experiments.
1469	pCiNeo-NHA-nvGW182 (Addgene 82419)	pCiNeo	NHA-nvGW182	*N. vectensis*		
1474	pCiNeo-HA-nvGW182-ΔCED (Addgene 82420)	pCiNeo	HA-nvGW182-Nterminus (aa 1-1158)	*N. vectensis*	NED of nvGW182 was amplified using primers mch1735&1795 and pMCh1429 as a template. CED using primers 1736&1796 and p1429 as a template. The resulting fragments were digested with SbfI-NotI and cloned in SbfI-NotI cut and dephosphorylated p1125 (pCiNeo-HA) and p1124 (pCiNeo-NHA) vectors.	Expression constructs for HA and NHA tagged N-terminal and C-terminal domain of nvGW182. Used in tethering experiments.
1475	pCiNeo-HA-nvGW182-CED (Addgene 82421)	pCiNeo	HA-nvGW182-Cterminus (aa 1159-1698)	*N. vectensis*		
1476	pCiNeo-NHA-nvGW182-ΔCED (Addgene 82422)	pCiNeo	NHA-nvGW182-Nterminus (aa 1-1158)	*N. vectensis*		
1477	pCiNeo-NHA-nvGW182-CED (Addgene 82423)	pCiNeo	NHA-nvGW182-Cterminus (aa 1159-1698)	*N. vectensis*		
1478	pEBG-nvGW182 (Addgene 82424)	pEBG	Full length nvGW182	*N. vectensis*	fl-Nv-GW182 was amplified using primers 1735&1736 and p1429 as a template; NED using primers mch1735&1795 and pMCh1429 as a template; CED using primers 1736&1796 and p1429 as a template. The resulting fragments were digested with SbfI-NotI and cloned in SbfI-NotI cut and dephosphorylated p805 (pEBG-GST).	Plasmid for high-yield expression of the GST-fused full length, NED or CED of nvGW182 in mammalian cells (for pull-downs and mass-spec)
1479	pEBG-nvGW182-ΔCED (Addgene 82425)	pEBG	nvGW182-Nterminus (aa 1-1158)	*N. vectensis*		
1480	pEBG-nvGW182-CED (Addgene 82426)	pEBG	nvGW182-Cterminus (aa 1159-1698)	*N. vectensis*		
1488	pCiNeo-NHA-nvGW182 W1657A	pCiNeo	NHA-nvGW182-1W1A	*N. vectensis*	Use oligos 1833&1834 and p1469 as template to mutate W1657A	To generate a mutant nvGW182 with 11 W-motifs within the CED
1489	pCiNeo-NHA-nv	pCiNeo	NHA-nvGW182-	*N.*	Use oligos 1831&1832 and	

pMCh	Name	Vector	Insert	Insert species	Cloning strategy	Purpose
	GW182 W1657, 1638A		2W2A	*vectensis*	p1488 as template to mutate W1638A	mutated to Ala
1490	pCiNeo-NHA-nvGW182 W1657, 1638, 1627A	pCiNeo	NHA-nvGW182-3W3A	*N. vectensis*	Use oligos 1829&1830 and p1489 as template to mutate W1627A	
1491	pCiNeo-NHA-nvGW182 W1657, 1638, 1627, 1589A	pCiNeo	NHA-nvGW182-4W4A	*N. vectensis*	Use oligos 1827&1828 and p1490 as template to mutate W1589A	
1492	pCiNeo-NHA-nvGW182 W1657, 1638, 1627, 1589, 1574A	pCiNeo	NHA-nvGW182-5W5A	*N. vectensis*	Use oligos 1825&1826 and p1491 as template to mutate W1574A	
1493	pCiNeo-NHA-nvGW182 W1657, 1638, 1627, 1589, 1574, 1453A	pCiNeo	NHA-nvGW182-6W6A	*N. vectensis*	Use oligos 1823&1824 and p1492 as template to mutate W1453A	
1494	pCiNeo-NHA-nvGW182 W1657, 1638, 1627, 1589, 1574, 1453, 1391A	pCiNeo	NHA-nvGW182-7W7A	*N. vectensis*	Use oligos 1821&1822 and p1493 as template to mutate W1391A	
1495	pCiNeo-NHA-nvGW182 W1657, 1638, 1627, 1589, 1574, 1453, 1391, 1309A	pCiNeo	NHA-nvGW182-8W8A	*N. vectensis*	Use oligos 1819&1820 and p1494 as template to mutate W1309A	
1496	pCiNeo-NHA-nvGW182 W1657, 1638, 1627, 1589, 1574, 1453, 1391, 1309, 1227A	pCiNeo	NHA-nvGW182-9W9A	*N. vectensis*	Use oligos 1817&1818 and p1495 as template to mutate W1227A	
1497	pCiNeo-NHA-nvGW182 W1657, 1638, 1627, 1589, 1574, 1453, 1391, 1309, 1227, 1183A	pCiNeo	NHA-nvGW182-10W10A	*N. vectensis*	Use oligos 1815&1816 and p1496 as template to mutate W1183A	
1498	pCiNeo-NHA-nvGW182 W1657, 1638, 1627, 1589, 1574, 1453, 1391, 1309, 1227, 1183, 1167A	pCiNeo	NHA-nvGW182-11W11A	*N. vectensis*	Use oligos 1813&1814 and p1497 as template to mutate W1167A	

pMCh	Name	Vector	Insert	Insert species	Cloning strategy	Purpose
	(Addgene 82427)					
1510	pCiNeo-NHA-Δdnaj-nvGW182	pCiNeo	Δdnaj-nvGW182	*N. vectensis*	Fragments were amplified using oligos 1855&1736 and 1855&1795, SbfI-NotI digested and cloned into SbfI-NotI-cut p1124	Constructs to tether Δdnaj-nvGW182 and its NED to mRNAs. Used with p1468 and p1474, respectively as negative controls
1511	pCiNeo-NHA-Δdnaj-ΔCED nvGW182	pCiNeo	Δdnaj-ΔCED nvGW182	*N. vectensis*		
1517	pEBG-Δdnaj-nvGW182	pEBG	Δdnaj-nvGW182	*N. vectensis*	Fragments were amplified using oligos 1855&1736 and 1855&1795, SbfI-NotI digested and cloned into SbfI-NotI-cut p805	Constructs encoding GST-fusions of Δdnaj-GW182 and Δdnaj-NED. Used in GST pull-down assays
1518	pEBG- Δdnaj-ΔCED nvGW182	pEBG	Δdnaj-ΔCED nvGW182	*N. vectensis*		
1519	pEBG-nv-dnaj	pEBG	DNAJ domain nv GW182	*N. vectensis*	Fragments were amplified using oligos 1735&1861, SbfI-NotI digested and cloned into SbfI-NotI-cut p805 and p1124	Construct for GST pulldowns
1520	pCiNeo-NHA-nv-dnaj	pCiNeo	DNAJ domain nv GW182	*N. vectensis*		Construct for tethering
1522	pEBG-nv-GW182-CED_11W11A (W1657, 1638, 1627, 1589, 1574, 1453, 1391, 1309, 1227, 1183, 1167A) (Addgene 82428)	pEBG	nvGW182-Cterminus (aa 1159-1698) with 11 W-motifs mutated to A	*N. vectensis*	Fragments were amplified using oligos 1796&1736, p1498, p1494, p1490 and p1488 were used as templates, respectively. Amplicons were SbfI-NotI digested and cloned into SbfI-NotI-cut p1124	Construct for GST pulldowns
1523	pCiNeo-NHA-nv-GW182-CED_1W1A (W1657A)	pCiNeo	nvGW182-Cterminus (aa 1159-1698) with 1 W-motif mutated to A	*N. vectensis*		Constructs for tethering
1524	pCiNeo-NHA-nv-GW182-CED_3W3A (W1657, 1638, 1627A)	pCiNeo	nvGW182-Cterminus (aa 1159-1698) with 3 W-motifs mutated to A	*N. vectensis*		
1525	pCiNeo-NHA-nv-GW182-CED_7W7A (W1657, 1638, 1627, 1589, 1574, 1453, 1391A)	pCiNeo	nvGW182-Cterminus (aa 1159-1698) with 7 W-motifs mutated to A	*N. vectensis*		

pMCh	Name	Vector	Insert	Insert species	Cloning strategy	Purpose
1526	pCiNeo-NHA-nv-GW182-CED_11W11A (W1657, 1638, 1627, 1589, 1574, 1453, 1391, 1309, 1227, 1183, 1167A) (Addgene 82429)	pCiNeo	nvGW182-Cterminus (aa 1159-1698) with 11 W-motifs mutated to A	*N. vectensis*		
1527	pCiNeo-NHA-nv-GW182-CED_8W8A W1657, 1638, 1627, 1589, 1574, 1453, 1391, 1309A	pCiNeo	nvGW182-Cterminus (aa 1159-1698) with 8 W-motifs mutated to A	*N. vectensis*	Fragments were amplified using oligos 1796&1736, p1495, p1496 and p1497 were used as templates, respectively. Amplicons were SbfI-NotI digested and cloned into SbfI-NotI-cut pCiNeo-NHA (p1124)	
1528	pCiNeo-NHA-nv-GW182-CED_9W9A W1657, 1638, 1627, 1589, 1574, 1453, 1391, 1309, 1227A	pCiNeo	nvGW182-Cterminus (aa 1159-1698) with 9 W-motifs mutated to A	*N. vectensis*		
1529	pCiNeo-NHA-nv-GW182-CED_10W10A W1657, 1638, 1627, 1589, 1574, 1453, 1391, 1309, 1227, 1183A	pCiNeo	nvGW182-Cterminus (aa 1159-1698) with 10 W-motifs mutated to A	*N. vectensis*		
1533	pEBG-3xflag-hAP2B full length	pEBG without GST-tag	3xflag tag-hAP2B	H. sapiens	Plasmid was generated by amplifying AP2B from HEK293 cDNA with 1889&1890, digesting it with SbfI-NotI and cloning it into p1238 NotI-SbfI digested	Vector for high level expression (EF1A promotor) of flag-taged proteins, used for pulldown/OE experiments. AP2B can be cut out with Sbfi-NotI.
1534	pEBG-3xflag-hAP2B appendage	pEBG without GST-tag	3xflag tag-hAP2B-appendage	H. sapiens	Plasmid was generated by amplifying AP2B appendage region from plasmid p1318 with oligos 1894&1187, digesting it with SbfI-NotI and cloning it into p1238	Vector for high level expression (EF1A promotor) of flag-taged proteins, used for pulldown/OE

pMCh	Name	Vector	Insert	Insert species	Cloning strategy	Purpose
					NotI-SbfI digested	experiments. AP2B appendage can be cut out with Sbfi-NotI.
1535	pCiNeo-NHA-nv-GW182-CED_1st4W4A (W 1309, 1227, 1183, 1167A)	pCiNeo	Nv GW182-Cterminus (aa 1159-1698) with the most N-terminal 4 W-motifs mutated to A	*N. vectensis*	Plasmid was generated by amplifying an N-terminus fragment of Nv CED with 4W4A with oligos 1796&1907 using p1498 as template and a C-terinal fragment with oligos 1908&1736 and p1468 as template. The two overlapping fragments were amplified using oligos 1796&1736. Final amplicon was SbfI-NotI digested and cloned into p1124 NotI-SbfI digested.	Plasmid used in tethering assays to test whether these 4 W-motifs are crucial for silencing
1536	pEBG-nv-GW182-CED_1st4W4A (W 1309, 1227, 1183, 1167A)	pEBG	Nv GW182-Cterminus (aa 1159-1698) with the most N-terminal 4 W-motifs mutated to A	*N. vectensis*	Plasmid was generated by amplifying an N-terminus fragment of Nv CED with 4W4A with oligos 1796&1907 using p1498 as template and a C-terinal fragment with oligos 1908&1736 and p1468 as template. The two overlapping fragments were amplified using oligos 1796&1736. Final amplicon was SbfI-NotI digested and cloned into p805 NotI-SbfI digested.	Plasmid used in GST pull-down assays to test whether these 4 W-motifs are crucial for CCR4-NOT binding
1537	pCiNeo-NHA-hybrid GW182 (siR insensitive) (Addgene 82430)	pCiNeo	Chimera GW182 with N-terminus from human TNRC6A iso2 and C-terminus of Nematostella GW182	*Homo sapiens* + *N. vectensis*	Plasmid was generated by amplifying an N-terminus fragment of hTNRC6A with oligos 1209&1899 using p1377 as template and a C-terminal fragment of NvGW182 with oligos 1900&1736 and p1468 (wt) or p1498 (mut) as template. The two overlapping fragments were amplified using oligos 1209&1736. Final amplicon was SbfI-NotI digested and cloned into p1124 NotI-SbfI digested.	HA- and NHA-fusions used in rescue assays
1538	pCiNeo-NHA-hybrid GW182 mut (siR insensitive) (Addgene 82431)	pCiNeo	Chimera GW182 with N-terminus from human TNRC6A iso2 and mutant C-terminus of Nematostella GW182	*Homo sapiens* + *N. vectensis*		

pMCh	Name	Vector	Insert	Insert species	Cloning strategy	Purpose
			(11W11A)			
1539	pEBG-hybrid GW182 (siR insensitive) (Addgene 82432)	pEBG	Chimera GW182 with N-terminus from human TNRC6A iso2 and C-terminus of Nematostella GW182	*Homo sapiens* + *N. vectensis*	Plasmid was generated by amplifying an N-terminus fragment of hTNRC6A with oligos 1209&1899 using p1377 as template and a C-terminal fragment of NvGW182 with oligos 1900&1736 and p1468 (wt) or p1498 (mut) as template. The two overlapping fragments were amplified using oligos 1209&1736. Final amplicon was SbfI-NotI digested and cloned into p805 NotI-SbfI digested.	GST-fusions used in GST pull-down assays to test for AGO and CCR4-NOT binding
1540	pEBG-hybrid GW182 mut (siR insensitive) (Addgene 82433)	pEBG	Chimera GW182 with N-terminus from human TNRC6A iso2 and mutant C-terminus of Nematostella GW182 (11W11A)	*Homo sapiens* + *N. vectensis*		
1545	pEBG-3xflag-nvAGO1	pEBG without GST-tag	Nematostella Ago1	*N. vectensis*	Ago1 and Ago2 were amplified with oligos 1909&1910 and p1541 and 1542 as templates, respectively; digested with SbfI-NotI and cloned into SbfI-NotI digested p1238 and p1239	Plamsids co-transfected with GST-nvGW182 and its domains to test interaction between nvGW182 and nvAgo1 and 2 in GST pull-down assays
1546	pEBG-3xflag-nvAGO2	pEBG without GST-tag	Nematostella Ago2	*N. vectensis*		
1547	pEBG-HA-nvAGO1 (Addgene 82434)	pEBG without GST-tag	Nematostella Ago1	*N. vectensis*		
1548	pEBG-HA-nvAGO2 (Addgene 82435)	pEBG without GST-tag	Nematostella Ago2	*N. vectensis*		
1552	pEBG-nv-GW182-CED_4W4A (W1657, 1638, 1627, 1589A)	pEBG	nvGW182 CED (aa 1159-1698) with the last 4 W-motifs mutated to A	*N. vectensis*	CED was amplified using oligos 1796&1736 and p1491 as templates. Amplicons were SbfI-NotI digested and cloned into SbfI-NotI-cut p805	GST-fusion used in pull-down assays together with 1st 4W4A mut o test whether the position of W-motifs is relevant for silencing and CNOT/AGO binding
1553	pCiNeo-NHA-nv-GW182-CED_4W4A (W1657, 1638, 1627, 1589A)	pCiNeo	nvGW182 CED (aa 1159-1698) with the last 4 W-motifs mutated to A	*N. vectensis*	CED was amplified using oligos 1796&1736 and p1491 as templates. Amplicons were SbfI-NotI digested and cloned into SbfI-NotI-cut p1124	NHA-fusion used in tethering assays together with 1st 4W4A mut to test whether the position of mutated W-motifs is relevant for

pMCh	Name	Vector	Insert	Insert species	Cloning strategy	Purpose
						silencing
1554	pEBG-nvGW182 W1657, 1638, 1627, 1589, 1574, 1453, 1391, 1309, 1227, 1183, 1167A	pEBG	nvGW182 11W11A mut	*N. vectensis*	nvGW182 was amplified using oligos 1735&1736 and p1498 as templates. Amplicons were SbfI-NotI digested and cloned into SbfI-NotI-cut p805	GST-fusion used in pull-down assays to test for CNOT/AGO binding
1555	pEBG-TNRC6A siR resi	pEBG	TNRC6A	*H. sapiens*	TNRC6A was amplified using oligos 1209&660 and p1377 as templates. Amplicons were SbfI-NotI digested and cloned into SbfI-NotI-cut p805	Used in pull-down assays as positive control for CNOT/AGO binding
1556	pEBG-TNRC6A 8W8A mut siR resi	pEBG	TNRC6A 8W8A mut	*H. sapiens*	TNRC6A 8W8A mut was amplified using oligos 1209&660 and p1378 as templates. Amplicons were SbfI-NotI digested and cloned into SbfI-NotI-cut p805	Used in pull-down assays as positive control for AGO binding and negative control on CNOT binding
1570	pEBG-3xflag-Caf1 mut	pEBG without GST-tag	CNOT7/CAF1 D40A	(Zheng et al., 2008), Ann-Bin Shyu;	Oligos 2026&2027 and 2024&2059 were used to amplify CNOT7 and CNOT6 cat mut from vectors 1530 and 1531, respectively.	High expression vectors for CCR4-NOT catalytic mutants. Used in tethering
1571	pEBG-3xflag-Ccr4a mut	pEBG without GST-tag	Ccr4a/CNOT6 E240A	(Chang et al., 2004) - Ann-Bin Shyu;	Amplicons were SbfI-NotI digested and cloned into SbfI-NotI digested pEBG-3xflag (p1545)	experiment to test if silencing is truly mediated by the deadenylase activity of the CCR4-NOT complex
1591	pCiNeo-NHA-nv-GW182-CED_1st1W1A (W1167A)	pCiNeo	Nv GW182-Cterminus (aa 1159-1698) with the most N-terminal 1 W-motifs mutated to A	*N. vectensis*	Plasmid was generated by site-directed mutagenesis of p1477 with oligos 1813&1814.	Used in tethering assays to discriminate whether is the number or the position (or both) of mutated W-motifs that mostly affects silencing
1592	pCiNeo-NHA-nv-GW182-CED_1st2W2A (W1167, 1183A)	pCiNeo	Nv GW182-Cterminus (aa 1159-1698) with the most N-terminal24 W-motifs mutated to A	*N. vectensis*	Plasmid was generated by site-directed mutagenesis of p1591 with oligos 1815&1816.	
1593	pCiNeo-NHA-nv-GW182-	pCiNeo	Nv GW182-Cterminus (aa	*N. vectensi*	Plasmid was generated by site-directed mutagenesis of	

pMCh	Name	Vector	Insert	Insert species	Cloning strategy	Purpose
	CED_1st3W3A (W1167, 1183, 1227A)		1159-1698) with the most N-terminal 3 W-motifs mutated to A	*s*	p1592 with oligos 1817&1818.	
1594	pCiNeo-NHA-nv-GW182-CED_last2W2A (W1657, 1638A)	pCiNeo	Nv GW182-Cterminus (aa 1159-1698) with the most C-terminal 2 W-motifs mutated to A	*N. vectensis*	Plasmid was generated by site-directed mutagenesis of p1523 with oligos 1831&1832.	
1597	pEBG-nvΔCED mut 1 (aa 441-1158)	pEBG	nvNED	N. vectensis	Plasmids were generated by amplifying nvNED deletion mutants with 2166&1795, 2167&1795, 2168&1795, 2169&1795, respectively. Amplicons were then digested with SbfI-NotI and cloned into NotI-SbfI digested p805.	Vectors for high level expression (EF1A promotor) of GST-tagged nvNED deletion mutants, used for pulldown/OE experiments to understand which GW-motifs are necessary for Nematostella Ago-binding
1598	pEBG-nvΔCED mut 2 (aa 497-1158)	pEBG	nvNED	N. vectensis		
1599	pEBG-nvΔCED mut 3 (aa 565-1158)	pEBG	nvNED	N. vectensis		
1600	pEBG-nvΔCED mut 4 (aa 643-1158)	pEBG	nvNED	N. vectensis		
1607	pCiNeo-NHA-nvAGO1	pCiNeo	Nematostella Ago1	*N. vectensis*	Ago1 and Ago2 were amplified with oligos 1909&1910 and p1541 and 1542 as templates, respectively; digested with SbfI-NotI and cloned into SbfI-NotI digested p1124 (pCiNeo-NHA) and p1125 (pCiNeo-HA)	Constructs for tethering
1608	pCiNeo-NHA-nvAGO2	pCiNeo	Nematostella Ago2	*N. vectensis*		
1609	pCiNeo-HA-nvAGO1	pCiNeo	Nematostella Ago1	*N. vectensis*		Negative controls for tethering. Used with the corresponding tethered nvAGOs encoded by p1607 and p1608
1610	pCiNeo-HA-nvAGO2	pCiNeo	Nematostella Ago2	*N. vectensis*		
1612	pCiNeo-HA-hAgo2	pCiNeo	human Ago2	*H. sapiens*	hAgo2 was amplified from p1189 with oligos 995&996; digested with SbfI-NotI and cloned into SbfI-NotI digested and dephosphorylated p1125	Negative control for tethering. To be used with the corresponding tethered hAgo2 encoded by p1192
1620	pEBG-NOnvΔCED mut 1 (aa 1-440)	pEBG	nvNED non overlapping del mut	*N. vectensis*	Non-overlapping fragments of nvNED were amplified with the following oligos and templates: mut1 1735&2240, mut2 2166&2237; mut3	Vectors for high level expression of GST-tagged non-overlapping nvNED deletion mutants.
1621	pEBG-	pEBG	nvNED non	*N.*		

pMCh	Name	Vector	Insert	Insert species	Cloning strategy	Purpose
	NOnvΔCED mut 2 (aa 441-496)		overlapping del mut	*vectensis*	2167&2238; mut4 2168&2239. p1429 was used as template. Amplicons were then digested with SbfI-NotI and cloned into NotI-SbfI digested p805.	Used for pulldown/OE experiments to understand which GW-motifs are necessary for *Nematostella* Ago-binding
1622	pEBG-NOnvΔCED mut 3 (aa 497-564)	pEBG	nvNED non overlapping del mut	*N. vectensis*		
1623	pEBG-NOnvΔCED mut 4 (aa 565-642)	pEBG	nvNED non overlapping del mut	*N. vectensis*		

Colleagues or collaborators cloned plasmids listed below; the source is cited:

pMCh	Name	Vector	Insert	Insert species	Purpose	Source
124	pCiNeo-NHA-TNRC6C	pCiNeo	NHA-TNRC6C	*H. sapiens*	Tethering construct for expression of NHA-TNRC6C in mammalian cell	J. Zipprich
133	pCiNeo-NHA-TNRC6C CED	pCiNeo	NHA-TNRC6C-CED	*H. sapiens*	Tethering construct for expression of NHA-TNRC6C-CED in mammalian cells	J. Zipprich
436	pCiNeo-HA-TNRC6B	pCiNeo	HA-TNRC6B	*H. sapiens*	Untethered control for TNRC6 tethering experiments	J. Zipprich
437	pCiNeo-HA-TNRC6C	pCiNeo	HA-TNRC6C	*H. sapiens*	Untethered control for TNRC6 tethering experiments	J. Zipprich
466	pEBG-CED	pEBG	TNRC6C CED	*H. sapiens*	High level expression of GST-fused TNRC6C CED in mammalian cells (for pull-downs and mass-spec)	H. Mathys
607	pCiNeo-NHA-CED 7W7A	pCiNeo	TNRC6C-CED-W1445,1487,1494,1504,1605,1648,1659A	*H. sapiens*	Tethering construct for CED with mutated W-motifs	M. Chekulaeva
633	pEBG-CED 7W7A	pEBG	TNRC6C-CED-W1445,1487,1494,1504,1605,1648,1659A	*H. sapiens*	High level expression of the GST-fused CED 7W7A in mammalian cells (for pull-downs and mass-spec)	M. Chekulaeva
729	pCiNeo-HA	pCiNeo	HA		Construct serving as negative control in tethering assay, can be used as filler DNA	J. Zipprich
730	pCiNeo-NHA	pCiNeo	NHA	*Lambda phage*	Construct serving as negative control in tethering assay, can be used as filler DNA	J. Zipprich

pMCh	Name	Vector	Insert	Insert species	Purpose	Source
731	pCiNeo-NHA-lacZ	pCiNeo	NHA-LacZ	*Lambda phage, E. coli*	Construct serving as negative control in tethering assay, can be used as filler DNA	J. Zipprich
1016	pCiNeo-HA-CED	pCiNeo	HA-TNRC6C CED	*H. sapiens*	Untethered control for CED tethering experiments	J. Zipprich
1019	pCiNeo-NHA-TNRC6B	pCiNeo	NHA-TNRC6B	*H. sapiens*	Tethering construct for expression of NHA-TNRC6B in mammalian cell	J. Zipprich
1049	pEGFP-N1		enhanced GFP	*A. victoria*	Transfection control; can be used as filler DNA	J. Schmoranzer
1070	pCiNeo-NHA-CED 7W7Y	pCiNeo	TNRC6C-CED-W1445,1487,1494,1504,1605,1648,1659Y	*H. sapiens*	Tethering construct for CED with mutated W-motifs	M. Chekulaeva
1075	pEBG-CED 7W7Y	pEBG	TNRC6C-CED-W1445,1487,1494,1504,1605,1648,1659Y	*H. sapiens*	High level expression construct of GST-fused 7W7Y CED (for pull-downs and MS)	M. Chekulaeva
1192	pCiNeo-NHA-hsAGO2	pCiNeo	NHA-hsAGO2	*H. sapiens*	Human AGO2 tethering construct	M. Chekulaeva/ S.J Hermann
1218	pCiNeo-NHA-TNRC6A-siRNAresi	pCiNeo	TNRC6A iso2 siRNA resistant	*H. sapiens*	To be used in rescue assays	E. Izaurralde
1238	pEBG-3xflag-sic	pEBG without GST-tag	3xflag tag sic		High level expression of flag-tagged sic peptide, to be used as filler DNA for pulldowns.	M. Chekulaeva
1243	GFP-AP1Gamma	pEGFP-N1 (Clontech)	GFP-AP 1 Gamma subunit	*M. musculus*	Expression of GFP tagged (C-terminal) Adaptor Protein complex 1 gamma subunit (isoform 2)	J. Bonifacino
1244	GFP-AP1Beta	pEGFP-N1 (Clontech)	GFP-AP 1 Beta subunit	*H. sapiens*	Expression of GFP tagged (C-terminal) Adaptor Protein complex 1 beta subunit (isoform 2)	J. Bonifacino
1305	pEBG-TNRC6CΔCED	pEBG	TNRC6CΔCED	*H. sapiens*	High level expression of GST-fused TNRC6C delta CED (for pull-downs and MS)	C.C. Mattioli
1492	nvGW182	pMA-RQ	Humanized nvGW182	*N. vectensis*		Y. Moran lab
1530	pSR-HA-Caf1 mut (CNOT7)	pSRD5	CAF1 D40A	*H. sapiens*		A. B. Shyu
1531	pSR-HA-Ccr4a mut	pSRD5	E240A	*H. sapiens*		A. B. Shyu

pMCh	Name	Vector	Insert	Insert species	Purpose	Source
	(CNOT6)					
1541	nvAGO1	pGEM-T easy	Nematostella Ago1 (cDNA)	*N. vectensis*		Y. Moran lab
1542	nvAGO2	pGEM-T easy	Nematostella Ago2 (cDNA)	*N. vectensis*		Y. Moran lab

Luciferase reporter plasmids are listed below:

pMCh	Name	Description	Source
673	pRLuc-3Xb	RLuc miRNA repoter with 3 artificial let-7 sites in 3'-UTR, for expression in mammalian cells	R. Pillai[412]
674	pRLuc-3Xb mut	Negative control for p673 (with let-7 sites mutated)	R. Pillai[412]
755	pSF3-FLuc/RLuc-hmga2-wt	Dox-inducible miRNA RLuc reporter with hmga2 3'-UTR targeted by let-7 (FL serves as negative control) for expression in mammalian cells	J. Bethune[392]
756	pSF3-FLuc/RLuc-hmga2-mut	Dox-inducible negative control for p755 (with let-7 sites mutated)	J. Bethune[392]
1028	pRLuc-5boxB	Tethering RLuc reporter for expression in mammalian cells	R. Pillai[309]
678	pFLuc	Fluc transfection control for expression in mammalian cells	R. Pillai[309]

4.9 Antibodies

Name	Host	Raised against	Working dilution	Catalogue number	Source
anti-AGO2 (11A9)	rat	human	IP 1:130; IF 1:500; WB 1:4000	11A9	Ascenion GmbH, Helmholtz Zentrum München, Elisabeth Kremmer
anti-AGO2 (M01)	mouse	human	WB 1:2000	H00027161-M01	Abnova
anti-AP2α	mouse	mouse	WB 1:2000	610502	BD Transduction Laboratories (gift from M. Krauss, FMP)
anti-AP2μ	mouse	human	WB 1:500		BD Transduction Laboratories (gift from M. Krauss, FMP)
anti-CLTC	mouse	rat, human	WB 1:5000; IF 1:250	610499	BD Biosciences
anti-CNOT1	rabbit	human, mouse, rat	WB 1:500; IHC 1:25-1:100	14276-1-AP	Proteintech
anti-CNOT7 (M01A)	mouse	human	WB 1:2000	H00029883-M01A	Abnova
anti-CNOT9 (RQCD1)	rabbit	human	WB 1:5000; IHC 1:20-1:200; IF 1:20-1:200	22503-1-AP	Proteintech
anti-FLAG M2, Clone M2	mouse		WB 1:5000-1:10.000; IF 1:250	F3165	Sigma-Aldrich
anti-GAPDH (6C5)	mouse	rabbit	WB 1:1000; IP: 1-2ug per 100-500ug of tot protein; IF 1:50-1:500	sc-32233	Santa Cruz Biotechnology
anti-GFP	mouse		WB 1:1000; IP 1:150	11814460001	Roche
anti-GST-HRP conjugate	rabbit		WB 1:5000-1:10000		Abcam
anti-GW182 (TNRC6A) A329	rabbit	human	WB 1:5000	A302-329A	Bethyl Laboratories/biomol
anti-GW182 (TNRC6A) A330	rabbit	human	IP 1:200	A302-330A	Bethyl Laboratories/biomol
anti-HA high affinity (3F10)	rat		WB 1:5000; IP 1:200-1:400; ELISA 1:50-1:200	11867431001	Roche
anti-αTubulin	mouse	sea urchin, reacts with human, fly	WB 1:4000; IF 1:2000	T5168	Sigma-Aldrich
Anti-mouse IgG(L)-HRP conjugate	rat	mouse	WB 1:5000-1:100000	ab99632	Abcam
Anti-rat-HRP conjugate	goat	rat	WB 1:5000-1:200000	31470	Thermo Fisher
Anti-rabbit-HRP conjugate	mouse	rabbit	WB 1:5000-1:100000	ab99697	Abcam

4.10 Polyacrylamide gel compositions

Sodium dodecyl sulfate polyacrylamide gels (SDS-PAG) consist of an upper layer of stacking gel and a lower layer of separating gel. Stacking gel contains a low percentage of acrylamide:methylenebisacrylamide (AA:MBA) and buffer conditions that allow proteins to migrate fast and concentrate into a narrow band before entering the separating gel where proteins are resolved according to their molecular weight. Separating gels can have different percentages of AA:MBA, depending on the size range of proteins to be analyzed. To solve big proteins (150-250 kDa) low percentages of AA:MBA are preferred, while for small proteins (10-30 kDa) high percentages are better. To solve a wide range of protein sizes a 10% separating gel is recommended (20-200 kDa).

5% stacking gel:

Reagents	**Volumes**
H_2O	2.2 ml
Acrylamide:Bis 30% 37.5:1	0.5 ml
1.5 M Tris pH 6.8	0.25 ml
20% SDS	0.015 ml
10% APS	0.03 ml
TEMED	0.003 ml
Final volume	3 ml

Separating gels:

Reagents	**7.5%**	**10%**	**12.5%**	**15%**
H_2O	2.9 ml	2.4 ml	1.9 ml	1.4 ml
Acrylamide:Bis 30% 37.5:1	1.5 ml	2 ml	2.5 ml	3 ml
1.5 M Tris pH 8.8	1.5 ml	1.5 ml	1.5 ml	1.5 ml
20% SDS	0.03 ml	0.03 ml	0.03 ml	0.03 ml
10% APS	0.06 ml	0.06 ml	0.06 ml	0.06 ml
TEMED	0.005 ml	0.005 ml	0.005 ml	0.005 ml
Final volume	6 ml	6 ml	6 ml	6 ml

4.11 Softwares

Software name	Provider	Use
Serial Cloner v2.6.1	Serialbasics.free.fr	Molecular cloning
Serial List v2.3	Serialbasics.free.fr	List comparison
SnapGene Viewer v3.1	GSL Biotech	Chromatogram visualization
Imagequant LAS 4000	GE Healthcare (Chicago, IL, USA)	WB
ImageJ	Imagej.nih.gov/ij	Image processing
AlphaView	Proteinsimple (San Jose, CA, USA)	DNA gel imaging
Perseus	Perseus-framework.org	Proteomic data analysis
MikroWin	MikroTek, Germany	Multiplate reader (luciferase assays)
Adobe Photoshop CS6	Adobe Systems (San Jose, CA, USA)	Photo editing
Adobe Illustrator CS6	Adobe Systems (San Jose, CA, USA)	Vector graphics editing (figure assembly)
Prism v7	GraphPad Software Inc. (La Jolla, CA, USA)	Graphing, statistics, data organization
Edu PyMOL v1.7.4	Pymol.org	Structure visualization
DinoXcope v1.9.7	Dino-Lite Europe (The Netherlands)	Inverted light microscope image acquisition
Papers	Papersapp.com	Managing bibliographies

5. Methods

5.1 Cell Culture

Human embryonic kidney fibroblasts (HEK293) and Henrietta Lacks cervical cancer (HeLa) cells were grown in Dulbecco's modified Eagle's medium supplemented High glucose (4.5 g/L) with GlutaMAX™ (DMEM+GlutaMAX, GIBCO) and 10% (v/v) FBS (GIBCO), named complete medium. Cells were grown at 37°C in 5% CO_2. Culture medium was replaced every 2-3 days depending on the growth rate of cells. To split cells the medium was removed, cells were washed once with 5 ml D-PBS without Ca^{2+} and Mg^{2+} (PAN Biotech) and detached by treatment with 1 ml Trypsin-EDTA (0.25%-0.02%; PAN Biotech) at 37°C for 2 to 5 minutes. To inhibit trypsin cells were resuspended in fresh medium and split (1:2-1:20) in a final volume of 9 ml per 10 cm dish. For other formats, amounts were adjusted proportionally. Alternatively, after incubation with trypsin-EDTA cells were resuspended in fresh medium, transferred in a 15 ml falcon and centrifuged at 350 g for 3 minutes. The supernatant was discarded and cells were resuspended in the desired volume of complete medium and distributed to new cell culture flasks or dishes. Cells were cultured for a maximum of 30 passages and then discarded. In order to freeze cells for long term storage low passage cells were re-suspended in freezing medium (90% FBS or 90% complete DMEM, and 10% DMSO) after centrifugation; 1 ml of cell suspension was placed in cryovials; cryovials were stored overnight in a Nalgene freezing container filled with isopropanol at -80°C and transferred in liquid N_2 the following day. Cells were routinely checked for mycoplasma contamination.

For stable isotope labeling using amino acids in cell culture (SILAC) HEK293 cells were grown for at least five passages in SILAC media: Dulbecco's modified eagle medium (DMEM) High glucose (4.5 g/L) depleted of L-arginine, L-lysine and L-glutamine (PAA, custom preparation) supplemented with 10% (v/v) sterile-filtered dialyzed fetal bovine serum (dFBS, Sigma-Aldrich), 4mM stable glutamine (L-alanyl-L-glutamine, PAA), 100 U/ml penicillin-streptomycin (Invitrogen), and with 28 mg/L L-arginine and 48 mg/L L-lysine, either as the light version (L-arginine monohydrochloride, "Arg0" and L-lysine monohydrochloride, "Lys0" Sigma-Aldrich), the medium heavy version ($^{13}C_6$ $^{14}N_4$-L-arginine

monohydrochloride, “Arg6”; 4,4,5,5-D_4-L-lysine monohydrochloride, “Lys4”; Sigma-Aldrich) or the heavy version ($^{13}C_6$ $^{15}N_4$-L-arginine monohydrochloride, “Arg10”; $^{13}C_6$ $^{15}N_2$-L-lysine monohydrochloride, “Lys8”; Sigma-Aldrich).

5.2 DNA work

5.2.1 DNA Extraction with Phenol-Chloroform

DNA was extracted from clarified cell lysates by adding an equal volume of phenol:chloroform:isoamyl alcohol (25:24:1) equilibrated with Tris:HCl pH 8.0 to the DNA containing solution (1:1 ratio). Samples were centrifuged at 15000 *g* for 15 min at 4°C. The aqueous phase (upper phase) was then transferred into a new tube and an equal volume of chloroform was added to the solution (1:1 ratio). Samples were vortexed and centrifuged at 15000 *g* for 15 min at 4°C. The upper layer was transferred in a new eppendorf and the DNA was precipitated by adding 0.1 volumes of 3 M NaOAc pH 5.2 and 2.5 volumes of 100% ethanol. Samples were incubated at -80°C for 1 h to ON (overnight) and centrifuged at 15000 *g* for 1 h at 4°C. Supernatants were discarded, 800 µl of 70% ethanol was added and samples were centrifuged at 15000 *g* for 15 min at 4°C. Pellets were air-dried and resuspended in sterile water.

5.2.2 Agarose gel electrophoresis

Agarose gel electrophoresis was used to visualize and separate nucleic acids according to their size. Electrophoresis was carried out using a horizontal gel electrophoresis apparatus (Carl Roth) connected to a power supply (Biorad, Powerpac Basic). Tris-Borate-EDTA (TBE) buffer (90 mM Tris-Borate, 2mM EDTA) was used as a running buffer. In order to prepare 0.5-2% (w/v) agarose gels, the desired amount of agarose powder (Applichem) was mixed with TBE buffer and dissolved using a microwave. Upon cooling of the solution to ~60°C 0.5 µg/ml of ethidium bromide (Carl Roth) was added and mixed well. The agarose solution was then transferred to a horizontal gel tray or alternatively stored at 60°C up to two weeks. Wells in the gel were formed with combs of the appropriate size. After jellification occurred, combs were removed and DNA or RNA samples were loaded. As a DNA size marker 6 µl of GeneRuler 1kb DNA ladder (ThermoFisher) were used. Samples (200 ng-5 µg) were resuspended in 10x DNA loading dye (ThermoFisher) and loaded. The electrophoretic run was carried out at 60-120 V.

DNA bands were visualized under ultraviolet (UV) light with an AlphaImager HP system (ProteinSimple) system using the AlphaView software (ProteinSimple).

5.2.3 Cloning

Plasmids produced in this study were cloned with PCR-based methods. Sequences of interest were PCR amplified from plasmids or cDNA/gDNA templates. Primers used for PCR reactions contained extra nucleotides in their 5'-end for the addition of desired restriction sites to the ends of the PCR amplicon. PCR products were digested with the desired restriction enzymes and cloned into digested and dephosphorylated vectors with compatible DNA ends.

In order to digest the vector two restriction enzymes producing non-compatible ends were used. The restriction digest reaction was assembled as follows (amounts are given per one reaction):

Reagents	Amounts
10x CutSmart buffer (NEB)/ compatible buffer	5 µl
Restriction enzyme I (20 U/µl)	0.5 µl
Restriction enzyme I (20 U/µl)	0.5 µl
Plasmid	5 µg
H_2O	Add to 50 µl
Final volume	50 µl

As a negative control no restriction enzymes were added. Reactions were incubated at 37°C 4 h-ON. Digested samples and undigested controls were run on a 0.5-1% agarose gel (depending on the plasmid size) to determine whether digestion was successful. Digested fragments of interest were cut out from the gel and purified using the GeneJET Gel Extraction kit (ThermoFisher) according to the manufacturer instruction. Digested vectors were eluted in 30 µl elution buffer and dephosphorylated using thermosensitive alkaline phosphatase (FastAP, ThermoFisher) according to the following mixture (amounts are given per one reaction):

Reagents	Amounts
10x FastAP buffer	3 µl
FastAP (1 U/µl)	1 µl
Digested vector	1-5 µg
H_2O	Add to 30 µl
Final volume	30 µl

Reactions were incubated 1-2 h at 37°C. Digested and dephosphorylated vectors were purified using the GeneJET PCR Purification kit (ThermoFisher) according to the manufacturer instruction and eluted in 50 µl elution buffer.
Inserts were PCR amplified using the Phusion polymerase kit (ThermoFisher) according to the following mix (amounts are given per one reaction):

Reagents	Amounts
5x DNA Polymerase buffer	10 µl
10 mM dNTP mix	1 µl
10 µM forward primer	2.5 µl
10 µM reverse primer	2.5 µl
2 U/µl Phusion DNA polymerase	0.5 µl
Template DNA	25-50 ng plasmid DNA; ~250 ng cDNA/gDNA
H_2O	Add to 50 µl
Final volume	50 µl

As a negative control a reaction mix without template was used. Enzymes were always kept on -20°C cold block.

PCR program:

Step	Description	Purpose
1	3 min 98°C	Denature
2	10 sec 98°C	Denature
3	10 sec Ta	Annealing
4	30 sec per kb 72°C	Elongation
5	Go to 2 30x	Amplification
6	5-10 min 72°C	
7	hold 8°C	

In order to calculate T_m and T_a of the oligos the web-based Tm calculator from ThermoFisher was used: Thermofisher Tm Calculator. PCR amplicons were run on a 1-2% agarose gel (depending on the size of the product) to determine whether amplification was successful. Fragments of interest were cut out from the gel and purified using the GeneJET Gel Extraction kit (ThermoFisher) according to the manufacturer instruction and eluted in 50 µl elution buffer. In order to digest the amplicons the two restriction enzymes recognizing the restriction sites introduced via PCR were used. The restriction digest reaction was assembled as follows (amounts are given per one reaction):

Reagents	Amounts
10x CutSmart buffer (NEB)/ compatible buffer	5 µl
Restriction enzyme I (20 U/µl)	0.5 µl
Restriction enzyme I (20 U/µl)	0.5 µl
PCR amplicon	44 µl
Final volume	50 µl

Reactions were incubated at 37°C ON. Digested fragments were purified using the GeneJET PCR Purification kit (ThermoFisher) according to the manufacturer instruction. Digested inserts were eluted in 30 µl elution buffer. Ligation of processed inserts and vectors was performed using the T4 DNA Ligation kit (ThermoFisher). Reactions were assembled as follows (amounts are given per one reaction):

Reagents	Amounts
10x T4 Ligase buffer	1 µl
Vector (~100 ng)	2 µl
Insert (3x molar excess than vector)	6 µl
T4 DNA ligase	1 µl
Final volume	10 µl

As a negative control on vector re-ligation a reaction mix without insert was used. Ligation reactions were incubated at room temperature (RT) 1 h-ON. 5 µl of ligation product were transformed into chemically competent Xl1b or Mach1 *E. coli* cells. Briefly, competent *E. coli* cells (competency above 10^7-10^8) were thaw on ice. 5µl of ligation mix were added to 50 µl of competent cells and cells were kept on ice for 10 min. Cells were then heat shocked for 1 min at 42°C and transferred back on ice for 2 additional min. 200µl of LB medium were added to each vial and cells were grown at 37°C with shaking for 45 min. Cultures were then spread on LB agars plates containing the corresponding selective antibiotic (resistance encoded from the vector). On the next day, bacteria colonies were counted. If a good ratio of colonies between the positive and negative control was observed, 2-4 colonies from the positive samples were grown in mini cultures of 5 ml LB and antibiotic ON at 37°C shaking at 180 rpm. Plasmid isolation was carried out using the Plasmid Miniprep DNA kit (Roboklon) according to the manufacturer instructions. The success of the cloning was confirmed by screening PCR or restriction digest and DNA sequencing (LGC Genomics). Screening PCRs were

performed using the DreamTaq PCR kit (ThermoFisher). PCR reactions were assembled as follows (amounts are given per one reaction):

Reagents	Amounts
10x DreamTaq Polymerase buffer	2 µl
10 mM dNTP mix	0.4 µl
10 µM forward primer	0.6 µl
10 µM reverse primer	0.6 µl
5 U/µl DreamTaq DNA polymerase	0.08 µl
Template plasmid DNA	10-50 ng
H_2O	Add to 20 µl
Final volume	20 µl

Enzymes were always kept on -20°C cold block.

PCR program:

Step	Description	Purpose
1	3 min 95°C	Polymerase activation
2	30 sec 95°C	Denature
3	45 sec Ta	Annealing
4	1 min per kb 72°C	Elongation
5	Go to 2 30-35x	Amplification
6	5-10 min 72°C	
7	hold 8°C	

5.2.4 Mutagenesis

Site directed mutagenesis was performed according to Zheng et al., 2004[689]. In short, primers used to introduce the mutation were designed according to the following four requirements: (I) minimum 4 nt from the change at the 5'-end, minimum 6 nt from the change at the 3'-end, 8 nt non-overlapping at the 3'-end of each primer; (II) up to 7 nt change for a 40 nt primer; (III) C or G at the primer 3'-end; (IV) primers T_m above 74°C, ΔT_m between primers below 2°C. The PCR reaction was performed according to the following mix using the Phusion polymerase kit (ThermoFisher); amounts are given per one reaction:

Reagents	Amounts
5x DNA Polymerase buffer	4 µl
10 mM dNTP mix	0.4 µl
10 µM forward primer	1 µl
10 µM reverse primer	1 µl
2 U/µl Phusion DNA polymerase	0.2 µl
Template plasmid DNA	25-50 ng
H_2O	Add to 20 µl
Final volume	20 µl

As a negative control a reaction mix without primers was used. Enzymes were always kept on -20°C cold block.

PCR program:

Step	Description	Purpose
1	30 sec 98°C	Polymerase activation
2	10 sec 98°C	Denature
3	10 sec 72°C	Annealing
4	30 sec per kb 72°C	Elongation
5	Go to 2 25x	Amplification of mutated plasmid
6	hold 8°C	

To eliminate the wild type template plasmid, each PCR reaction was incubated with 0.5 µl of the restriction enzyme DpnI (20 U/µl) at 37°C for 30 min (up to overnight, ON). The negative control is used to assess the background given by the undigested template. 5 µl were then used to transform 50 µl of chemically competent Xl1b or Mach1 *E. coli* cells as described in the previous cloning chapter. Bacteria cultures were spread on LB agar plates containing the antibiotic whose resistance gene is present in the template plasmid. On the next day, bacteria colonies were counted. If a good ratio of colonies between the positive

and negative control was observed, 2-4 colonies from the positive samples were grown in mini cultures of 5 ml liquid LB and antibiotic ON at 37°C shaking at 180 rpm. Plasmid isolation was carried out using the Plasmid Miniprep DNA kit (Roboklon) according to the manufacturer instructions. The success of the mutagenesis was confirmed by DNA sequencing (LGC Genomics).

5.3 RNA work

All experimental procedures dealing with RNA were done using nuclease-free water, filter tips and nuclease-free tubes. Reactions were always assembled on ice and enzymes were kept on a -20°C block. Unless otherwise indicated RNA work was performed in an RNA-dedicated hood to minimize the risk of cross contamination with DNA and nucleases.

5.3.1 RNA isolation

Cells were lysed with cytoplasmic RNA lysis buffer (50 mM Tris-HCl pH 7.4, 150 mM KCl, 0.5% Triton X-100, 0.2 mM Pefabloc prepared in DEPC-treated water), clarified and split for luciferase, western blotting and qRT-PCR assay. To isolate RNA, 250 µl of clarified lysates were mixed with 750 µl of TriFast FL (Peqlab) by pipetting the mix up and down several times. After 5 min incubation at RT, 200 µl of chloroform were added, samples were mixed by inversion for 15-20 times and incubated 5 min at RT. Tubes were centrifuged at 12000 *g* for 15 min at 4°C. The upper aqueous phase (~550 µl) was transferred into new tubes and if the expected RNA yield was low (<10 µg) 1 µl of 15 mg/ml GlycoBlue (Ambion) was added as a carrier for precipitation. To precipitate the RNA 500 µl of isopropanol were added, samples were vortexed and incubated 10 min at RT. All steps described above were performed in a laminar flow hood. After incubation, tubes were centrifuged at 12000 *g* for 10 min at 4°C. Samples were then transferred on ice, the supernatant was discarded and pellets were washed by adding 1 ml 70% EtOH, vortexing and centrifuging at 12000 *g* for 5 min at 4°C. Supernatants were discarded and RNA pellets were briefly air dried and then resuspended in DEPC-treated H_2O. RNA concentration and absorbance was estimated using an Eppendorf Biospectrometer or Qubit 2.0 fluorometer (Life Technologies). Only samples with $OD_{260/280}$ between 1.6-2.0 were used for downstream analysis.

5.3.2 cDNA synthesis

1 pg-5 µg of pure RNA (not degraded and with no traces of phenol) was resuspended in 8 µL DEPC-treated H_2O. Within a single experiment the same amount of RNA per each sample was used (i.e. 1 µg). To remove genomic DNA contaminant RNA samples were first treated with RQ1 RNase-free DNase (Promega) according to the following mixture (amounts are given per sample):

Reagents	Amounts
RQ1 DNase 10x buffer	1 µl
RQ1 DNase (1 U/µl)	1 U/µg
RNA	1 pg-5µg
Final volume	10 µl

Samples were incubated at 37°C for 30 min; 1 µL of DNase stop solution (Promega) was then added to the mix to inhibit DNase digestion and samples were incubated at 65°C for 10 min. DNase-treated RNA was immediately used for first strand cDNA synthesis performed with a mixture of random hexamers and oligo-dT primers. Components of the Maxima first strand cDNA synthesis kit (Thermo Fisher) were assembled according to the following formulation (amounts are given per sample):

Reagents	Amounts
5x Reaction mix	4 µl
Enzyme mix	2 µl
RNA	1 pg-4µg
H_2O	To 20 µl
Final volume	20 µl

For each reaction a corresponding “NO RT control” without enzyme and 5x reaction mix was used.

PCR program:

Step	Description
1	10 min 25°C
2	15 min 50°C
3	5 min 85°C
4	Hold 4°C

cDNA samples were stored at -20°C.

5.3.3 qRT-PCR

To estimate relative RNA expression levels of a set of transcripts across samples quantitative real time PCR (qRT-PCR) was performed using the sensiFAST SYBR® No ROX kit (Bioline) and primers listed in section 4.6.4. First, the amplification efficiency (*E*) of each primer pair used was estimated using a series of 10 fold cDNA dilutions and the following formula:

$$E = 10^{-1/slope}$$

Only primer pairs with good amplification efficiency (*E*-1=0.9-1.1; 90%-110%) 1.9≤ *E* ≤2.1 were used. Technical and biological duplicates for each sample and for the respective NO RT controls were run in a CFX96™ real time machine (Biorad). No template controls were added for each primer pair tested.

qRT-PCR mixes were assembled according to the following formulation (amounts are given per sample):

Reagents	Amounts
2x sensiFAST SYBR No ROX mix	5 µl
10 µM forward primer	0.4 µl
10 µM reverse primer	0.4 µl
Template plasmid DNA	5 ng
H_2O	Add to 10 µl
Final volume	10 µl

The following PCR program was used:

Step	Description	Purpose
1	2 min 95°C	Polymerase activation
2	5 sec 95°C	Denature
3	10 sec 60°C	Annealing
4	15 sec 72°C	Elongation
5	Read fluorescence	Quantification
6	Go to 2 40x	Amplification
7	Melting curve 1°C intervals	Check specificity of amplification
8	Hold 8°C	
	Lid 105°C	

At the end of the PCR reaction the amplification curves of all samples were visualized on the Biorad CFX Manager software in a graph plotting cycle numbers (*y* axis) against the $\log_2$ function of the fluorescence intensity derived from the intercalating SYBR green dye (*x* axis). A cycle threshold (Ct), intersecting the linear regions of all curves, was arbitrarily placed and Ct values were exported. Before proceeding to the analysis, Ct values for NO RT and NO template samples

were checked and a minimal difference of 6 Ct values between negative controls and test samples was accepted. Melting curves were also checked to detect the eventual presence of multiple peaks indicating aspecific amplification products. If specificity was achieved, RNA expression levels were calculated using the ΔΔCt method and normalized to reference *GAPDH* or *FLuc* mRNA. Briefly, the mean Ct values obtained from technical replicates and another mean between biological replicates were calculated. The biological mean Ct value of reference mRNA was subtracted from the biological mean Ct value of target mRNA for both the test samples and the control samples according to the following formula:

$$\Delta Ct = Ct_{target} - Ct_{reference}$$

The standard deviation (SD) of ΔCt was calculated as follows:

$$SD = \sqrt{{s_{target}}^2 + {s_{reference}}^2}$$

Where *s* is the standard deviation of either target or reference *Ct* values

Subsequently a ΔΔCt was calculated according to the following formula:

$$\Delta\Delta Ct = \Delta Ct_{test\ sample} - \Delta Ct_{control}$$

Where SD of ΔΔCt corresponds to SD of ΔCt of the test sample. Lastly, the fold difference was calculated as shown below

$$2^{-\Delta\Delta Ct}$$

And the standard deviation was incorporated in the fold difference as follows:

$2^{-(\Delta\Delta Ct+SD)}$ and $2^{-(\Delta\Delta Ct-SD)}$

5.4 Protein work

5.4.1 Protein Extraction

For protein extraction cells were placed on ice, rinsed with ice-cold PBS and lysed in the following lysis buffer:

Lysis buffer
50 mM Tris-HCl pH 7.5
150 mM KCl
0.2 mM Pefabloc or 1 tablet EDTA-free Roche protease inhibitor cocktail
0.5% (v/) Triton X-100

Cells were mechanically scraped in 1 ml lysis buffer per 10 cm dish. For other formats the amount of lysis buffer was adjusted proportionally. Lysates were placed on ice for 5 min, incubated 10 min at 4°C on a rotating wheel and clarified by centrifugation at 1000 *g* for 5 min at 4°C.

5.4.2 Determination of protein concentration

The colorimetric Bradford assay was used to estimate protein concentration. The assay relies on a shift in the color, and consequently the absorbance, of the Comassie Brilliant Blue G-250 dye caused by binding to various concentrations of proteins. The absorbance of the protein bound form of the dye peaks at a wavelength of 595 nm. In order to estimate protein concentrations of cell lysates a series of bovine serum albumin (BSA) dilutions to final concentrations of 100, 250, 500, 750, 1000 and 1500 µg/ml were used as protein standards. As blank sample, 5 µl of lysis buffer were diluted 1:4 in H_2O in a total volume of 20 µl. 5 µl of lysates from test samples (lysed in 1ml) were also diluted 1:4 in H_2O in a total volume of 20 µl. 20 µl of blank, BSA standards and test samples were transferred in 1.5 ml cuvettes; 1 ml of 1x Biorad protein assay (Biorad) containing the G-250 dye was added to each cuvette and mixed by pipetting. A spectrophotometer was adjusted to a wavelength of 595 nm; the absorbance of the blank sample was measured and used as a baseline; standards were then measured. The eppendorf spectrophotometer automatically plots the absorbance of the standards (*y* axis) against their concentration (*x* axis) to derive a standard curve. Linear regression of the data point is calculated. Regression coefficient (R^2) values close to 1 (0.9-1)

had to be obtained in order to proceed with the measurements of test samples. OD_{595} of test samples was then measured and their concentration (C) was automatically derived according to the Beer-Lambert law:

$$C = \frac{OD_{595}}{\varepsilon L} * dilution\ factor$$

Where ε is the slope of the standard curve and L is the length of the cuvette. Concentrations were reliable with OD_{595} values between 0.1-1. If absorbance exceeded this range samples were further diluted.

5.4.3 GST pull-down

HEK293 cells were seeded to 10 cm dishes to reach 70% confluency on the next day. The following day, 0.2-10 µg of plasmids encoding GST fusions (or GST alone) were transfected into HEK293 cells using the transfection reagent polyethylenimine (PEI; Polysciences Inc.) in a 1:5 w/w ratio (DNA:PEI). Within each experiment the same amount of DNA per sample was transfected. In order to obtain comparable expression levels of GST-fusions of considerably different sizes different amounts of GST-fusions were transfected and filler DNA (encoding for the yeast peptide sic) was used to top up to same final amounts (**Figures 20B, 22A, 23B, S3**). Transfection mixtures were assembled by adding first the DNA, secondly 500 µl DMEM without FBS, and lastly PEI (amounts are given per sample). Mix were vortexed, briefly spinned down and incubated 10 min at RT to allow complex formation. Transfection mixes were then added dropwise to the cells.

In order to perform GST pull-down of GST fusions upon knockdown of CCR4-NOT and CCV components (**Figure 15**) $2.5x10^5$ HEK293 cells were seeded per 10 cm dish. One day after seeding, cells were transfected with siRNAs to a final concentration of 20 nM using jetPRIME (Polyplus transfection). siRNAs were resuspended in 500 µl of jetPRIME, 20 µl of jetPRIME transfection reagent were added and mixes were vortexed. After 10 min of incubation at RT, mixes were added dropwise to the cells. 48 h post siRNA transfection a second siRNA transfection round was performed using siRNA to a final concentration of 30 nM. Transfection was performed with jetPRIME as described above. 24 h after the second round of siRNA tranfection cells were transfected with 5 µg GST-fusions

using PEI in a 1:5 ratio (5 µg DNA: 30 µg PEI). Cells were lysed on the next day as described below.

24 h post-transfection of GST-fusions cells were placed on ice, media was removed and cells were rinsed in ice-cold PBS. PBS was removed and cells kept on ice were scraped with 1 ml of lysis buffer [50 mM Tris-HCl pH 7.5, 150 mM KCl, 0.2 mM Pefabloc, 0.5% (v/v) Triton X-100] per dish. In case of co-expression of GST-fusions and HA-fusions (**Figure 22A, 23B**) the percentage of Triton-X-100 in the lysis buffer was lowered to 0.25%. Lysates were incubated 15 min at 4°C on a rotating wheel and clarified by centrifugation at 1000 *g* for 5 min at 4°C. To exclude the identification of protein interactions mediated by nucleic acids clarified lysates (1.5 mg/ml) were treated with one of the following nucleases: (I) 10 ng/µl S7 micrococcal nuclease (Roche) and 1 mM $CaCl_2$ shaking for 30 min at RT (**Figures 8-10, 12, S3**) (II) 300 U/ml micrococcal nuclease (ThermoFisher) and 1 mM $CaCl_2$ shaking for 30 min at RT (**Figures 20B, 20C, 23B**) (III) 10 U/µl RNase T1 (ThermoFisher) shaking for 10 min at 37°C (**Figure 19, 20A, 22A, 23B**). During lysates nuclease treatment, 20 µl of glutathione (GSH)-Sepharose beads (GE Healthcare) per sample were equilibrated 2x in 1 ml washing buffer [50 mM Tris-HCl, pH 7.5, 150 mM KCl, 0.2 mM Pefabloc, 0.1% (v/v) Triton X-100] and 1x in 1 ml lysis buffer. Between each wash beads were spinned down at 1000 *g* for 5 min at 4°C and the supernatants were discarded. Protein concentration of each lysate was assessed by Bradford assays; lysates concentrations were equalized and then incubated with 20 µl of equilibrated beads for 2-4 h at 4 °C on a rotating wheel. Beads were washed three times with washing buffer. Next, washed beads were incubated for 1 h at 4°C on a rotating wheel with 60 µl elution buffer (50 mM GSH in washing buffer, pH adjusted to 7.5 with Tris). Per each experiment, heavy, medium heavy and light SILAC labeled GST-fusions were pooled together and eluted in 8 M guanidinium hydrochloride. Eluates to be used for mass spectrometry were precipitated ON by adding 1 µl of 15 mg/ml GlycoBlue (Ambion) and 10 volumes of 100% EtOH. Samples destined to SDS-PAGE and western blotting were boiled 5 min at 95°C upon addition of 0.2 volumes of 5xSDS-loading buffer [50% glycerol, 300 mM Tris-HCl pH 6.8, 5% 14.3 M β2-mercapto-ethanol, 0.1% (w/v) bromophenol blue, 10% (w/v) SDS].

5.4.4 TNRC6A IP

Per each IP a confluent 10 cm dish of HeLa rtTA cells was used. Cells were lysed in 1 ml lysis buffer [50 mM Tris-HCl pH 7.5, 150 mM KCl, 0.5% (v/v) Triton X-100, 1 tablet of Roche protease inhibitor cocktail complete EDTA free in 10 ml buffer] per 10 cm dish. Lysates were clarified and nuclease treated as described for GST pull-down in section 5.4.3. Protein G Dynabeads slurry (Invitrogen) was mixed by inversion and 50 µl magnetic beads per IP were transferred in an eppendorf tube. Beads were washed three times in PBS-T [PBS with 0.1% (v/v) Tween-20], resuspended in 250 µl PBS-T and 10 µg of TNRC6A A330 antibody (Bethyl) were added. Beads were incubated 3 h to ON on a rotating wheel at 4°C to permit antibody binding. With the help of a magnetic rack the unbound antibody was removed and beads were resuspended in 900 µl cell lysate (~1 mg proteins). TNRC6A IP was performed by incubating samples for 2-4 h on a rotating wheel at 4°C. Beads were then washed three times with washing buffer [50 mM Tris-HCl pH 7.5, 150 mM KCl, 0.1% (v/v) Triton X-100, 1 tablet of Roche protease inhibitor cocktail complete EDTA free in 10 ml buffer], resuspended in 60 µl 1x SDS loading buffer [50% glycerol, 300 mM Tris-HCl pH 6.8, 5% 14.3 M β2-mercapto-ethanol, 0.1% (w/v) bromophenol blue, 10% (w/v) SDS] and boiled 5 min at 95°C. Magnetic beads were removed with the help of a magnetic rack and samples were then analyzed by western blotting.

5.4.5 *Nematostella* AGO1 and CNOT9 IP

For *Nematostella* AGO1-IP a custom antibody raised against the synthetic peptide CMMDRDKEAGNDNSS derived from nvAGO1 was generated in rabbit (GenScript, USA). 10 µg of αnvAGO1 (GenScript) or αCNOT9 (OriGene) antibodies were coupled with protein A magnetic beads (Bio-Rad). *Nematostella* embryos were lyzed in lysis buffer [25 mM Tris-HCl pH 7.5, 150 mM KCl, 25 mM EDTA, 0.5 % NP-40, 1 mM DTT, complete Ultra (Roche) and 2 Set III (Merck) protease inhibitor cocktails] 48 h post-fertilization and 500 µg of lysate were used per each IP. After IP the beads were washed with the wash buffer [50 mM Tris-HCl pH 7.5, 300 mM NaCl, 5 mM $MgCl_2$, 0.05 % NP-40, complete Ultra (Roche) and Set III (Merck) protease inhibitor cocktails], and bound proteins were eluted with SDS-PAGE sample buffer. Inputs and IPs were analyzed by westrn blotting using the following antibodies: a custom αnvGW182 antibody raised against a

recombinant fragment spanning amino acid positions 1301-1698 of nvGW182 in guinea pig (GenScript, USA) 1:1000; αCNOT9 (OriGene) 1:1000; αnvAGO1 (GenScript, described above) 1:1000. *In vivo Nematostella* IPs were performed by Dr. Yehu Moran Lab.

5.4.6 SILAC and Mass Spectrometry

For SILAC and mass spectrometry described in chapter 2.1, labeled HEK293 cells were expanded to one 70% confluent 15 cm dish per affinity purification. Heavy, medium heavy and light labelled cells were transiently transfected with 10-15 µg of the following GST-fusions: TNRC6C CED wt, 7W7A mutant and a GST control on background binders. Alternatively cells were transfected with: CED wt, 7W7A mutant and 7W7Y mutant. Transfections were performed using polyethylenimine transfection reagent (PEI; Polysciences Inc.) in a 1:2 ratio DNA: PEI. Each experiment consisted of a forward replicate and a reverse replicate, in which the labels were swapped to exclude eventual biases introduced by the labelling procedure.

For mass spectrometry experiments described in chapter 2.3, HEK293 cells were expanded to one 70% confluent 10 cm dish per affinity purification. Cells were transiently transfected with 4 µg of the indicated GST-fusions (GST control, nvGW182, nvDNAJ, nvΔCED, nvCED, nvCED11W11A) using PEI in a 1:5 ratio.

In both setups, 24 h post-transfection cells were lysed and nuclease-treated lysates were used in GST pull-downs as described in section 5.4.3. GST pull-downs were eluted in 2 ml eppendorfs and precipitated by adding up to 2 ml 100% EtOH (~20 volumes). Protein precipitates were resuspended in denaturation buffer [6 M urea/2 M thiourea in 10 mM HEPES pH 8.0] then reduced for 30 min at RT in 10 mM dithiothreitol solution, followed by alkylation by 55 mM iodacetamide for 20 min in the dark at RT. The endoproteinase LysC (Wako, Japan) was added following a protein:enzyme ratio of 50:1 and incubated for 4 h at RT. After dilution of the sample with 4x digestion buffer [50 mM ammonium bi-carbonate in water, pH 8.0], sequence grade modified trypsin (Promega) was added (same protein:enzyme ratio as for LysC) and digested overnight. Finally, trypsin and Lys-C activity were quenched by acidification of the reaction mixtures with TFA to pH~2. Afterwards, peptides were extracted and desalted using StageTips[690]. Peptide mixtures were separated by reversed phase chromatography using the

EASY-nLC system (Thermo Scientific) on in-house manufactured 20 cm fritless silica microcolumns with an inner diameter of 75 µm. Columns were packed with ReproSil-Pur C18-AQ 3 µm resin (Dr. Maisch GmbH). Peptides were separated on a 8-60% acetonitrile gradient (224 min) with 0.5% formic acid at a nanoflow rate of 250 nl/min. Eluting peptides were directly ionized by electrospray ionization and transferred into a Q Exactive mass spectrometer (Thermo Scientific). Mass spectrometry was performed in the data dependent positive mode with one full scan (m/z range = 300-1700; R = 70000; target value: 5×10^6; maximum injection time = 120 ms). The ten most intense ions with a charge state greater than one were selected (R = 35000, target value = 5×10^5; isolation window = 4 m/z; maximum injection time = 120 ms). Dynamic exclusion for selected precursor ions was set to 30 s.

MS/MS data were analyzed by MaxQuant[691] software v1.3 (for data shown in chapter 2.1) and v1.5.1.2 (for data shown in chapter 2.3). The internal Andromeda search engine[692] was used to search MS/MS spectra against a decoy human UniProt database (HUMAN.2012 for data in chapter 2.1 and HUMAN.2014-10 for data in chapter 2.3) containing forward and reverse sequences supplemented with the bait sequences. The search included variable modifications of methionine oxidation and N-terminal acetylation, and fixed modification of carbamidomethyl cysteine. Minimal peptide length was set to six amino acids, trypsin was set as the selected protease and a maximum of two missed cleavages was allowed. The FDR was set to 0.01 for peptide and protein identifications.

In SILAC-MS/MS (data in chapter 2.1) corresponding forward and reverse experiments were analyzed together. Subsequent analysis was done using Perseus v1.5.6.0 (MaxQuant environment). First, the data from five experiments (each with forward and reverse; n=9 since one forward experiment had to be excluded due to protein precipitation) were combined using their Uniprot identifier. The mean $\log_2$ fold change (avg $\log_2$FC) of the transformed normalized ratios given by MaxQuant was calculated for each of the following comparisons (both forward and reverse): wt/mut (either 7W7A or 7W7Y), wt/7W7A mut, wt/7W7Y mut, 7W7A/7W7Y. Each mean is representative of 2-5 independent experiments. Proteins were considered enriched interactors if the mean $\log_2$FC of both forward and reverse experiments was above 0.4 (1.3 fold enrichment). Threshold was set to 0.4 to avoid missing low affinity interactions. The 80 W-motif specific interactors

were identified using a one-sample t-test plotting the mean log_2FC wt/mut against the t-test p-value (mean log_2 wt/mut≥ 0.4; p-value< 0.05). Only interactors that were also enriched in comparison to the GST control (mean log_2FC wt/GST≥ 0.4) were considered.

Label-free quantification (LFQ) (data in chapter 2.3) was performed in MaxQuant as described[693]. Unique and razor peptides were considered for quantification with a minimum ratio count of 1. Retention times were recalibrated based on the built-in nonlinear time-rescaling algorithm. MS/MS identifications were transferred between LC-MS/MS runs with the "Match between runs" option, in which the maximal retention time window was set to 2 min. Subsequent analysis was done using Perseus v1.5.6.0 (MaxQuant environment). LFQ intensity values were logarithmized and missing values were imputed with random numbers from a normal distribution whose mean and standard deviation were chosen to best simulate low abundance values below the noise level (width = 0.3; shift= 1.8). nvGW182 GST-fusions pull-downs and GST control were defined as groups of 2 biological replicates and 3 technical replicates; significantly enriched proteins were determined by a volcano plot-based strategy, combining standard two-sample t-test p-values with ratio information. Significance corresponding to an FDR of 0.05 was determined by a permutation-based method[694]. A total of 2275 proteins were identified; to exclude background (GST control) binders from further analysis, only proteins enriched with nvGW182 as compared to GST (log_2 ratio nvGW182/GST> 0; 1337 proteins) were used as inputs of t-tests comparing nvGW182 domains to GST. MS runs and MaxQuant analysis were performed by Dr. Marieluise Kirchner (Selbach Lab).

5.4.7 Western blotting

Proteins were separated by SDS-PAGE according to their size using linear polyacrylamide gels listed in section 4.10. Electrophoresis was performed in a Biorad minitank filled with running buffer [25 mM Tris-base, 191 mM glycine, 0.1% SDS] and ran first at 80 V while samples crossed the stacking gel and at 110 V in the separating gel for ~2.5 h. In order to transfer proteins from a polyacrylamide gel to a PVDF membrane (Millipore) two types of transfer were used: a wet transfer, preferentially for big proteins (above 100 kDa) and lowly expressed proteins or a semi-dry transfer, for proteins between 10-200 kDa and for routine

checks. Once an SDS-PAGE run was over, polyacrilammide gels were removed from their glass support, the stacking gel was cut and the separating gel was wet in transfer buffer [25 mM Tris-base, 191 mM glycine, 20% (v/v) MetOH] for 2 min. PVDF membranes (Millipore) of the same size of the gel were activated for 30 sec in MetOH. For a wet transfer a transfer cassette was assemble by placing the following items in this order: 1 filter pad and 3 filter papers wet in transfer buffer, the gel, an activated PVDF membrane, 2 additional filter papers and a filter pad wet in transfer buffer. The cassette was closed, placed in the transfer module with the membrane side facing the anode, the module was then transferred in a Biorad mini-tank filled with transfer buffer and 0.025-0.1% SDS (for efficient transfer of proteins between 200-250 kDa). Transfer was performed ON at 4°C at 30 V or 1 h at 4°C at 100 V.

For a semi-dry transfer, 7 pieces of filter pads (Biorad) wet in transfer buffer were placed on the bottom (anode) of the transfer cassette (Biorad). The activated membrane was then placed on top, followed by the gel and other 7 wet filter pads. The cassette was closed and transfer was performed for 30 min at 25 V.

After transfer, membranes were blocked in blocking solution [5% (w/v) milk (or BSA) in PBS-T (or TBS-T), PBS with 0.1% (v/v) Tween-20] for 1 h at RT and incubated ON at 4°C in blocking buffer containing the specified primary antibody amongst the ones listed in section 4.9 at the stated working dilution. After primary staining, membranes were washed 3 times for 10 min at RT in PBS-T (or TBS-T); incubated for 1 h at RT with the corresponding HRP-conjugated secondary antibody listed in section 4.9 at the dilution specified and washed 3 times for 10 min at RT in PBS-T (or TBS-T). In order to detect the chemiluminescent signal membrane was incubated with constant shaking in 10 ml ECL reagent [10 ml 100 mM Tris-HCl pH 8.5, 25 μl 90 mM coumaric acid, 50 μl 250 mM luminol and 3 μl 30% (w/w) H_2O_2] for 30 sec and exposed in an ImageQuant LAS 4000 (GE Healthcare) chemiluminescent analyzer. In case the chemiluminescent signal was low the 10x more sensitive Femto kit (Thermo Fisher) was used instead of homemade ECL. Images were acquired and later processed with Photoshop (Adobe). Only minimal adjustments, such as contrast increase, were performed. When explicitly stated signals were quantified using ImageJ64 software.

5.5 CCVs Isolation from HeLa cells

CCV-enriched fractions were prepared as described in[664], with the omission of the RNase A treatment and subsequent pelleting of partially digested ribosomes. Briefly, per each condition tested four confluent 15 cm dishes of HeLa cells were rinsed in ice-cold D-PBS without Ca^{2+} and Mg^{2+} (PAN Biotech) and scraped into 800 μl/dish hypotonic buffer A (0.1 M MES, pH 6.5 adjusted with NaOH, 0.2 mM EGTA, and 0.5 mM $MgCl_2$), resulting in ~4 ml cell suspension per condition. Cells were homogenized with a motorized glass homogenizer with the power head set at 1500 rpm (20 strokes) and the homogenates were clarified by centrifugation at 4100 g for 30 min at 4°C. Membranes were pelleted by centrifugation at 55000 rpm (209900 *g* RCF_{max}) for 40 min in a S110-AT rotor (Thermo Scientific) at 4°C. Pellets were resuspended in 300 μl buffer A with a 1 ml Dounce homogenizer, mixed with an equal volume of FS buffer (12.5% (w/v) ficoll and 12.5% (w/v) sucrose in buffer A) and centrifuged at 20000 rpm (21700 *g* RCF_{max}) for 35 min in a S55-A2 rotor (Thermo Scientific) at 4°C. The following centrifugation steps were performed in an S110-AT rotor (Thermo Scientific). Supernatants were diluted with four volumes of buffer A and centrifuged at 20000 rpm (21700 *g* RCF_{max}) for 15 min at 4°C. Supernatants were centrifuged at 35000 rpm (66500 *g* RCF_{max}) for 30 min at 4°C to obtain the CCV-enriched fraction (pellet). Pellets were resuspended in 100 μl buffer A with a micro-tube sample pestle and used for downstream analysis (yield: 0.3-0.5%). Fractions were snap-frozen in liquid N_2 and stored at -80°C. All steps described above were performed at 4°C and all reagents used were prepared with diethylpyrocarbonate (DEPC)-treated water. HeLa cells stably integrating dox-inducible wt and mut let-7 reporters (HeLa rtTA-755 and HeLa rtTA-756) were induced ON with 1 μg/ml doxycycline prior to CCVs isolation (**Figure 13**).

5.6 Tethering assays

On the first day, $7x10^3$ HEK293 cells were seeded per well of a 96-well plate. The following day cells were transfected with 2 ng RLuc-5BoxB and 30 ng FLuc (transfection control), and 10 ng HA- or NHA-fusion constructs per well of a 96-well plate. Transfections were performed using polyethylenimine (PEI) in a 1:5 ratio DNA:PEI, as described in section 5.4.3. In tethering experiments shown in **Figure 21**, increasing amounts of plasmids encoding $CNOT6_{cat}$ and $CNOT7_{cat}$ (50,

100, and 200 ng) were co-transfected. Transfections containing less than 200 ng of $CNOT_{cat}$ plasmids were topped up to 200 ng with LacZ-encoding plasmid. For other formats, the amounts of plasmids were adjusted proportionally. The media was removed 24 h post transfection, cells were lysed and lysates were used for downstream applications, such as luciferase assays, western blotting and qRT-PCR.

5.7 miRNA reporter assays

HeLa cells stably expressing Tet-On machinery (HeLa rtTA) were used in miRNA reporter assays[685]. In experiments shown in **Figure 14A** (left), $4x10^4$ HeLa rtTA cells were seeded per well of a 96-well plate. Shortly after seeding, cells were co-transfected with 10 ng of dox-inducible wt or mut Fluc/RLuc-hmga2 reporters, 190 ng of filler DNA (pCiNeo-NHA) per well of a 96-well plate and the indicated siRNAs to a final concentration of 10 nM. Transfections were performed using 0.75 μl/well attractene reagent (Qiagen) according to the manufacturer instructions. 6-24 h post transfection medium was replaced to minimize the toxic effects of attractene. 48 h post transfection the expression of the reporters was induced with 0.2 μg/ml doxycycline. 4 h after induction, the media was aspirated and cells were lysed in 1x Passive lysis buffer (Promega) for luciferase assays. In experiments shown in **Figure 14A** (right), $4x10^3$ HeLa rtTA cells stably integrating wt or mut dox-inducible Fluc/RLuc-hmga2 reporters[392] were seeded per well of a 96-well plate. The day after, cells were transfected with the indicated siRNAs to a final concentration of 10 nM using 0.6 μl/well of jetPRIME transfection reagent (Polyplus Transfection) according to the manufacturer instructions. 48 h post transfection, the expression of the reporters was induced with 1 μg/ml doxycycline. 4 h after induction, cells were lysed as described above. In experiments shown in **Figure S5**, $4x10^3$ HeLa rtTA cells were seeded per well of a 96-well plate. The day after, cells were co-transfected with 30 ng Fluc, 1 ng Rluc-3xb artificial let-7 reporter[412], and 19 ng of filler DNA (pCiNeo-NHA) per well of a 96-well plate and the indicated siRNAs to a final concentration of 40 nM. Co-transfection was performed using 0.6 μl/well of jetPRIME transfection reagent (Polyplus Transfection) according to the manufacturer instructions. 48 h post transfection, cells were lysed as described above.

5.8 TNRC6 rescue assays

On the first day, $3x10^3$ HeLa rtTA ("no knockdown" control) and Hela rtTA-TNRC6-KD cells were seeded per well of a 96-well plate. shRNA-mediated TNRC6A&B knockdown was induced for 2 days with doxycycline (1 µg/ml). On day 2, doxycycline was removed and cells were transfected with 0.5 ng/well of FLuc/RLuc-hmga2-wt or FLuc/RLuc-hmga2-mut dox-inducible let7 reporters[275,392], and increasing amounts (50, 100 and 200 ng/well) of the indicated rescue constructs. The same vector backbone encoding LacZ was used as a filler, to top up each transfection to the same total amount of DNA. Transfections were performed using polyethylenimine (PEI) in a 1:5 ratio DNA:PEI, as described in section 5.4.3. On day 3, expression of the reporters was induced with doxycycline (1 µg/ml) for 4 h prior media removal and cell lysis in 1x Passive lysis buffer (Promega). RLuc and FLuc expression was measured via luciferase assays.

5.9 Luciferase assays

Cells transfected with *Renilla* and Firefly luciferase reporters were lysed 24 h after transfection or 4 h after induction when experiments were done using inducible reporters. Media was aspirated and 40 µl of 1x Passive lysis buffer (Promega) were added per well of a 96-well plate. Cells were lysed for 15 min at RT on an orbital shaker. 5 µl lysate per sample were then transferred in a Greiner white microplate and luciferase activities were measured with a homemade luciferase reporter assay system. 45 µl of FLuc reagent (75 mM Hepes pH 8.0, 0.1 mM EDTA, 4 mM $MgSO_4$, 530 µM ATP, 270 µM Coenzyme A, 470 µM DTT and 470 µM luciferin) per sample were used to measure firefly luciferase activity. After firefly quantification, the reaction was quenched and *Renilla* activity measured by adding 45 µl of RLuc reagent (2.2 mM Na_2EDTA, 220 mM K_3PO_4 pH 5.1, 0.44 mg/ml BSA, 1.1 M NaCl, 1.3 mM NaN_3 and 0.6 µg/ml colenterazine) to the same sample. RLuc values were then normalized to the corresponding FLuc values and expressed as percentage of the experimental negative control: samples expressing untethered fusions for tethering assay, and samples expressing mut miRNA reporter without depletion for miRNA reporter assays and rescue assays.

5.10 Transferrin uptake assays

HeLa cells seeded in a 6-well plate were transfected with siRNAs (final concentration: 100 nM) targeting TNRC6A/B, or a non-targeting scrambled control siRNA 48 h before conducting the uptake assay. 24 h before the assay siRNA-treated cells were seeded on Matrigel-coated coverslips. Cells were starved in serum-free DMEM for 1 h and then incubated with 25 µg/ml Transferrin-Alexa647 (Life Technologies; spun down at 15000 *g* for 3 min to remove ligand precipitates; diluted in serum-free DMEM) for 10 min at 37°C. Cells were washed twice with ice-cold PBS containing $MgCl_2$ (10 mM) and a 1min acid wash on ice (0.2 M NaCl, 0.1 M NaOAc pH 5.3) was used to remove surface bound transferrin from the cells followed by two times washing with ice-cold PBS-$MgCl_2$ and fixation with ice-cold PFA (4% PFA, 4% sucrose) for 45 min at room temperature. For the surface labeling, cells were serum-starved for 1 h and then incubated at 4°C with 25 µg/ml Transferrin-Alexa647 for 45min. Cells were washed two times with ice-cold PBS-$MgCl_2$ followed by fixation with ice-cold PFA (4% PFA, 4% sucrose) for 45 min at room temperature. After fixation, PFA was quenched with 50 mM NH_4C in PBS and coverslips were mounted with immomount (with Dapi, 50 µg/ml) and Transferrin uptake and surface labeling was analyzed by epifluorescent microscopy. Per conditions, 15-20 images with a total number of 200-400cells were analyzed. After background subtraction the total fluorescence intensities per cells were calculated and values were normalized to scrambled control cells (**Figure S6A**). The ratio of internalized Tfn to surface-bound Tfn was used to distinguish between uptake and recycling defects. Tfn uptake assays were performed by Dr. Caroline Bruns (Haucke Lab).

5.11 GO and KEGG pathways enrichment analysis

Gene ontology (GO) and KEGG pathway enrichment analysis was performed for the W-motif-specific interactome (80 proteins) using the whole proteome detected by Mass Spectrometry (2609 proteins) as background. Overrepresentation of GO terms and KEGG pathways was identified using a Fisher Exact test via the online tool DAVID v6.7[662,663], requiring at least 3 protein hits per term/pathway and adjusted p-values< 0.01 (**Figure 8C**).

5.12 Motif analysis

The MEME motif finder tool available online at http://meme-suite.org/ was used to identify consensus motifs across stretches of amino acids. As inputs eleven (**Figure S2**) and thirteen (**Figure S9**) amino acid long regions of the indicated proteins were used. Only sequences surrounding tryptophan residues were chosen and tryptophan was always placed centrally. MEME was asked to find a maximum of three motifs with a minimal length of 6 amino acids. The motif with the top score is displayed.

6. Appendix

6.1 Supplementary Figures

> hsTNRC6C_Q9HCJ0_1690 aa

MATGSAQGNFTGHTKKTNGNNGTNGALVQSPSNQSALGAGGANSNGSAARVWGVATGSSSG-
LAHCSVSGGDGKMDTMIGDGRSQNCWGASNSNAGINLNLNPNANPAAWPVLGHEGTVATGNPSSICSPVSAIGQNMGNQNGNPT
GTLGAWGNLLPQESTEPQTSTSQNVSFSAQPQNLNTDGPNNTNPMNSSPNPINAMQTNGLPNWGMAVGMGAIIPPHLQGLPGAN
GSSVSQVSGGSAEGISNSVWGLSPGNPATGNSNSGFSQGNGDTVNSALSAKQNGSSSAVQKEGSGGNAWDSGPPAGPGILAWG
RGSGNNGVGNIHSGAWGHPSRSTSNGVNGEWGKPPNQHSNSDINGKGSTGWESPSVTSQNPTVQPGGEHMNSWAKAASSGTT
ASEGSSDGSGNHNEGSTGREGTGEGRRRDKGIIDQGHIQLPRNDLDPRVLSNTGWGQTPVKQNTAWEFEESPRSERKNDNGTEA
WGCAATQASNSGGKNDGSIMNSTNTSSVSGWVNAPPAAVPANTGWGDSNNKAPSGPGVWGDSISSTAVSTAAAAKSGHAWSGA
ANQEDKSPTWGEPPKPKSQHWGDGQRSNPAWSAGGGDWADSSSVLGHLGDGKKNGSGWDADSNRSGSGWNDTTRSGNSG
WGNSTNTKANPGTNWGETLKPGPQQNWASKPQDNNVSNWGGAASVKQTGTGWIGGPVPVKQKDSSEATGWEEPSPPSIRRKM
EIDDGTSAWGDPSNYNNKTVNMWDRNNPVIQSSTTTNTTTTTTTTTSNTTHRVEPPHQAGTQLNRSPLLGPGRKVSSGWGEMPN
VHSKTENSWGEPSSPSTLVDNGTAAWGKPPSSGSGWGDHPAEPPVAFGRAGAPVAASALCKPASKSMQEGWGSGGDEMNLSTS
QWEDEEGDVWNNAASQESTSSCSSWGNAPKKGLQKGMKTSGKQDEAWIMSRLIKQLTDMGFPREPAEEALKSNNMNLDQAMSA
LLEKKVDVDKRGLGVTDHNGMAAKPLGCRPPISKESSVDRPTFLDKDGGLVEEPTPSPFLPSPSLKLPLSHSALPSQALGGIASGLG
MQNLNSSRQIPSGNLGMFGNSGAAQARTMQQPPQPPVQPLNSSQPSLRAQVPQFLSPQVQAQLLQFAAKNIGLNPALLTSPINPQ
HMTMLNQLYQLQLAYQRLQIQQQMLQAQRNVSGSMRQQEQQVARTITNLQQQIQQHQRQLAQALLVKQPPPPPPPPHLSLHPSA
GKSAMDSFPSHPQTPGLPDLQTKEQQSSPNTFAPYPLAGLNPNMNVNSMDMTGGLSVKDPSQSQSRLPQWTHPNSMDNLPSAA
SPLEQNPSKHGAIPGGLSIGPPGKSSIDDSYGRYDLIQNSESPASPPVAVPHSWSRAKSDSDKISNGSSINWPPEFHPGVPWKGLQ
NIDPENDPDVTPGSVPTGPTINTTIQDVNRYLLKSGGKLSDIKSTWSSGPTSHTQASLSHELWKVPRNSTAPTRPPPGLTNPKPSST
WGASPLGWTSSYSSGSAWSTDTSGRTSSWLVLRNLTPQIDGSTLRTLCLQHGPLITFHLNLTQGNAVVRYSSKEEAAKAQKSLHMC
VLGNTTILAEFAGEEEVNRFLAQGQALPPTSSWQSSSASSQPRLSAAGSSHGLVRSDAGHWNAPCLGGKGSSELLWGGVPQYSS
SLWGPPSADDSRVIGSPTPLTTLLPGDLLSGESL

Features:
UBA: [aa 933-978]

CED: [aa 1369-1690]
PAM2: [aa 1381-1399]
RRM: [aa 1565-1632]
W_1 : [aa 1445]
W_2: [aa 1487]
W_3: [aa 1494]
W_4: [aa 1504]
W_5: [aa 1605]
W_6: [aa 1648]
W_7: [aa 1659]

Figure S 1. Human TNRC6C amino acid sequence Amino acid sequence of *Homo sapiens* TNRC6C isoform 1 (Uniprot identifier: Q9HCJ10-1). The C-terminal effector domain (CED) used in this study corresponds to the region between residues 1369-1690 and is highlighted in blue. The two structured domains Ubiquitin Associated Domain (UBA) and RNA Recognition Motif (RRM) are shown in purple and red, respectively. The PABP Associated Motif (PAM2) is shown in cyan and seven CED W-motifs are highlighted in green. Exactly these seven tryptophan residues were mutated to either tyrosine or alanine in the 7W7Y and 7W7A mutants, respectively. Amino acid positions of the domains and motifs are annotated below the sequence.

	amino acid:	A	C	D	E	F	G	H	I	K	L	M	N	P	Q	R	S	T	V	W	Y
position in W-motif:	**consensus motif**																				
1st residue	**[PS]**	0	0	0	0	0	1	0	2	0	0	0	0	5	0	0	7	0	0	0	0
2d residue	**T**	0	0	0	1	0	3	0	0	2	1	0	0	1	0	0	3	4	0	0	0
3d residue	**S**	0	0	0	0	0	1	0	0	0	3	0	0	1	0	0	10	0	0	0	0
4th residue	**[TL]**	2	0	0	0	0	3	0	0	0	4	0	0	0	0	0	2	4	0	0	0
5th residue	**W**	0	0	0	0	0	0	0	0	0	0	0	0	0	0	0	0	0	0	15	0
6th residue	**[GS]**	0	0	1	0	0	7	0	0	0	1	0	0	0	2	0	4	1	0	0	0

>TNRC6A_W1673
PSTSAWSSIRA

>TNRC6A_W1703
DSKLTWSPGSV

>TNRC6A_W1747
PPLSTWDNSPL

>TNRC6A_W1758
RIGGGWGNSDA

>TNRC6A_W1771
TPGSSWGESSS

>TNRC6A_W1872
TPSPGWQSLGS

>TNRC6A_W1919
HGTSLWGTPHY

>TNRC6A_W1929
YSTSLWGPPSS

>TNRC6C_W1445
DIKSTWSSGPT

>TNRC6C_W1487
KPSSTWGASPL

>TNRC6C_W1494
ASPLGWTSSYS

>TNRC6C_W1504
SSGSAWSTDTS

>TNRC6C_W1605
PPTSSWQSSSA

>TNRC6C_W1648
SSELLWGGVPQ

>TNRC6C_W1659
YSSSLWGPPSA

Figure S 2. Consensus human W-motif and the corresponding count matrix Motif was derived using MEME Suite (Bailey and Elkan, 1994)[661] with a set of experimentally validated W-motifs from TNRC6A (Q8NDV7-1) and TNRC6C (Q9HCJ0-1) proteins. Sequences used as inputs are provided below the count matrix. The number after W refers to the amino acid position of the tryptophan (W) residue in the corresponding full-length protein.

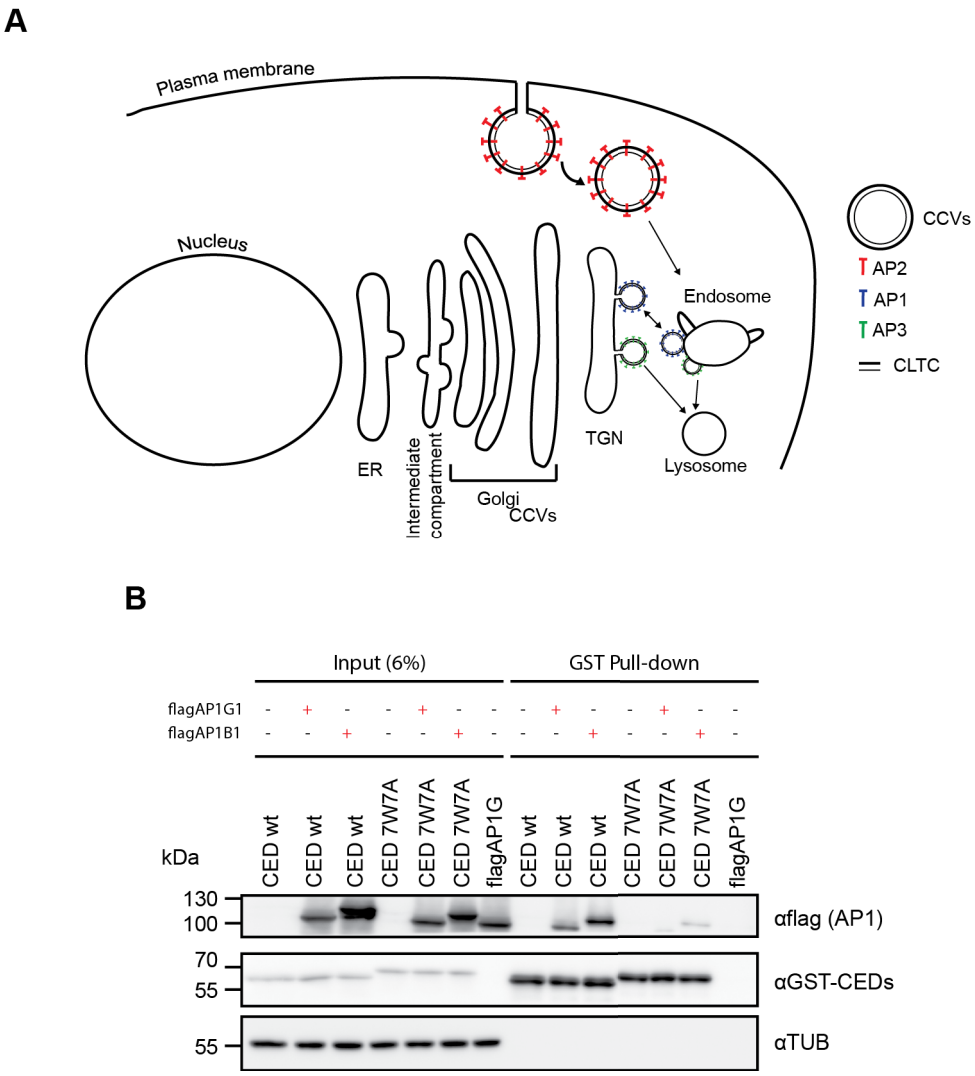

Figure S 3. TNRC6C CED interacts with AP1 proteins via W-motifs (A) Illustration representing an eukaryotic animal cell with budding clathrin-coated vesicles (CCVs) associated to different type of adaptor proteins: AP1 (green), AP2 (red) and AP3 (blue). AP1 mediate internal trafficking between the transgolgi network (TGN) and endosomes, AP2 mediate trafficking from the plasma membrane to endosomes and AP3 additionally mediate endo-lysosomal trafficking. **(B)** HEK293 cells were co-transfected with plasmids encoding GST-fusions of TNRC6C CED and plasmids encoding flag-tagged AP21G or AP1B subunits (or filler DNA encoding flag-sic peptide). Nuclease-treated cell lysates were used in GST pull-down, and inputs (6%) and GST pull-downs were analyzed by western blotting with the indicated antibodies. Cells transfected with only flag-AP1G were used as negative control on unspecific precipitation.

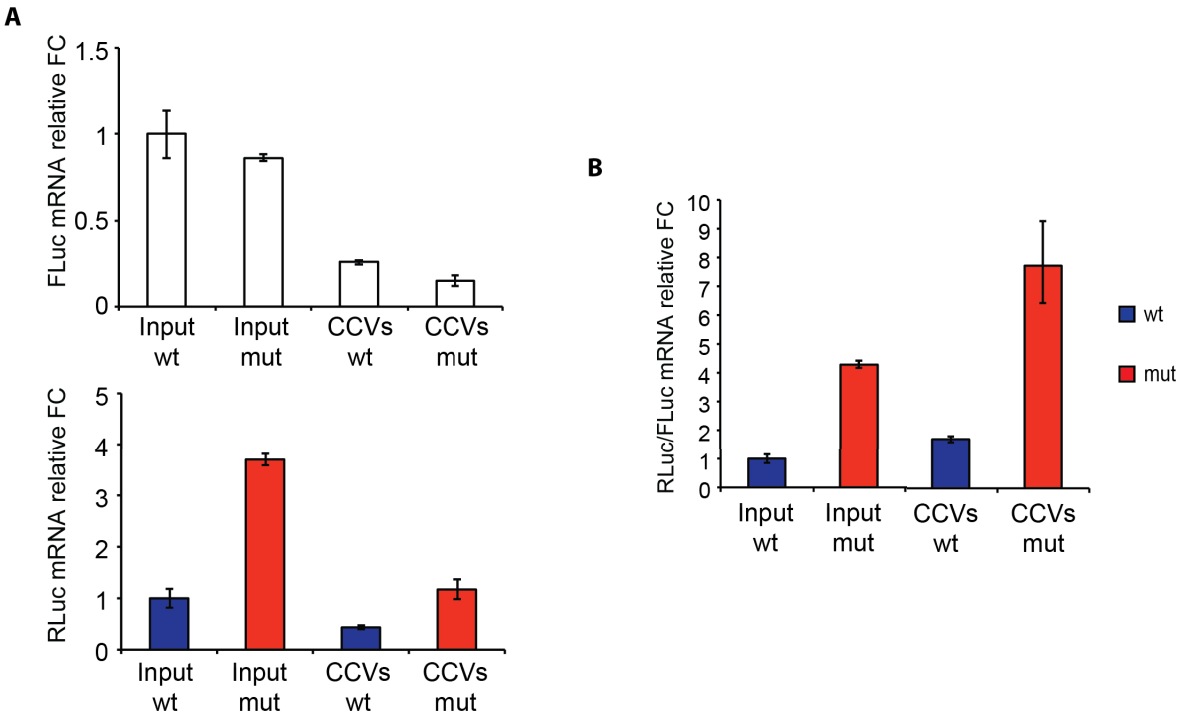

Figure S 4. Ratio of wt to mut RLuc-hmga2 reporter does not vary between input-isolated and CCV-isolated RNA (A) FLuc (top) and RLuc (bottom) mRNA levels were expressed as fold-change (FC) relative to Input wt (always set to 1). **(B)** RLuc mRNA levels were normalized to that of Fluc and expressed as fold-change relative to Input wt (set to 1). Not normalized and normalized RLuc-hmga2 wt is shown in blue, mutant in red. Values represent means ± SD from 3 technical replicates.

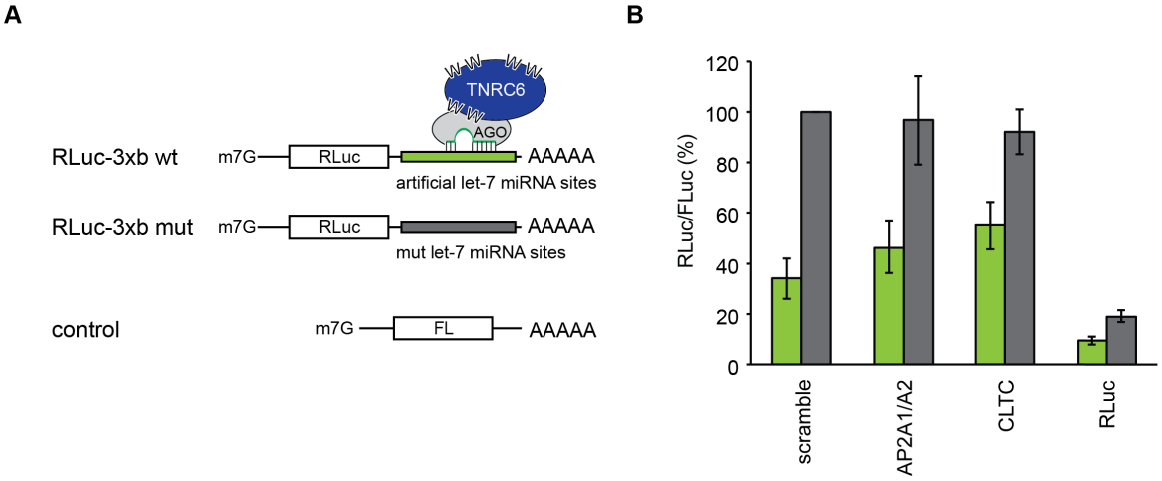

Figure S 5. Knockdown of AP2A proteins does not enhance miRNA repression when using RLuc-3xb artificial miRNA reporters (A) Schematic representation of RLuc-3xb reporters expressing RLuc fused to an artificial 3'UTR sensitive to let-7 miRNA (wt, green) or its mutant version with disrupted let-7 sites (mut, grey). FLuc insensitive to let-7 miRNA is used as a control. Reporters were previously described in[412] **(B)** siRNAs against the indicated genes were co-transfected with plasmids encoding wt or mut RLuc-3xb let-7 reporters and FLuc control as illustrated in (A) (means ± SEM, n=4). RLuc activity was normalized to that of FLuc and expressed as a percentage of RLuc activity produced by 3xb-mut reporter in samples co-transfected with scramble siRNA (set to 100%). Knockdown of RLuc was used as a proxy for knockdown efficiency (~5-fold).

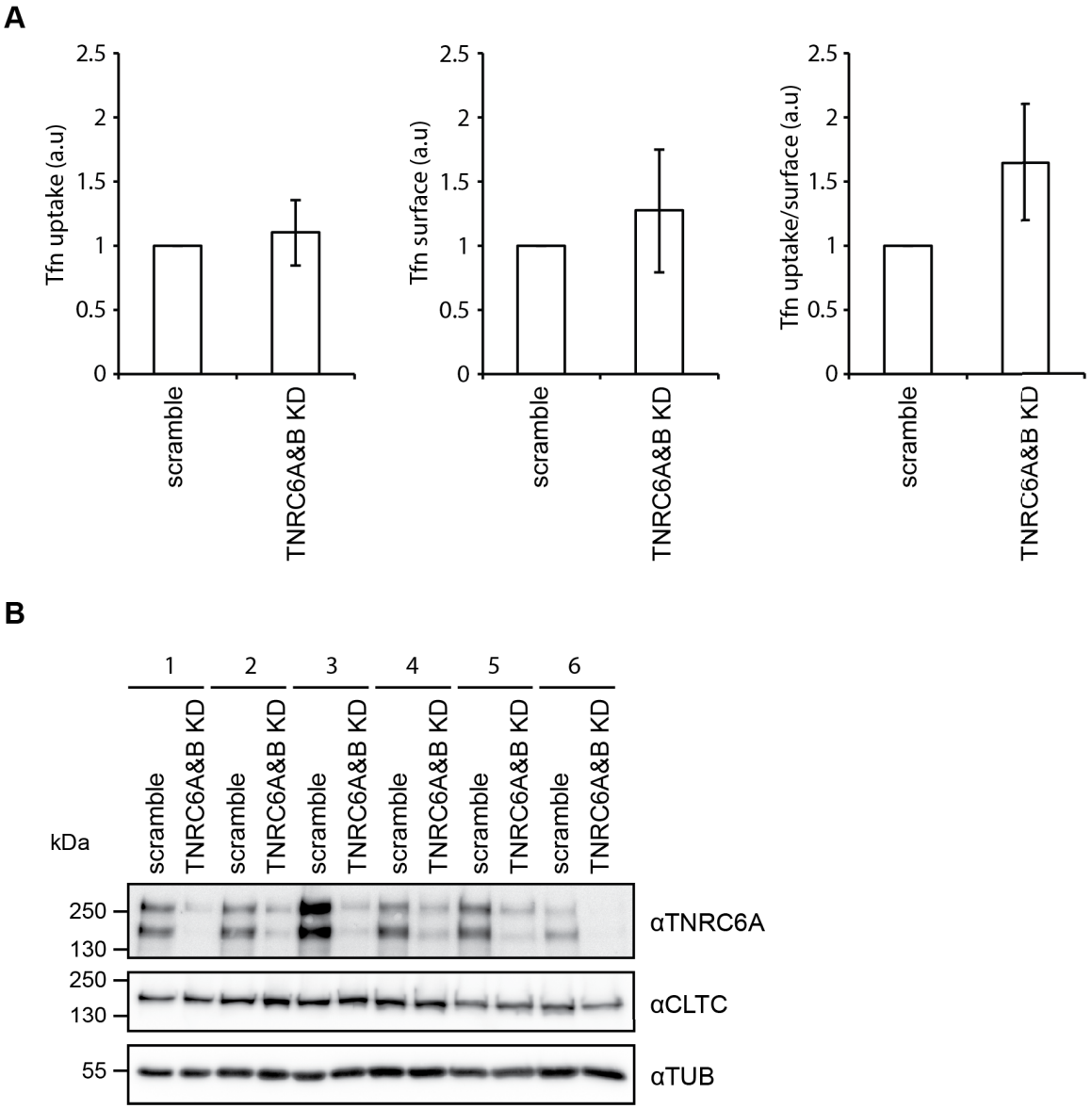

Figure S 6. Knockdown of TNRC6 proteins does not significantly affect CCV-mediated endocytosis (A) HeLa cells transfected with siRNAs targeting TNRC6A and B or with a non-targeting siRNA (scramble) were stained using an Alexa Fluor 647-conjugated transferrin (Tfn) (ligand of Tfn receptors). The fluorescence signals coming from the internalized receptor (Tfn uptake, histogram on the left) and from the ligand-bound surface receptor were quantified (Tfn surface; central histogram). Tfn uptake normalized to Tfn on the cell surface is shown on the right histogram (means ± SEM; n=6, biological replicates). Values are expressed as fold change of Tfn fluorescence in samples transfected with siRNA targeting TNRC6 proteins as compared to samples transfected with scramble siRNA (set to 1). None of the differences observed is significant (two-samples t-test). **(B)** TNRC6 KD is efficient and does not affect CLTC expression levels. Lysates of samples used in (A) were analyzed by western blotting with the indicated antibodies. Numbers 1 to 6 correspond to the different biological replicates.

> nvGW182_1698 aa

MPKDDKKEFLKSLGVDTLSSENDIKRAYKKIALQCHPDKNPSDTSARKQFEEVSKAFEYLVHDGINDSLKDYDKVFFDFL
RDILFGSDGASDFFTYFCGSKQHSCISTDTDPDFRYQDDDEEEDIDGEQELESLLEIVKNRRKRGKPVPDEFHEEKLQEL
KTRLSQHKEDMKKDGSKKQAVKKGKAVSVPVAKPKPKSKKQLLAEQRRRAKEMEQIAMELEEKRKEEEEKEKQRKQLEVE
KQKRLEEERIRSQNEERKRREREQKEREKQQKLDMEKEERRRRQQEEEKKRREEEEKRKKVEKEKQEREKAAKKAALQAA
KEKEEQAKAASKNQNIKRQQQQQRTDQQQYPREIPPRFQKMKRQQQQQQLQTPNLPPPAPTGSPAQLNKFQSKPQQQPVG
KKKDPNRFASKEYADLVDEVDDAGWNKGSQCKGSGWEGTSEDWEENIAEKWGADRQWGSKEGSSNQLVVDRTDGDSWPTV
GSKSAIGDKPNSSLENSNSKNSSETVPVGTIGSKPPSSNWNSNRNSGGLPLSENWDTTCDESIDRALDATESKGSVGPGG
VNWVGMGTGGLGGIIGTPLGWEPSKENRDIDKTASKSGWCGEQNSTVDSWNKTPGKGPKTQVFGGSAPTWGGTPADSSSA
WVETSGTETNKPNSSGWNSKVSSGLSQGNSSSMASVDSTDNKPTDNKPAPSGWGEAGPSWAVQASVTGTACWDTATTTSP
KKPLDSKDSKLSHDKVSGWLETSVTSTSVTADWNGDSNADQEDYYEEAWDGWTTASSKRNKAPKPAPTNDSNAWMSRSLK
QLLDMGFKQEDAEKALRANHMNIESAISDLLSLTASQIEEASRASSANTGEPDPAEACRMQQQNTTTSKPNRKQRRKTQQ
QLQQQQASQAKQESKQTDIYDANSQSGSSDSTVKDPKSESNKDKEGQAAEGQSNKPSNQGASDGKGNASKTTENSPHLSP
GKSNAGQKRATTGLIQTPALGTPTPMRTPMTHPLLHQQFLHQVQLHQLRMAQGGLLQPPINPQQVALLQQMAQLQMVQHR
IAQQQLTQKHNIQAQQQLYQQQQQIALMMGQLQQQVMQQHNHQIAGSRFPSPGFQQSTLPPQSSSAQPGTPPQNAKNSTK
ATSTEPSQSKPEEPPKVSTADKPVTTVASGERITQQSPAPQSRLTQWKQPLLPDPETSHGETWGMPKIEQMSLLSGPVVS
SSLEQQHGAPNLSPQANRIADPVSSRWGVDASLKLSADPPEFKPGVPWRPRGEGEEKSGSSGSSMESSPQGMPASGKTQI
TDNPNKQPGFPGGFSSASQFPYSIASSPWQNTEPTDSLNKTQANPSSIRPPPGLNTSTSSGLPDTPSVEERPAWMKNLMD
GGTQQSFAQGPNPGNFQLGLRLGFSASGNSWSTQDGMSVSGLTPNSQPWAAPGGPSSSSTPSSDPSAEAASSTANAVTSA
EQLKPQDEGISSWSTNQPIPSAEEKQQQPPVAQGPRMGSGRGGANPMSTWLVLRNLSPRADPTAMRAVCQQYGPLLTFTL
NLRHGNSLIRYSNKDQAASARNNLNGMMVKGMQLIADFATDSDIGGFFEQTPDWSNNPMPPNPSFGNPWSFGTVDPNRPL
GSTQGLEKTPQGPPPQMPAMVPPGMQWGSSSQLPAQLWGNSHPGAATGFPSQVPSMWSFSGGAPRDVEPQSGTNENGLVS
PSMTTFLPPGLLNGGESV

Features:
DNAJ: [aa 11-61]
UBA: [aa 797-827]

CED: [aa 1159-1698]
PAM2: [aa 1234-1252]
RRM: [aa 1491-1554]
W_1 : [aa 1167]
W_2: [aa 1183]
W_3: [aa 1227]
W_4: [aa 1309]
W_5: [aa 1391]
W_6: [aa 1453]
W_7: [aa 1574]
W_8: [aa 1589]
W_9: [aa 1627]
W_10: [aa 1638]
W_11: [aa 1657]

Figure S 7. Nematostella GW182 (nvGW182) amino acid sequence Amino acid sequence of full-length *Nematostella vectensis* GW182. Starting from the N-terminus, DNAJ domain characteristic of nvGW182 is shown in yellow, Ubiquitin Associated Domain (UBA) is shown in purple. The C-terminal effector domain (nvCED) used in this study corresponds to the region between residues 1159-1698 and is highlighted in blue. Within nvCED the structured RNA Recognition Motif (RRM) is shown in red and the PABP Associated Motif (PAM2) in cyan. Eleven W-motifs are highlighted in green. Exactly these eleven tryptophan residues were mutated to alanine in the 11W11A mutant. Amino acid positions of the domains and motifs are annotated below the sequence.

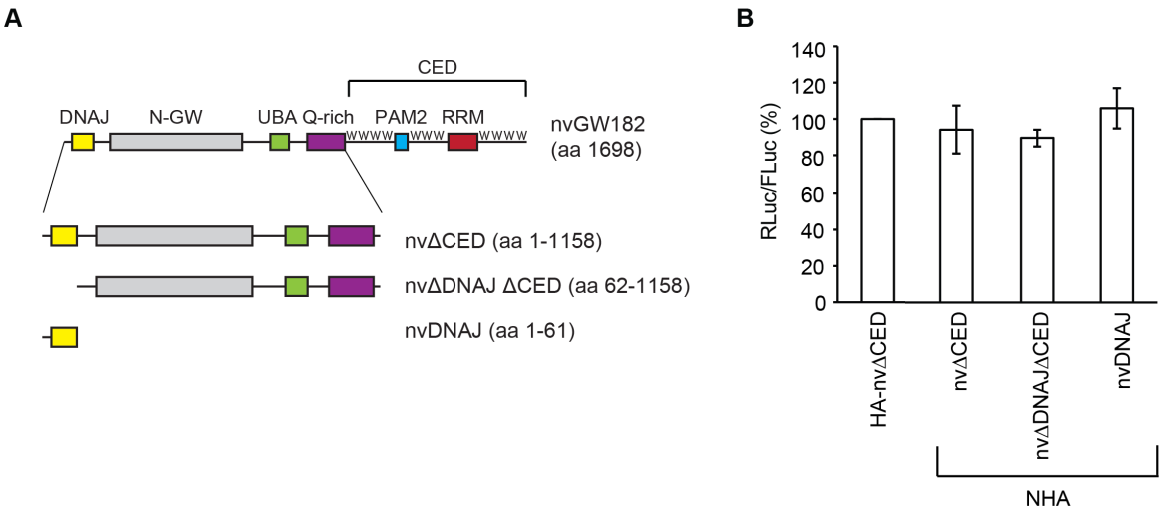

Figure S 8. Tethering of nvΔCED does not affect mRNA repression (A) Schematic representation of nvGW182 and the C-terminal deletion mutants used in (B). DNAJ domain (yellow); N-GW: GW-repeat–rich region (grey); UBA: ubiquitin associated domain (green); PAM2: PABP associated motif 2 (light blue); RRM: RNA-recognition motif (red). The C-terminal effector domain (CED) is formed by RRM, PAM2 and the unstructured flanking regions with tryptophan-containing motifs, or W-motifs (W). Numbers correspond to the amino acid positions. **(B)** Expression of RLuc-boxB mRNA is not affected by tethering NHA-nvGW182 C-terminal and DNAJ deletion mutants. Human HEK293 cells were co-transfected with plasmids encoding RLuc-boxB, FLuc, and the indicated NHA-nvGW182 deletion mutants. As negative control, a plasmid encoding untethered HA-fusion was used. RLuc activity was normalized to that of FLuc and presented as a percentage of RLuc produced in the presence of the untethered HA-fusion (means ± SD; n=3-8).

	amino acid:	A	C	D	E	F	G	H	I	K	L	M	N	P	Q	R	S	T	V	W	Y
position in W-motif:	**consensus motif**																				
1st residue	**[PS]**	1	0	0	1	1	4	1	2	0	0	0	0	8	1	1	8	2	2	0	0
2d residue	**[SG]**	2	0	0	1	0	7	0	1	2	2	0	3	2	0	0	8	4	0	0	0
3d residue	**S**	0	0	0	2	0	1	1	0	1	3	1	3	2	1	0	14	3	0	0	0
4th residue	**T**	1	0	2	0	0	4	0	0	0	6	1	1	2	2	1	5	7	0	0	0
5th residue	**W**	0	0	0	0	0	0	0	0	0	0	0	0	0	0	0	0	0	0	32	0
6th residue	**[GS]**	0	0	1	0	0	12	0	0	1	1	0	0	0	3	0	11	3	0	0	0

>dmGW182_W942
DNENKDWSVAQPT
>dmGW182_W1024
SLSSSTWSFNPNQ
>dmGW182_W1037
NYPSHSWSDNSQQ
>dmGW182_W1051
TATSELWTSPLNK
>dmGW182_W1092
TGGANGWLQPRSG
>dmGW182_W1107
QTTNTNWTGGNTT
>dmGW182_W1114
TGGNTTWGSSWLL

>hsTNRC6A_W1703
SDSKLTWSPGSVT
>hsTNRC6A_W1747
KPPLSTWDNSPLR
>hsTNRC6A_W1758
LRIGGGWGNSDAR
>hsTNRC6A_W1771
YTPGSSWGESSSG
>hsTNRC6A_W1872
LTPSPGWQSLGSS
>hsTNRC6A_W1919
LHGTSLWGTPHYS
>hsTNRC6A_W1929
HYSTSLWGPPSSS
>hsTNRC6C_W1445
SDIKSTWSSGPTS
>hsTNRC6C_W1487
PKPSSTWGASPLG
>hsTNRC6C_W1494
GASPLGWTSSYSS
>hsTNRC6C_W1504
YSSGSAWSTDTSG
>hsTNRC6C_W1605
LPPTSSWQSSSAS
>hsTNRC6C_W1648
GSSELLWGGVPQY
>hsTNRC6C_W1659
QYSSSLWGPPSAD

>nvGW182_W1167
QSRLTQWKQPLLP
>nvGW182_W1183
TSHGETWGMPKIE
>nvGW182_W1227
DPVSSRWGVDASL
>nvGW182_W1309
SIASSPWQNTEPT
>nvGW182_W1391
SASGNSWSTQDGM
>nvGW182_W1453
DEGISSWSTNQPI
>nvGW182_W1574
FEQTPDWSNNPMP
>nvGW182_W1589
PSFGNPWSFGTVD
>nvGW182_W1627
VPPGMQWGSSSQL
>nvGW182_W1638
QLPAQLWGNSHPG
>nvGW182_W1657
SQVPSMWSFSGGA

Figure S 9. Consensus W-motif and the corresponding count matrix Consensus W-motif and the corresponding count matrix, derived using MEME Suite (Bailey and Elkan,1994)[661] with a set of validated W-motifs from human TNRC6A (Q8NDV7-1) and TNRC6C (Q9HCJ0-1), *Drosophila* GW182 (Q8SY33-1) and *Nematostella* GW182 proteins. Sequences of validated W-motifs used as input in MEME motif prediction are provided below the count matrix. The numbers after W refer to the amino acid position of the corresponding tryptophan (W) in the indicated TNRC6/GW182 proteins.

Figure S 10. Sequence alignment of human and Nematostella DDX6 Sequence alignment of hsDDX6 and nvDDX6 was performed with Clustal Omega (EBI) and visualized with Jalview. Percentage of identity (ID) is shown below the alignment.

HRPA1 (*C. elegans*) Uniprot identifier: Q22037_Heterogeneous nuclear ribonucleoprotein A1

MTDVEIKAENGSGDASLEPENLRKIFVGGLTSNTTDDLMREFYSQFGEITDIIVMRDPTT
KRSRGFGFVTFSGKTEVDAAMKQRPHIIDGKTVDPKRAVPRDDKNRSESNVSTKRLYVSG
VREDHTEDMLTEYFTKYGTVTKSEIILDKATQKPRGFGFVTFDDHDSVDQCVLQKSHMVN
GHRCDVRKGLSKDEMSKAQMNRDRETRGGRSRDGQRGGYNGGGGGGGGWGGPAQRGGPGA
YGGPGGGGQGGYGGDYGGGWGQQGGGGQGGWGGPQQQQGGGGWGQQGGGGQGGWGGPQQQ
QQGGWGGPQQGGGGGGWGGQGQQQGGWGGQSGAQQWAHAQGGNRNY

SPT5 C-terminus aa 897-1063 (*S. cerevisiae*) Uniprot identifier: P27692_Transcription elongation factor

SSGLSGGMTPGWSSFDGGKTPAVNAHGGSGGGGVSSWGGASTWGGQGNGGASAWGGAGGGASAW
GGQGTGATSTWGGASAWGNKSSWGGASTWASGGESNGAMSTWGGTGDRSAYGGASTWGGN
NNNKSTRDGGASAWGNQDDGNRSAWNNQGNKSNYGGNSTWGGH

Ipod (*D. melanogaster*) Uniprot identifier: Q9W2X1_Interaction partner of Dnmt2

MKVFICLLATICACNATFLSLLGGGGGGGGGGGSKTTYNVIATPSSGGGGGGGGGGGGGGG
GHGYSYAQGGGGGHGYAQGHGYGHGHGGSPQIIKVILQEGCGYSNAGGSAGGIVSSEGHG
YSHGHGHGYASGHGSYGGQQAQIYKIIEQAPAPVPAPAPVPIPISIPAPAPPAAPIAYHA
ASGSNGYSYDQGHSHSYGQSYASGHGYGGGASFDTQQFNAILPQIIQLVLQEDSFGGGGG
GSADVAAINGQLINTFGSKGKAIILKADQAQGAFFKSGHVVQRGTLKVMRVQEQQQSQSA
GGSKGGWGSGGGAISGGWSSGGGAASGGWSSGGGAASGGWSSGGPPSAW

Osiris 12 (*D. melanogaster*) Uniprot identifier: Q9VNN2

MIFKQWPWQALISLLSVLFLASSCGAATEQLGSPPGPSPSQSAGARTLLRVYDECTRAEA
GFVPCLKKKAISFIDRLAPIDAINVAEGIKLVRLETAPRPPATSENELESSLPRSGSDRD
AKLTNMLIERLSYFFNGHSLQVSFPKLTSDEIGRGLEEGRGKMKKMMGMMMMGMAMKMMG
MIPIAMGALYILAGKALIISKIALLLAGIIGLKKLMSGKSSGGSSGWSSGGGGGGGGWSS
GGGGGGGGGWDRRSLTEAQELAYRAHHQEQVAHAQSRPQLQHLHPKAAAPQVTKS

CG12998 (*D. melanogaster*) Uniprot identifier: Q8SXV9

MKVFIVLCALVACVSAGLVRSSGWGSNPWGGSSSGWNSGWVAQQPQVIKVIKIGGGGGSG
WGGNSGWGGNSGWGSNSGWGGNSGWGGNSGWSSGNSGWNSNGWSSSSSNSGWW

CG13376 (*D. melanogaster*) Uniprot identifier: Q59E78

MKAFVCLMLIGAASVTANPKPGGGSSWSSGGSGGGWSSGGGGGGGHGGGGDVQIIKVITE
SGSSGGGGGGGGWSSGGGGGGGGWSSGGGGGGGGWSSGGGGGGWSSGGGGGSGSDVKLIK
IISLGGGGGGHSGGGGGWSSGGGGGGWSSGGSGGHGSSGGGDTKVIKIIKLSSGGHGGAG
GGGGHGGGGGGGWQPAGGWA

CG34327 (*D. melanogaster*) Uniprot identifier: A8JV30
MQTTITTRRLGLLGLLVVLGCIVAQGKPHGWSSGGGGGGWSSGGSGGGSKVIISAWPSSGG
GGWSSGGGSGGWKSGGDGGGGWSSGGSGGGWKSGGGSSGWKSGGGSGGWSSGGSSGWPSS
GSSGWKSGGSSGLSSALSSLSSWKSQALGSLSSGWKSGGGGGGWSSGGSSGGGWKSGGGS
GGWSSGGSSAWPSKISSGWSSGGGGGGWSPGGGGGSGWSW

C6orf15 (*H. sapiens*) Uniprot identifier: Q6UXA7

MQGRVAGSCAPLGLLLVCLHLPGLFARSIGVVEEKVSQNLGTNLPQLGQPSSTGPSNSEH
PQPALDPRSNDLARVPLKLSVPASDGFPPAGGSAVQRWPPSWGLPAMDSWPPEDPWQMMA
AAAEDRLGEALPEELSYLSSAAALAPGSGPLPGESSPDATGLSPKASLLHQDSESRRLPR
SNSLGAGGKILSQRPPWSLIHRVLPDHPWGTLNPSVSWGGGGPGTGWGTRPMPHPEGIWG
INNQPPGTSWGNINRYPGGSWGNINRYPGGSWGNINRYPGGSWGNIHLYPGINNPFPPGV
LRPPGSSWNIPAGFPNPPSPRLQWG

Figure S 11. Proteins other than TNRC6 containing W-motifs W-motif-containing proteins across species. Amino acid sequences of proteins containing W-motifs are shown; the central tryptophan residue of W-motifs is highlighted in red. Uniprot identifiers of the sequence used are provided.

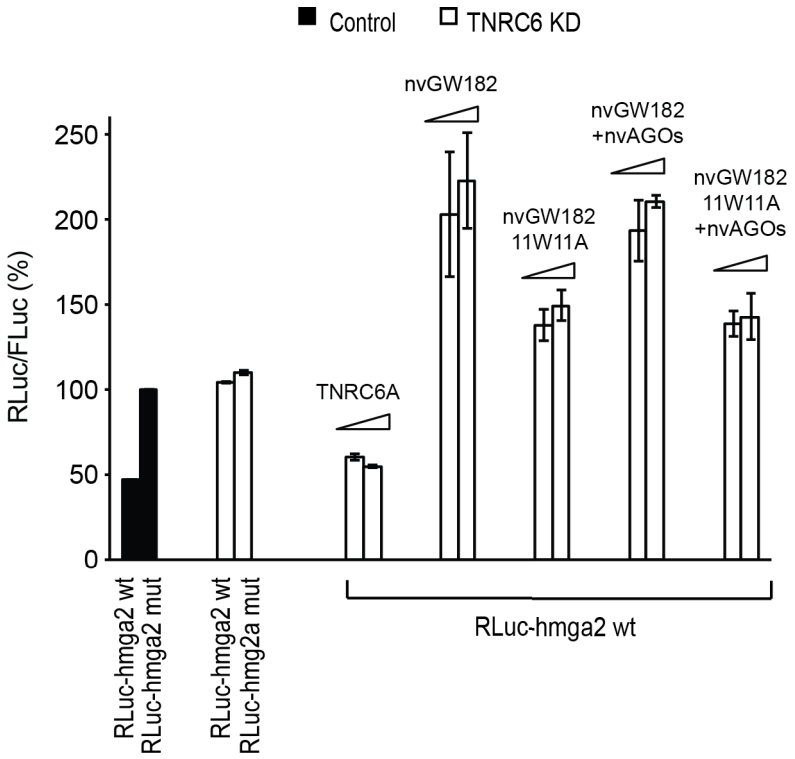

Figure S 12. Coexpression of nvGW182 and nvAGOs cannot rescue TNRC6 depletion in mammalian cells HeLa cell line carrying stably integrated inducible shRNAs construct against endogenous TNRC6A and B was used for TNRC6 knockdown experiments (open bars); HeLa cells not expressing TNRC6-directed shRNAs was used as a control (filled bars). Expression of shRNAs was induced for 2 days prior to transfection of miRNA reporters and rescue constructs. Cells were transfected with RLuc-hmga2 reporter containing let-7 sites (RLuc-hmga2 wt) or its mutant version (RLuc-hmga2 mut), and increasing amounts (50 ng and 100 ng) of plasmids expressing nvGW182 wt or its 11W11A mutant cotransfected with 100 ng of a filler plasmid encoding LacZ or 100 ng nvAGOs (50 ng nvAGO1 and 50 ng nvAGO2). TNRC6A was used as a positive control. Values represent percentages of RLuc activity produced by hmga2-mut reporter without TNRC6 depletion (means ± SD; n=3).

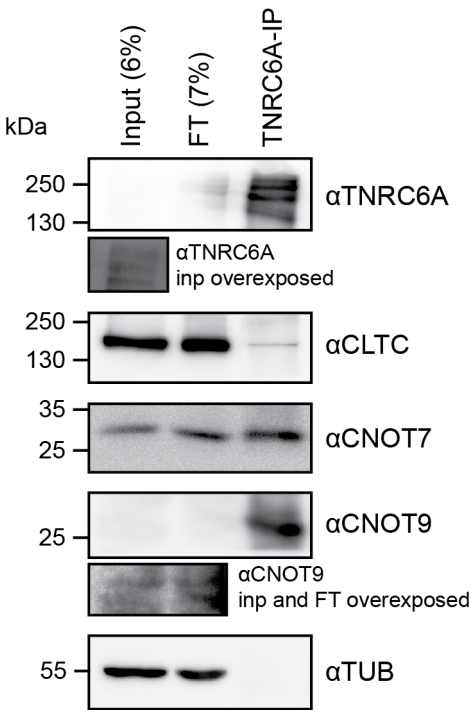

Figure S 13. Affinity purification of endogenous TNRC6A shows abundant interactions with CCR4-NOT and less abundant interactions with CLTC Nuclease-treated HeLa cell lysate was used to pull-down endogenous TNRC6A, and input (6%), flow through (FT, 7%) and TNRC6A IP were analyzed by western blotting with the indicated antibodies.

6.2 Supplementary Tables

Table S1. W-motif enriched interactors identified by SILAC followed by AP-MS/MS 80 W-motif specific interactors identified by SILAC-AP-MS/MS, their mean log_2 ratio wt/mut and the corresponding t-test p-values are shown. Proteins that resulted specific wt CED binders (enriched over GST by at least 1.3 fold) and were significantly enriched (p-value< 0.05) with wt TNRC6 CED as compared to either 7W7Y and 7W7A CED mutants by at least 1.3 fold (log_2=0.4) are listed (one sample t-test; p-value< 0.05; n= 9, biological replicates, 4 forward and 5 reverse).

Gene name	Mean log_2 wt CED/mut	-log_{10} p-value
CNOT3	2.43	7.53
CNOT9	2.27	5.24
PYCRL	2.13	4.79
CNOT1	2.00	5.92
CNOT2	1.92	8.34
CNOT10	1.89	5.81
TIMM13	1.75	5.03
AP2A1	1.72	5.33
AP2S1	1.67	2.19
CNOT7	1.60	3.80
CNOT8	1.59	4.84
AP2B1	1.53	5.02
PHGDH	1.50	6.54
CLTC	1.36	4.52
TIMM8A	1.25	2.69
TUBB4B	1.20	1.85
AP2M1	1.19	2.42
CAD	1.17	3.19
TIMM8B	1.14	3.15
SSBP1	1.13	2.38
CLTA	1.12	4.02
CNOT6	1.11	2.32

Gene name	Mean log_2 wt CED/mut	$-log_{10}$ p-value
SLC25A11	1.05	2.22
SLC25A5	0.99	2.64
PABPC1	0.99	3.19
DCAF7	0.97	5.10
GIGYF2	0.95	4.40
CPNE1	0.92	1.93
CCZ1	0.90	1.57
AP2A2	0.89	2.36
PPP2R1A	0.88	3.46
PABPC4	0.87	2.53
TUBB4	0.84	2.46
ATP12A	0.83	1.93
CNOT6L	0.83	1.90
PRKDC	0.82	2.07
DNAJA1	0.79	4.17
TIPRL	0.78	2.49
PPP2CA	0.78	2.27
OGT	0.78	2.88
TUBB	0.76	2.47
SLC25A6	0.74	2.60
DNAJA2	0.71	2.82
CTPS	0.69	1.38
FXR1	0.69	1.85
ABCF2	0.68	1.75
TUBB3	0.68	2.17
RPL36	0.67	1.39
USP9X	0.66	2.13
CDK4	0.66	2.94
RPN1	0.62	2.38
MLLT1	0.62	1.77

Gene name	Mean log_2 wt CED/mut	$-log_{10}$ p-value
HSPB1	0.60	2.14
FAM98A	0.59	1.42
ATAD3A	0.59	1.70
RPS27A	0.58	1.79
SLC25A3	0.57	2.22
XPO1	0.57	1.44
RPL18	0.55	1.90
DKC1	0.55	1.82
PCBP1	0.54	1.68
DDX46	0.52	1.48
YWHAB	0.51	1.30
C14orf166	0.51	1.85
DDX20	0.50	1.55
FMR1	0.49	1.35
NUP93	0.48	1.48
SF3B3	0.47	1.33
EIF4E2	0.46	1.60
TUBB2A	0.46	1.64
KHSRP	0.46	2.74
TPM1	0.45	1.38
RPS4X	0.44	1.49
NUP205	0.44	1.79
DYNLL1	0.42	2.49
LARP4	0.42	1.69
HSPD1	0.42	1.93
CLINT1	0.41	1.69
RPL29	0.41	2.14
PDHB	0.41	1.62

Table S2. nvGW182 MS results Quantitative mass spectrometric analysis of proteins associated with nvGW182. Table listing the 43 proteins that are significantly enriched with nvGW182 full-length as compared to the negative control GST (two sample t-test; FDR≤ 0.05; S0= 0.1; n= 2, biological replicates). The logarithmic ratios of protein intensities, and the corresponding t-test p-values are shown.

Gene name	Mean $\log_2$ nvGW182/GST	$-\log_{10}$ p-value
SNAPC4	8.28	4.01
MRPS22	6.09	5.01
NOP2	5.80	5.30
SND1	5.68	3.64
CNOT1	5.61	4.79
NONO	5.01	3.37
HNRNPR	4.87	3.25
STAU1	4.63	3.21
TOP1	4.48	3.96
SLC25A10	4.27	6.05
FAU	4.27	3.54
HADHA	4.23	3.37
MAPRE2	4.18	2.88
ILF3	4.13	2.83
PABPC4	3.91	2.98
DNAJB6	3.90	4.14
ABCD3	3.84	4.04
SRRT	3.78	2.87
RMDN3	3.74	3.05
HP1BP3	3.62	3.69
PRC1	3.60	3.54
TFAM	3.42	4.46
IGF2BP3	3.34	2.98
MRPS28	3.32	2.91
POLR2H	3.25	3.86
DAP3	3.09	3.45
DIMT1	3.06	3.01
CNOT9	3.04	4.38

Gene name	Mean log_2 nvGW182/GST	$-log_{10}$ p-value
MYO1B	3.04	4.35
EDC3	2.98	3.02
SART3	2.86	3.03
WDR75	2.80	3.86
MAP7D3	2.79	3.38
MRPS21	2.41	7.17
PCBP2	2.15	3.99
ACTB	2.14	3.56
RPL13A	2.04	4.28
MYO1C	1.93	4.53
RPL10	1.69	4.50
RPL28	1.55	3.98
RPL10A	1.42	5.16
RPLP2	1.25	4.22
RPL38	0.97	4.27

Table S3. nvΔCED MS results Quantitative mass spectrometric analysis of proteins associated with nvΔCED. Table listing the 174 proteins that are significantly enriched with nvΔCED as compared to the negative control GST (two sample t-test; FDR ≤ 0.05; S0= 0.1; n= 2, individual experiments). The logarithmic ratios of protein intensities and the corresponding t-test p-values are shown. As input for the t-test only proteins that showed logarithmic ratios nvGW182/GST above 0 were considered in order to filter out background interactors.

Gene name	Mean log_2 nvΔCED/GST	$-log_{10}$ p-value
SNAPC4	9.48	7.12
NONO	6.52	4.15
SND1	6.49	5.07
MRPS22	6.15	4.91
NOP2	6.09	5.99
YTHDF2	5.90	8.47
POLR1C	5.83	7.48
ZNF768	5.66	2.29
PYCRL	5.49	4.64
ZC3H7A	5.33	5.47
STAU1	5.23	3.42
MRPS27	4.81	5.79
CKAP4	4.79	3.47
HNRNPR	4.77	3.38
HADHA	4.70	3.71
SPG7	4.67	2.01
RPL10	4.65	1.98
IGF2BP3	4.55	4.54
PTPLAD1	4.53	4.09
USP7	4.47	5.38
GNL3	4.44	3.23
NKRF	4.31	2.21
MRPS31	4.27	6.23
EIF3C	4.20	3.43

Gene name	Mean log_2 nv∆CED/GST	$-log_{10}$ p-value
PRPS1	4.19	3.78
RFC2	4.15	4.34
EIF3B	4.15	4.08
IRS4	4.15	2.84
ASCC3	4.10	4.70
ANKRD17	4.09	2.95
RPS11	4.06	1.99
SLC25A10	4.03	5.79
FAU	4.00	2.10
GNL2	3.99	2.00
LARP4B	3.98	2.83
ILF3	3.98	1.93
MRPS34	3.93	2.29
KPNA1	3.92	3.06
NOP14	3.88	3.59
COPG1	3.83	3.24
MAPRE2	3.81	2.83
MRPS18B	3.73	3.01
DNAJB6	3.72	4.01
DIMT1	3.71	3.90
MRPS26	3.67	6.64
HADHB	3.66	2.74
SRRM1	3.66	2.00
SF3B1	3.65	2.77
SFPQ	3.64	2.54
POLR2H	3.64	5.58
PPAN	3.54	2.81
PPP2CA; PPP2CB	3.49	4.05
LTV1	3.46	3.18
EIF2S3; EIF2S3L	3.43	2.72

Gene name	Mean $\log_2$ nvΔCED/GST	$-\log_{10}$ p-value
EIF3F	3.37	2.57
TMPO	3.36	2.01
PTCD3	3.36	4.92
MRPL24	3.34	3.72
C11orf48	3.34	3.36
CTNND1	3.32	3.59
EIF3E	3.31	2.94
SLC25A13	3.28	3.89
NOC4L	3.28	2.62
EIF3D	3.22	2.32
ABCD3	3.20	3.72
MYO1B	3.19	4.04
MYO1C	3.16	5.86
PCBP2	3.13	5.30
MRPS28	3.12	3.04
MRPS6	3.11	2.77
RPS5	3.11	3.50
PES1	3.11	2.82
FARSA	3.08	4.20
NOP16	3.08	2.77
IGF2BP2	3.07	2.06
MRPL23	2.98	2.50
MRPS9	2.96	2.96
EXOSC2	2.96	3.52
DDX20	2.91	2.43
CNOT1	2.91	2.00
HNRNPH2	2.91	2.47
RPS3A	2.90	2.05
IPO7	2.89	2.69
MRPS35	2.89	2.66

Gene name	Mean log_2 nv∆CED/GST	$-log_{10}$ p-value
BLM	2.83	2.76
SRP72	2.83	2.29
MRPS14	2.82	1.96
DDX39A; DDX39	2.79	1.99
NDUFA10	2.78	2.72
MRPL3	2.77	2.48
IMPDH1	2.76	2.03
RPL19	2.75	2.29
HBS1L	2.73	2.08
RFC3	2.72	2.94
RPS8	2.66	2.99
MSH6	2.66	2.10
FAF2	2.65	3.79
GNB2L1	2.64	2.91
DPM1	2.62	2.86
RRP12	2.57	2.79
RPL36	2.57	2.22
PELO	2.56	3.10
PPP2R1A	2.53	2.16
AHCYL1	2.53	2.12
HIGD1A	2.52	3.21
AIMP2	2.51	2.34
TSR1	2.51	2.11
SF3B2	2.50	3.17
IPO5	2.49	4.45
RPS6	2.47	2.38
MKI67IP	2.46	2.06
MTCH2	2.43	2.59
RPS15	2.42	2.52
DAP3	2.41	3.17

Gene name	Mean log_2 nv∆CED/GST	$-log_{10}$ p-value
PRPF4	2.40	2.35
WDR75	2.35	2.46
RPS2	2.34	2.70
LUC7L	2.34	2.21
RPL13A	2.34	6.05
IGF2BP1	2.33	3.36
UBAP2	2.28	2.22
EIF2AK2	2.27	2.56
ESF1	2.26	3.75
USP9X	2.14	2.40
MRPS21	2.10	6.19
RPL18A	2.09	4.60
CNOT10	2.08	2.28
RPL24	2.07	2.49
RPL35A	2.05	2.07
RPS26	2.04	2.36
RPL10A	2.02	3.75
UTP14A; UTP14C	2.01	2.52
GCDH	2.00	2.08
MRPL41	1.98	2.09
RPL27A	1.93	3.31
RPL28	1.92	4.68
RPL26; KRBA2	1.91	4.01
RPL13	1.90	2.86
RBM39	1.90	3.50
RPL8	1.89	3.72
RPS27	1.85	2.36
RPS24	1.83	2.70
RPL18	1.83	4.43
RPL32	1.83	5.79

Gene name	Mean $\log_2$ nv∆CED/GST	$-\log_{10}$ p-value
RPS3	1.82	2.58
HNRNPC	1.74	2.68
RPL10; RPL10L	1.73	4.04
RPL29	1.72	4.53
SLC25A6	1.68	6.41
RPLP2	1.67	3.01
RPS13	1.67	3.30
ACTB	1.65	2.39
LSM14B	1.65	2.37
RPL6	1.61	4.49
RPL4	1.57	2.80
RPL23A	1.54	2.32
NOP58	1.53	2.20
POLR2B	1.52	2.52
RPL3	1.47	4.64
RPL21	1.44	3.81
SMC2	1.39	3.77
RPS25	1.37	2.36
RPL27	1.36	4.25
RPL7	1.34	2.69
RPL7A	1.34	4.83
SRSF7	1.31	2.72
SURF4	1.29	2.36
RPS19	1.24	3.56
PGAM5	1.24	3.12
RPL15	1.18	2.78
RPL34	1.14	3.33
C22orf28	1.10	2.61
RPS16	1.01	2.87
HNRNPM	0.83	2.90

Table S4. nvDNAJ MS results Quantitative mass spectrometric analysis of proteins associated with nvDNAJ domain. Table listing the 375 proteins that are significantly enriched with nvDNAJ as compared to the negative control GST (two sample t-test; FDR≤ 0.05; S0= 0.1; n= 2, biological replicates). The logarithmic ratios of protein intensities and the corresponding t-test p-values are shown. As input for the t-test only proteins that showed logarithmic ratios nvGW182/GST above 0 were considered in order to filter out background interactors.

Gene name	Mean log_2 nvDNAJ/GST	$-log_{10}$ p-value
PTPLAD1	7.82	7.80
ECM29; KIAA0368	7.64	7.93
ATP2A2	7.34	7.65
PPP2R2A	7.32	4.52
USP9X	7.25	7.63
STT3A	7.16	8.15
NUP205	7.14	7.10
TMEM33	7.11	8.11
LRPPRC	6.94	3.65
IMMT	6.84	4.89
SLC25A10	6.82	8.08
QKI	6.78	7.29
MSH2	6.56	4.41
SLC25A1	6.55	5.46
HADHA	6.53	4.76
SLC1A5	6.53	9.11
HEATR2	6.51	5.70
KDM1A	6.39	4.78
PSMC6	6.36	4.21
SLC25A3	6.34	2.96
PRKDC	6.32	3.54
MTCH2	6.31	6.70
PRC1	6.29	7.56
SFXN1	6.23	4.76

Gene name	Mean log_2 nvDNAJ/GST	$-log_{10}$ p-value
PDS5A	6.21	7.27
IPO7	6.06	4.07
CAND1	6.06	3.58
MTHFD2	6.04	5.37
PPP2R1A	5.95	5.33
NCLN	5.94	5.09
GNB1; GNB2	5.93	10.40
MAPRE2	5.88	5.23
SLC25A11	5.83	4.69
NCAPD2	5.81	5.25
TBRG4	5.72	5.43
TRIP13	5.71	3.99
G6PD	5.69	8.21
COMT	5.69	6.19
SLC25A13	5.68	6.58
EMD	5.66	4.33
NUP93	5.65	4.45
SMC3	5.65	2.95
PSMD14	5.64	4.30
FAF2	5.63	8.11
CUL1	5.62	4.78
SEC63	5.62	4.27
EARS2	5.61	5.39
AFG3L2	5.61	6.36
PRPS1	5.54	4.77
CAD	5.51	2.48
TUBB4A	5.49	6.23
DHCR24	5.39	8.19
NCDN	5.39	4.71
PSMC3	5.37	3.59

Gene name	Mean log_2 nvDNAJ/GST	$-log_{10}$ p-value
COPG1	5.35	3.07
SMC4	5.35	2.48
ABCD3	5.34	5.38
IPO5	5.33	6.25
NDUFA9	5.31	5.49
UQCRC2	5.30	3.12
PYCRL	5.23	4.34
NUP107	5.21	5.57
BAG2	5.19	6.42
CCT2	5.19	1.95
KPNA2	5.18	3.05
MTCH1	5.18	5.89
RCOR1	5.17	6.14
UCK2	5.17	4.27
SMC2	5.16	5.25
XPO7	5.16	6.61
MCM7	5.15	2.75
NDUFS2	5.15	3.60
CHCHD3	5.12	5.05
GCDH	5.09	6.38
PPP2R5B	5.07	5.33
MMS19	5.05	2.73
ARL1	5.02	5.94
TIMM23; TIMM23B	5.01	5.15
POLR1C	5.01	2.22
MAPK14	4.95	3.73
THOC3	4.95	3.33
PELO	4.95	7.28
PSMC4	4.93	3.81
SKP1	4.91	3.07

Gene name	Mean log_2 nvDNAJ/GST	$-log_{10}$ p-value
NDUFA4	4.89	2.80
PPP2CA; PPP2CB	4.89	3.72
NDUFS8	4.88	5.00
CCT3	4.88	1.86
SCD	4.86	6.61
CCT6A	4.85	1.88
POLR2B	4.85	4.51
SLC16A1	4.83	2.68
AIFM1	4.83	4.30
MSH6	4.82	4.24
CCT5	4.78	2.01
PPM1G	4.77	2.48
LBR	4.77	3.18
TIMMDC1	4.76	4.86
PHGDH	4.76	2.22
DPM1	4.74	6.20
DNAJA1	4.71	3.58
NDUFA13; YJEFN3	4.71	4.75
PSMD6	4.70	2.12
NSF	4.69	1.58
COPB2	4.69	3.37
RPN1	4.69	2.77
PDXDC1	4.68	1.91
TBC1D9B	4.67	1.71
OPA1	4.67	3.96
DCXR	4.62	4.84
TELO2	4.59	2.94
VPS16	4.51	8.52
AGK	4.50	3.69
PGRMC1	4.46	2.69

Gene name	Mean log_2 nvDNAJ/GST	$-log_{10}$ p-value
DNAJA2	4.44	2.86
CANX	4.44	2.69
TUBA1C	4.44	3.02
RFC2	4.42	5.99
CTPS1	4.41	2.34
HSP90AB2P	4.37	3.18
FARSA	4.35	2.71
TOMM22	4.33	4.35
TNPO3	4.33	2.96
DNAJB6	4.31	4.24
EIF2S3; EIF2S3L	4.31	3.10
DDX39A; DDX39	4.30	3.10
PFKM	4.28	1.67
CDIPT	4.26	4.70
DDX20	4.25	2.87
RFC5	4.24	5.02
AKAP1	4.24	2.57
EIF3F	4.22	4.11
IRS4	4.18	2.22
TCP1	4.17	1.77
MST4	4.17	2.79
STUB1	4.14	2.00
UBXN1	4.13	3.31
TECR	4.13	2.14
YTHDF2	4.12	4.33
MARCKSL1	4.12	1.64
HSPBP1	4.11	4.60
NPEPPS	4.11	1.59
ADCK3	4.09	3.82
NSDHL	4.08	2.73

Gene name	Mean log_2 nvDNAJ/GST	$-log_{10}$ p-value
FARSB	4.05	3.18
GEMIN5	4.04	2.62
CUL4B	4.04	3.85
SMN1	4.02	3.58
SCRIB	4.01	7.37
HMOX2	3.99	2.22
SURF4	3.98	2.61
DNAJA3	3.97	3.68
VPS33A	3.97	5.05
CKAP4	3.93	5.18
CNP	3.93	2.86
PUM1	3.93	2.06
MRFAP1	3.92	3.79
HSD17B10	3.91	3.52
TUBGCP2	3.91	5.15
COPG2	3.90	2.69
TMPO	3.90	2.37
AAAS	3.89	4.08
GNPAT	3.89	1.61
TXNDC5	3.88	3.49
SPTLC1	3.86	6.89
AHCYL1	3.85	7.20
RUVBL2	3.84	1.80
ACADM	3.84	1.48
TRAP1	3.84	3.87
TAGLN2	3.84	1.58
PCBP2	3.83	6.15
CTBP1	3.83	4.40
EIF2B2	3.83	3.70
VDAC1	3.82	1.84

Gene name	Mean log_2 nvDNAJ/GST	$-log_{10}$ p-value
QIL1	3.81	4.56
STAT1	3.81	1.77
MRPS6	3.81	4.54
HAUS8	3.80	2.68
PA2G4	3.80	1.52
SRPRB	3.80	4.46
POLR2H	3.79	5.46
CECR5	3.78	2.34
TIMM50	3.77	4.09
FDFT1	3.76	6.43
USP7	3.76	4.59
ATAD3A	3.75	1.63
HDAC1	3.75	1.89
FKBP8	3.75	1.74
SLC25A24	3.75	1.83
CTNND1	3.74	2.86
MCM3	3.73	1.94
PCID2	3.71	2.23
ABCF2	3.70	1.86
HELLS	3.69	2.08
RBBP7	3.68	1.53
CCT4	3.67	3.27
RUVBL1	3.67	1.72
DLD	3.66	1.73
NCKAP1	3.65	1.74
FRYL	3.63	3.61
YME1L1	3.63	2.16
POLD3	3.63	1.84
AUP1	3.61	3.43
POLD2	3.59	2.69

Gene name	Mean log_2 nvDNAJ/GST	$-log_{10}$ p-value
MTHFD1L	3.58	1.77
RBFOX2; RBM9; RBFOX1	3.56	2.16
QARS	3.56	1.72
CDK1	3.55	1.54
MTA2	3.52	2.27
AIMP2	3.49	3.69
EIF2B5	3.49	2.05
KCTD12	3.48	1.72
RRP1	3.48	3.60
TRMT10C	3.46	1.56
MAGT1	3.43	3.26
IMPDH1	3.43	2.70
TARS2	3.42	2.32
ATP5J2; PTCD1	3.42	5.26
EIF3M	3.37	4.40
CPSF2	3.36	3.98
TCEB1	3.36	2.50
IRAK1	3.35	2.58
SLC7A1	3.35	4.31
TBL2	3.34	2.13
SRM	3.33	1.75
SLC39A7	3.33	2.71
SNRNP70	3.32	5.60
MRPL37	3.32	1.81
SCO2	3.32	2.56
HSDL1	3.31	3.32
CSRP2	3.31	1.92
EIF3E	3.31	2.81
C12orf45	3.27	5.27
HSPA9	3.27	2.16

Gene name	Mean log_2 nvDNAJ/GST	$-log_{10}$ p-value
UBAC2	3.27	6.30
ATP5O	3.26	3.44
AAR2	3.25	4.30
GCAT	3.23	2.98
BYSL	3.22	1.77
CYC1	3.21	1.99
PMPCB	3.21	3.63
EIF2B4	3.19	4.19
SLC25A5	3.18	4.23
EEF1E1; hCG_2043275	3.17	2.05
ALDH9A1	3.16	1.53
ADAR	3.14	1.56
ARFGAP1	3.13	2.81
TTK	3.13	6.63
DERL1	3.13	4.21
RCL1	3.12	2.53
VDAC2	3.12	4.07
GMPPA	3.10	1.89
TPP1	3.10	3.79
KPNA1	3.10	2.51
SCAMP1	3.09	3.58
RFC3	3.08	2.18
PRDX3	3.07	2.12
MRPS22	3.07	1.72
GCFC2	3.07	2.50
WDR70	3.05	1.66
ELOVL1	3.04	2.98
MYL6	3.04	2.28
SEH1L	3.03	1.73
UBE2G2	3.03	2.42

Gene name	Mean log_2 nvDNAJ/GST	$-log_{10}$ p-value
NDUFA10	3.03	2.90
TCEB2	3.03	1.59
CDC45	3.01	4.56
RBBP4	3.00	2.05
FPGS	2.99	4.85
NUP160	2.96	3.13
RANGAP1	2.95	1.78
DSG2	2.95	1.52
PGRMC2	2.94	2.44
FAR1	2.93	3.24
FAM115A	2.93	1.65
UQCRQ	2.93	2.24
EIF3K	2.92	2.52
RMDN3	2.90	1.83
TSG101	2.85	2.98
UBA5	2.85	1.82
FAM96B	2.84	4.35
UBR4	2.82	1.73
PFN2	2.81	2.77
USP11	2.81	1.93
SNRPD2	2.81	1.71
NCAPG2	2.81	1.79
BCR	2.81	1.51
GTF3C4	2.79	3.04
HBS1L	2.77	1.91
PRIM1	2.77	2.27
HLTF	2.77	5.22
NOC4L	2.73	3.83
MAGED1	2.73	1.63
NTPCR	2.73	1.87

Gene name	Mean log_2 nvDNAJ/GST	$-log_{10}$ p-value
RHOT2	2.72	2.61
SKIV2L2	2.72	4.25
MRPL11	2.72	1.71
AAGAB	2.71	3.26
HSP90AB1	2.70	1.70
HNRNPAB	2.69	1.81
AKAP8L	2.69	4.07
PTGES2	2.67	2.60
ERAL1	2.65	2.22
POLE	2.61	2.37
NDUFB10	2.59	1.53
GTF3C5	2.57	1.86
TMEM165	2.56	3.43
STEAP3	2.55	1.80
EXOSC9	2.55	4.19
KIF2A	2.55	1.95
CUL3	2.55	3.53
ECD	2.54	4.27
PYCR2	2.51	2.12
LRRC41	2.50	2.45
AP3D1	2.50	1.97
ZNF207	2.48	1.83
GEMIN4	2.48	1.97
HIGD1A	2.48	2.38
ELAC2	2.47	1.78
TFB2M	2.46	2.30
EIF2B3	2.45	2.08
CMSS1	2.41	2.74
PSME4	2.40	2.16
SF3B5	2.39	1.56

Gene name	Mean log_2 nvDNAJ/GST	$-log_{10}$ p-value
EXOSC7	2.37	2.61
UBXN4	2.36	2.17
SMARCAD1	2.36	2.30
LIN7C; LIN7A	2.35	2.51
WDR3	2.34	2.22
ERGIC1	2.33	1.92
NUP43	2.31	1.84
SDAD1	2.31	2.20
MYO1C	2.31	4.34
C5orf51	2.27	1.88
TARBP1	2.26	3.45
DARS2	2.20	1.73
MRPS27	2.20	3.17
DNAJB11	2.19	2.27
SRPR	2.19	2.03
SRP72	2.14	1.65
PPFIA1	2.12	2.17
ASCC3	2.10	2.33
ZC3H11A	2.08	2.20
CDC20	2.03	2.18
TMEM109	2.01	3.01
ATXN2	2.00	1.86
HSD17B4	1.99	1.88
RFC4	1.98	2.49
ARAF; BRAF	1.94	1.88
MCU	1.91	1.63
DHX36	1.89	2.16
XRN2	1.88	2.23
SLC25A6	1.86	2.16
PDIA6	1.82	2.03

Gene name	Mean log_2 nvDNAJ/GST	$-log_{10}$ p-value
LAMTOR5	1.81	2.04
SUPT4H1	1.81	1.91
TMPO	1.79	1.99
GTPBP1	1.77	2.35
GOLGA2	1.74	1.88
DIMT1	1.70	1.76
PET112	1.69	1.65
EXOSC4	1.65	1.81
WDR6	1.64	2.45
FAM213A	1.57	2.15
EIF4A1	1.54	1.81
PRKCI	1.50	2.31
HCCS	1.49	2.12
WDR82	1.46	2.00
ERP44	1.44	2.60
CDKAL1	1.42	2.02
MYBBP1A	1.31	2.75
CCNB1	1.26	1.75
GNG12	1.23	1.90
UBR5	1.20	1.83
NMNAT1	0.90	1.97

Table S5. nvCED MS results Quantitative mass spectrometric analysis of proteins associated with nvCED domain. Table listing the 214 proteins that are significantly enriched with nvCED as compared to the negative control GST (two sample t-test; FDR≤ 0.05; S0= 0.1; n= 2, biological replicates). The logarithmic ratios of protein intensities and the corresponding t-test p-values are shown. As input for the t-test only proteins that showed logarithmic ratios nvGW182/GST above 0 were considered in order to filter out background interactors.

Gene name	Mean log_2 nvCED/GST	$-log_{10}$ p-value
CNOT1	10.96	8.81
MAPRE2	8.85	7.85
SLC25A1	8.55	6.28
SLC25A13	8.42	8.18
SLC25A11	8.17	5.66
SLC25A10	7.98	8.47
PABPC4	7.95	4.79
CNOT3	7.89	7.72
SFXN1	7.65	5.36
MTCH2	7.65	7.70
CNOT2	7.48	8.93
STT3A	7.27	6.39
FAF2	7.17	8.13
SLC25A3	7.17	3.21
NUP205	6.95	5.04
UQCRC2	6.91	3.99
CAD	6.90	3.20
NSDHL	6.85	3.79
PTPLAD1	6.85	6.08
SLC1A5	6.83	10.17
PFKM	6.74	4.27
GCDH	6.69	6.77
MTCH1	6.65	7.51
BAG2	6.62	6.34

Gene name	Mean log_2 nvCED/GST	$-log_{10}$ p-value
RBFOX2; RBM9; RBFOX1	6.60	4.76
CNOT9	6.60	7.27
POLR2H	6.56	7.77
SLC16A1	6.50	3.97
EARS2	6.45	6.41
TIMMDC1	6.43	6.26
ATP2A2	6.42	4.89
CNOT10	6.39	5.93
MSH2	6.38	2.75
MCM7	6.37	2.89
TIMM23; TIMM23B	6.34	7.08
ATP5A1	6.28	2.19
CECR5	6.27	3.39
SMC3	6.26	3.13
HSPA9	6.12	4.09
FARSA	6.06	4.20
DPM1	6.05	7.05
YTHDF2	6.05	6.17
NUP93	6.04	4.51
TMEM33	5.94	6.70
DHCR24	5.86	6.43
PRKDC	5.77	3.16
EMD	5.74	4.61
NDUFA13; YJEFN3	5.72	4.98
TUBB2B	5.70	5.06
NONO	5.61	1.98
IMMT	5.52	2.24
SCD	5.49	6.07
DNAJA3	5.49	4.86
TUBGCP2	5.42	5.16

Gene name	Mean log_2 nvCED/GST	$-log_{10}$ p-value
PHGDH	5.40	2.37
NDUFA12	5.32	3.52
YARS	5.30	1.69
HIGD1A	5.23	4.64
TUBA1C	5.23	3.60
PELO	5.23	4.28
SPTLC1	5.21	6.74
PABPC1	5.21	4.19
ABCD3	5.19	5.59
LBR	5.17	2.62
TUBB4A	5.16	6.38
PUM1	5.14	1.88
TCP1	5.13	2.26
TOMM22	5.10	4.92
QIL1	5.07	7.14
SPCS2	5.07	1.69
FAR1	5.04	4.86
NDUFA9	5.02	3.44
TECR	4.99	2.36
PDHB	4.95	1.95
NDUFA10	4.93	4.76
TIMM50	4.91	5.07
NDUFS2	4.87	3.02
HADHA	4.85	2.31
RPN1	4.85	2.55
UCK2	4.81	3.75
ARL1	4.81	6.04
ABCF2	4.77	2.43
NDUFS8	4.77	2.49
AIFM1	4.74	3.05

Gene name	Mean log_2 nvCED/GST	$-log_{10}$ p-value
CAND1	4.72	2.36
TBRG4	4.71	2.56
RBM14	4.71	2.06
MSH6	4.71	3.18
DNAJA1	4.70	3.54
KPNA2	4.70	2.50
MAGED1	4.66	2.97
DNAJA4	4.62	4.60
CNOT8	4.61	1.94
ABCB7	4.61	4.59
RFC5	4.58	5.22
TPP1	4.58	2.83
TARS2	4.57	1.79
PCBP2	4.53	5.23
DNAJA2	4.50	2.90
MPC2	4.49	4.74
TELO2	4.49	3.96
LARP4B	4.46	2.52
HNRNPA0	4.45	2.40
ATP5J2; PTCD1	4.44	3.77
CNOT7	4.39	2.14
SRM	4.39	1.88
QARS	4.38	1.78
DDX39A; DDX39	4.36	2.77
AGK	4.35	3.52
COQ5	4.34	4.50
SFXN3	4.33	2.75
ELOVL1	4.30	3.60
ECM29; KIAA0368	4.30	1.88
PRPS1	4.26	2.54

Gene name	Mean log_2 nvCED/GST	$-log_{10}$ p-value
NDUFA4	4.26	2.01
BYSL	4.18	1.75
POLR1D	4.15	2.30
POLR2B	4.15	1.81
ERAL1	4.13	3.46
CTPS1	4.09	1.72
GNB1; GNB2	4.09	2.40
DNAJB6	4.08	2.42
AUP1	4.06	4.25
VDAC1	4.05	3.10
IPO5	4.05	6.65
MCM3	4.03	2.20
PPP2R1A	4.03	2.75
SLC25A5	4.00	5.74
HNRNPH2	3.99	3.12
ADCK3	3.99	4.42
IRS4	3.94	2.11
HEATR2	3.92	3.76
AKAP8L	3.90	4.16
SLC25A6	3.87	4.21
AIMP2	3.86	4.09
EIF2S3; EIF2S3L	3.84	1.93
PSMD10	3.83	1.87
IPO7	3.82	3.51
PGRMC1	3.82	2.23
CYFIP1	3.79	2.48
CNOT6	3.77	4.05
COMT	3.72	2.03
MLF2	3.71	2.30
EEF1E1; hCG_2043275	3.71	2.47

Gene name	Mean log_2 nvCED/GST	$-log_{10}$ p-value
CNOT11	3.68	1.77
ATP5C1	3.67	1.91
PLK1	3.66	4.54
TMEM165	3.59	3.51
MARCKSL1	3.57	2.13
AAAS	3.56	2.24
UBE2G2	3.56	3.82
TMCO1	3.47	1.97
PYCRL	3.45	1.78
NCAPD2	3.45	3.02
UBAP2L	3.43	2.91
CDIPT	3.40	2.38
VMP1; TMEM49	3.39	2.34
ATAD3B	3.38	2.80
USP9X	3.34	1.94
VPS33A	3.33	3.19
MMS19	3.33	3.49
LARP4	3.32	2.48
HSP90AB2P	3.29	1.96
TRAP1	3.29	1.83
PMPCB	3.27	1.85
ATXN2	3.25	2.08
XPO7	3.21	1.79
RFC2	3.18	1.89
MRPL11	3.13	2.36
FPGS	3.10	2.64
FDFT1	3.09	3.87
PSME4	3.09	1.85
SURF4	3.09	4.45
CCT4	3.09	2.01

Gene name	Mean log_2 nvCED/GST	$-log_{10}$ p-value
SRRT	3.07	2.32
SRPR	3.06	3.55
MPC1; BRP44L	3.02	1.90
ZNF703	2.97	2.43
HSD17B11	2.93	2.67
ECSIT	2.87	1.94
MCU	2.83	2.23
UBE2E1; UBE2E2	2.82	2.19
QKI	2.79	1.79
EIF2B5	2.78	1.93
CDC45	2.77	1.98
MRPL37	2.74	1.99
DERL1	2.74	2.58
RCL1	2.71	2.01
NSUN4	2.66	2.42
SMARCAD1	2.66	2.36
UBAC2	2.62	2.29
HSD17B4	2.61	2.23
TTK	2.57	3.55
EIF4E2	2.53	2.99
AASS	2.47	1.84
VDAC2	2.47	2.01
IMPDH1	2.42	1.91
UTP20	2.35	2.12
EIF2S1	2.29	1.85
DHX36	2.22	2.57
SLC7A1	2.20	2.22
GNE	2.18	2.64
SF3B5	2.14	1.86
HNRNPH1	2.14	2.89

Gene name	Mean log_2 nvCED/GST	$-log_{10}$ p-value
ARFGAP1	2.13	2.12
EIF4A1	2.10	4.06
FAM213A	2.06	2.74
SCRIB	2.01	2.24
TXNDC5	1.95	2.40
RBM39	1.66	2.68
MRPS6	1.53	2.22
CPSF2	1.43	2.19
ECD	1.39	2.33
ASCC3	1.36	2.95

Table S6. W-motif enriched interactors detected in b-isoxazol precipitates 21 TNRC6C W-motif-specific interactors, as well as TNRC6 proteins, were identified by Kato and colleagues and Han and colleagues as components of b-isoxazol precipitates from the indicated cell lysates[676,677]. Comparison of RNase treated and untreated U-2 OS b-isox precipitates revealed whether the presence of these proteins is RNA independent (--), RNA insensitive (-) or RNA dependent (+).

Gene Name	B-isoxazole precipitates	RNA dependency
KHSRP	U-2 OS, NIH-3T3, mESC cells, mouse brain, mouse testis	- -
SLC25A5	U-2 OS cells	- -
TUBB	U-2 OS cells, NIH-3T3, mESC cells, mouse brain, mouse testis	- -
CLTC	U-2 OS cells	-
FAM98A	U-2 OS cells, NIH-3T3, mESC cells, mouse brain, mouse testis	-
HSPB1	U-2 OS cells	-
PABPC1	U-2 OS cells, NIH-3T3, mESC cells, mouse brain, mouse testis	-
PABPC4	U-2 OS cells, NIH-3T3, mESC cells, mouse brain, mouse testis	-
PCBP1	U-2 OS cells, NIH-3T3, mESC cells, mouse brain, mouse testis	-
C14orf166	U-2 OS cells	+
FXR1	U-2 OS cells, NIH-3T3, mESC cells, mouse brain, mouse testis	+
RPL18	U-2 OS cells, S2 cells	+
RPL36	U-2 OS cells, S2 cells	+
RPLP0	U-2 OS cells, S2 cells	+
RPS4X	U-2 OS cells	+
AP2A2	NIH-3T3, mESC cells, mouse brain, mouse testis	not tested
AP2B1	NIH-3T3, mESC cells, mouse brain, mouse testis	not tested
FMR1	S2 cells	not tested

7. Abbreviations

AGO	Argonaute
AP	Adaptor protein
CAF1	CCR4-associated factor 1
CCR4	Carbon catabolite repressor protein 4 homolog
CCV	Clathrin-coated vesicle
cDNA	Complementary deoxyribonucleic acid
CDS	Coding Sequence
CED	C-terminal effector domain
CNOT	CCR4-NOT transcription complex subunit
CrPV	Cricket paralysis virus
CVD	Cardiovascular Disease
DAZL	Deleted in azoospermia-like
DCP1	mRNA-decapping enzyme 1
Dgcr8	DiGeorge syndrome critical region gene 8
Dhh1	DEAD box helicase homolog 1
DNA	Deoxyribonucleic acid
DNase	Deoxyribonuclease
Dnd1	Dead-end 1
EDC3	Enhancer of mRNA-decapping protein 3
EDD	E3 ubiquitin-protein ligase UBR5
eIF3	Eukaryotic translation initiation factor 3
eIF4A	Eukaryotic translation initiation factor 4A
eIF4E	Eukaryotic translation initiation factor 4E
eIF4G	Eukaryotic translation initiation factor 4G
eIF6	Eukaryotic translation initiation factor 6
EMCV	Encephalomyocarditis virus
ER	Endoplasmatic reticulum
ES cells	Embryonic stem cells
ESCRT	complex Endosomal sorting complex required for transport complex
EtOH	Ethanol
FC	Fold change
FLuc	Firefly luciferase
GO	Gene ontology
GST	Glutathione S-transferase
GTP	Guanosine triphosphate
HA	Hemagglutinin
HCV	Hepatitis C virus
HRP	Horseradish peroxidase
hs	Homo sapiens
HSL	Histone stem-loop
i.e.	that is
IP	Immunoprecipitation
IRES	Internal ribosomal entry site
ITAFs	Internal ribosome-entry site (IRES) trans-acting factors
KEGG	Kyoto encyclopedia of genes and genomes
LC	Liquid Chromatography
LFQ	Label Free Quantification
m7G	7-methyl-guanylate cap

miR	MicroRNA
miRNA	MicroRNA
MNase	Microccocal nuclease
mRNA	Messenger ribonucleic acid
MS	Mass spectrometry
mut	Mutant
MVBs	Multivesicular bodies
MW	Molecular Weight
NED	N-terminal effector domain
nv	Nematostella vectensis
ORF	Open reading frame
PABP	Polyadenylate-binding protein
PAM2	PABP-interacting motif 2
PAN2	PABP-dependent poly(A)-specific ribonuclease subunit 2
PAN3	PABP-dependent poly(A)-specific ribonuclease subunit 3
PAZ	domain Piwi-Argonaute-Zwille domain
PBS	Phosphate Buffered Saline
PCR	Polymerase Chain Reaction
pH	Potential of Hydrogen
PIC	Pre-Initiation Complex
piRNA	Piwi-interacting RNA
qRT-PCR	Quantitative real time PCR
RBP	RNA binding proteins
RISC	RNA-induced silencing complex
RLuc	Renilla luciferase
RNA	Ribonucleic acid
RNAi	RNA interference
RRM	RNA recognition motif
RT	Room temperature or Reverse Transcriptase, can be inferred from context
SD	standard deviation
SDS-PAGE	Sodium dodecyl sulfate polyacrylamide gel electrophoresis
SEM	Standard error of the mean
shRNA	short hairpin RNA
SILAC	Stable isotope labelling with amino acids in cell culture
siRNA	Small interfering RNA
TNRC6A	Trinucleotide repeat containing gene 6A protein
TNRC6B	Trinucleotide repeat containing gene 6B protein
TNRC6C	Trinucleotide repeat containing gene 6C protein
TRBP	TAR RNA-binding protein
tRNA	Transfer ribonucleic acid
UTR	Untranslated region
W	tryptophan
wt	Wild type
XRN1	5’-3’ exoribonuclease 1

8. Symbols and Units

%	Percentage
%v/v	Percentage volume/ volume
%w/v	Percentage weight/ volume
°C	Degree Celsius
bp	Base pairs
g	Gram
g	Acceleration of gravity (see RCF)
h	Hour
kb	Kilobase
kDa	Kilodalton
L	Liter
mg	Milligram
min	Minute
µl	Microliter
ml	Milliliter
µM	Micromolar
mM	Millimolar
ng	Nanogram
nt	Nucleotide
rcf (g)	Relative centrifugal force
rpm	Revolutions per minute
µg	Microgram

9. Bibliography

1. Miescher, F. *Die histochemischen und physiologischen Arbeiten von Friedrich Miescher*. (1897).
2. Avery, O. T., Macleod, C. M. & McCarty, M. STUDIES ON THE CHEMICAL NATURE OF THE SUBSTANCE INDUCING TRANSFORMATION OF PNEUMOCOCCAL TYPES : INDUCTION OF TRANSFORMATION BY A DESOXYRIBONUCLEIC ACID FRACTION ISOLATED FROM PNEUMOCOCCUS TYPE III. *J. Exp. Med.* **79,** 137–158 (1944).
3. Watson, J. D. & CRICK, F. H. Molecular structure of nucleic acids; a structure for deoxyribose nucleic acid. *Nature* **171,** 737–738 (1953).
4. CRICK, F. H., BARNETT, L., BRENNER, S. & WATTS-TOBIN, R. J. General nature of the genetic code for proteins. *Nature* **192,** 1227–1232 (1961).
5. NIRENBERG, M. W. & MATTHAEI, J. H. The dependence of cell-free protein synthesis in E. coli upon naturally occurring or synthetic polyribonucleotides. *Proc. Natl. Acad. Sci. U.S.A.* **47,** 1588–1602 (1961).
6. Crick, F. Central dogma of molecular biology. *Nature* **227,** 561–563 (1970).
7. Kruger, K. *et al.* Self-splicing RNA: autoexcision and autocyclization of the ribosomal RNA intervening sequence of Tetrahymena. *Cell* **31,** 147–157 (1982).
8. Guerrier-Takada, C., Gardiner, K., Marsh, T., Pace, N. & Altman, S. The RNA moiety of ribonuclease P is the catalytic subunit of the enzyme. *Cell* **35,** 849–857 (1983).
9. Gesteland, R. F., Cech, T. & Atkins, J. F. *The RNA World*. (CSHL Press, 2006).
10. ENCODE Project Consortium *et al.* Identification and analysis of functional elements in 1% of the human genome by the ENCODE pilot project. *Nature* **447,** 799–816 (2007).
11. Amaral, P. P., Dinger, M. E., Mercer, T. R. & Mattick, J. S. The eukaryotic genome as an RNA machine. *Science* **319,** 1787–1789 (2008).
12. Cech, T. R. & Steitz, J. A. The noncoding RNA revolution-trashing old rules to forge new ones. *Cell* **157,** 77–94 (2014).
13. Jaenisch, R. & Bird, A. Epigenetic regulation of gene expression: how the genome integrates intrinsic and environmental signals. *Nat. Genet.* **33 Suppl,** 245–254 (2003).
14. Mattick, J. S. The central role of RNA in human development and cognition. *FEBS Lett* **585,** 1600–1616 (2011).
15. Ponting, C. P. & Hardison, R. C. What fraction of the human genome is functional? *Genome Res.* **21,** 1769–1776 (2011).
16. Holoch, D. & Moazed, D. RNA-mediated epigenetic regulation of gene expression. *Nat. Rev. Genet.* **16,** 71–84 (2015).
17. Ponting, C. P., Oliver, P. L. & Reik, W. Evolution and functions of long noncoding RNAs. *Cell* **136,** 629–641 (2009).
18. Ghildiyal, M. & Zamore, P. D. Small silencing RNAs: an expanding

universe. *Nat. Rev. Genet.* **10,** 94–108 (2009).
19. Rands, C. M., Meader, S., Ponting, C. P. & Lunter, G. 8.2% of the Human genome is constrained: variation in rates of turnover across functional element classes in the human lineage. *PLoS Genet.* **10,** e1004525 (2014).
20. Chen, L.-L. The biogenesis and emerging roles of circular RNAs. *Nat Rev Mol Cell Biol* **17,** 205–211 (2016).
21. Kondo, T. *et al.* Small peptides switch the transcriptional activity of Shavenbaby during Drosophila embryogenesis. *Science* **329,** 336–339 (2010).
22. Mackowiak, S. D. *et al.* Extensive identification and analysis of conserved small ORFs in animals. *Genome Biol.* **16,** 179 (2015).
23. Hellens, R. P., Brown, C. M., Chisnall, M. A. W., Waterhouse, P. M. & Macknight, R. C. The Emerging World of Small ORFs. *Trends Plant Sci.* **21,** 317–328 (2016).
24. Fire, A. *et al.* Potent and specific genetic interference by double-stranded RNA in Caenorhabditis elegans. *Nature* **391,** 806–811 (1998).
25. Zhao, B. S., Roundtree, I. A. & He, C. Post-transcriptional gene regulation by mRNA modifications. *Nat Rev Mol Cell Biol* (2016). doi:10.1038/nrm.2016.132
26. Carmell, M. A. & Hannon, G. J. RNase III enzymes and the initiation of gene silencing. *Nat Struct Mol Biol* **11,** 214–218 (2004).
27. Czech, B. *et al.* An endogenous small interfering RNA pathway in Drosophila. *Nature* **453,** 798–802 (2008).
28. Kawamura, Y. *et al.* Drosophila endogenous small RNAs bind to Argonaute 2 in somatic cells. *Nature* **453,** 793–797 (2008).
29. Ghildiyal, M. *et al.* Endogenous siRNAs derived from transposons and mRNAs in Drosophila somatic cells. *Science* **320,** 1077–1081 (2008).
30. Okamura, K. *et al.* The Drosophila hairpin RNA pathway generates endogenous short interfering RNAs. *Nature* **453,** 803–806 (2008).
31. Magny, E. G. *et al.* Conserved regulation of cardiac calcium uptake by peptides encoded in small open reading frames. *Science* **341,** 1116–1120 (2013).
32. Slavoff, S. A., Heo, J., Budnik, B. A., Hanakahi, L. A. & Saghatelian, A. A human short open reading frame (sORF)-encoded polypeptide that stimulates DNA end joining. *J. Biol. Chem.* **289,** 10950–10957 (2014).
33. Lee, C. *et al.* The mitochondrial-derived peptide MOTS-c promotes metabolic homeostasis and reduces obesity and insulin resistance. *Cell Metab.* **21,** 443–454 (2015).
34. Anderson, D. M. *et al.* A micropeptide encoded by a putative long noncoding RNA regulates muscle performance. *Cell* **160,** 595–606 (2015).
35. D'Lima, N. G. *et al.* A human microprotein that interacts with the mRNA decapping complex. *Nat. Chem. Biol.* (2016). doi:10.1038/nchembio.2249
36. Zamore, P. D. & Haley, B. Ribo-gnome: the big world of small RNAs. *Science* **309,** 1519–1524 (2005).
37. Hannon, G. J., Rivas, F. V., Murchison, E. P. & Steitz, J. A. The expanding universe of noncoding RNAs. *Cold Spring Harb. Symp. Quant. Biol.* **71,** 551–564 (2006).
38. Rana, T. M. Illuminating the silence: understanding the structure and function of small RNAs. *Nat Rev Mol Cell Biol* **8,** 23–36 (2007).
39. Grosshans, H. & Filipowicz, W. Molecular biology: the expanding world of small RNAs. *Nature* **451,** 414–416 (2008).

40. Wang, X.-H. *et al.* RNA interference directs innate immunity against viruses in adult Drosophila. *Science* **312,** 452–454 (2006).
41. van Rij, R. P. *et al.* The RNA silencing endonuclease Argonaute 2 mediates specific antiviral immunity in Drosophila melanogaster. *Genes & Development* **20,** 2985–2995 (2006).
42. Pak, J. & Fire, A. Distinct populations of primary and secondary effectors during RNAi in C. elegans. *Science* **315,** 241–244 (2007).
43. Colmenares, S. U., Buker, S. M., Buhler, M., Dlakić, M. & Moazed, D. Coupling of double-stranded RNA synthesis and siRNA generation in fission yeast RNAi. *Molecular Cell* **27,** 449–461 (2007).
44. Shabalina, S. A. & Koonin, E. V. Origins and evolution of eukaryotic RNA interference. *Trends Ecol. Evol. (Amst.)* **23,** 578–587 (2008).
45. Gottesman, S. & Storz, G. Bacterial small RNA regulators: versatile roles and rapidly evolving variations. *Cold Spring Harb Perspect Biol* **3,** (2011).
46. Bushati, N. & Cohen, S. M. microRNA functions. *Annu. Rev. Cell Dev. Biol.* **23,** 175–205 (2007).
47. Schwarz, D. S. *et al.* Asymmetry in the assembly of the RNAi enzyme complex. *Cell* **115,** 199–208 (2003).
48. Khvorova, A., Reynolds, A. & Jayasena, S. D. Functional siRNAs and miRNAs exhibit strand bias. *Cell* **115,** 209–216 (2003).
49. Matranga, C., Tomari, Y., Shin, C., Bartel, D. P. & Zamore, P. D. Passenger-strand cleavage facilitates assembly of siRNA into Ago2-containing RNAi enzyme complexes. *Cell* **123,** 607–620 (2005).
50. Rand, T. A., Petersen, S., Du, F. & Wang, X. Argonaute2 cleaves the anti-guide strand of siRNA during RISC activation. *Cell* **123,** 621–629 (2005).
51. Leuschner, P. J. F., Ameres, S. L., Kueng, S. & Martinez, J. Cleavage of the siRNA passenger strand during RISC assembly in human cells. *EMBO Rep.* **7,** 314–320 (2006).
52. Filipowicz, W. RNAi: the nuts and bolts of the RISC machine. *Cell* **122,** 17–20 (2005).
53. Castel, S. E. & Martienssen, R. A. RNA interference in the nucleus: roles for small RNAs in transcription, epigenetics and beyond. *Nat. Rev. Genet.* **14,** 100–112 (2013).
54. Borges, F. & Martienssen, R. A. The expanding world of small RNAs in plants. *Nat Rev Mol Cell Biol* **16,** 727–741 (2015).
55. Kim, V. N., Han, J. & Siomi, M. C. Biogenesis of small RNAs in animals. *Nat Rev Mol Cell Biol* **10,** 126–139 (2009).
56. Carthew, R. W. & Sontheimer, E. J. Origins and Mechanisms of miRNAs and siRNAs. *Cell* **136,** 642–655 (2009).
57. Ross, R. J., Weiner, M. M. & Lin, H. PIWI proteins and PIWI-interacting RNAs in the soma. *Nature* **505,** 353–359 (2014).
58. Houseley, J. & Tollervey, D. The many pathways of RNA degradation. *Cell* **136,** 763–776 (2009).
59. Vagin, V. V. *et al.* A distinct small RNA pathway silences selfish genetic elements in the germline. *Science* **313,** 320–324 (2006).
60. Saito, K. *et al.* Pimet, the Drosophila homolog of HEN1, mediates 2 '-O-methylation of PIWI-interacting RNAs at their 3 ' ends. *Genes & Development* **21,** 1603–1608 (2007).
61. Horwich, M. D. *et al.* The Drosophila RNA methyltransferase, DmHen1, modifies germline piRNAs and single-stranded siRNAs in RISC. *Curr. Biol.* **17,** 1265–1272 (2007).

62. Kirino, Y. & Mourelatos, Z. Mouse Piwi-interacting RNAs are 2 '-O-methylated at their 3 ' termini. *Nat Struct Mol Biol* **14,** 347–348 (2007).
63. Ohara, T. *et al.* The 3 ' termini of mouse Piwi-interacting RNAs are 2 '-O-methylated. *Nat Struct Mol Biol* **14,** 349–350 (2007).
64. Brennecke, J. *et al.* Discrete small RNA-generating loci as master regulators of transposon activity in Drosophila. *Cell* **128,** 1089–1103 (2007).
65. Aravin, A. A. *et al.* Double-stranded RNA-mediated silencing of genomic tandem repeats and transposable elements in the D. melanogaster germline. *Curr. Biol.* **11,** 1017–1027 (2001).
66. Aravin, A. A. *et al.* The small RNA profile during Drosophila melanogaster development. *Dev. Cell* **5,** 337–350 (2003).
67. Saito, K. *et al.* Specific association of Piwi with rasiRNAs derived from retrotransposon and heterochromatic regions in the Drosophila genome. *Genes & Development* **20,** 2214–2222 (2006).
68. Nishida, K. M. *et al.* Gene silencing mechanisms mediated by Aubergine-piRNA complexes in Drosophila male gonad. *RNA* **13,** 1911–1922 (2007).
69. Gunawardane, L. S. *et al.* A slicer-mediated mechanism for repeat-associated siRNA 5' end formation in Drosophila. *Science* **315,** 1587–1590 (2007).
70. Cox, D. N. *et al.* A novel class of evolutionarily conserved genes defined by piwi are essential for stem cell self-renewal. *Genes & Development* **12,** 3715–3727 (1998).
71. Cox, D. N., Chao, A. & Lin, H. F. piwi encodes a nucleoplasmic factor whose activity modulates the number and division rate of germline stem cells. *Development* **127,** 503–514 (2000).
72. Sarot, E., Payen-Groschene, G., Bucheton, A. & Pelisson, A. Evidence for a piwi-dependent RNA silencing of the gypsy endogenous retrovirus by the Drosophila melanogaster flamenco gene. *Genetics* **166,** 1313–1321 (2004).
73. Szakmary, A., Cox, D. N., Wang, Z. & Lin, H. F. Regulatory relationship among piwi, pumilio, and bag-of-marbles in Drosophila germline stem cell self-renewal and differentiation. *Curr. Biol.* **15,** 171–178 (2005).
74. Kalmykova, A. I., Klenov, M. S. & Gvozdev, V. A. Argonaute protein PIWI controls mobilization of retrotransposons in the Drosophila male germline. *Nucleic Acids Research* **33,** 2052–2059 (2005).
75. Siomi, M. C., Sato, K., Pezic, D. & Aravin, A. A. PIWI-interacting small RNAs: the vanguard of genome defence. *Nat Rev Mol Cell Biol* **12,** 246–258 (2011).
76. Chowdhury, D., Choi, Y. E. & Brault, M. E. DNA DAMAGE - OPINION Charity begins at home: non-coding RNA functions in DNA repair. *Nat Rev Mol Cell Biol* **14,** 181–189 (2013).
77. Stuwe, E., Toth, K. F. & Aravin, A. A. Small but sturdy: small RNAs in cellular memory and epigenetics. *Genes & Development* **28,** 423–431 (2014).
78. Ishizu, H., Siomi, H. & Siomi, M. C. Biology of PIWI-interacting RNAs: new insights into biogenesis and function inside and outside of germlines. *Genes & Development* **26,** 2361–2373 (2012).
79. Ha, H. *et al.* A comprehensive analysis of piRNAs from adult human testis and their relationship with genes and mobile elements. *BMC Genomics* **15,** (2014).

80. Griffiths-Jones, S., Saini, H. K., van Dongen, S. & Enright, A. J. miRBase: tools for microRNA genomics. *Nucleic Acids Research* **36,** D154–8 (2008).
81. Huntzinger, E. & Izaurralde, E. Gene silencing by microRNAs: contributions of translational repression and mRNA decay. *Nat. Rev. Genet.* **12,** 99–110 (2011).
82. Brower-Toland, B. *et al.* Drosophila PIWI associates with chromatin and interacts directly with HP1a. *Genes & Development* **21,** 2300–2311 (2007).
83. Malone, C. D. *et al.* Specialized piRNA pathways act in germline and somatic tissues of the Drosophila ovary. *Cell* **137,** 522–535 (2009).
84. Lee, E. J. *et al.* Identification of piRNAs in the central nervous system. *RNA* **17,** 1090–1099 (2011).
85. Rouget, C. *et al.* Maternal mRNA deadenylation and decay by the piRNA pathway in the early Drosophila embryo. *Nature* **467,** 1128–1132 (2010).
86. Gou, L.-T. *et al.* Pachytene piRNAs instruct massive mRNA elimination during late spermiogenesis. *Cell Res.* **24,** 680–700 (2014).
87. Reinhart, B. J. *et al.* The 21-nucleotide let-7 RNA regulates developmental timing in Caenorhabditis elegans. *Nature* **403,** 901–906 (2000).
88. Kozomara, A. & Griffiths-Jones, S. miRBase: annotating high confidence microRNAs using deep sequencing data. *Nucleic Acids Research* **42,** D68–73 (2014).
89. Ha, M. & Kim, V. N. Regulation of microRNA biogenesis. *Nat Rev Mol Cell Biol* **15,** 509–524 (2014).
90. Jonas, S. & Izaurralde, E. Towards a molecular understanding of microRNA-mediated gene silencing. *Nat. Rev. Genet.* **16,** 421–433 (2015).
91. Wilczynska, A. & Bushell, M. The complexity of miRNA-mediated repression. *Cell Death Differ.* **22,** 22–33 (2015).
92. Lee, R. C., Feinbaum, R. L. & Ambros, V. The C. elegans heterochronic gene lin-4 encodes small RNAs with antisense complementarity to lin-14. *Cell* **75,** 843–854 (1993).
93. Wightman, B., Ha, I. & Ruvkun, G. Posttranscriptional regulation of the heterochronic gene lin-14 by lin-4 mediates temporal pattern formation in C. elegans. *Cell* **75,** 855–862 (1993).
94. Pasquinelli, A. E. *et al.* Conservation of the sequence and temporal expression of let-7 heterochronic regulatory RNA. *Nature* **408,** 86–89 (2000).
95. Bartel, D. P. MicroRNAs: target recognition and regulatory functions. *Cell* **136,** 215–233 (2009).
96. Reinhart, B. J., Weinstein, E. G., Rhoades, M. W., Bartel, B. & Bartel, D. P. MicroRNAs in plants. *Genes & Development* **16,** 1616–1626 (2002).
97. Lagos-Quintana, M. *et al.* Identification of tissue-specific microRNAs from mouse. *Curr. Biol.* **12,** 735–739 (2002).
98. Lim, L. P. *et al.* The microRNAs of Caenorhabditis elegans. *Genes & Development* **17,** 991–1008 (2003).
99. Lewis, B. P., Burge, C. B. & Bartel, D. P. Conserved seed pairing, often flanked by adenosines, indicates that thousands of human genes are microRNA targets. *Cell* **120,** 15–20 (2005).
100. Bentwich, I. *et al.* Identification of hundreds of conserved and nonconserved human microRNAs. *Nat. Genet.* **37,** 766–770 (2005).
101. Zhao, T. *et al.* A complex system of small RNAs in the unicellular green alga Chlamydomonas reinhardtii. *Genes & Development* **21,** 1190–1203 (2007).

102. Molnár, A., Schwach, F., Studholme, D. J., Thuenemann, E. C. & Baulcombe, D. C. miRNAs control gene expression in the single-cell alga Chlamydomonas reinhardtii. *Nature* **447,** 1126–1129 (2007).
103. Lai, E. C. Micro RNAs are complementary to 3' UTR sequence motifs that mediate negative post-transcriptional regulation. *Nat. Genet.* **30,** 363–364 (2002).
104. Suh, N. & Blelloch, R. Small RNAs in early mammalian development: from gametes to gastrulation. *Development* **138,** 1653–1661 (2011).
105. Friedman, R. C., Farh, K. K.-H., Burge, C. B. & Bartel, D. P. Most mammalian mRNAs are conserved targets of microRNAs. *Genome Res.* **19,** 92–105 (2009).
106. Jackson, A. L. & Levin, A. A. Developing microRNA therapeutics: approaching the unique complexities. *Nucleic Acid Ther* **22,** 213–225 (2012).
107. Chen, K. & Rajewsky, N. Natural selection on human microRNA binding sites inferred from SNP data. *Nat. Genet.* **38,** 1452–1456 (2006).
108. Chen, K. & Rajewsky, N. The evolution of gene regulation by transcription factors and microRNAs. *Nat. Rev. Genet.* **8,** 93–103 (2007).
109. Cai, X., Hagedorn, C. H. & Cullen, B. R. Human microRNAs are processed from capped, polyadenylated transcripts that can also function as mRNAs. *RNA* **10,** 1957–1966 (2004).
110. Lee, Y. *et al.* MicroRNA genes are transcribed by RNA polymerase II. *EMBO J* **23,** 4051–4060 (2004).
111. Parizotto, E. A., Dunoyer, P., Rahm, N., Himber, C. & Voinnet, O. In vivo investigation of the transcription, processing, endonucleolytic activity, and functional relevance of the spatial distribution of a plant miRNA. *Genes & Development* **18,** 2237–2242 (2004).
112. Lagos-Quintana, M., Rauhut, R., Lendeckel, W. & Tuschl, T. Identification of novel genes coding for small expressed RNAs. *Science* **294,** 853–858 (2001).
113. Lee, Y., Jeon, K., Lee, J.-T., Kim, S. & Kim, V. N. MicroRNA maturation: stepwise processing and subcellular localization. *EMBO J* **21,** 4663–4670 (2002).
114. Monteys, A. M. *et al.* Structure and activity of putative intronic miRNA promoters. *RNA* **16,** 495–505 (2010).
115. Ozsolak, F. *et al.* Chromatin structure analyses identify miRNA promoters. *Genes & Development* **22,** 3172–3183 (2008).
116. Lee, Y. *et al.* The nuclear RNase III Drosha initiates microRNA processing. *Nature* **425,** 415–419 (2003).
117. Goldberg, R., Motzkin, B., Marion, R., Scambler, P. J. & Shprintzen, R. J. Velo-cardio-facial syndrome: a review of 120 patients. *Am. J. Med. Genet.* **45,** 313–319 (1993).
118. Shiohama, A., Sasaki, T., Noda, S., Minoshima, S. & Shimizu, N. Molecular cloning and expression analysis of a novel gene DGCR8 located in the DiGeorge syndrome chromosomal region. *Biochem. Biophys. Res. Commun.* **304,** 184–190 (2003).
119. Wang, Y., Medvid, R., Melton, C., Jaenisch, R. & Blelloch, R. DGCR8 is essential for microRNA biogenesis and silencing of embryonic stem cell self-renewal. *Nat. Genet.* **39,** 380–385 (2007).
120. Chong, M. M. W. *et al.* Canonical and alternate functions of the microRNA biogenesis machinery. *Genes & Development* **24,** 1951–1960 (2010).

121. Yi, R., Qin, Y., Macara, I. G. & Cullen, B. R. Exportin-5 mediates the nuclear export of pre-microRNAs and short hairpin RNAs. *Genes & Development* **17,** 3011–3016 (2003).
122. Bohnsack, M. T., Czaplinski, K. & Görlich, D. Exportin 5 is a RanGTP-dependent dsRNA-binding protein that mediates nuclear export of pre-miRNAs. *RNA* **10,** 185–191 (2004).
123. Lund, E., Güttinger, S., Calado, A., Dahlberg, J. E. & Kutay, U. Nuclear export of microRNA precursors. *Science* **303,** 95–98 (2004).
124. Bernstein, E., Caudy, A. A., Hammond, S. M. & Hannon, G. J. Role for a bidentate ribonuclease in the initiation step of RNA interference. *Nature* **409,** 363–366 (2001).
125. Grishok, A. *et al.* Genes and mechanisms related to RNA interference regulate expression of the small temporal RNAs that control C. elegans developmental timing. *Cell* **106,** 23–34 (2001).
126. Hutvágner, G. *et al.* A cellular function for the RNA-interference enzyme Dicer in the maturation of the let-7 small temporal RNA. *Science* **293,** 834–838 (2001).
127. Ketting, R. F. *et al.* Dicer functions in RNA interference and in synthesis of small RNA involved in developmental timing in C. elegans. *Genes & Development* **15,** 2654–2659 (2001).
128. Knight, S. W. & Bass, B. L. A role for the RNase III enzyme DCR-1 in RNA interference and germ line development in Caenorhabditis elegans. *Science* **293,** 2269–2271 (2001).
129. Bernstein, E. *et al.* Dicer is essential for mouse development. *Nat. Genet.* **35,** 215–217 (2003).
130. Kanellopoulou, C. *et al.* Dicer-deficient mouse embryonic stem cells are defective in differentiation and centromeric silencing. *Genes & Development* **19,** 489–501 (2005).
131. Murchison, E. P., Partridge, J. F., Tam, O. H., Cheloufi, S. & Hannon, G. J. Characterization of Dicer-deficient murine embryonic stem cells. *Proc. Natl. Acad. Sci. U.S.A.* **102,** 12135–12140 (2005).
132. Iwasaki, S. *et al.* Hsc70/Hsp90 chaperone machinery mediates ATP-dependent RISC loading of small RNA duplexes. *Molecular Cell* **39,** 292–299 (2010).
133. Miyoshi, K., Miyoshi, T., Hartig, J. V., Siomi, H. & Siomi, M. C. Molecular mechanisms that funnel RNA precursors into endogenous small-interfering RNA and microRNA biogenesis pathways in Drosophila. *RNA* **16,** 506–515 (2010).
134. Förstemann, K., Horwich, M. D., Wee, L., Tomari, Y. & Zamore, P. D. Drosophila microRNAs are sorted into functionally distinct argonaute complexes after production by dicer-1. *Cell* **130,** 287–297 (2007).
135. Yoda, M. *et al.* ATP-dependent human RISC assembly pathways. *Nat Struct Mol Biol* **17,** 17–23 (2010).
136. Kawamata, T., Seitz, H. & Tomari, Y. Structural determinants of miRNAs for RISC loading and slicer-independent unwinding. *Nat Struct Mol Biol* **16,** 953–960 (2009).
137. Tomari, Y., Du, T. & Zamore, P. D. Sorting of Drosophila small silencing RNAs. *Cell* **130,** 299–308 (2007).
138. Lau, N. C., Lim, L. P., Weinstein, E. G. & Bartel, D. P. An abundant class of tiny RNAs with probable regulatory roles in Caenorhabditis elegans. *Science* **294,** 858–862 (2001).

139. Hu, H. Y. *et al.* Sequence features associated with microRNA strand selection in humans and flies. *BMC Genomics* **10,** 413 (2009).
140. Czech, B. *et al.* Hierarchical rules for Argonaute loading in Drosophila. *Molecular Cell* **36,** 445–456 (2009).
141. Okamura, K., Liu, N. & Lai, E. C. Distinct mechanisms for microRNA strand selection by Drosophila Argonautes. *Molecular Cell* **36,** 431–444 (2009).
142. Ghildiyal, M., Xu, J., Seitz, H., Weng, Z. & Zamore, P. D. Sorting of Drosophila small silencing RNAs partitions microRNA* strands into the RNA interference pathway. *RNA* **16,** 43–56 (2010).
143. Czech, B. & Hannon, G. J. Small RNA sorting: matchmaking for Argonautes. *Nat. Rev. Genet.* **12,** 19–31 (2011).
144. Steiner, F. A. *et al.* Structural features of small RNA precursors determine Argonaute loading in Caenorhabditis elegans. *Nat Struct Mol Biol* **14,** 927–933 (2007).
145. Jannot, G., Boisvert, M.-E. L., Banville, I. H. & Simard, M. J. Two molecular features contribute to the Argonaute specificity for the microRNA and RNAi pathways in C. elegans. *RNA* **14,** 829–835 (2008).
146. Meister, G. *et al.* Human Argonaute2 mediates RNA cleavage targeted by miRNAs and siRNAs. *Molecular Cell* **15,** 185–197 (2004).
147. Liu, J. *et al.* Argonaute2 is the catalytic engine of mammalian RNAi. *Science* **305,** 1437–1441 (2004).
148. Babiarz, J. E., Ruby, J. G., Wang, Y., Bartel, D. P. & Blelloch, R. Mouse ES cells express endogenous shRNAs, siRNAs, and other Microprocessor-independent, Dicer-dependent small RNAs. *Genes & Development* **22,** 2773–2785 (2008).
149. Berezikov, E., Chung, W.-J., Willis, J., Cuppen, E. & Lai, E. C. Mammalian mirtron genes. *Molecular Cell* **28,** 328–336 (2007).
150. Okamura, K., Hagen, J. W., Duan, H., Tyler, D. M. & Lai, E. C. The mirtron pathway generates microRNA-class regulatory RNAs in Drosophila. *Cell* **130,** 89–100 (2007).
151. Ruby, J. G., Jan, C. H. & Bartel, D. P. Intronic microRNA precursors that bypass Drosha processing. *Nature* **448,** 83–86 (2007).
152. Ender, C. *et al.* A human snoRNA with microRNA-like functions. *Molecular Cell* **32,** 519–528 (2008).
153. Flynt, A. S., Greimann, J. C., Chung, W.-J., Lima, C. D. & Lai, E. C. MicroRNA biogenesis via splicing and exosome-mediated trimming in Drosophila. *Molecular Cell* **38,** 900–907 (2010).
154. Cazalla, D., Xie, M. & Steitz, J. A. A primate herpesvirus uses the integrator complex to generate viral microRNAs. *Molecular Cell* **43,** 982–992 (2011).
155. Cifuentes, D. *et al.* A novel miRNA processing pathway independent of Dicer requires Argonaute2 catalytic activity. *Science* **328,** 1694–1698 (2010).
156. Yang, J.-S. *et al.* Conserved vertebrate mir-451 provides a platform for Dicer-independent, Ago2-mediated microRNA biogenesis. *Proc. Natl. Acad. Sci. U.S.A.* **107,** 15163–15168 (2010).
157. Cheloufi, S., Santos, Dos, C. O., Chong, M. M. W. & Hannon, G. J. A dicer-independent miRNA biogenesis pathway that requires Ago catalysis. *Nature* **465,** 584–589 (2010).
158. Heo, I. *et al.* Mono-uridylation of pre-microRNA as a key step in the biogenesis of group II let-7 microRNAs. *Cell* **151,** 521–532 (2012).

159. Lewis, B. P., Shih, I.-H., Jones-Rhoades, M. W., Bartel, D. P. & Burge, C. B. Prediction of mammalian microRNA targets. *Cell* **115,** 787–798 (2003).
160. Doench, J. G. & Sharp, P. A. Specificity of microRNA target selection in translational repression. *Genes & Development* **18,** 504–511 (2004).
161. Nielsen, C. B. *et al.* Determinants of targeting by endogenous and exogenous microRNAs and siRNAs. *RNA* **13,** 1894–1910 (2007).
162. Baek, D. *et al.* The impact of microRNAs on protein output. *Nature* **455,** 64–71 (2008).
163. Ha, I., Wightman, B. & Ruvkun, G. A bulged lin-4/lin-14 RNA duplex is sufficient for Caenorhabditis elegans lin-14 temporal gradient formation. *Genes & Development* **10,** 3041–3050 (1996).
164. Vella, M. C., Choi, E.-Y., Lin, S.-Y., Reinert, K. & Slack, F. J. The C. elegans microRNA let-7 binds to imperfect let-7 complementary sites from the lin-41 3'UTR. *Genes & Development* **18,** 132–137 (2004).
165. Didiano, D. & Hobert, O. Perfect seed pairing is not a generally reliable predictor for miRNA-target interactions. *Nat Struct Mol Biol* **13,** 849–851 (2006).
166. Tay, Y., Zhang, J., Thomson, A. M., Lim, B. & Rigoutsos, I. MicroRNAs to Nanog, Oct4 and Sox2 coding regions modulate embryonic stem cell differentiation. *Nature* **455,** 1124–1128 (2008).
167. Hutvagner, G. & Zamore, P. D. A microRNA in a multiple-turnover RNAi enzyme complex. *Science* **297,** 2056–2060 (2002).
168. Yekta, S., Shih, I.-H. & Bartel, D. P. MicroRNA-directed cleavage of HOXB8 mRNA. *Science* **304,** 594–596 (2004).
169. Kloosterman, W. P., Wienholds, E., Ketting, R. F. & Plasterk, R. H. A. Substrate requirements for let-7 function in the developing zebrafish embryo. *Nucleic Acids Research* **32,** 6284–6291 (2004).
170. Easow, G., Teleman, A. A. & Cohen, S. M. Isolation of microRNA targets by miRNP immunopurification. *RNA* **13,** 1198–1204 (2007).
171. Lytle, J. R., Yario, T. A. & Steitz, J. A. Target mRNAs are repressed as efficiently by microRNA-binding sites in the 5‘ UTR as in the 3’ UTR. *Proc. Natl. Acad. Sci. U.S.A.* **104,** 9667–9672 (2007).
172. Hafner, M. *et al.* Transcriptome-wide identification of RNA-binding protein and microRNA target sites by PAR-CLIP. *Cell* **141,** 129–141 (2010).
173. Grosswendt, S. *et al.* Unambiguous identification of miRNA:target site interactions by different types of ligation reactions. *Molecular Cell* **54,** 1042–1054 (2014).
174. Grimson, A. *et al.* MicroRNA targeting specificity in mammals: determinants beyond seed pairing. *Molecular Cell* **27,** 91–105 (2007).
175. Farh, K. K.-H. *et al.* The widespread impact of mammalian MicroRNAs on mRNA repression and evolution. *Science* **310,** 1817–1821 (2005).
176. Selbach, M. *et al.* Widespread changes in protein synthesis induced by microRNAs. *Nature* **455,** 58–63 (2008).
177. Sood, P., Krek, A., Zavolan, M., Macino, G. & Rajewsky, N. Cell-type-specific signatures of microRNAs on target mRNA expression. *Proc. Natl. Acad. Sci. U.S.A.* **103,** 2746–2751 (2006).
178. Mu, P. *et al.* Genetic dissection of the miR-17~92 cluster of microRNAs in Myc-induced B-cell lymphomas. *Genes & Development* **23,** 2806–2811 (2009).
179. Hausser, J. & Zavolan, M. Identification and consequences of miRNA-target interactions--beyond repression of gene expression. *Nat. Rev.*

Genet. **15,** 599–612 (2014).
180. Gu, S., Jin, L., Zhang, F., Sarnow, P. & Kay, M. A. Biological basis for restriction of microRNA targets to the 3' untranslated region in mammalian mRNAs. *Nat Struct Mol Biol* **16,** 144–150 (2009).
181. Hausser, J., Syed, A. P., Bilen, B. & Zavolan, M. Analysis of CDS-located miRNA target sites suggests that they can effectively inhibit translation. *Genome Res.* **23,** 604–615 (2013).
182. Lee, I. *et al.* New class of microRNA targets containing simultaneous 5'-UTR and 3'-UTR interaction sites. *Genome Res.* **19,** 1175–1183 (2009).
183. Guo, H., Ingolia, N. T., Weissman, J. S. & Bartel, D. P. Mammalian microRNAs predominantly act to decrease target mRNA levels. *Nature* **466,** 835–840 (2010).
184. Eichhorn, S. W. *et al.* mRNA destabilization is the dominant effect of mammalian microRNAs by the time substantial repression ensues. *Molecular Cell* **56,** 104–115 (2014).
185. Yoo, A. S. & Greenwald, I. LIN-12/Notch activation leads to microRNA-mediated down-regulation of Vav in C. elegans. *Science* **310,** 1330–1333 (2005).
186. Lu, Y., Thomson, J. M., Wong, H. Y. F., Hammond, S. M. & Hogan, B. L. M. Transgenic over-expression of the microRNA miR-17-92 cluster promotes proliferation and inhibits differentiation of lung epithelial progenitor cells. *Dev. Biol.* **310,** 442–453 (2007).
187. He, L. *et al.* A microRNA component of the p53 tumour suppressor network. *Nature* **447,** 1130–1134 (2007).
188. Wang, Y. *et al.* Embryonic stem cell-specific microRNAs regulate the G1-S transition and promote rapid proliferation. *Nat. Genet.* **40,** 1478–1483 (2008).
189. Rosa, A., Spagnoli, F. M. & Brivanlou, A. H. The miR-430/427/302 family controls mesendodermal fate specification via species-specific target selection. *Dev. Cell* **16,** 517–527 (2009).
190. Frost, R. J. A. & Olson, E. N. Control of glucose homeostasis and insulin sensitivity by the Let-7 family of microRNAs. *Proc. Natl. Acad. Sci. U.S.A.* **108,** 21075–21080 (2011).
191. Miska, E. A. *et al.* Most Caenorhabditis elegans microRNAs are individually not essential for development or viability. *PLoS Genet.* **3,** e215 (2007).
192. Park, C. Y. *et al.* A resource for the conditional ablation of microRNAs in the mouse. *Cell Rep* **1,** 385–391 (2012).
193. Ambros, V. *et al.* A uniform system for microRNA annotation. *RNA* **9,** 277–279 (2003).
194. Hertel, J. *et al.* The expansion of the metazoan microRNA repertoire. *BMC Genomics* **7,** 25 (2006).
195. Lee, Y. S. *et al.* Distinct roles for Drosophila Dicer-1 and Dicer-2 in the siRNA/miRNA silencing pathways. *Cell* **117,** 69–81 (2004).
196. Fukuda, T. *et al.* DEAD-box RNA helicase subunits of the Drosha complex are required for processing of rRNA and a subset of microRNAs. *Nat. Cell Biol.* **9,** 604–611 (2007).
197. Martin, R. *et al.* A Drosophila pasha mutant distinguishes the canonical microRNA and mirtron pathways. *Mol. Cell. Biol.* **29,** 861–870 (2009).
198. Krek, A. *et al.* Combinatorial microRNA target predictions. *Nat. Genet.* **37,** 495–500 (2005).
199. Brennecke, J., Stark, A., Russell, R. B. & Cohen, S. M. Principles of

microRNA-target recognition. *PLoS Biol.* **3,** e85 (2005).
200. Xie, X. *et al.* Systematic discovery of regulatory motifs in human promoters and 3' UTRs by comparison of several mammals. *Nature* **434,** 338–345 (2005).
201. Chalfie, M., Horvitz, H. R. & Sulston, J. E. Mutations that lead to reiterations in the cell lineages of C. elegans. *Cell* **24,** 59–69 (1981).
202. Morita, S. *et al.* One Argonaute family member, Eif2c2 (Ago2), is essential for development and appears not to be involved in DNA methylation. *Genomics* **89,** 687–696 (2007).
203. Jiang, Z. *et al.* Trinucleotide repeat containing 6a (Tnrc6a)-mediated microRNA function is required for development of yolk sac endoderm. *J. Biol. Chem.* **287,** 5979–5987 (2012).
204. Fukagawa, T. *et al.* Dicer is essential for formation of the heterochromatin structure in vertebrate cells. *Nat. Cell Biol.* **6,** 784–791 (2004).
205. Kim, Y.-K., Kim, B. & Kim, V. N. Re-evaluation of the roles of DROSHA, Export in 5, and DICER in microRNA biogenesis. *Proc. Natl. Acad. Sci. U.S.A.* **113,** E1881–9 (2016).
206. Wu, Q. *et al.* The RNase III enzyme DROSHA is essential for microRNA production and spermatogenesis. *J. Biol. Chem.* **287,** 25173–25190 (2012).
207. Su, H., Trombly, M. I., Chen, J. & Wang, X. Essential and overlapping functions for mammalian Argonautes in microRNA silencing. *Genes & Development* **23,** 304–317 (2009).
208. Kim, D. H., Grün, D. & van Oudenaarden, A. Dampening of expression oscillations by synchronous regulation of a microRNA and its target. *Nat. Genet.* **45,** 1337–1344 (2013).
209. Johnson, C. D. *et al.* The let-7 microRNA represses cell proliferation pathways in human cells. *Cancer Res.* **67,** 7713–7722 (2007).
210. Flynt, A. S. & Lai, E. C. Biological principles of microRNA-mediated regulation: shared themes amid diversity. *Nat. Rev. Genet.* **9,** 831–842 (2008).
211. Melton, C., Judson, R. L. & Blelloch, R. Opposing microRNA families regulate self-renewal in mouse embryonic stem cells. *Nature* **463,** 621–626 (2010).
212. Pauli, A., Rinn, J. L. & Schier, A. F. Non-coding RNAs as regulators of embryogenesis. *Nat. Rev. Genet.* **12,** 136–149 (2011).
213. Cordes, K. R. *et al.* miR-145 and miR-143 regulate smooth muscle cell fate and plasticity. *Nature* **460,** 705–710 (2009).
214. Xin, M. *et al.* MicroRNAs miR-143 and miR-145 modulate cytoskeletal dynamics and responsiveness of smooth muscle cells to injury. *Genes & Development* **23,** 2166–2178 (2009).
215. Cheng, Y. *et al.* MicroRNA-145, a novel smooth muscle cell phenotypic marker and modulator, controls vascular neointimal lesion formation. *Circ. Res.* **105,** 158–166 (2009).
216. Chivukula, R. R. *et al.* An essential mesenchymal function for miR-143/145 in intestinal epithelial regeneration. *Cell* **157,** 1104–1116 (2014).
217. Vidigal, J. A. & Ventura, A. The biological functions of miRNAs: lessons from in vivo studies. *Trends in Cell Biology* **25,** 137–147 (2015).
218. Staton, A. A., Knaut, H. & Giraldez, A. J. miRNA regulation of Sdf1 chemokine signaling provides genetic robustness to germ cell migration. *Nat. Genet.* **43,** 204–211 (2011).

219. Wang, X. *et al.* Regulation of let-7 and its target oncogenes (Review). *Oncol Lett* **3,** 955–960 (2012).
220. Giraldez, A. J. *et al.* Zebrafish MiR-430 promotes deadenylation and clearance of maternal mRNAs. *Science* **312,** 75–79 (2006).
221. Tan, C. L. *et al.* MicroRNA-128 governs neuronal excitability and motor behavior in mice. *Science* **342,** 1254–1258 (2013).
222. Wang, D. *et al.* MicroRNA-205 controls neonatal expansion of skin stem cells by modulating the PI(3)K pathway. *Nat. Cell Biol.* **15,** 1153–1163 (2013).
223. Bushati, N., Stark, A., Brennecke, J. & Cohen, S. M. Temporal reciprocity of miRNAs and their targets during the maternal-to-zygotic transition in Drosophila. *Curr. Biol.* **18,** 501–506 (2008).
224. Lund, E., Liu, M., Hartley, R. S., Sheets, M. D. & Dahlberg, J. E. Deadenylation of maternal mRNAs mediated by miR-427 in Xenopus laevis embryos. *RNA* **15,** 2351–2363 (2009).
225. Wu, E. *et al.* Pervasive and cooperative deadenylation of 3'UTRs by embryonic microRNA families. *Molecular Cell* **40,** 558–570 (2010).
226. Caudy, A. A., Myers, M., Hannon, G. J. & Hammond, S. M. Fragile X-related protein and VIG associate with the RNA interference machinery. *Genes & Development* **16,** 2491–2496 (2002).
227. Ishizuka, A., Siomi, M. C. & Siomi, H. A Drosophila fragile X protein interacts with components of RNAi and ribosomal proteins. *Genes & Development* **16,** 2497–2508 (2002).
228. Jin, P. *et al.* Biochemical and genetic interaction between the fragile X mental retardation protein and the microRNA pathway. *Nat. Neurosci.* **7,** 113–117 (2004).
229. Soifer, H. S., Rossi, J. J. & Saetrom, P. MicroRNAs in disease and potential therapeutic applications. *Mol. Ther.* **15,** 2070–2079 (2007).
230. Ventura, A. & Jacks, T. MicroRNAs and cancer: short RNAs go a long way. *Cell* **136,** 586–591 (2009).
231. Ardekani, A. M. & Naeini, M. M. The Role of MicroRNAs in Human Diseases. *Avicenna J Med Biotechnol* **2,** 161–179 (2010).
232. Ameres, S. L. & Zamore, P. D. Diversifying microRNA sequence and function. *Nat Rev Mol Cell Biol* **14,** 475–488 (2013).
233. Tüfekci, K. U., Oner, M. G., Meuwissen, R. L. J. & Genç, S. The role of microRNAs in human diseases. *Methods Mol. Biol.* **1107,** 33–50 (2014).
234. Oberlé, I. *et al.* Instability of a 550-base pair DNA segment and abnormal methylation in fragile X syndrome. *Science* **252,** 1097–1102 (1991).
235. Verkerk, A. J. *et al.* Identification of a gene (FMR-1) containing a CGG repeat coincident with a breakpoint cluster region exhibiting length variation in fragile X syndrome. *Cell* **65,** 905–914 (1991).
236. Kremer, E. J. *et al.* Mapping of DNA instability at the fragile X to a trinucleotide repeat sequence p(CCG)n. *Science* **252,** 1711–1714 (1991).
237. Ashley, C. T., Wilkinson, K. D., Reines, D. & Warren, S. T. FMR1 protein: conserved RNP family domains and selective RNA binding. *Science* **262,** 563–566 (1993).
238. Feng, Y. *et al.* FMRP associates with polyribosomes as an mRNP, and the I304N mutation of severe fragile X syndrome abolishes this association. *Molecular Cell* **1,** 109–118 (1997).
239. Laggerbauer, B., Ostareck, D., Keidel, E. M., Ostareck-Lederer, A. & Fischer, U. Evidence that fragile X mental retardation protein is a negative

regulator of translation. *Hum. Mol. Genet.* **10,** 329–338 (2001).
240. Li, Y. & Kowdley, K. V. MicroRNAs in common human diseases. *Genomics Proteomics Bioinformatics* **10,** 246–253 (2012).
241. Li, Z. & Rana, T. M. Therapeutic targeting of microRNAs: current status and future challenges. *Nat Rev Drug Discov* **13,** 622–638 (2014).
242. Ipsaro, J. J. & Joshua-Tor, L. From guide to target: molecular insights into eukaryotic RNA-interference machinery. *Nat Struct Mol Biol* **22,** 20–28 (2015).
243. Calin, G. A. *et al.* Frequent deletions and down-regulation of micro- RNA genes miR15 and miR16 at 13q14 in chronic lymphocytic leukemia. *Proc. Natl. Acad. Sci. U.S.A.* **99,** 15524–15529 (2002).
244. Cimmino, A. *et al.* miR-15 and miR-16 induce apoptosis by targeting BCL2. *Proc. Natl. Acad. Sci. U.S.A.* **102,** 13944–13949 (2005).
245. Calin, G. A. *et al.* Human microRNA genes are frequently located at fragile sites and genomic regions involved in cancers. *Proc. Natl. Acad. Sci. U.S.A.* **101,** 2999–3004 (2004).
246. Lu, J. *et al.* MicroRNA expression profiles classify human cancers. *Nature* **435,** 834–838 (2005).
247. Chan, J. A., Krichevsky, A. M. & Kosik, K. S. MicroRNA-21 is an antiapoptotic factor in human glioblastoma cells. *Cancer Res.* **65,** 6029–6033 (2005).
248. Jopling, C. L., Yi, M., Lancaster, A. M., Lemon, S. M. & Sarnow, P. Modulation of hepatitis C virus RNA abundance by a liver-specific MicroRNA. *Science* **309,** 1577–1581 (2005).
249. Lanford, R. E. *et al.* Therapeutic silencing of microRNA-122 in primates with chronic hepatitis C virus infection. *Science* **327,** 198–201 (2010).
250. Gatto, G. *et al.* Epstein-Barr virus latent membrane protein 1 trans-activates miR-155 transcription through the NF-kappaB pathway. *Nucleic Acids Research* **36,** 6608–6619 (2008).
251. Linnstaedt, S. D., Gottwein, E., Skalsky, R. L., Luftig, M. A. & Cullen, B. R. Virally induced cellular microRNA miR-155 plays a key role in B-cell immortalization by Epstein-Barr virus. *J. Virol.* **84,** 11670–11678 (2010).
252. Gottwein, E. *et al.* A viral microRNA functions as an orthologue of cellular miR-155. *Nature* **450,** 1096–1099 (2007).
253. Junker, A. *et al.* MicroRNA profiling of multiple sclerosis lesions identifies modulators of the regulatory protein CD47. *Brain* **132,** 3342–3352 (2009).
254. Martins, M. *et al.* Convergence of miRNA expression profiling, α-synuclein interacton and GWAS in Parkinson's disease. *PLoS ONE* **6,** e25443 (2011).
255. Kim, J. *et al.* A MicroRNA feedback circuit in midbrain dopamine neurons. *Science* **317,** 1220–1224 (2007).
256. Hébert, S. S. *et al.* Loss of microRNA cluster miR-29a/b-1 in sporadic Alzheimer's disease correlates with increased BACE1/beta-secretase expression. *Proc. Natl. Acad. Sci. U.S.A.* **105,** 6415–6420 (2008).
257. Willem, M. *et al.* Control of peripheral nerve myelination by the beta-secretase BACE1. *Science* **314,** 664–666 (2006).
258. van Rooij, E. *et al.* Control of stress-dependent cardiac growth and gene expression by a microRNA. *Science* **316,** 575–579 (2007).
259. Montgomery, R. L. *et al.* Therapeutic inhibition of miR-208a improves cardiac function and survival during heart failure. *Circulation* **124,** 1537–1547 (2011).

260. Krol, J., Loedige, I. & Filipowicz, W. The widespread regulation of microRNA biogenesis, function and decay. *Nat. Rev. Genet.* **11,** 597–610 (2010).
261. Fabian, M. R. & Sonenberg, N. The mechanics of miRNA-mediated gene silencing: a look under the hood of miRISC. *Nat Struct Mol Biol* **19,** 586–593 (2012).
262. Hendrickson, D. G. *et al.* Concordant regulation of translation and mRNA abundance for hundreds of targets of a human microRNA. *PLoS Biol.* **7,** e1000238 (2009).
263. Subtelny, A. O., Eichhorn, S. W., Chen, G. R., Sive, H. & Bartel, D. P. Poly(A)-tail profiling reveals an embryonic switch in translational control. *Nature* **508,** 66–71 (2014).
264. Schirle, N. T. & MacRae, I. J. The Crystal Structure of Human Argonaute2. *Science* **336,** 1037–1040 (2012).
265. Elkayam, E. *et al.* The structure of human argonaute-2 in complex with miR-20a. *Cell* **150,** 100–110 (2012).
266. Schirle, N. T., Sheu-Gruttadauria, J. & MacRae, I. J. Structural basis for microRNA targeting. *Science* **346,** 608–613 (2014).
267. Mathys, H. *et al.* Structural and Biochemical Insights to the Role of the CCR4-NOT Complex and DDX6 ATPase in MicroRNA Repression. *Molecular Cell* **54,** 751–765 (2014).
268. Chen, Y. *et al.* A DDX6-CNOT1 complex and W-binding pockets in CNOT9 reveal direct links between miRNA target recognition and silencing. *Molecular Cell* **54,** 737–750 (2014).
269. Christie, M., Boland, A., Huntzinger, E., Weichenrieder, O. & Izaurralde, E. Structure of the PAN3 Pseudokinase Reveals the Basis for Interactions with the PAN2 Deadenylase and the GW182 Proteins. *Molecular Cell* **51,** 360–373 (2013).
270. Tritschler, F. *et al.* Structural basis for the mutually exclusive anchoring of P body components EDC3 and Tral to the DEAD box protein DDX6/Me31B. *Molecular Cell* **33,** 661–668 (2009).
271. Meister, G. *et al.* Identification of novel argonaute-associated proteins. *Curr. Biol.* **15,** 2149–2155 (2005).
272. Liu, J., Valencia-Sanchez, M. A., Hannon, G. J. & Parker, R. MicroRNA-dependent localization of targeted mRNAs to mammalian P-bodies. *Nat. Cell Biol.* **7,** 719–723 (2005).
273. Jakymiw, A. *et al.* Disruption of GW bodies impairs mammalian RNA interference. *Nat. Cell Biol.* **7,** 1267–1274 (2005).
274. Ding, L., Spencer, A., Morita, K. & Han, M. The developmental timing regulator AIN-1 interacts with miRISCs and may target the argonaute protein ALG-1 to cytoplasmic P bodies in C. elegans. *Molecular Cell* **19,** 437–447 (2005).
275. Chekulaeva, M. *et al.* miRNA repression involves GW182-mediated recruitment of CCR4–NOT through conserved W-containing motifs. *Nat Struct Mol Biol* **18,** 1218–1226 (2011).
276. Braun, J. E., Huntzinger, E., Fauser, M. & Izaurralde, E. GW182 Proteins Directly Recruit Cytoplasmic Deadenylase Complexes to miRNA Targets. *Molecular Cell* **44,** 120–133 (2011).
277. Fabian, M. R. *et al.* miRNA-mediated deadenylation is orchestrated by GW182 through two conserved motifs that interact with CCR4–NOT. *Nat Struct Mol Biol* **18,** 1211–1217 (2011).

278. Brengues, M., Teixeira, D. & Parker, R. Movement of eukaryotic mRNAs between polysomes and cytoplasmic processing bodies. *Science* **310,** 486–489 (2005).
279. Bhattacharyya, S. N., Habermacher, R., Martine, U., Closs, E. I. & Filipowicz, W. Relief of microRNA-mediated translational repression in human cells subjected to stress. *Cell* **125,** 1111–1124 (2006).
280. Anderson, P. & Kedersha, N. RNA granules. *The Journal of Cell Biology* **172,** 803–808 (2006).
281. Schratt, G. M. *et al.* A brain-specific microRNA regulates dendritic spine development. *Nature* **439,** 283–289 (2006).
282. Banerjee, S., Neveu, P. & Kosik, K. S. A coordinated local translational control point at the synapse involving relief from silencing and MOV10 degradation. *Neuron* **64,** 871–884 (2009).
283. Muddashetty, R. S. *et al.* Reversible inhibition of PSD-95 mRNA translation by miR-125a, FMRP phosphorylation, and mGluR signaling. *Molecular Cell* **42,** 673–688 (2011).
284. Bazzini, A. A., Lee, M. T. & Giraldez, A. J. Ribosome profiling shows that miR-430 reduces translation before causing mRNA decay in zebrafish. *Science* **336,** 233–237 (2012).
285. Kundu, P., Fabian, M. R., Sonenberg, N., Bhattacharyya, S. N. & Filipowicz, W. HuR protein attenuates miRNA-mediated repression by promoting miRISC dissociation from the target RNA. *Nucleic Acids Research* **40,** 5088–5100 (2012).
286. Jinek, M., Fabian, M. R., Coyle, S. M., Sonenberg, N. & Doudna, J. A. Structural insights into the human GW182-PABC interaction in microRNA-mediated deadenylation. *Nat Struct Mol Biol* **17,** 238–240 (2010).
287. Kozlov, G., Safaee, N., Rosenauer, A. & Gehring, K. Structural basis of binding of P-body-associated proteins GW182 and ataxin-2 by the MIle domain of poly(A)-binding protein. *J. Biol. Chem.* **285,** 13599–13606 (2010).
288. Schäfer, I. B., Rode, M., Bonneau, F., Schüssler, S. & Conti, E. The structure of the Pan2-Pan3 core complex reveals cross-talk between deadenylase and pseudokinase. *Nat Struct Mol Biol* (2014). doi:10.1038/nsmb.2834
289. Wolf, J. *et al.* Structural basis for Pan3 binding to Pan2 and its function in mRNA recruitment and deadenylation. *EMBO J* **33,** 1514–1526 (2014).
290. Jonas, S. *et al.* An asymmetric PAN3 dimer recruits a single PAN2 exonuclease to mediate mRNA deadenylation and decay. *Nat Struct Mol Biol* (2014). doi:10.1038/nsmb.2837
291. Petit, A.-P. *et al.* The structural basis for the interaction between the CAF1 nuclease and the NOT1 scaffold of the human CCR4-NOT deadenylase complex. *Nucleic Acids Research* **40,** 11058–11072 (2012).
292. Basquin, J. *et al.* Architecture of the nuclease module of the yeast Ccr4-not complex: the Not1-Caf1-Ccr4 interaction. *Molecular Cell* **48,** 207–218 (2012).
293. Rouya, C. *et al.* Human DDX6 effects miRNA-mediated gene silencing via direct binding to CNOT1. *RNA* **20,** 1398–1409 (2014).
294. Fromm, S. A. *et al.* The structural basis of Edc3- and Scd6-mediated activation of the Dcp1:Dcp2 mRNA decapping complex. *EMBO J* **31,** 279–290 (2012).
295. She, M. *et al.* Structural basis of dcp2 recognition and activation by dcp1.

Molecular Cell **29,** 337–349 (2008).
296. Braun, J. E. *et al.* A direct interaction between DCP1 and XRN1 couples mRNA decapping to 5' exonucleolytic degradation. *Nat Struct Mol Biol* **19,** 1324–1331 (2012).
297. Jonas, S. & Izaurralde, E. The role of disordered protein regions in the assembly of decapping complexes and RNP granules. *Genes & Development* **27,** 2628–2641 (2013).
298. Hammond, S. M., Bernstein, E., Beach, D. & Hannon, G. J. An RNA-directed nuclease mediates post-transcriptional gene silencing in Drosophila cells. *Nature* **404,** 293–296 (2000).
299. Hammond, S. M., Boettcher, S., Caudy, A. A., Kobayashi, R. & Hannon, G. J. Argonaute2, a link between genetic and biochemical analyses of RNAi. *Science* **293,** 1146–1150 (2001).
300. Tuschl, T., Zamore, P. D., Lehmann, R., Bartel, D. P. & Sharp, P. A. Targeted mRNA degradation by double-stranded RNA in vitro. *Genes & Development* **13,** 3191–3197 (1999).
301. Rand, T. A., Ginalski, K., Grishin, N. V. & Wang, X. Biochemical identification of Argonaute 2 as the sole protein required for RNA-induced silencing complex activity. *Proc. Natl. Acad. Sci. U.S.A.* **101,** 14385–14389 (2004).
302. Tabara, H. *et al.* The rde-1 gene, RNA interference, and transposon silencing in C. elegans. *Cell* **99,** 123–132 (1999).
303. Fagard, M., Boutet, S., Morel, J. B., Bellini, C. & Vaucheret, H. AGO1, QDE-2, and RDE-1 are related proteins required for post-transcriptional gene silencing in plants, quelling in fungi, and RNA interference in animals. *Proc. Natl. Acad. Sci. U.S.A.* **97,** 11650–11654 (2000).
304. Rivas, F. V. *et al.* Purified Argonaute2 and an siRNA form recombinant human RISC. *Nat Struct Mol Biol* **12,** 340–349 (2005).
305. Miyoshi, K., Tsukumo, H., Nagami, T., Siomi, H. & Siomi, M. C. Slicer function of Drosophila Argonautes and its involvement in RISC formation. *Genes & Development* **19,** 2837–2848 (2005).
306. Bartel, D. P. MicroRNAs: genomics, biogenesis, mechanism, and function. *Cell* **116,** 281–297 (2004).
307. Liu, J. *et al.* A role for the P-body component GW182 in microRNA function. *Nat. Cell Biol.* **7,** 1261–1266 (2005).
308. Bohmert, K. *et al.* AGO1 defines a novel locus of Arabidopsis controlling leaf development. *EMBO J* **17,** 170–180 (1998).
309. Pillai, R. S., Artus, C. G. & Filipowicz, W. Tethering of human Ago proteins to mRNA mimics the miRNA-mediated repression of protein synthesis. *RNA* **10,** 1518–1525 (2004).
310. Rehwinkel, J., Behm-Ansmant, I., Gatfield, D. & Izaurralde, E. A crucial role for GW182 and the DCP1:DCP2 decapping complex in miRNA-mediated gene silencing. *RNA* **11,** 1640–1647 (2005).
311. Behm-Ansmant, I. *et al.* mRNA degradation by miRNAs and GW182 requires both CCR4:NOT deadenylase and DCP1:DCP2 decapping complexes. *Genes & Development* **20,** 1885–1898 (2006).
312. Landthaler, M. *et al.* Molecular characterization of human Argonaute-containing ribonucleoprotein complexes and their bound target mRNAs. *RNA* **14,** 2580–2596 (2008).
313. Azuma-Mukai, A. *et al.* Characterization of endogenous human Argonautes and their miRNA partners in RNA silencing. *Proc. Natl. Acad. Sci. U.S.A.*

105, 7964–7969 (2008).
314. Meister, G. Argonaute proteins: functional insights and emerging roles. *Nat. Rev. Genet.* **14,** 447–459 (2013).
315. Peters, L. & Meister, G. Argonaute proteins: mediators of RNA silencing. *Molecular Cell* **26,** 611–623 (2007).
316. O'Carroll, D. *et al.* A Slicer-independent role for Argonaute 2 in hematopoiesis and the microRNA pathway. *Genes & Development* **21,** 1999–2004 (2007).
317. Pfaff, J. & Meister, G. Argonaute and GW182 proteins: an effective alliance in gene silencing. *Biochemical Society transactions* **41,** 855–860 (2013).
318. Lingel, A., Simon, B., Izaurralde, E. & Sattler, M. Structure and nucleic-acid binding of the Drosophila Argonaute 2 PAZ domain. *Nature* **426,** 465–469 (2003).
319. Yan, K. S. *et al.* Structure and conserved RNA binding of the PAZ domain. *Nature* **426,** 468–474 (2003).
320. Ma, J.-B., Ye, K. & Patel, D. J. Structural basis for overhang-specific small interfering RNA recognition by the PAZ domain. *Nature* **429,** 318–322 (2004).
321. Ma, J.-B. *et al.* Structural basis for 5'-end-specific recognition of guide RNA by the A. fulgidus Piwi protein. *Nature* **434,** 666–670 (2005).
322. Parker, J. S., Roe, S. M. & Barford, D. Structural insights into mRNA recognition from a PIWI domain-siRNA guide complex. *Nature* **434,** 663–666 (2005).
323. Jinek, M. & Doudna, J. A. A three-dimensional view of the molecular machinery of RNA interference. *Nature* **457,** 405–412 (2009).
324. Wang, Y. *et al.* Structure of an argonaute silencing complex with a seed-containing guide DNA and target RNA duplex. *Nature* **456,** 921–926 (2008).
325. Song, J.-J., Smith, S. K., Hannon, G. J. & Joshua-Tor, L. Crystal structure of Argonaute and its implications for RISC slicer activity. *Science* **305,** 1434–1437 (2004).
326. Yuan, Y.-R. *et al.* Crystal structure of A. aeolicus argonaute, a site-specific DNA-guided endoribonuclease, provides insights into RISC-mediated mRNA cleavage. *Molecular Cell* **19,** 405–419 (2005).
327. Frank, F., Sonenberg, N. & Nagar, B. Structural basis for 5'-nucleotide base-specific recognition of guide RNA by human AGO2. *Nature* **465,** 818–822 (2010).
328. Nakanishi, K., Weinberg, D. E., Bartel, D. P. & Patel, D. J. Structure of yeast Argonaute with guide RNA. *Nature* **486,** 368–374 (2012).
329. Hauptmann, J. *et al.* Turning catalytically inactive human Argonaute proteins into active slicer enzymes. *Nat Struct Mol Biol* **20,** 814–817 (2013).
330. Faehnle, C. R., Elkayam, E., Haase, A. D., Hannon, G. J. & Joshua-Tor, L. The making of a slicer: activation of human Argonaute-1. *Cell Rep* **3,** 1901–1909 (2013).
331. Pfaff, J. *et al.* Structural features of Argonaute-GW182 protein interactions. *Proc. Natl. Acad. Sci. U.S.A.* **110,** E3770–9 (2013).
332. Miyoshi, K., Okada, T. N., Siomi, H. & Siomi, M. C. Characterization of the miRNA-RISC loading complex and miRNA-RISC formed in the Drosophila miRNA pathway. *RNA* **15,** 1282–1291 (2009).
333. Till, S. *et al.* A conserved motif in Argonaute-interacting proteins mediates

functional interactions through the Argonaute PIWI domain. *Nat Struct Mol Biol* **14,** 897–903 (2007).
334. El-Shami, M. *et al.* Reiterated WG/GW motifs form functionally and evolutionarily conserved ARGONAUTE-binding platforms in RNAi-related components. *Genes & Development* **21,** 2539–2544 (2007).
335. Eulalio, A., Helms, S., Fritzsch, C., Fauser, M. & Izaurralde, E. A C-terminal silencing domain in GW182 is essential for miRNA function. *RNA* **15,** 1067–1077 (2009).
336. Chekulaeva, M., Filipowicz, W. & Parker, R. Multiple independent domains of dGW182 function in miRNA-mediated repression in Drosophila. *RNA* **15,** 794–803 (2009).
337. Lazzaretti, D., Tournier, I. & Izaurralde, E. The C-terminal domains of human TNRC6A, TNRC6B, and TNRC6C silence bound transcripts independently of Argonaute proteins. *RNA* **15,** 1059–1066 (2009).
338. Zipprich, J. T., Bhattacharyya, S., Mathys, H. & Filipowicz, W. Importance of the C-terminal domain of the human GW182 protein TNRC6C for translational repression. *RNA* **15,** 781–793 (2009).
339. Lian, S. L. *et al.* The C-terminal half of human Ago2 binds to multiple GW-rich regions of GW182 and requires GW182 to mediate silencing. *RNA* **15,** 804–813 (2009).
340. Takimoto, K., Wakiyama, M. & Yokoyama, S. Mammalian GW182 contains multiple Argonaute-binding sites and functions in microRNA-mediated translational repression. *RNA* **15,** 1078–1089 (2009).
341. Eystathioy, T. *et al.* A phosphorylated cytoplasmic autoantigen, GW182, associates with a unique population of human mRNAs within novel cytoplasmic speckles. *Mol. Biol. Cell* **13,** 1338–1351 (2002).
342. Sen, G. L. & Blau, H. M. Argonaute 2/RISC resides in sites of mammalian mRNA decay known as cytoplasmic bodies. *Nat. Cell Biol.* **7,** 633–636 (2005).
343. Eystathioy, T. *et al.* The GW182 protein colocalizes with mRNA degradation associated proteins hDcp1 and hLSm4 in cytoplasmic GW bodies. *RNA* **9,** 1171–1173 (2003).
344. Sheth, U. & Parker, R. Decapping and decay of messenger RNA occur in cytoplasmic processing bodies. *Science* **300,** 805–808 (2003).
345. Cougot, N., Babajko, S. & Séraphin, B. Cytoplasmic foci are sites of mRNA decay in human cells. *The Journal of Cell Biology* **165,** 31–40 (2004).
346. Eulalio, A., Tritschler, F. & Izaurralde, E. The GW182 protein family in animal cells: New insights into domains required for miRNA-mediated gene silencing. *RNA* **15,** 1433–1442 (2009).
347. Zhang, L. *et al.* Systematic identification of C. elegans miRISC proteins, miRNAs, and mRNA targets by their interactions with GW182 proteins AIN-1 and AIN-2. *Molecular Cell* **28,** 598–613 (2007).
348. Su, V. & Lau, A. F. Ubiquitin-like and ubiquitin-associated domain proteins: significance in proteasomal degradation. *Cell. Mol. Life Sci.* **66,** 2819–2833 (2009).
349. Cléry, A., Blatter, M. & Allain, F. H.-T. RNA recognition motifs: boring? Not quite. *Curr. Opin. Struct. Biol.* **18,** 290–298 (2008).
350. Fabian, M. R., Sonenberg, N. & Filipowicz, W. Regulation of mRNA Translation and Stability by microRNAs. *Annu. Rev. Biochem.* **79,** 351–379 (2010).
351. Eulalio, A. *et al.* The RRM domain in GW182 proteins contributes to

miRNA-mediated gene silencing. *Nucleic Acids Research* **37,** 2974–2983 (2009).
352. Mishima, Y. *et al.* Translational inhibition by deadenylation-independent mechanisms is central to microRNA-mediated silencing in zebrafish. *Proc. Natl. Acad. Sci. U.S.A.* **109,** 1104–1109 (2012).
353. Huntzinger, E. *et al.* The interactions of GW182 proteins with PABP and deadenylases are required for both translational repression and degradation of miRNA targets. *Nucleic Acids Research* **41,** 978–994 (2013).
354. Braun, J. E., Huntzinger, E. & Izaurralde, E. in *link.springer.com* **768,** 147–163 (Springer New York, 2012).
355. Chekulaeva, M., Parker, R. & Filipowicz, W. The GW/WG repeats of Drosophila GW182 function as effector motifs for miRNA-mediated repression. *Nucleic Acids Research* **38,** 6673–6683 (2010).
356. Chen, Y. *et al.* A DDX6-CNOT1 Complex and W-Binding Pockets in CNOT9 Reveal Direct Links between miRNA Target Recognition and Silencing. *Molecular Cell*
357. Kuzuoğlu-Öztürk, D., Huntzinger, E., Schmidt, S. & Izaurralde, E. The Caenorhabditis elegans GW182 protein AIN-1 interacts with PAB-1 and subunits of the PAN2-PAN3 and CCR4-NOT deadenylase complexes. *Nucleic Acids Research* **40,** 5651–5665 (2012).
358. Bhandari, D., Raisch, T., Weichenrieder, O., Jonas, S. & Izaurralde, E. Structural basis for the Nanos-mediated recruitment of the CCR4–NOT complex and translational repression. *Genes & Development* **28,** 888–901 (2014).
359. Raisch, T. *et al.* Distinct modes of recruitment of the CCR4-NOT complex by Drosophila and vertebrate Nanos. *EMBO J* **35,** 974–990 (2016).
360. Huntzinger, E., Braun, J. E., Heimstädt, S., Zekri, L. & Izaurralde, E. Two PABPC1-binding sites in GW182 proteins promote miRNA-mediated gene silencing. *EMBO J* **29,** 4146–4160 (2010).
361. Fabian, M. R. *et al.* Mammalian miRNA RISC recruits CAF1 and PABP to affect PABP-dependent deadenylation. *Molecular Cell* **35,** 868–880 (2009).
362. Zekri, L., Huntzinger, E., Heimstädt, S. & Izaurralde, E. The silencing domain of GW182 interacts with PABPC1 to promote translational repression and degradation of microRNA targets and is required for target release. *Mol. Cell. Biol.* **29,** 6220–6231 (2009).
363. Tarun, S. Z. & Sachs, A. B. Association of the yeast poly(A) tail binding protein with translation initiation factor eIF-4G. *EMBO J* **15,** 7168–7177 (1996).
364. Le, H. *et al.* Translation initiation factors eIF-iso4G and eIF-4B interact with the poly(A)-binding protein and increase its RNA binding activity. *Journal of Biological Chemistry* **272,** 16247–16255 (1997).
365. Imataka, H., Gradi, A. & Sonenberg, N. A newly identified N-terminal amino acid sequence of human eIF4G binds poly(A)-binding protein and functions in poly(A)-dependent translation. *EMBO J* **17,** 7480–7489 (1998).
366. Wakiyama, M., Imataka, H. & Sonenberg, N. Interaction of eIF4G with poly(A)-binding protein stimulates translation and is critical for Xenopus oocyte maturation. *Curr. Biol.* **10,** 1147–1150 (2000).
367. Moretti, F., Kaiser, C., Zdanowicz-Specht, A. & Hentze, M. W. PABP and the poly(A) tail augment microRNA repression by facilitated miRISC binding. *Nat Struct Mol Biol* **19,** 603–608 (2012).

368. Beilharz, T. H. *et al.* microRNA-mediated messenger RNA deadenylation contributes to translational repression in mammalian cells. *PLoS ONE* **4,** e6783 (2009).
369. Walters, R. W., Bradrick, S. S. & Gromeier, M. Poly(A)-binding protein modulates mRNA susceptibility to cap-dependent miRNA-mediated repression. *RNA* **16,** 239–250 (2010).
370. Zekri, L., Kuzuoğlu-Öztürk, D. & Izaurralde, E. GW182 proteins cause PABP dissociation from silenced miRNA targets in the absence of deadenylation. *EMBO J* **32,** 1052–1065 (2013).
371. Ricci, E. P. *et al.* miRNA repression of translation in vitro takes place during 43S ribosomal scanning. *Nucleic Acids Research* **41,** 586–598 (2013).
372. Fukaya, T. & Tomari, Y. PABP is not essential for microRNA-mediated translational repression and deadenylation in vitro. *EMBO J* **30,** 4998–5009 (2011).
373. Wu, L., Fan, J. & Belasco, J. G. MicroRNAs direct rapid deadenylation of mRNA. *Proc. Natl. Acad. Sci. U.S.A.* **103,** 4034–4039 (2006).
374. Eulalio, A., Huntzinger, E. & Izaurralde, E. GW182 interaction with Argonaute is essential for miRNA-mediated translational repression and mRNA decay. *Nat Struct Mol Biol* **15,** 346–353 (2008).
375. Wahle, E. & Winkler, G. S. RNA decay machines: deadenylation by the Ccr4-not and Pan2-Pan3 complexes. *Biochim. Biophys. Acta* **1829,** 561–570 (2013).
376. Yamashita, A. *et al.* Concerted action of poly(A) nucleases and decapping enzyme in mammalian mRNA turnover. *Nat Struct Mol Biol* **12,** 1054–1063 (2005).
377. Chen, C.-Y. A., Zheng, D., Xia, Z. & Shyu, A.-B. Ago-TNRC6 triggers microRNA-mediated decay by promoting two deadenylation steps. *Nat Struct Mol Biol* **16,** 1160–1166 (2009).
378. Eulalio, A. *et al.* Deadenylation is a widespread effect of miRNA regulation. *RNA* **15,** 21–32 (2009).
379. Brown, C. E. & Sachs, A. B. Poly(A) tail length control in Saccharomyces cerevisiae occurs by message-specific deadenylation. *Mol. Cell. Biol.* **18,** 6548–6559 (1998).
380. Tucker, M. *et al.* The transcription factor associated Ccr4 and Caf1 proteins are components of the major cytoplasmic mRNA deadenylase in Saccharomyces cerevisiae. *Cell* **104,** 377–386 (2001).
381. Bönisch, C., Temme, C., Moritz, B. & Wahle, E. Degradation of hsp70 and other mRNAs in Drosophila via the 5‘ 3’ pathway and its regulation by heat shock. *Journal of Biological Chemistry* **282,** 21818–21828 (2007).
382. Collart, M. A. & Panasenko, O. O. The Ccr4–Not complex. *Gene* **492,** 42–53 (2012).
383. Temme, C., Simonelig, M. & Wahle, E. Deadenylation of mRNA by the CCR4-NOT complex in Drosophila: molecular and developmental aspects. *Front Genet* **5,** 143 (2014).
384. Siddiqui, N. *et al.* Poly(A) nuclease interacts with the C-terminal domain of polyadenylate-binding protein domain from poly(A)-binding protein. *Journal of Biological Chemistry* **282,** 25067–25075 (2007).
385. Presnyak, V. & Coller, J. The DHH1/RCKp54 family of helicases: an ancient family of proteins that promote translational silencing. *Biochim. Biophys. Acta* **1829,** 817–823 (2013).

386. Bhaskar, V. *et al.* Structure and RNA-binding properties of the Not1-Not2-Not5 module of the yeast Ccr4-Not complex. *Nat Struct Mol Biol* **20,** 1281–1288 (2013).
387. Boland, A. *et al.* Structure and assembly of the NOT module of the human CCR4-NOT complex. *Nat Struct Mol Biol* **20,** 1289–1297 (2013).
388. Chicoine, J. *et al.* Bicaudal-C recruits CCR4-NOT deadenylase to target mRNAs and regulates oogenesis, cytoskeletal organization, and its own expression. *Dev. Cell* **13,** 691–704 (2007).
389. Suzuki, A., Saba, R., Miyoshi, K., Morita, Y. & Saga, Y. Interaction between NANOS2 and the CCR4-NOT deadenylation complex is essential for male germ cell development in mouse. *PLoS ONE* **7,** e33558 (2012).
390. Piao, X., Zhang, X., Wu, L. & Belasco, J. G. CCR4-NOT deadenylates mRNA associated with RNA-induced silencing complexes in human cells. *Mol. Cell. Biol.* **30,** 1486–1494 (2010).
391. Cooke, A., Prigge, A. & Wickens, M. Translational repression by deadenylases. *Journal of Biological Chemistry* **285,** 28506–28513 (2010).
392. Béthune, J., Artus-Revel, C. G. & Filipowicz, W. Kinetic analysis reveals successive steps leading to miRNA-mediated silencing in mammalian cells. *EMBO Rep.* **13,** 716–723 (2012).
393. Bawankar, P., Loh, B., Wohlbold, L., Schmidt, S. & Izaurralde, E. NOT10 and C2orf29/NOT11 form a conserved module of the CCR4-NOT complex that docks onto the NOT1 N-terminal domain. *RNA Biol* **10,** 228–244 (2013).
394. Bartlam, M. & Yamamoto, T. The structural basis for deadenylation by the CCR4-NOT complex. *Protein Cell* **1,** 443–452 (2010).
395. Behm-Ansmant, I., Rehwinkel, J. & Izaurralde, E. MicroRNAs silence gene expression by repressing protein expression and/or by promoting mRNA decay. *Cold Spring Harb. Symp. Quant. Biol.* **71,** 523–530 (2006).
396. Jeske, M., Meyer, S., Temme, C., Freudenreich, D. & Wahle, E. Rapid ATP-dependent deadenylation of nanos mRNA in a cell-free system from Drosophila embryos. *Journal of Biological Chemistry* **281,** 25124–25133 (2006).
397. Lau, N.-C. *et al.* Human Ccr4-Not complexes contain variable deadenylase subunits. *Biochem. J.* **422,** 443–453 (2009).
398. Shirai, Y.-T., Suzuki, T., Morita, M., Takahashi, A. & Yamamoto, T. Multifunctional roles of the mammalian CCR4-NOT complex in physiological phenomena. *Front Genet* **5,** 286 (2014).
399. Ohrt, T., Muetze, J., Svoboda, P. & Schwille, P. Intracellular localization and routing of miRNA and RNAi pathway components. *Curr Top Med Chem* **12,** 79–88 (2012).
400. Robb, G. B., Brown, K. M., Khurana, J. & Rana, T. M. Specific and potent RNAi in the nucleus of human cells. *Nat Struct Mol Biol* **12,** 133–137 (2005).
401. Rüdel, S., Flatley, A., Weinmann, L., Kremmer, E. & Meister, G. A multifunctional human Argonaute2-specific monoclonal antibody. *RNA* **14,** 1244–1253 (2008).
402. Gagnon, K. T., Li, L., Chu, Y., Janowski, B. A. & Corey, D. R. RNAi factors are present and active in human cell nuclei. *Cell Rep* **6,** 211–221 (2014).
403. Nishi, K., Nishi, A., Nagasawa, T. & Ui-Tei, K. Human TNRC6A is an Argonaute-navigator protein for microRNA-mediated gene silencing in the nucleus. *RNA* **19,** 17–35 (2012).

404. Schraivogel, D. *et al.* Importin-β facilitates nuclear import of human GW proteins and balances cytoplasmic gene silencing protein levels. *Nucleic Acids Research* (2015). doi:10.1093/nar/gkv705
405. Eulalio, A., Behm-Ansmant, I. & Izaurralde, E. P bodies: at the crossroads of post-transcriptional pathways. *Nat Rev Mol Cell Biol* **8,** 9–22 (2007).
406. Parker, R. & Sheth, U. P bodies and the control of mRNA translation and degradation. *Molecular Cell* **25,** 635–646 (2007).
407. Shyu, A.-B., Wilkinson, M. F. & van Hoof, A. Messenger RNA regulation: to translate or to degrade. *EMBO J* **27,** 471–481 (2008).
408. Eulalio, A., Huntzinger, E. & Izaurralde, E. Getting to the root of miRNA-mediated gene silencing. *Cell* **132,** 9–14 (2008).
409. Andrei, M. A. *et al.* A role for eIF4E and eIF4E-transporter in targeting mRNPs to mammalian processing bodies. *RNA* **11,** 717–727 (2005).
410. Ferraiuolo, M. A. *et al.* A role for the eIF4E-binding protein 4E-T in P-body formation and mRNA decay. *The Journal of Cell Biology* **170,** 913–924 (2005).
411. Teixeira, D., Sheth, U., Valencia-Sanchez, M. A., Brengues, M. & Parker, R. Processing bodies require RNA for assembly and contain nontranslating mRNAs. *RNA* **11,** 371–382 (2005).
412. Pillai, R. S. *et al.* Inhibition of translational initiation by Let-7 MicroRNA in human cells. *Science* **309,** 1573–1576 (2005).
413. Eulalio, A., Behm-Ansmant, I., Schweizer, D. & Izaurralde, E. P-body formation is a consequence, not the cause, of RNA-mediated gene silencing. *Mol. Cell. Biol.* **27,** 3970–3981 (2007).
414. Yang, Z. *et al.* GW182 is critical for the stability of GW bodies expressed during the cell cycle and cell proliferation. *J. Cell. Sci.* **117,** 5567–5578 (2004).
415. Leung, A. K. L., Calabrese, J. M. & Sharp, P. A. Quantitative analysis of Argonaute protein reveals microRNA-dependent localization to stress granules. *Proc. Natl. Acad. Sci. U.S.A.* **103,** 18125–18130 (2006).
416. Gallois-Montbrun, S. *et al.* Antiviral protein APOBEC3G localizes to ribonucleoprotein complexes found in P bodies and stress granules. *J. Virol.* **81,** 2165–2178 (2007).
417. Pare, J. M. *et al.* Hsp90 regulates the function of argonaute 2 and its recruitment to stress granules and P-bodies. *Mol. Biol. Cell* **20,** 3273–3284 (2009).
418. Kedersha, N. L., Gupta, M., Li, W., Miller, I. & Anderson, P. RNA-binding proteins TIA-1 and TIAR link the phosphorylation of eIF-2 alpha to the assembly of mammalian stress granules. *The Journal of Cell Biology* **147,** 1431–1442 (1999).
419. Kedersha, N. *et al.* Dynamic shuttling of TIA-1 accompanies the recruitment of mRNA to mammalian stress granules. *The Journal of Cell Biology* **151,** 1257–1268 (2000).
420. Kedersha, N. *et al.* Evidence that ternary complex (eIF2-GTP-tRNA(i)(Met))-deficient preinitiation complexes are core constituents of mammalian stress granules. *Mol. Biol. Cell* **13,** 195–210 (2002).
421. Wilczynska, A., Aigueperse, C., Kress, M., Dautry, F. & Weil, D. The translational regulator CPEB1 provides a link between dcp1 bodies and stress granules. *J. Cell. Sci.* **118,** 981–992 (2005).
422. Kedersha, N. *et al.* Stress granules and processing bodies are dynamically linked sites of mRNP remodeling. *The Journal of Cell Biology* **169,** 871–

884 (2005).
423. Souquere, S. *et al.* Unravelling the ultrastructure of stress granules and associated P-bodies in human cells. *J. Cell. Sci.* **122,** 3619–3626 (2009).
424. Lee, Y. S. *et al.* Silencing by small RNAs is linked to endosomal trafficking. *Nat. Cell Biol.* **11,** 1150–1156 (2009).
425. Gibbings, D. J., Ciaudo, C., Erhardt, M. & Voinnet, O. Multivesicular bodies associate with components of miRNA effector complexes and modulate miRNA activity. *Nat. Cell Biol.* **11,** 1143–1149 (2009).
426. Cikaluk, D. E. *et al.* GERp95, a membrane-associated protein that belongs to a family of proteins involved in stem cell differentiation. *Mol. Biol. Cell* **10,** 3357–3372 (1999).
427. Wu, P.-H., Isaji, M. & Carthew, R. W. Functionally diverse microRNA effector complexes are regulated by extracellular signaling. *Molecular Cell* **52,** 113–123 (2013).
428. Li, S. *et al.* MicroRNAs inhibit the translation of target mRNAs on the endoplasmic reticulum in Arabidopsis. *Cell* **153,** 562–574 (2013).
429. Stalder, L. *et al.* The rough endoplasmatic reticulum is a central nucleation site of siRNA-mediated RNA silencing. *EMBO J* **32,** 1115–1127 (2013).
430. Antic, S., Wolfinger, M. T., Skucha, A., Hosiner, S. & Dorner, S. General and MicroRNA-Mediated mRNA Degradation Occurs on Ribosome Complexes in Drosophila Cells. *Mol. Cell. Biol.* **35,** 2309–2320 (2015).
431. Kim, D. H., Villeneuve, L. M., Morris, K. V. & Rossi, J. J. Argonaute-1 directs siRNA-mediated transcriptional gene silencing in human cells. *Nat Struct Mol Biol* **13,** 793–797 (2006).
432. Janowski, B. A. *et al.* Involvement of AGO1 and AGO2 in mammalian transcriptional silencing. *Nat Struct Mol Biol* **13,** 787–792 (2006).
433. Weinmann, L. *et al.* Importin 8 is a gene silencing factor that targets argonaute proteins to distinct mRNAs. *Cell* **136,** 496–507 (2009).
434. Sonenberg, N. & Hinnebusch, A. G. Regulation of translation initiation in eukaryotes: mechanisms and biological targets. *Cell* **136,** 731–745 (2009).
435. Gingras, A. C., Raught, B. & Sonenberg, N. eIF4 initiation factors: effectors of mRNA recruitment to ribosomes and regulators of translation. *Annu. Rev. Biochem.* **68,** 913–963 (1999).
436. Jackson, R. J., Hellen, C. U. T. & Pestova, T. V. The mechanism of eukaryotic translation initiation and principles of its regulation. *Nat Rev Mol Cell Biol* **11,** 113–127 (2010).
437. Hinnebusch, A. G. The scanning mechanism of eukaryotic translation initiation. *Annu. Rev. Biochem.* **83,** 779–812 (2014).
438. Dever, T. E. & Green, R. The elongation, termination, and recycling phases of translation in eukaryotes. *Cold Spring Harb Perspect Biol* **4,** a013706 (2012).
439. Nierhaus, K. H. The allosteric three-site model for the ribosomal elongation cycle: features and future. *Biochemistry* **29,** 4997–5008 (1990).
440. Uemura, S. *et al.* Real-time tRNA transit on single translating ribosomes at codon resolution. *Nature* **464,** 1012–1017 (2010).
441. Chen, C. *et al.* Allosteric vs. spontaneous exit-site (E-site) tRNA dissociation early in protein synthesis. *Proc. Natl. Acad. Sci. U.S.A.* **108,** 16980–16985 (2011).
442. Stansfield, I. *et al.* The products of the SUP45 (eRF1) and SUP35 genes interact to mediate translation termination in Saccharomyces cerevisiae. *EMBO J* **14,** 4365–4373 (1995).

443. Zhouravleva, G. *et al.* Termination of translation in eukaryotes is governed by two interacting polypeptide chain release factors, eRF1 and eRF3. *EMBO J* **14,** 4065–4072 (1995).
444. Kozak, M. Selection of initiation sites by eucaryotic ribosomes: effect of inserting AUG triplets upstream from the coding sequence for preproinsulin. *Nucleic Acids Research* **12,** 3873–3893 (1984).
445. Kessler, S. H. & Sachs, A. B. RNA recognition motif 2 of yeast Pab1p is required for its functional interaction with eukaryotic translation initiation factor 4G. *Mol. Cell. Biol.* **18,** 51–57 (1998).
446. Gray, N. K., Coller, J. M., Dickson, K. S. & Wickens, M. Multiple portions of poly(A)-binding protein stimulate translation in vivo. *EMBO J* **19,** 4723–4733 (2000).
447. Cakmakci, N. G., Lerner, R. S., Wagner, E. J., Zheng, L. & Marzluff, W. F. SLIP1, a factor required for activation of histone mRNA translation by the stem-loop binding protein. *Mol. Cell. Biol.* **28,** 1182–1194 (2008).
448. Pestova, T. V., Hellen, C. U. & Shatsky, I. N. Canonical eukaryotic initiation factors determine initiation of translation by internal ribosomal entry. *Mol. Cell. Biol.* **16,** 6859–6869 (1996).
449. Pestova, T. V., Shatsky, I. N. & Hellen, C. U. Functional dissection of eukaryotic initiation factor 4F: the 4A subunit and the central domain of the 4G subunit are sufficient to mediate internal entry of 43S preinitiation complexes. *Mol. Cell. Biol.* **16,** 6870–6878 (1996).
450. de Breyne, S., Yu, Y., Unbehaun, A., Pestova, T. V. & Hellen, C. U. T. Direct functional interaction of initiation factor eIF4G with type 1 internal ribosomal entry sites. *Proc. Natl. Acad. Sci. U.S.A.* **106,** 9197–9202 (2009).
451. Pestova, T. V., Shatsky, I. N., Fletcher, S. P., Jackson, R. J. & Hellen, C. U. A prokaryotic-like mode of cytoplasmic eukaryotic ribosome binding to the initiation codon during internal translation initiation of hepatitis C and classical swine fever virus RNAs. *Genes & Development* **12,** 67–83 (1998).
452. Siridechadilok, B., Fraser, C. S., Hall, R. J., Doudna, J. A. & Nogales, E. Structural roles for human translation factor eIF3 in initiation of protein synthesis. *Science* **310,** 1513–1515 (2005).
453. Schüler, M. *et al.* Structure of the ribosome-bound cricket paralysis virus IRES RNA. *Nat Struct Mol Biol* **13,** 1092–1096 (2006).
454. Wilson, J. E., Pestova, T. V., Hellen, C. U. & Sarnow, P. Initiation of protein synthesis from the A site of the ribosome. *Cell* **102,** 511–520 (2000).
455. Baranick, B. T. *et al.* Splicing mediates the activity of four putative cellular internal ribosome entry sites. *Proc. Natl. Acad. Sci. U.S.A.* **105,** 4733–4738 (2008).
456. Jackson, R. J. Alternative mechanisms of initiating translation of mammalian mRNAs. *Biochemical Society transactions* **33,** 1231–1241 (2005).
457. Olsen, P. H. & Ambros, V. The lin-4 regulatory RNA controls developmental timing in Caenorhabditis elegans by blocking LIN-14 protein synthesis after the initiation of translation. *Dev. Biol.* **216,** 671–680 (1999).
458. Seggerson, K., Tang, L. & Moss, E. G. Two genetic circuits repress the Caenorhabditis elegans heterochronic gene lin-28 after translation initiation. *Dev. Biol.* **243,** 215–225 (2002).
459. Maroney, P. A., Yu, Y., Fisher, J. & Nilsen, T. W. Evidence that microRNAs are associated with translating messenger RNAs in human cells. *Nat Struct*

Mol Biol **13,** 1102–1107 (2006).
460. Nottrott, S., Simard, M. J. & Richter, J. D. Human let-7a miRNA blocks protein production on actively translating polyribosomes. *Nat Struct Mol Biol* **13,** 1108–1114 (2006).
461. Petersen, C. P., Bordeleau, M.-E., Pelletier, J. & Sharp, P. A. Short RNAs repress translation after initiation in mammalian cells. *Molecular Cell* **21,** 533–542 (2006).
462. Kim, J. *et al.* Identification of many microRNAs that copurify with polyribosomes in mammalian neurons. *Proc. Natl. Acad. Sci. U.S.A.* **101,** 360–365 (2004).
463. Nelson, P. T., Hatzigeorgiou, A. G. & Mourelatos, Z. miRNP:mRNA association in polyribosomes in a human neuronal cell line. *RNA* **10,** 387–394 (2004).
464. Humphreys, D. T., Westman, B. J., Martin, D. I. K. & Preiss, T. MicroRNAs control translation initiation by inhibiting eukaryotic initiation factor 4E/cap and poly(A) tail function. *Proc. Natl. Acad. Sci. U.S.A.* **102,** 16961–16966 (2005).
465. Huang, J. *et al.* Derepression of microRNA-mediated protein translation inhibition by apolipoprotein B mRNA-editing enzyme catalytic polypeptide-like 3G (APOBEC3G) and its family members. *Journal of Biological Chemistry* **282,** 33632–33640 (2007).
466. Clancy, J. L. *et al.* mRNA isoform diversity can obscure detection of miRNA-mediated control of translation. *RNA* **17,** 1025–1031 (2011).
467. Ding, X. C. & Grosshans, H. Repression of C. elegans microRNA targets at the initiation level of translation requires GW182 proteins. *EMBO J* **28,** 213–222 (2009).
468. Karaa, Z. S. *et al.* The VEGF IRESes are differentially susceptible to translation inhibition by miR-16. *RNA* **15,** 249–254 (2009).
469. Thermann, R. & Hentze, M. W. Drosophila miR2 induces pseudo-polysomes and inhibits translation initiation. *Nature* **447,** 875–878 (2007).
470. Mathonnet, G. *et al.* MicroRNA inhibition of translation initiation in vitro by targeting the cap-binding complex eIF4F. *Science* **317,** 1764–1767 (2007).
471. Wang, B., Love, T. M., Call, M. E., Doench, J. G. & Novina, C. D. Recapitulation of short RNA-directed translational gene silencing in vitro. *Molecular Cell* **22,** 553–560 (2006).
472. Wakiyama, M., Takimoto, K., Ohara, O. & Yokoyama, S. Let-7 microRNA-mediated mRNA deadenylation and translational repression in a mammalian cell-free system. *Genes & Development* **21,** 1857–1862 (2007).
473. Iwasaki, S., Kawamata, T. & Tomari, Y. Drosophila argonaute1 and argonaute2 employ distinct mechanisms for translational repression. *Molecular Cell* **34,** 58–67 (2009).
474. Zdanowicz, A. *et al.* Drosophila miR2 primarily targets the m7GpppN cap structure for translational repression. *Molecular Cell* **35,** 881–888 (2009).
475. Kamenska, A. *et al.* Human 4E-T represses translation of bound mRNAs and enhances microRNA-mediated silencing. *Nucleic Acids Research* **42,** 3298–3313 (2014).
476. Nishimura, T. *et al.* The eIF4E-Binding Protein 4E-T Is a Component of the mRNA Decay Machinery that Bridges the 5‘ and 3’ Termini of Target mRNAs. *Cell Rep* **11,** 1425–1436 (2015).
477. Waghray, S., Williams, C., Coon, J. J. & Wickens, M. Xenopus CAF1

requires NOT1-mediated interaction with 4E-T to repress translation in vivo. *RNA* **21,** 1335–1345 (2015).
478. Chu, C.-Y. & Rana, T. M. Translation repression in human cells by microRNA-induced gene silencing requires RCK/p54. *PLoS Biol.* **4,** e210 (2006).
479. Eulalio, A. *et al.* Target-specific requirements for enhancers of decapping in miRNA-mediated gene silencing. *Genes & Development* **21,** 2558–2570 (2007).
480. Nishihara, T., Zekri, L., Braun, J. E. & Izaurralde, E. miRISC recruits decapping factors to miRNA targets to enhance their degradation. *Nucleic Acids Research* **41,** 8692–8705 (2013).
481. Meijer, H. A. *et al.* Translational repression and eIF4A2 activity are critical for microRNA-mediated gene regulation. *Science* **340,** 82–85 (2013).
482. Galicia-Vázquez, G., Chu, J. & Pelletier, J. eIF4AII is dispensable for miRNA-mediated gene silencing. *RNA* **21,** 1826–1833 (2015).
483. Fukaya, T., Iwakawa, H.-O. & Tomari, Y. MicroRNAs block assembly of eIF4F translation initiation complex in Drosophila. *Molecular Cell* **56,** 67–78 (2014).
484. Fukao, A. *et al.* MicroRNAs trigger dissociation of eIF4AI and eIF4AII from target mRNAs in humans. *Molecular Cell* **56,** 79–89 (2014).
485. Fukaya, T. & Tomari, Y. MicroRNAs mediate gene silencing via multiple different pathways in drosophila. *Molecular Cell* **48,** 825–836 (2012).
486. Kuzuoğlu-Öztürk, D. *et al.* miRISC and the CCR4-NOT complex silence mRNA targets independently of 43S ribosomal scanning. *EMBO J* **35,** 1186–1203 (2016).
487. Elfakess, R. *et al.* Unique translation initiation of mRNAs-containing TISU element. *Nucleic Acids Research* **39,** 7598–7609 (2011).
488. Su, H. *et al.* Mammalian hyperplastic discs homolog EDD regulates miRNA-mediated gene silencing. *Molecular Cell* **43,** 97–109 (2011).
489. Lim, L. P. *et al.* Microarray analysis shows that some microRNAs downregulate large numbers of target mRNAs. *Nature* **433,** 769–773 (2005).
490. Krützfeldt, J. *et al.* Silencing of microRNAs in vivo with 'antagomirs'. *Nature* **438,** 685–689 (2005).
491. Bagga, S. *et al.* Regulation by let-7 and lin-4 miRNAs results in target mRNA degradation. *Cell* **122,** 553–563 (2005).
492. Wu, L. & Belasco, J. G. Micro-RNA regulation of the mammalian lin-28 gene during neuronal differentiation of embryonal carcinoma cells. *Mol. Cell. Biol.* **25,** 9198–9208 (2005).
493. Rehwinkel, J. *et al.* Genome-wide analysis of mRNAs regulated by Drosha and Argonaute proteins in Drosophila melanogaster. *Mol. Cell. Biol.* **26,** 2965–2975 (2006).
494. Schmitter, D. *et al.* Effects of Dicer and Argonaute down-regulation on mRNA levels in human HEK293 cells. *Nucleic Acids Research* **34,** 4801–4815 (2006).
495. Garneau, N. L., Wilusz, J. & Wilusz, C. J. The highways and byways of mRNA decay. *Nat Rev Mol Cell Biol* **8,** 113–126 (2007).
496. Liu, H., Rodgers, N. D., Jiao, X. & Kiledjian, M. The scavenger mRNA decapping enzyme DcpS is a member of the HIT family of pyrophosphatases. *EMBO J* **21,** 4699–4708 (2002).
497. Lim, J. *et al.* Uridylation by TUT4 and TUT7 marks mRNA for degradation.

Cell **159,** 1365–1376 (2014).
498. Semotok, J. L. *et al.* Smaug recruits the CCR4/POP2/NOT deadenylase complex to trigger maternal transcript localization in the early Drosophila embryo. *Curr. Biol.* **15,** 284–294 (2005).
499. Goldstrohm, A. C., Hook, B. A., Seay, D. J. & Wickens, M. PUF proteins bind Pop2p to regulate messenger RNAs. *Nat Struct Mol Biol* **13,** 533–539 (2006).
500. Igreja, C. & Izaurralde, E. CUP promotes deadenylation and inhibits decapping of mRNA targets. *Genes & Development* **25,** 1955–1967 (2011).
501. Van Etten, J. *et al.* Human Pumilio proteins recruit multiple deadenylases to efficiently repress messenger RNAs. *J. Biol. Chem.* **287,** 36370–36383 (2012).
502. Fabian, M. R. *et al.* Structural basis for the recruitment of the human CCR4-NOT deadenylase complex by tristetraprolin. *Nat Struct Mol Biol* **20,** 735–739 (2013).
503. Leppek, K. *et al.* Roquin promotes constitutive mRNA decay via a conserved class of stem-loop recognition motifs. *Cell* **153,** 869–881 (2013).
504. Djuranovic, S., Nahvi, A. & Green, R. miRNA-mediated gene silencing by translational repression followed by mRNA deadenylation and decay. *Science* **336,** 237–240 (2012).
505. Newman, M. A. & Hammond, S. M. Emerging paradigms of regulated microRNA processing. *Genes & Development* **24,** 1086–1092 (2010).
506. Zeng, Y., Sankala, H., Zhang, X. & Graves, P. R. Phosphorylation of Argonaute 2 at serine-387 facilitates its localization to processing bodies. *Biochem. J.* **413,** 429–436 (2008).
507. Horman, S. R. *et al.* Akt-mediated phosphorylation of argonaute 2 downregulates cleavage and upregulates translational repression of MicroRNA targets. *Molecular Cell* **50,** 356–367 (2013).
508. Rüdel, S. *et al.* Phosphorylation of human Argonaute proteins affects small RNA binding. *Nucleic Acids Research* **39,** 2330–2343 (2011).
509. Shen, J. *et al.* EGFR modulates microRNA maturation in response to hypoxia through phosphorylation of AGO2. *Nature* **497,** 383–387 (2013).
510. Wu, C. *et al.* Hypoxia potentiates microRNA-mediated gene silencing through posttranslational modification of Argonaute2. *Mol. Cell. Biol.* **31,** 4760–4774 (2011).
511. Qi, H. H. *et al.* Prolyl 4-hydroxylation regulates Argonaute 2 stability. *Nature* **455,** 421–424 (2008).
512. Sahin, U., Lapaquette, P., Andrieux, A., Faure, G. & Dejean, A. Sumoylation of human argonaute 2 at lysine-402 regulates its stability. *PLoS ONE* **9,** e102957 (2014).
513. Leung, A. K. L. *et al.* Poly(ADP-ribose) regulates stress responses and microRNA activity in the cytoplasm. *Molecular Cell* **42,** 489–499 (2011).
514. Bronevetsky, Y. *et al.* T cell activation induces proteasomal degradation of Argonaute and rapid remodeling of the microRNA repertoire. *J. Exp. Med.* **210,** 417–432 (2013).
515. Smibert, P., Yang, J.-S., Azzam, G., Liu, J.-L. & Lai, E. C. Homeostatic control of Argonaute stability by microRNA availability. *Nat Struct Mol Biol* **20,** 789–795 (2013).
516. Martinez, N. J. & Gregory, R. I. Argonaute2 expression is post-transcriptionally coupled to microRNA abundance. *RNA* **19,** 605–612

(2013).
517. Iakoucheva, L. M. *et al.* The importance of intrinsic disorder for protein phosphorylation. *Nucleic Acids Research* **32,** 1037–1049 (2004).
518. Huang, K.-L., Chadee, A. B., Chen, C.-Y. A., Zhang, Y. & Shyu, A.-B. Phosphorylation at intrinsically disordered regions of PAM2 motif-containing proteins modulates their interactions with PABPC1 and influences mRNA fate. *RNA* **19,** 295–305 (2013).
519. Lau, N.-C. *et al.* Phosphorylation of Not4p functions parallel to BUR2 to regulate resistance to cellular stresses in Saccharomyces cerevisiae. *PLoS ONE* **5,** e9864 (2010).
520. Brook, M. *et al.* The multifunctional poly(A)-binding protein (PABP) 1 is subject to extensive dynamic post-translational modification, which molecular modelling suggests plays an important role in co-ordinating its activities. *Biochem. J.* **441,** 803–812 (2012).
521. Le, H., Browning, K. S. & Gallie, D. R. The phosphorylation state of poly(A)-binding protein specifies its binding to poly(A) RNA and its interaction with eukaryotic initiation factor (eIF) 4F, eIFiso4F, and eIF4B. *Journal of Biological Chemistry* **275,** 17452–17462 (2000).
522. Denli, A. M., Tops, B. B. J., Plasterk, R. H. A., Ketting, R. F. & Hannon, G. J. Processing of primary microRNAs by the Microprocessor complex. *Nature* **432,** 231–235 (2004).
523. Gregory, R. I. *et al.* The Microprocessor complex mediates the genesis of microRNAs. *Nature* **432,** 235–240 (2004).
524. Han, J. *et al.* The Drosha-DGCR8 complex in primary microRNA processing. *Genes & Development* **18,** 3016–3027 (2004).
525. Landthaler, M., Yalcin, A. & Tuschl, T. The human DiGeorge syndrome critical region gene 8 and Its D. melanogaster homolog are required for miRNA biogenesis. *Curr. Biol.* **14,** 2162–2167 (2004).
526. Han, J. *et al.* Posttranscriptional crossregulation between Drosha and DGCR8. *Cell* **136,** 75–84 (2009).
527. Yeom, K.-H., Lee, Y., Han, J., Suh, M. R. & Kim, V. N. Characterization of DGCR8/Pasha, the essential cofactor for Drosha in primary miRNA processing. *Nucleic Acids Research* **34,** 4622–4629 (2006).
528. Kadener, S. *et al.* Genome-wide identification of targets of the drosha-pasha/DGCR8 complex. *RNA* **15,** 537–545 (2009).
529. Tang, X., Li, M., Tucker, L. & Ramratnam, B. Glycogen synthase kinase 3 beta (GSK3β) phosphorylates the RNAase III enzyme Drosha at S300 and S302. *PLoS ONE* **6,** e20391 (2011).
530. Tang, X., Zhang, Y., Tucker, L. & Ramratnam, B. Phosphorylation of the RNase III enzyme Drosha at Serine300 or Serine302 is required for its nuclear localization. *Nucleic Acids Research* **38,** 6610–6619 (2010).
531. Tang, X. *et al.* Acetylation of drosha on the N-terminus inhibits its degradation by ubiquitination. *PLoS ONE* **8,** e72503 (2013).
532. Wada, T., Kikuchi, J. & Furukawa, Y. Histone deacetylase 1 enhances microRNA processing via deacetylation of DGCR8. *EMBO Rep.* **13,** 142–149 (2012).
533. Herbert, K. M., Pimienta, G., DeGregorio, S. J., Alexandrov, A. & Steitz, J. A. Phosphorylation of DGCR8 increases its intracellular stability and induces a progrowth miRNA profile. *Cell Rep* **5,** 1070–1081 (2013).
534. Cheng, T.-L. *et al.* MeCP2 suppresses nuclear microRNA processing and dendritic growth by regulating the DGCR8/Drosha complex. *Dev. Cell* **28,**

547–560 (2014).
535. Davis, B. N., Hilyard, A. C., Lagna, G. & Hata, A. SMAD proteins control DROSHA-mediated microRNA maturation. *Nature* **454,** 56–61 (2008).
536. Warner, D. R. *et al.* Functional interaction between Smad, CREB binding protein, and p68 RNA helicase. *Biochem. Biophys. Res. Commun.* **324,** 70–76 (2004).
537. Bates, G. J. *et al.* The DEAD box protein p68: a novel transcriptional coactivator of the p53 tumour suppressor. *EMBO J* **24,** 543–553 (2005).
538. Suzuki, H. I. *et al.* Modulation of microRNA processing by p53. *Nature* **460,** 529–533 (2009).
539. Yamagata, K. *et al.* Maturation of microRNA is hormonally regulated by a nuclear receptor. *Molecular Cell* **36,** 340–347 (2009).
540. Endoh, H. *et al.* Purification and identification of p68 RNA helicase acting as a transcriptional coactivator specific for the activation function 1 of human estrogen receptor alpha. *Mol. Cell. Biol.* **19,** 5363–5372 (1999).
541. Trabucchi, M. *et al.* The RNA-binding protein KSRP promotes the biogenesis of a subset of microRNAs. *Nature* **459,** 1010–1014 (2009).
542. Viswanathan, S. R. & Daley, G. Q. Lin28: A microRNA regulator with a macro role. *Cell* **140,** 445–449 (2010).
543. Hagan, J. P., Piskounova, E. & Gregory, R. I. Lin28 recruits the TUTase Zcchc11 to inhibit let-7 maturation in mouse embryonic stem cells. *Nat Struct Mol Biol* **16,** 1021–1025 (2009).
544. Heo, I. *et al.* TUT4 in concert with Lin28 suppresses microRNA biogenesis through pre-microRNA uridylation. *Cell* **138,** 696–708 (2009).
545. Lehrbach, N. J. *et al.* LIN-28 and the poly(U) polymerase PUP-2 regulate let-7 microRNA processing in Caenorhabditis elegans. *Nat Struct Mol Biol* **16,** 1016–1020 (2009).
546. Guil, S. & Cáceres, J. F. The multifunctional RNA-binding protein hnRNP A1 is required for processing of miR-18a. *Nat Struct Mol Biol* **14,** 591–596 (2007).
547. Michlewski, G., Guil, S., Semple, C. A. & Cáceres, J. F. Posttranscriptional regulation of miRNAs harboring conserved terminal loops. *Molecular Cell* **32,** 383–393 (2008).
548. Di Carlo, V. *et al.* TDP-43 regulates the microprocessor complex activity during in vitro neuronal differentiation. *Mol. Neurobiol.* **48,** 952–963 (2013).
549. Kawahara, Y. & Mieda-Sato, A. TDP-43 promotes microRNA biogenesis as a component of the Drosha and Dicer complexes. *Proc. Natl. Acad. Sci. U.S.A.* **109,** 3347–3352 (2012).
550. Fukunaga, R. *et al.* Dicer partner proteins tune the length of mature miRNAs in flies and mammals. *Cell* **151,** 533–546 (2012).
551. Liu, X. *et al.* Dicer-1, but not Loquacious, is critical for assembly of miRNA-induced silencing complexes. *RNA* **13,** 2324–2329 (2007).
552. Park, J. K., Liu, X., Strauss, T. J., McKearin, D. M. & Liu, Q. The miRNA pathway intrinsically controls self-renewal of Drosophila germline stem cells. *Curr. Biol.* **17,** 533–538 (2007).
553. Chendrimada, T. P. *et al.* TRBP recruits the Dicer complex to Ago2 for microRNA processing and gene silencing. *Nature* **436,** 740–744 (2005).
554. Haase, A. D. *et al.* TRBP, a regulator of cellular PKR and HIV-1 virus expression, interacts with Dicer and functions in RNA silencing. *EMBO Rep.* **6,** 961–967 (2005).
555. Lee, Y. *et al.* The role of PACT in the RNA silencing pathway. *EMBO J* **25,**

522–532 (2006).
556. Chakravarthy, S., Sternberg, S. H., Kellenberger, C. A. & Doudna, J. A. Substrate-specific kinetics of Dicer-catalyzed RNA processing. *J. Mol. Biol.* **404,** 392–402 (2010).
557. Lee, H. Y. & Doudna, J. A. TRBP alters human precursor microRNA processing in vitro. *RNA* **18,** 2012–2019 (2012).
558. Paroo, Z., Ye, X., Chen, S. & Liu, Q. Phosphorylation of the human microRNA-generating complex mediates MAPK/Erk signaling. *Cell* **139,** 112–122 (2009).
559. Auyeung, V. C., Ulitsky, I., McGeary, S. E. & Bartel, D. P. Beyond secondary structure: primary-sequence determinants license pri-miRNA hairpins for processing. *Cell* **152,** 844–858 (2013).
560. Calin, G. A. *et al.* A MicroRNA signature associated with prognosis and progression in chronic lymphocytic leukemia. *N. Engl. J. Med.* **353,** 1793–1801 (2005).
561. Jazdzewski, K. *et al.* Common SNP in pre-miR-146a decreases mature miR expression and predisposes to papillary thyroid carcinoma. *Proc. Natl. Acad. Sci. U.S.A.* **105,** 7269–7274 (2008).
562. Tian, T. *et al.* A functional genetic variant in microRNA-196a2 is associated with increased susceptibility of lung cancer in Chinese. *Cancer Epidemiol. Biomarkers Prev.* **18,** 1183–1187 (2009).
563. Jazdzewski, K. *et al.* Polymorphic mature microRNAs from passenger strand of pre-miR-146a contribute to thyroid cancer. *Proc. Natl. Acad. Sci. U.S.A.* **106,** 1502–1505 (2009).
564. Ryan, B. M., Robles, A. I. & Harris, C. C. Genetic variation in microRNA networks: the implications for cancer research. *Nat. Rev. Cancer* **10,** 389–402 (2010).
565. Yang, W. *et al.* Modulation of microRNA processing and expression through RNA editing by ADAR deaminases. *Nat Struct Mol Biol* **13,** 13–21 (2006).
566. Kawahara, Y., Zinshteyn, B., Chendrimada, T. P., Shiekhattar, R. & Nishikura, K. RNA editing of the microRNA-151 precursor blocks cleavage by the Dicer-TRBP complex. *EMBO Rep.* **8,** 763–769 (2007).
567. Xhemalce, B., Robson, S. C. & Kouzarides, T. Human RNA methyltransferase BCDIN3D regulates microRNA processing. *Cell* **151,** 278–288 (2012).
568. Rüegger, S. & Grosshans, H. MicroRNA turnover: when, how, and why. *Trends Biochem. Sci.* **37,** 436–446 (2012).
569. Hwang, H.-W., Wentzel, E. A. & Mendell, J. T. A hexanucleotide element directs microRNA nuclear import. *Science* **315,** 97–100 (2007).
570. Gatfield, D. *et al.* Integration of microRNA miR-122 in hepatic circadian gene expression. *Genes & Development* **23,** 1313–1326 (2009).
571. Baccarini, A. *et al.* Kinetic analysis reveals the fate of a microRNA following target regulation in mammalian cells. *Curr. Biol.* **21,** 369–376 (2011).
572. Rajasethupathy, P. *et al.* Characterization of small RNAs in Aplysia reveals a role for miR-124 in constraining synaptic plasticity through CREB. *Neuron* **63,** 803–817 (2009).
573. Sethi, P. & Lukiw, W. J. Micro-RNA abundance and stability in human brain: specific alterations in Alzheimer's disease temporal lobe neocortex. *Neurosci. Lett.* **459,** 100–104 (2009).

574. Krol, J. *et al.* Characterizing light-regulated retinal microRNAs reveals rapid turnover as a common property of neuronal microRNAs. *Cell* **141,** 618–631 (2010).
575. Ameres, S. L. *et al.* Target RNA-directed trimming and tailing of small silencing RNAs. *Science* **328,** 1534–1539 (2010).
576. Libri, V. *et al.* Murine cytomegalovirus encodes a miR-27 inhibitor disguised as a target. *Proc. Natl. Acad. Sci. U.S.A.* **109,** 279–284 (2012).
577. Xie, J. *et al.* Long-term, efficient inhibition of microRNA function in mice using rAAV vectors. *Nat. Methods* **9,** 403–409 (2012).
578. la Mata, de, M. *et al.* Potent degradation of neuronal miRNAs induced by highly complementary targets. *EMBO Rep.* (2015). doi:10.15252/embr.201540078
579. Haas, G. *et al.* Identification of factors involved in target RNA-directed microRNA degradation. *Nucleic Acids Research* **44,** 2873–2887 (2016).
580. Marcinowski, L. *et al.* Degradation of cellular mir-27 by a novel, highly abundant viral transcript is important for efficient virus replication in vivo. *PLoS Pathog.* **8,** e1002510 (2012).
581. Buck, A. H. *et al.* Post-transcriptional regulation of miR-27 in murine cytomegalovirus infection. *RNA* **16,** 307–315 (2010).
582. Lee, S. *et al.* Selective degradation of host MicroRNAs by an intergenic HCMV noncoding RNA accelerates virus production. *Cell Host Microbe* **13,** 678–690 (2013).
583. Heo, I. *et al.* Lin28 mediates the terminal uridylation of let-7 precursor MicroRNA. *Molecular Cell* **32,** 276–284 (2008).
584. Chang, H.-M., Triboulet, R., Thornton, J. E. & Gregory, R. I. A role for the Perlman syndrome exonuclease Dis3l2 in the Lin28-let-7 pathway. *Nature* **497,** 244–248 (2013).
585. Ustianenko, D. *et al.* Mammalian DIS3L2 exoribonuclease targets the uridylated precursors of let-7 miRNAs. *RNA* **19,** 1632–1638 (2013).
586. Backes, S. *et al.* Degradation of host microRNAs by poxvirus poly(A) polymerase reveals terminal RNA methylation as a protective antiviral mechanism. *Cell Host Microbe* **12,** 200–210 (2012).
587. Katoh, T. *et al.* Selective stabilization of mammalian microRNAs by 3' adenylation mediated by the cytoplasmic poly(A) polymerase GLD-2. *Genes & Development* **23,** 433–438 (2009).
588. Rissland, O. S., Hong, S.-J. & Bartel, D. P. MicroRNA destabilization enables dynamic regulation of the miR-16 family in response to cell-cycle changes. *Molecular Cell* **43,** 993–1004 (2011).
589. Suzuki, H. I. *et al.* MCPIP1 ribonuclease antagonizes dicer and terminates microRNA biogenesis through precursor microRNA degradation. *Molecular Cell* **44,** 424–436 (2011).
590. Upton, J.-P. *et al.* IRE1α cleaves select microRNAs during ER stress to derepress translation of proapoptotic Caspase-2. *Science* **338,** 818–822 (2012).
591. Das, S. K. *et al.* Human polynucleotide phosphorylase selectively and preferentially degrades microRNA-221 in human melanoma cells. *Proc. Natl. Acad. Sci. U.S.A.* **107,** 11948–11953 (2010).
592. Thomas, M. F. *et al.* Eri1 regulates microRNA homeostasis and mouse lymphocyte development and antiviral function. *Blood* **120,** 130–142 (2012).
593. Bail, S. *et al.* Differential regulation of microRNA stability. *RNA* **16,** 1032–

1039 (2010).
594. Chatterjee, S. & Grosshans, H. Active turnover modulates mature microRNA activity in Caenorhabditis elegans. *Nature* **461,** 546–549 (2009).
595. Chatterjee, S., Fasler, M., Büssing, I. & Grosshans, H. Target-mediated protection of endogenous microRNAs in C. elegans. *Dev. Cell* **20,** 388–396 (2011).
596. Ramachandran, V. & Chen, X. Degradation of microRNAs by a family of exoribonucleases in Arabidopsis. *Science* **321,** 1490–1492 (2008).
597. Wang, J. *et al.* CREB up-regulates long non-coding RNA, HULC expression through interaction with microRNA-372 in liver cancer. *Nucleic Acids Research* **38,** 5366–5383 (2010).
598. Cesana, M. *et al.* A long noncoding RNA controls muscle differentiation by functioning as a competing endogenous RNA. *Cell* **147,** 358–369 (2011).
599. Hansen, T. B. *et al.* Natural RNA circles function as efficient microRNA sponges. *Nature* **495,** 384–388 (2013).
600. Memczak, S. *et al.* Circular RNAs are a large class of animal RNAs with regulatory potency. *Nature* **495,** 333–338 (2014).
601. Denzler, R., Agarwal, V., Stefano, J., Bartel, D. P. & Stoffel, M. Assessing the ceRNA hypothesis with quantitative measurements of miRNA and target abundance. *Molecular Cell* **54,** 766–776 (2014).
602. Mishima, Y. *et al.* Differential regulation of germline mRNAs in soma and germ cells by zebrafish miR-430. *Curr. Biol.* **16,** 2135–2142 (2006).
603. Kedde, M. *et al.* RNA-binding protein Dnd1 inhibits microRNA access to target mRNA. *Cell* **131,** 1273–1286 (2007).
604. Nolde, M. J., Saka, N., Reinert, K. L. & Slack, F. J. The Caenorhabditis elegans pumilio homolog, puf-9, is required for the 3'UTR-mediated repression of the let-7 microRNA target gene, hbl-1. *Dev. Biol.* **305,** 551–563 (2007).
605. Miles, W. O., Tschöp, K., Herr, A., Ji, J.-Y. & Dyson, N. J. Pumilio facilitates miRNA regulation of the E2F3 oncogene. *Genes & Development* **26,** 356–368 (2012).
606. Galgano, A. *et al.* Comparative analysis of mRNA targets for human PUF-family proteins suggests extensive interaction with the miRNA regulatory system. *PLoS ONE* **3,** e3164 (2008).
607. Wulczyn, F. G., Cuevas, E., Franzoni, E. & Rybak, A. MiRNA need a TRIM regulation of miRNA activity by Trim-NHL proteins. *Adv. Exp. Med. Biol.* **700,** 85–105 (2010).
608. Schwamborn, J. C., Berezikov, E. & Knoblich, J. A. The TRIM-NHL protein TRIM32 activates microRNAs and prevents self-renewal in mouse neural progenitors. *Cell* **136,** 913–925 (2009).
609. Hammell, C. M., Lubin, I., Boag, P. R., Blackwell, T. K. & Ambros, V. nhl-2 Modulates microRNA activity in Caenorhabditis elegans. *Cell* **136,** 926–938 (2009).
610. Neumüller, R. A. *et al.* Mei-P26 regulates microRNAs and cell growth in the Drosophila ovarian stem cell lineage. *Nature* **454,** 241–245 (2008).
611. Rybak, A. *et al.* The let-7 target gene mouse lin-41 is a stem cell specific E3 ubiquitin ligase for the miRNA pathway protein Ago2. *Nat. Cell Biol.* **11,** 1411–1420 (2009).
612. Chang, H.-M. *et al.* Trim71 cooperates with microRNAs to repress Cdkn1a expression and promote embryonic stem cell proliferation. *Nat Commun* **3,** 923 (2012).

613. Kim, H. H. *et al.* HuR recruits let-7/RISC to repress c-Myc expression. *Genes & Development* **23,** 1743–1748 (2009).
614. Xue, Y. *et al.* Direct conversion of fibroblasts to neurons by reprogramming PTB-regulated microRNA circuits. *Cell* **152,** 82–96 (2013).
615. Ashraf, S. I., McLoon, A. L., Sclarsic, S. M. & Kunes, S. Synaptic protein synthesis associated with memory is regulated by the RISC pathway in Drosophila. *Cell* **124,** 191–205 (2006).
616. Cook, H. A., Koppetsch, B. S., Wu, J. & Theurkauf, W. E. The Drosophila SDE3 homolog armitage is required for oskar mRNA silencing and embryonic axis specification. *Cell* **116,** 817–829 (2004).
617. Tomari, Y. *et al.* RISC assembly defects in the Drosophila RNAi mutant armitage. *Cell* **116,** 831–841 (2004).
618. Szostak, E. & Gebauer, F. Translational control by 3'-UTR-binding proteins. *Brief Funct Genomics* **12,** 58–65 (2013).
619. Cerutti, H. & Casas-Mollano, J. A. On the origin and functions of RNA-mediated silencing: from protists to man. *Curr. Genet.* **50,** 81–99 (2006).
620. Chapman, E. J. & Carrington, J. C. Specialization and evolution of endogenous small RNA pathways. *Nat. Rev. Genet.* **8,** 884–896 (2007).
621. Matranga, C. & Zamore, P. D. Small silencing RNAs. *Curr. Biol.* **17,** R789–93 (2007).
622. Makarova, K. S., Grishin, N. V., Shabalina, S. A., Wolf, Y. I. & Koonin, E. V. A putative RNA-interference-based immune system in prokaryotes: computational analysis of the predicted enzymatic machinery, functional analogies with eukaryotic RNAi, and hypothetical mechanisms of action. *Biol. Direct* **1,** 7 (2006).
623. Majdalani, N., Vanderpool, C. K. & Gottesman, S. Bacterial small RNA regulators. *Crit. Rev. Biochem. Mol. Biol.* **40,** 93–113 (2005).
624. Aiba, H. Mechanism of RNA silencing by Hfq-binding small RNAs. *Curr. Opin. Microbiol.* **10,** 134–139 (2007).
625. Marraffini, L. A. & Sontheimer, E. J. CRISPR interference: RNA-directed adaptive immunity in bacteria and archaea. *Nat. Rev. Genet.* **11,** 181–190 (2010).
626. Lillestøl, R. K., Redder, P., Garrett, R. A. & Brügger, K. A putative viral defence mechanism in archaeal cells. *Archaea* **2,** 59–72 (2006).
627. Barrangou, R. *et al.* CRISPR provides acquired resistance against viruses in prokaryotes. *Science* **315,** 1709–1712 (2007).
628. Deveau, H. *et al.* Phage response to CRISPR-encoded resistance in Streptococcus thermophilus. *J. Bacteriol.* **190,** 1390–1400 (2008).
629. Horvath, P. *et al.* Diversity, activity, and evolution of CRISPR loci in Streptococcus thermophilus. *J. Bacteriol.* **190,** 1401–1412 (2008).
630. Aravind, L., Walker, D. R. & Koonin, E. V. Conserved domains in DNA repair proteins and evolution of repair systems. *Nucleic Acids Research* **27,** 1223–1242 (1999).
631. Aravind, L., Watanabe, H., Lipman, D. J. & Koonin, E. V. Lineage-specific loss and divergence of functionally linked genes in eukaryotes. *Proc. Natl. Acad. Sci. U.S.A.* **97,** 11319–11324 (2000).
632. MacRae, I. J. & Doudna, J. A. Ribonuclease revisited: structural insights into ribonuclease III family enzymes. *Curr. Opin. Struct. Biol.* **17,** 138–145 (2007).
633. Iyer, L. M., Koonin, E. V. & Aravind, L. Evolutionary connection between the catalytic subunits of DNA-dependent RNA polymerases and eukaryotic

RNA-dependent RNA polymerases and the origin of RNA polymerases. *BMC Struct. Biol.* **3,** 1 (2003).
634. Salgado, P. S. *et al.* The structure of an RNAi polymerase links RNA silencing and transcription. *PLoS Biol.* **4,** e434 (2006).
635. Hutvagner, G. & Simard, M. J. Argonaute proteins: key players in RNA silencing. *Nat Rev Mol Cell Biol* **9,** 22–32 (2008).
636. Schauer, S. E., Jacobsen, S. E., Meinke, D. W. & Ray, A. DICER-LIKE1: blind men and elephants in Arabidopsis development. *Trends Plant Sci.* **7,** 487–491 (2002).
637. Reinhart, B. J. & Bartel, D. P. Small RNAs correspond to centromere heterochromatic repeats. *Science* **297,** 1831 (2002).
638. Drinnenberg, I. A. *et al.* RNAi in budding yeast. *Science* **326,** 544–550 (2009).
639. Weinberg, D. E., Nakanishi, K., Patel, D. J. & Bartel, D. P. The inside-out mechanism of Dicers from budding yeasts. *Cell* **146,** 262–276 (2011).
640. Djikeng, A., Shi, H., Tschudi, C. & Ullu, E. RNA interference in Trypanosoma brucei: cloning of small interfering RNAs provides evidence for retroposon-derived 24-26-nucleotide RNAs. *RNA* **7,** 1522–1530 (2001).
641. Llave, C., Kasschau, K. D., Rector, M. A. & Carrington, J. C. Endogenous and silencing-associated small RNAs in plants. *Plant Cell* **14,** 1605–1619 (2002).
642. Ambros, V., Lee, R. C., Lavanway, A., Williams, P. T. & Jewell, D. MicroRNAs and other tiny endogenous RNAs in C. elegans. *Curr. Biol.* **13,** 807–818 (2003).
643. Okamura, K. & Lai, E. C. Endogenous small interfering RNAs in animals. *Nat Rev Mol Cell Biol* **9,** 673–678 (2008).
644. Allen, E. *et al.* Evolution of microRNA genes by inverted duplication of target gene sequences in Arabidopsis thaliana. *Nat. Genet.* **36,** 1282–1290 (2004).
645. Jones-Rhoades, M. W., Bartel, D. P. & Bartel, B. MicroRNAS and their regulatory roles in plants. *Annu Rev Plant Biol* **57,** 19–53 (2006).
646. Prochnik, S. E., Rokhsar, D. S. & Aboobaker, A. A. Evidence for a microRNA expansion in the bilaterian ancestor. *Dev. Genes Evol.* **217,** 73–77 (2007).
647. Floyd, S. K. & Bowman, J. L. Gene regulation: ancient microRNA target sequences in plants. *Nature* **428,** 485–486 (2004).
648. Arteaga-Vázquez, M., Caballero-Pérez, J. & Vielle-Calzada, J.-P. A family of microRNAs present in plants and animals. *Plant Cell* **18,** 3355–3369 (2006).
649. Voinnet, O. Origin, biogenesis, and activity of plant microRNAs. *Cell* **136,** 669–687 (2009).
650. Gruber, J. J. *et al.* Ars2 links the nuclear cap-binding complex to RNA interference and cell proliferation. *Cell* **138,** 328–339 (2009).
651. Sabin, L. R. *et al.* Ars2 regulates both miRNA- and siRNA- dependent silencing and suppresses RNA virus infection in Drosophila. *Cell* **138,** 340–351 (2009).
652. Axtell, M. J., Westholm, J. O. & Lai, E. C. Vive la différence: biogenesis and evolution of microRNAs in plants and animals. *Genome Biol.* **12,** 221 (2011).
653. Rodriguez, A., Griffiths-Jones, S., Ashurst, J. L. & Bradley, A. Identification of mammalian microRNA host genes and transcription units. *Genome Res.*

14, 1902–1910 (2004).
654. Moran, Y., Praher, D., Fredman, D. & Technau, U. The evolution of microRNA pathway protein components in Cnidaria. *Mol. Biol. Evol.* **30,** 2541–2552 (2013).
655. Grimson, A. *et al.* Early origins and evolution of microRNAs and Piwi-interacting RNAs in animals. *Nature* **455,** 1193–1197 (2008).
656. Maxwell, E. K., Ryan, J. F., Schnitzler, C. E., Browne, W. E. & Baxevanis, A. D. MicroRNAs and essential components of the microRNA processing machinery are not encoded in the genome of the ctenophore Mnemiopsis leidyi. *BMC Genomics* **13,** 714 (2012).
657. Wheeler, B. M. *et al.* The deep evolution of metazoan microRNAs. *Evol. Dev.* **11,** 50–68 (2009).
658. Krishna, S. *et al.* Deep sequencing reveals unique small RNA repertoire that is regulated during head regeneration in Hydra magnipapillata. *Nucleic Acids Research* **41,** 599–616 (2013).
659. Moran, Y. *et al.* Cnidarian microRNAs frequently regulate targets by cleavage. *Genome Res.* **24,** 651–663 (2014).
660. Gehring, N. H., Neu-Yilik, G., Schell, T., Hentze, M. W. & Kulozik, A. E. Y14 and hUpf3b form an NMD-activating complex. *Molecular Cell* **11,** 939–949 (2003).
661. Bailey, T. L. & Elkan, C. Fitting a mixture model by expectation maximization to discover motifs in biopolymers. *Proc Int Conf Intell Syst Mol Biol* **2,** 28–36 (1994).
662. Huang, D. W., Sherman, B. T. & Lempicki, R. A. Bioinformatics enrichment tools: paths toward the comprehensive functional analysis of large gene lists. *Nucleic Acids Research* **37,** 1–13 (2009).
663. Huang, D. W., Sherman, B. T. & Lempicki, R. A. Systematic and integrative analysis of large gene lists using DAVID bioinformatics resources. *Nat Protoc* **4,** 44–57 (2009).
664. Borner, G. H. H. *et al.* Multivariate proteomic profiling identifies novel accessory proteins of coated vesicles. *The Journal of Cell Biology* **197,** 141–160 (2012).
665. Frohn, A. *et al.* Dicer-dependent and -independent Argonaute2 protein interaction networks in mammalian cells. *Mol. Cell Proteomics* **11,** 1442–1456 (2012).
666. Robinson, M. S. Forty Years of Clathrin-coated Vesicles. *Traffic* **16,** 1210–1238 (2015).
667. Popova, N. V., Deyev, I. E. & Petrenko, A. G. Clathrin-mediated endocytosis and adaptor proteins. *Acta Naturae* **5,** 62–73 (2013).
668. Mauri, M. *et al.* Conservation of miRNA-mediated silencing mechanisms across 600 million years of animal evolution. *Nucleic Acids Research* (2016). doi:10.1093/nar/gkw792
669. Pisani, D. *et al.* Genomic data do not support comb jellies as the sister group to all other animals. *Proc. Natl. Acad. Sci. U.S.A.* **112,** 15402–15407 (2015).
670. Ryan, J. F. *et al.* The genome of the ctenophore Mnemiopsis leidyi and its implications for cell type evolution. *Science* **342,** 1242592 (2013).
671. Murthy, V. N. & De Camilli, P. Cell biology of the presynaptic terminal. *Annu. Rev. Neurosci.* **26,** 701–728 (2003).
672. Gustafson, E. A. & Wessel, G. M. DEAD-box helicases: posttranslational regulation and function. *Biochem. Biophys. Res. Commun.* **395,** 1–6

(2010).
673. Höck, J. *et al.* Proteomic and functional analysis of Argonaute-containing mRNA-protein complexes in human cells. *EMBO Rep.* **8,** 1052–1060 (2007).
674. Voronina, E. & Seydoux, G. The C. elegans homolog of nucleoporin Nup98 is required for the integrity and function of germline P granules. *Development* **137,** 1441–1450 (2010).
675. Frey, S., Richter, R. P. & Gorlich, D. FG-Rich Repeats of Nuclear Pore Proteins Form a Three-Dimensional Meshwork with Hydrogel-Like Properties. *Science* **314,** 815–817 (2006).
676. Kato, M. *et al.* Cell-free Formation of RNA Granules: Low Complexity Sequence Domains Form Dynamic Fibers within Hydrogels. *Cell* **149,** 753–767 (2012).
677. Han, T. W. *et al.* Cell-free Formation of RNA Granules: Bound RNAs Identify Features and Components of Cellular Assemblies. *Cell* **149,** 768–779 (2012).
678. Ross, C. A. & Poirier, M. A. Protein aggregation and neurodegenerative disease. *Nat. Med.* **10 Suppl,** S10–7 (2004).
679. Shastry, B. S. Neurodegenerative disorders of protein aggregation. *Neurochem. Int.* **43,** 1–7 (2003).
680. Zarnescu, D. C. *et al.* Fragile X protein functions with lgl and the par complex in flies and mice. *Dev. Cell* **8,** 43–52 (2005).
681. Pérez-González, A. *et al.* hCLE/C14orf166 associates with DDX1-HSPC117-FAM98B in a novel transcription-dependent shuttling RNA-transporting complex. *PLoS ONE* **9,** e90957 (2014).
682. Castello, A., Hentze, M. W. & Preiss, T. Metabolic Enzymes Enjoying New Partnerships as RNA-Binding Proteins. *Trends Endocrinol. Metab.* (2015). doi:10.1016/j.tem.2015.09.012
683. Li, P., Jiao, J., Gao, G. & Prabhakar, B. S. Control of mitochondrial activity by miRNAs. *J. Cell. Biochem.* **113,** 1104–1110 (2012).
684. Pazos, F. & Valencia, A. Protein co-evolution, co-adaptation and interactions. *EMBO J* **27,** 2648–2655 (2008).
685. Weidenfeld, I. *et al.* Inducible expression of coding and inhibitory RNAs from retargetable genomic loci. *Nucleic Acids Research* **37,** e50 (2009).
686. Ajiro, M. *et al.* Involvement of RQCD1 overexpression, a novel cancer-testis antigen, in the Akt pathway in breast cancer cells. *Int. J. Oncol.* **35,** 673–681 (2009).
687. Tanaka, M., Gupta, R. & Mayer, B. J. Differential inhibition of signaling pathways by dominant-negative SH2/SH3 adapter proteins. *Mol. Cell. Biol.* **15,** 6829–6837 (1995).
688. Berger, S. M. *et al.* Quantitative analysis of conditional gene inactivation using rationally designed, tetracycline-controlled miRNAs. *Nucleic Acids Research* **38,** e168 (2010).
689. Zheng, L., Baumann, U. & Reymond, J.-L. An efficient one-step site-directed and site-saturation mutagenesis protocol. *Nucleic Acids Research* **32,** e115 (2004).
690. Rappsilber, J., Ishihama, Y. & Mann, M. Stop and go extraction tips for matrix-assisted laser desorption/ionization, nanoelectrospray, and LC/MS sample pretreatment in proteomics. *Anal. Chem.* **75,** 663–670 (2003).
691. Cox, J. & Mann, M. MaxQuant enables high peptide identification rates, individualized p.p.b.-range mass accuracies and proteome-wide protein

quantification. *Nat. Biotechnol.* **26,** 1367–1372 (2008).
692. Cox, J. *et al.* Andromeda: a peptide search engine integrated into the MaxQuant environment. *J. Proteome Res.* **10,** 1794–1805 (2011).
693. Hubner, N. C. *et al.* Quantitative proteomics combined with BAC TransgeneOmics reveals in vivo protein interactions. *The Journal of Cell Biology* **189,** 739–754 (2010).
694. Tusher, V. G., Tibshirani, R. & Chu, G. Significance analysis of microarrays applied to the ionizing radiation response. *Proc. Natl. Acad. Sci. U.S.A.* **98,** 5116–5121 (2001).

Acknowledgements

First, I would like to thank my PhD advisor, Dr. Marina Chekulaeva, for direct supervision throughout these years, and for sharing her deep knowledge and experience in miRNA/RNA mechanistic research. I thank Marina, DAAD and MDC for having given me the opportunity to pursue my PhD studies. This experience, at times incredibly rugged, has taught me invaluable scientific and life lessons. Secondly, I would like to express my gratitude to Marie (Dr. Marieluise Kirchner) for an outstanding collaboration since the very first year of PhD; for extremely useful tips on proteomic analysis, and for professional and personal advises. I would like to thank all members of past PhD committees, Prof. Dr. Ana Pombo, Dr. Markus Landthaler, Prof. Dr. Matthias Selbach, Prof. Dr. Uwe Ohler and Dr. Robert Zinzen, for constructive feedback and guidance year by year. Particularly, I would like to thank Ana Pombo for mentoring all through my PhD.

A special mention goes to the whole lab for being so united and supportive throughout these years. I'd like to thank the core Cheku lab for the numerous adventures we shared, in the order in which they joined: Alessandra, David, Larissa and Camilla. Additionally all former members, students and fresh additions; especially Thies, Karthi and Konstantinia, with whom I started; the always happy Cinthia 'mi primera estudiante'; Sarah, who contributed to organize the lab and set up techniques, and Debbie; Olivier, Katja for sharing the A1, B1, C1 fun in the bay, and the pineapple lover Rutger. I am grateful to David, Larissa and Inga for their major help on the German version of this thesis abstract, and to Russ Hodge for constructive comments on the English abstract.

I would like to thank all the people who contributed to this work with experiments, scientific ideas or discussions; our collaborator Dr. Yehu Moran and its lab; and Dr. Caroline Bruns. Likewise I am thankful to the MDC staff and graduate office, especially Dr. Michaela Herzig and Rainer Leben, who continuously support students.

Thank also to all the Kuglerstrasse crew (Doro, Ines, Aga and Antonio), MDC friends, theatre friends and the 'spread around the world' ones for wonderful moments spent together and for support during difficult times.

I would like to say a big thank you to Eduardo, who thinks life could be split into "before a PhD and after a PhD" for coping with me all along, and giving really precious and concrete advises. Last, but not least I am extremely grateful to my whole family for their constant support, help, curiosity on what I do, and for offering alternative perspectives on puzzling situations. Finally, I would like to thank all of you who will take some time to read this thesis.